KATHOLIEKE UNIVERSITEIT LEUVEN
FACULTEIT TOEGEPASTE WETENSCHAPPEN
DEPARTEMENT COMPUTERWETENSCHAPPEN
AFDELING NUMERIEKE ANALYSE EN
TOEGEPASTE WISKUNDE
Celestijnenlaan 200A – B-3001 Heverlee

WAVELET THRESHOLDING AND NOISE REDUCTION

Promotor:
Prof. Dr. A. Bultheel

Proefschrift voorgedragen tot
het behalen van het doctoraat
in de toegepaste wetenschappen

door

Maarten JANSEN

April 2000

KATHOLIEKE UNIVERSITEIT LEUVEN
FACULTEIT TOEGEPASTE WETENSCHAPPEN
DEPARTEMENT COMPUTERWETENSCHAPPEN
AFDELING NUMERIEKE ANALYSE EN
TOEGEPASTE WISKUNDE
Celestijnenlaan 200A – B-3001 Heverlee

WAVELET THRESHOLDING AND NOISE REDUCTION

Jury:
Prof. Dr. ir. R. Govaerts, voorzitter
Prof. Dr. A. Bultheel, promotor
Prof. Dr. ir. D. Roose
Prof. Dr. W. Van Assche
Prof. Dr. J. Beirlant
Prof. Dr. ir. D. Vandermeulen
Prof. Dr. M. Unser
(Ecole Polytechnique Fédérale de Lausanne, Switzerland)

Proefschrift voorgedragen tot
het behalen van het doctoraat
in de toegepaste wetenschappen

door

Maarten JANSEN

U.D.C. 519.234, 519.25, 681.3$*$G.3+I.4.4

April 2000

D/2000/7515/08

ISBN 90-5682-235-7

Wavelet thresholding and noise reduction

Maarten Jansen
Katholieke Universiteit Leuven
Department of Computer Science

Abstract

A wavelet transform decomposes data into a sparse, multiscale representation. This dissertation uses both features in wavelet based noise reduction algorithms.

Sparsity is the key to wavelet thresholding: coefficients with magnitude below a threshold are replaced by zero. After an introduction to wavelets and their applications, this text discusses the minimum risk threshold. This threshold minimizes the expected mean square error of the output. This error cannot be computed exactly when the uncorrupted data are unknown. We present a procedure based on generalized cross validation (GCV) to estimate the optimal threshold. An asymptotic argument motivates this estimation method. To this end, we first study the asymptotic behavior of the minimum risk threshold. We compare these minimum risk and GCV thresholds with the well known universal threshold.

The multiresolution character of a wavelet decomposition allows for refinements of the general threshold scheme. Tree structured thresholding reduces false structures in the output. Scale dependent thresholds are necessary to deal with correlated noise or non-orthogonal wavelet transforms. The synthesis from a non-decimated wavelet transform has an additional smoothing effect. We also investigate noise reduction in the framework of integer wavelet transform.

The next part concentrates on images. An approximation theoretic argument learns that wavelets might not be the ultimate basis functions for image processing. Moreover, selecting the coefficients with large magnitude is a local approach. A Bayesian procedure could lead to a more structured coefficient selection, which better preserves edges in the output. The geometric prior model favors clusters of important coefficients.

The last part investigates the applicability of threshold algorithms for non-equidistant data and second generation wavelets. Experimental results indicate that instability of the wavelet transform hinders the classification of the coefficients according to their importance. We propose an algorithm to overcome this difficulty.

Key words and phrases: wavelet, noise, threshold, non-linear, non-parametric regression, generalized cross validation, minimum risk, mean square error, Bayes, Markov Random Field, non-equidistant

AMS 2000 Mathematics Subject Classification: 41A30, 42C40, 60G60, 62C12, 62F15, 62G08, 62G20, 62J07, 93E14, 94A08, 94A12

Waveletdrempels en ruisonderdrukking

Maarten Jansen
Katholieke Universiteit Leuven
Departement Computerwetenschappen

Situering en vulgariserende samenvatting

Wavelets vormen een wiskundige basis die bijzonder geschikt is voor bepaalde signaal- en beeldverwerkingsoperaties. Eén van die mogelijke toepassingen is beeldcompressie. Een waveletvoorstelling van een beeld bevat enkele grote getallen die de essentiële informatie dragen en vele kleine getallen voor de details. Een groot deel van die kleine getallen kan achterwege blijven zonder dat dit aanleiding geeft tot waarneembaar kwaliteitsverlies. Waar details (kleine getallen) toch een zichtbaar verschil uitmaken, gaat het dikwijls om ruis. Hetzelfde principe als dat van compressie ligt dus ook aan de basis van ruisonderdrukkingsschema's: laat de kleine getallen in de waveletvoorstelling weg. In dit proefschrift bestuderen we waar we de grens (de drempel) moeten trekken tussen belangrijke informatie en details of ruis. Als we de ruisvrije informatie kenden, zouden we de optimale grens exact kunnen berekenen. In deze tekst gaan we na hoe die optimale drempel zich globaal gedraagt en hoe we die kunnen schatten als we enkel over de gegevens met ruis beschikken. Daarna bespreken we enkele praktijkvoorbeelden. We stellen enkele eenvoudige verfijningen voor om het drempelprincipe ook te laten werken in meer complexe situaties. Vervolgens leiden we een techniek in om de randen in het uitvoerbeeld minder wazig te maken. Een laatste hoofdstuk vóór het algemeen besluit bestudeert de moeilijkheden die optreden wanneer de invoer niet bestaat uit een regelmatig signaal of een beeld maar uit waarnemingen op onregelmatige tijdstippen.

Korte inhoud

Een wavelettransformatie ontbindt gegevens in een ijle voorstelling die bovendien verschijnselen op verschillende schalen ontleedt. Dit proefschrift gebruikt beide eigenschappen in waveletgebaseerde ruisonderdrukkingsalgoritmen.

Ijlheid ligt aan de basis van methoden met waveletdrempels: coëfficiënten met absolute waarde onder een drempel worden nul. Na een inleiding tot wavelets en hun toepassingen bespreekt deze tekst de drempel met minimale kwadratische fout in de uitvoer. Deze fout kunnen we niet exact berekenen als de ruisvrije gegevens onbekend zijn. We stellen een procedure voor, gebaseerd op veralgemeende kruisvalidatie (GCV - generalized cross validation) om de drempel met minimale fout te schatten. We tonen aan dat deze procedure asymptotisch optimaal is. Hiertoe bestuderen we eerst het asymptotisch gedrag van de drempel met minimale fout. We

maken ook de vergelijking tussen deze drempel, de GCV-drempel en de bekende universele drempel.

Het multischaalkarakter van een waveletontbinding leidt tot verdere verfijning van het drempelalgoritme. Boomgestructureerde selectie van coëfficiënten vermindert het aantal storende, oneigenlijke structuren in de uitvoer. Schaalafhankelijke drempels zijn nodig als de ruis gecorreleerd (gekleurd) is of de transformatie niet orthogonaal is. Een niet-gedecimeerde wavelettransformatie veroorzaakt een bijkomende vereffening van de gegevens. We onderzoeken eveneens de mogelijkheden van een gehele-getallentransformatie in ruisonderdrukkingsschema's.

Een volgend deel gaat dieper in op toepassing op beelden. Een benaderingstheoretische redenering geeft aan dat wavelets voor tweedimensionale gegevens niet noodzakelijk de beste voorstelling opleveren. Bovendien is de selectie op basis van de grootte van iedere individuele coëfficiënt een erg lokale aanpak. Een Bayesiaanse procedure moet tot een meer gestructureerde selectie leiden, waarbij randen in de uitvoer beter bewaard blijven. Het ruimtelijk a priori model bevordert clusters van belangrijke coëfficiënten.

Het laatste deel onderzoekt de toepasbaarheid van drempelmethoden voor gegevens op onregelmatige afstand van elkaar. Hiervoor dienen wavelets van de tweede generatie. Experimentele resultaten wijzen op problemen ten gevolge van instabiliteiten in de transformatie: het is moeilijker het belang van een coëfficiënt af te lezen uit zijn grootte. We stellen een algoritme voor om deze moeilijkheden te omzeilen.

Voorwoord – *Preface*

“Se non è vero, è ben trovato.”
—Italiaans spreekwoord.

Verzen of verzonnen verhalen mogen dan wel een diepe waarheid verkondigen, feiten boeien blijkbaar sneller en langer. Nochtans is waarneming van feiten niet meer dan een eerste — weliswaar belangrijke — stap in iedere ontdekking. Alles begint met kijken, maar algemene waarheden, die zich in eerste instantie aandienen als abstracte idealen, laten zich zo handig vertalen in verhalen.

Voor dit werk was het de bedoeling feiten te verzinnen, en ze liefst nog te bewijzen ook. Beslist (voorwaar) niet altijd even gemakkelijk.

Koffie lust ik niet, of toch niet graag, dus van die kant kon ik geen hulp verwachten. Veel inspiratie heb ik ingeademd op de zwerftochtjes langsheen het Begijnhof of over de *licht* golvende heuvels rondom Leuven. Ik ben me maar al te goed bewust van het voorrecht schoonheid te kunnen zoeken en koesteren. Zonder de aanzet en de steun van velen was ik hier nooit geraakt.

Voor omstanders lag het voor de hand dat ik zou opteren voor de ‘positieve’ wetenschappen, zelf vond ik die stap veel minder vanzelfsprekend. Wellicht heeft de bedenking meegespeeld dat wiskunde nooit een bezigheid kon worden in de vrije tijd. En je maakt van je belangrijkste hobby best niet je beroep, wil je vermijden dat je met de zin voor het werk ook je interesses zou verliezen. Anderzijds was ik van bij het begin geboeid door kansrekening en statistiek, die, vanuit drie eenvoudige axioma’s en als geen andere wiskundige theorie, een werkelijkheid beschrijft en daarmee dus een soort ideaal benadert. Zoals dat meestal gaat bij een belangrijke beslissing, is ook daarna de twijfel nooit helemaal verdwenen. Dat heeft zeker te maken met de inzet en gedrevenheid van de leraars en leraressen op ‘ons Mals’ college (de woordspeling komt van één van hen). Het beroep van leraar of onderwijzer verdient alle waardering, zeker in deze tijd, en zeker in scholen met leerlingen uit minder bevoorrechte middens. Dat houdt, geachte excellentie, wel degelijk een aanpassing van het salaris in. Niet alleen voor de twijfel ben ik mijn lesgevers dankbaar, maar ook voor die momenten waarop je ontdekt hoeveel dingen je in die tijd hebt meegekregen waarvan je veel later pas de volle betekenis beseft. Dat geldt misschien vooral voor de zogeheten ‘humane’ vakken, hoewel, zijn ze dat niet allemaal in de ‘humaniora’? Ik kijk nu alvast uit naar de momenten die zo nog gaan komen.

Uiteindelijk is het dus kansrekenen en statistiek geworden, het zekere voor (en over) het onzekere, sluimerend in het begin, want de ingenieursopleiding bood niet meer. Toen één van de eindwerkvoorstellen gewag maakte van een statistische methode, was de keuze snel gemaakt. Maurits Malfait begeleidde me bij mijn eerste tocht over ‘het woelig ruisende water van de waveletzee’. Van bij het begin hield ook Wim Sweldens een oogje in het zeil. Meer dan eens trok hij me met zijn enthousiasme over de streep van mijn twijfels. En mijn promotor, prof. Adhemar Bultheel, had alle vertrouwen in mijn werk en een relativerende kijk op de problemen daarbij. Mijn schrijfsels heeft hij steeds in een mum van tijd nagelezen en becommentarieerd.

Met dezelfde promotor, maar ook met de steun van prof. Dirk Roose ben ik dan aangekomen in dit ‘Land van het Verstand’. Het is hier, al bij al, rustig leven. Zoals overal elders zijn er natuurlijk de mega-ego’s en de kleine kantjes, maar je kan hier heerlijk denken en dromen. Na al die jaren weet ik meestal wel de ruis van het signaal te onderscheiden. Naast dat onderscheidingsvermogen staan hier nog een aantal andere attitudes hoog aangeschreven: zin voor het subtiele, aandacht voor het detail en de nuance, voorzichtigheid met uitspraken over ongekende domeinen, openheid voor vernieuwing, niet te snel een besluit, maar alle mogelijke verklaringen onderzoeken. Niet dat we altijd naar deze mooie principes handelen, maar we doen ons best.

Hoog in de toren van gebouw A gaat het er meestal gemoedelijk, soms bijna speels aan toe. De discussies met mijn collega’s gingen gelukkig niet alleen over wiskunde en computers. In het bijzonder dank ik mijn kantoorgenoten, eerst Geert, daarna Caroline, voor hun geduld. In zijn Linux-lessen had Geert aan mij een behoorlijk kritische leerling. Voor een theoretisch vraagje klopte ik bij Jo aan. Bij het schrijven van de tekst en het voorbereiden van de presentatie kreeg ik hulp en computertips van Geert, Peter, Frank en Philippe. Voor praktische problemen van andere orde kon ik terecht bij onze secretaressen Margot Peeters en Denise Brams of bij onze bibliothecaresse Ria Vanhoof.

Onze proffen moedigden ons aan de wijde wereld in te trekken, en vooral Dirk Roose is altijd ijverig in de weer om het geld daarvoor bijeen te sprokkelen. *This is how I met several people in the wavelet world. I had interesting discussions with Michael Unser (National Institutes of Health at that time), with Rainer von Sachs and his student Véronique Delouille (U.C.L.) Bernard Silverman (Bristol University), Brani Vidakovic (Duke University). On my trips to the United States, I enjoyed the hospitality of Wim Sweldens and his wife Kirsten. Wim gave me the opportunity to present my work at Bell Labs and at Princeton University. He kindly introduced me to Mark Hansen (Bell Labs), Ingrid Daubechies (Princeton University), Bin Yu (University of California at Berkeley), Richard Baraniuk (Rice University) and many other, enthusiastic people.*

A cette occasion, je voudrais remercier également les professeurs Jean-Pierre

Antoine (U.C.L.) et Christine De Mol (U.L.B.) qui continuent d'organiser les journées belges des ondelettes. Non seulement ils ont rassemblé les chercheurs locaux, mais aussi ils nous ont donné une chance de plus de rencontrer des experts invités.

I spent six weeks at the statistics department of Stanford University. Prof. Iain Johnstone made this possible, showed his interest in my work, introduced me to Emmanual Candes and Xiaoming Huo, and last but not least, helped me in practical problems, such as housing. I also thank other people at Sequoia Hall for discussions and support. By the way, many of the results in this thesis were obtained with the aid of the free software WaveLab*, developed at Stanford University. These Californian weeks allowed me to quietly consider my research and to fill in some gaps. Most of the material of Chapter 3 is the result of this fruitful period. Evidently, all scientific responsibility rests with me.*

From Johan Van Horebeek, I also got the opportunity to teach a wavelet course at CIMAT, Guanajuato, Mexico. This was nice experience and a surprising discovery of a beautiful country.

Intussen kon ik me ook thuis uitleven in het lesgeven. Ik heb dat altijd graag gedaan, en dat dank ik natuurlijk ook aan de studenten met wie ik kon werken. In het bijzonder vermeld ik de twee meisjes die ik begeleidde bij hun eindwerk, Tineke Verhaeghe en Evelyne Vanraes. Ik heb hun geen gemakkelijke opgaven voorgelegd, maar hun werklust verzekerde toch mooie resultaten.

Naast Prof. Adhemar Bultheel en Prof. Roose van ons departement verklaarden ook Prof. Jan Beirlant en Prof. Walter Van Assche van het departement wiskunde zich bereid om een eerste versie van de tekst na te kijken, een behoorlijk zware opdracht, want een doctoraal proefschrift laat zich meestal niet lezen als een spannende roman (dat hoop ik toch). De leden van dit leescomité maken ook deel uit van de eigenlijke jury, waarin ook Prof. Dirk Vandermeulen wilde zetelen. *Prof. Michael Unser de l'Ecole Polytechnique Fédérale de Lausanne était bien interessé de retourner, cinq années après le doctorat de Maurits, à Louvain, pour participer au jury.*

Tot slot denk ik aan die mensen die er waren in mooie en moeilijke momenten. Tom gaat al mee sinds mijn tweede middelbaar, en heeft al die tijd zijn begijnhoffelijkheid weten te bewaren, zij het sinds enkele jaren met de niet onaardige steun van Liesbeth. Met Johan (en later 'ons' Ann) heb ik ontdekt dat toch niet alles even belangrijk is en zeker niet even boeiend. Christof blijft immer even stoffig: daar kan je dus staat op maken. Als geen ander weet Koen dat een doctoraat voorbereiden niet altijd even vlot verloopt. Koen en Liesbeth hebben me trouwens ook af en toe op professioneel vlak verder geholpen. Ook de mensen die me bij het zingen op toon en in toom hielden, en alle anderen die mee onderweg zijn geweest, wil ik niet vergeten. Ook al noem ik verder geen namen, wie zich aangesproken voelt, die laat dat gevoel rustig spreken.

Dankzij mijn ouders bleef Zoersel een plek om thuis te komen, om te rusten. Al het ongewone dat ze voor mij deden was voor hen heel gewoon en van het dagdagelijkse maakten ze iets bijzonders. Ik dank zus Karen voor haar vaak rake raad en broer Freek voor zijn soms wat rare raad, waarvan de ware aard altijd bestond uit oprechte bekommernis.

Als ik de tijd van mijn ingenieursthesis meetel, heb ik zes heerlijke jaren achter de rug. Een mooie periode loopt ten einde en wat de toekomst brengt, is nog onzeker. Alleszins blik ik tevreden terug op wat voorbij is, en dat is alvast een comfortabele uitgangspositie. Er is al heimwee op voorhand.

Allemaal hartelijk dank. *Thank you. Merci à tous. Grazie a tutti.*
Maarten, 3 maart 2000.

Nederlandse Samenvatting

Waveletdrempels en ruisonderdrukking

Over *denken en dromen*:

> *"Une certaine quantité de rêverie est bonne, comme un narcotique à dose discrète. Cela endort les fièvres, quelquefois dures, de l'intelligence en travail, et fait naître dans l'esprit une vapeur molle et fraîche qui corrige les contours trop âpres de la pensée pure, comble çà et là des lacunes et des intervalles, lie les ensembles et estompe les angles des idées. Mais trop de rêverie submerge et noie. Malheur au travailleur par l'esprit qui se laisse tomber tout entier de la pensée dans la rêverie! Il croit qu'il remontera aisément et il se dit qu'après c'est la même chose. Erreur! La pensée est le labeur de l'intelligence, la rêverie en est la volupté. Remplacer la pensée par la rêverie, c'est confondre un poison avec une nourriture."*
>
> —Victor Hugo, *(1802 – 1885), Les Misérables, Saint-Denis, Livre Deuxième (Eponine), Le Champ de l'alouette.*

1 Inleiding

1.1 Afbakening van het onderwerp

Heel wat fenomenen vertonen een verschillend gedrag naargelang de schaal waarop men observeert. In zulke gevallen is het logisch dat de analyse of verwerking van die waarnemingen ook schaal per schaal gebeurt. Wavelettheorie ondersteunt op een natuurlijke wijze het concept van een multischaalvoorstelling.

In dit proefschrift concentreren we ons op meerschalige, niet-parametrische regressie voor digitale gegevens. Niet-parametrisch betekent dat we vooraf geen vorm opleggen aan de curve die we doorheen de waarnemingen met ruis willen trekken. Het moet dus geen rechte zijn, parabool, sinusoïdale of exponentiële kromme. We willen alleen een uitvoer die samengesteld is uit basisfuncties op verschillende schalen, de wavelets. Waarnemingen met storingen (ruis) transformeren we eerst naar een multischaalvoorstelling. In deze voorstelling behouden we enkel de grootste getallen; getallen beneden een bepaalde drempelwaarde vervangen we door nul. Deze operatie vermindert de hoeveelheid ruis. De drempels geven de methode een niet-lineair karakter: ze behouden de grootste waarden, niet de eerste. Niet-lineaire methodes zijn meestal krachtiger maar moeilijker te beschrijven. In eerste instantie speelt niet zozeer het multischaalelement op zich een rol, als wel het feit dat dezelfde transformatie ook een ijle voorstelling van gegevens toelaat: hierdoor volstaan de grootste waarden om de essentie van een waarneming te vatten. In onze aanpak veronderstellen we dat we vooraf niet weten hoeveel ruis we mogen verwachten. Dit bemoeilijkt de opgave, maar stemt overeen met vele praktijkgevallen.

Een eerste belangrijke probleem in deze werkwijze vormt het optimaal bepalen van de drempels. Hiervoor verantwoorden en gebruiken we de methode van kruisvalidatie (cross validation). Daarna pas concentreren we ons op de mogelijkheden van de multischaalontbinding zelf: we maken de operaties schaalafhankelijk. In een derde stap passen we de algoritmen toe op beelden met ruis, en zorgen we voor een uitbreiding specifiek voor deze toepassing. Tenslotte bestuderen we de aanpassingen die nodig zijn om te werken met gegevens op onregelmatige roosters: als de waarnemingen onregelmatig gebeuren, is het moeilijker om vaste schalen te onderscheiden.

1.2 Opbouw van het proefschrift

Voor goed begrip van de tekst is geen voorkennis over wavelets nodig. Wel veronderstellen we vertrouwdheid met algemene wiskunde en statistiek. Na de invoering van de nodige basisbegrippen herhalen we in hoofdstuk 2 de beginselen van wavelettheorie die nodig zijn om het vervolg te verstaan. We formuleren daar ook het probleem van ruisverwijdering en leggen de stappen uit in een drempelalgoritme.

In hoofdstuk 3 bestuderen we het asymptotisch gedrag van de optimale drempel. Eerst definiëren we natuurlijk wat we verstaan onder “optimaal”. In twee stappen gaan we dan na hoe de drempel zich gedraagt als het aantal invoergegevens stijgt. Het aantal gegevens laten toenemen en kijken wat er dan gebeurt, is een klassieke werkwijze in de statistiek. Het resultaat dat we bekomen is interessant op zich omdat Donoho en Johnstone van de universiteit van Stanford volgens andere criteria gelijkaardige uitdrukkingen voor goede drempels ontwikkeld hebben. Omdat deze criteria en hun eigenschappen belangrijk en niet eenvoudig zijn, staan we in hoofdstuk 3 ook stil bij de betekenis ervan.

De eigenlijke reden voor de studie van het asymptotisch gedrag van de optimale drempel wordt pas duidelijk in hoofdstuk 4. Daar stellen we veralgemeende kruisvalidatie (generalized cross validation) voor om de optimale drempel in praktijk te schatten. Deze methode verantwoorden we met een asymptotisch argument: neigt het aantal observaties naar oneindig, dan wordt de schatting optimaal. Om dit te bewijzen, moeten we weten hoe de optimale drempel zelf evolueert bij een toenemend aantal observaties.

Het volgend hoofdstuk gebruikt het multiresolutie-aspect van een waveletontbinding om de drempelmethode te verbeteren. In hoofdstuk 6 concentreren we ons op beelden en combineren we het drempelalgoritme met een Bayesiaanse methode. Het doel is extra aandacht te besteden aan de randen in het beeld.

In veel toepassingen bestaat de invoer uit onregelmatige waarnemingen. Hoofdstuk 7 is een eerste kennismaking met dit door de waveletwereld nog vrijwel onontgonnen domein. We stuitten hierbij op een aantal hardnekkige problemen. Op dit ogenblik is het onderzoek daarvan aan het departement nog volop aan de gang.

Het laatste hoofdstuk bundelt enkele besluiten en mogelijke richtingen voor verder onderzoek.

Deze Nederlandse samenvatting volgt grotendeels dezelfde indeling. Voor de hoofdstukken 2 tot en met 5 heb ik geprobeerd de samenvatting zo eenvoudig mogelijk te maken. Dit stuk zou voor ieder met een minimum aan wiskundige achtergrond (niveau laatste middelbaar, sterke richting) en met wat wetenschappelijke interesse verstaanbaar moeten zijn, op voorwaarde dat men ook de figuren raadpleegt waarnaar ik in de tekst verwijs. Omdat hoofdstuk 6 specifiek gebaseerd is op een toepassing van de regel van Bayes voor een speciaal soort a priori model, was deze ambitie hier niet houdbaar. Ook hoofdstuk 7 gaat dieper in op een zeer specifiek probleem.

1.3 Motivering

Oorspronkelijk bouwde dit werk voort op resultaten van M. Malfait op het gebied van beeldverwerking. Dit domein beschouwen we nog steeds als één van de belangrijkste toepassingen. Op het vlak van geografische informatiesystemen (GIS) werkt het departement samen met enkele Vlaamse bedrijven. Over de resultaten van deze samenwerking bericht het doctoraat van Geert Uytterhoeven [140]. Voorts bestaat er interesse vanuit de sector van medische beeldverwerking. Natuurlijk verbeteren beeldvormingstechnieken nog steeds en beschikken we nu over beelden met duizenden grijswaarden, in plaats van de klassieke 256. Precies daarom stellen we ook steeds hogere eisen. Ons oog kan geen duizenden grijswaarden onderscheiden, en dikwijls spitst men de aandacht toe op een deel van het grijswaardenspectrum. Binnen dat deel verhoogt men het contrast zodat deze zone het hele bereik van zwart tot wit bestrijkt. Ook al is de ruis eerst onzichtbaar klein, door deze contrastverhoging kan ze toch weer storend worden.

Het verwijderen van ruis uit beelden blijft een belangrijke toepassingsmogelijkheid, en dit verklaart de verschillende illustraties met beelden in deze tekst. Geleidelijk aan zagen we in dat bijna alle materiaal (op het hoofdstuk 6 na) niet gericht hoeft te zijn op één welbepaalde toepassing. We willen die verbreding benadrukken en zelfs vermelden dat de methode van hoofdstuk 4 ook buiten een waveletaanpak van pas kan komen. Wavelets bieden in sommige gevallen niet noodzakelijk de beste oplossing, zoals we illustreren in hoofdstuk 6. Het besluit bij hoofdstuk 4 haalt een reden aan waarom we mogen hopen dat onze methode ook van dienst kan zijn bij eventuele nieuwe transformaties met betere eigenschappen dan de wavelettransformatie: we mogen verwachten dat die nieuwe methode ook met ijle voorstellingen zal werken.

Gegevens met ruis komen voor in een brede waaier van domeinen. We vermelden de financiële wereld, aardrijkskundige of aardkundige opmetingen, analyses in biomedische toepassingen, geluidssignalen. Voor al deze gevallen loont het de moeite een waveletaanpak te onderzoeken. Uiteraard is succes niet gegarandeerd, of zijn er gerichte aanpassingen nodig aan de eenvoudige, algemene schema's die we hier voorstellen.

2 Wavelets en drempels

2.1 Probleemstelling

De invoer van onze algoritmen bestaat uit een discreet signaal $\boldsymbol{f} \in \mathbb{R}^N$, dit is een eindige rij (reële) getallen. Die vector kan bijvoorbeeld een beeld zijn, waarbij de getallen f_i in de rij grijswaarden voorstellen. Typisch liggen de opeenvolgende getallen dicht bij elkaar en het is dan ook niet efficiënt die getallen zonder meer na elkaar op te slaan in de computer. Bovendien zegt een getal in deze voorstelling totaal niets over de *algemene evolutie* van het signaal: uit één beeldpunt kunnen we niet opmaken of we in de buurt van een rand in het beeld werken of ergens in een effen deel. Om een globale kijk op het signaal te krijgen, moeten we verschillende punten samennemen: al is een digitaal beeld een matrix van beeldpunten, zo kijken onze ogen niet.

Het zou dus veel interessanter zijn als we de invoer konden omzetten naar getallen die vrijwel onmiddellijk aangeven waar de belangrijke kenmerken van het signaal optreden en die tegelijk geen overbodige informatie leveren. Hiertoe nemen we de getallen samen in paren en berekenen van ieder paar het gemiddelde en het (halve) verschil:

$$\begin{aligned} a_1 &= \frac{f_1 + f_2}{2} \\ d_1 &= \frac{f_1 - f_2}{2} \end{aligned}$$

Deze operatie is omkeerbaar:

$$\begin{aligned} f_1 &= a_1 + d_1 \\ f_2 &= a_1 - d_1 \end{aligned}$$

Deze eigenschap van omkeerbaarheid heet *perfecte reconstructie*: het is een absolute voorwaarde voor iedere bruikbare gegevenstransformatie.

2.2 Visuele voorstelling

De rij getallen kunnen we ook visueel voorstellen als een stuksgewijs constante lijn over een doorlopende (continue) tijdsas, zoals bovenaan in figuur 2.1. De gegevens blijven natuurlijk discreet, dit is enkel een continue voorstelling, en het is zeker niet de enig mogelijke. De gemiddelde waarden visualiseren we op dezelfde manier, maar de verschillen vertalen we in twee lijnstukjes: eentje ligt boven de nullijn en vertelt hoeveel het ene invoergetal boven het gemiddelde ligt. Natuurlijk ligt het andere dan even ver onder het gemiddelde.

De rij van gemiddelden vormt een afgevlakte (uitgemiddelde) versie van de invoer, net alsof we met halfgesloten ogen naar een beeld kijken. Op deze rij kunnen we dezelfde operaties nog eens uitvoeren, en zo verder. De verschilwaarden in iedere stap geven details weer op opeenvolgende schalen.

De stuksgewijs constante lijn van de invoer is eigenlijk een combinatie van blokfuncties $\varphi_k(x)$, zoals in figuur 2.3, bovenaan. Ieder invoergetal f_k geeft weer hoe hoog de blokfunctie op die plaats moet zijn:

$$f(x) = \sum_k f_k \varphi_k(x).$$

Alle blokfuncties hebben natuurlijk dezelfde vorm: het zijn allemaal translaties (verschuivingen) van één *vader*functie. Ze heten ook *schaalfuncties*. De gemiddelde waarden na de eerste stap horen dan bij blokfuncties met dubbele breedte. De verschillen komen overeen met een blok*golfje* $\psi_k(x)$. Op alle schalen krijgen we golfjes van dezelfde vorm, ze zijn enkel uitgerokken (dilatatie) en verplaatst (translatie). Dit zijn de wavelets. Ze stammen af van één enkele *moeder*functie. Dit eenvoudig voorbeeld van een waveletontbinding staat bekend als de *Haar*-transformatie.

2.3 Ijle en locale voorstelling

Omdat twee naburige getallen dikwijls bijna even groot zijn, liggen de meeste verschilwaarden erg dicht bij nul. Figuur 2.2 geeft een voorbeeld. In deze figuur staan de verschilwaarden allemaal op een rij en de stippellijnen bakenen de schalen af. De figuur illustreert twee kenmerken van een wavelettransformatie:

1. de waveletcoëfficiënten zijn bijna allemaal zo goed als nul: men noemt dit het *decorrelerend vermogen* van een wavelettransformatie. Het zorgt voor een *ijle* voorstelling van de invoer, dit is een voorstelling met veel bijna-nullen, die we dikwijls kunnen verwaarlozen. Dit ligt aan de basis van allerhande compressie-algoritmen.

2. enkel als twee naburige getallen ver uit elkaar liggen, is hun verschil groot. In een signaal gebeurt dit op de plaats van een sprong of een plotse overgang, bijvoorbeeld aan de rand in een beeld. De grote waveletcoëfficiënten geven

dus aan waar belangrijke verschijnselen optreden. Bovendien heeft iedere wavelet een bepaalde schaal: de coëfficiënt geeft dus ook informatie over de schaal waarop een fenomeen zich voordoet: enkel lokaal of ook met bredere impact. Men zegt dat een waveletvoorstelling een goede *localiteit* heeft in *ruimte* of *tijd* én in *schaal* (frequentie). Als we de coëfficiënten bewerken, heeft dit ook maar een *locaal effect*, zowel in tijd als in frequentie, zodat we goede controle houden over wat we precies aan het doen zijn.

2.4 Multiresolutie

In plaats van gemiddelden en verschillen te berekenen, kunnen we ook meer dan twee getallen samennemen en ingewikkeldere combinaties maken. Dit komt overeen met andere basisfuncties, en dus ook een andere voorstelling op de continue tijdsas van de discrete invoer. We willen wel behouden dat alle basisfuncties afkomstig zijn van één vader- en moederfunctie, want we willen dat alle detailcoëfficiënten een gelijkaardige betekenis hebben. Hadden de basisfuncties verschillende vormen, dan hadden de bijhorende coëfficiënten elk een andere achtergrond. Deze voorwaarde leidt tot het begrip *multiresolutie-analyse* (MRA), waarvan definitie 2.1 een precieze beschrijving geeft. Alle functies die in deze definitie passen als moederfunctie zijn mogelijke wavelets. Wavelets zien er altijd uit als korte golfjes, wat hun naam verklaart: in het Engels betekent *wave-let* “kleine golf”. In feite is het diminutief afkomstig van het Franse woord “ondelette”: wavelets doken het eerst op in Frankrijk, in het begin van de tachtiger jaren. Een algemeen aanvaarde Nederlandse term voor wavelet bestaat (nog) niet. Voorstellen voor een vertaling zijn, o.a., golflet, golflein, golvelet, golfje, kabbel, zoempje, piefje, rimpel, wervel [134]. Voorbeelden van waveletfuncties staan in figuur 2.8.

3. Wavelets en multiresolutie-analyse gaan altijd samen. Dit is interessant, want vele fenomenen in de natuur bezitten uit zichzelf een meerschalig karakter. De manier waarop onze ogen beelden waarnemen, sluit bijvoorbeeld goed aan bij een multiresoltie-voorstelling: we zien eerst de grote lijnen van een beeld, en gaan daarna in op details.

4. Er zijn verschillende soorten wavelets, elk met hun eigen kenmerken. Voor iedere toepassing vindt men, mits wat zoeken en proberen, een geschikte waveletbasis.

2.5 Theoretisch onderbouwd en snelle algoritmen

De idee om met kortlopende golven te werken is natuurlijk niet nieuw. In feite is een muziekpartituur ook een voorstelling met korte golven, al gaat de analogie met wavelets niet volledig op. Men heeft ook al geprobeerd op verscheidene manieren klassieke sinusoïdale golven af te breken, maar meestal krijgt men dan te maken met knip- en plakwerk. Afgebroken sinussen passen niet in de wiskundige definitie van een multiresolutieschema.

5. waveletmethoden steunen daarentegen op een elegante (zij het niet eenvoudige) wiskundige theorie.

6. Bovendien verloopt een volledige wavelettransformatie bijzonder snel: de hoeveelheid rekenwerk is maar recht evenredig met de lengte van de invoervector N. Voor een snelle Fouriertransformatie is dit $N \log N$ en een algemene lineaire transformatie vergt orde N^2 berekeningen.

7. Tenslotte garandeert de theorie ook dat een wavelettransformatie stabiel blijft: fouten op de invoer zullen zich doorheen de transformatie niet te fel uitbreiden.

2.6 Wavelets en ruis

In veel toepassingen bestaat de invoer uit een signaal met ruis:

$$\boldsymbol{y} = \boldsymbol{f} + \boldsymbol{\eta}.$$

In dit model hangt de ruisvector $\boldsymbol{\eta}$ af van toevallige effecten en is het signaal $\boldsymbol{f}$ géén toevalsvector, maar afkomstig van een vaste, zacht verlopende functie. Van het stoorsignaal nemen we aan dat het overal even ‘krachtig’ is. Dit betekent dat de variantie (verwachte energiewaarde) σ^2, van de ruis constant is. De ruis heet dan homoscedastisch. Verder veronderstellen we voorlopig dat de opeenvolgende componenten $\eta_i, i = 1, \ldots, N$ onderling onafhankelijk zijn. De storing in één punt staat dan volledig los van de vorige en volgende waarneming. Dit heet witte ruis. Als we later gekleurde of gecorreleerde ruis bestuderen, veronderstellen we dat de correlatie tussen twee punten enkel afhangt van de onderlinge afstand tussen die punten, en niet van de plaats van die punten zelf. Dit is dan tweede-orde-stationaire ruis. Dit soort ruis altijd homoscedastisch: de variantie is immers de covariantie van een waarneming met zichzelf en die hangt niet af van de plaats van de waarneming, dus is de variantie een constante.

Op dit signaal passen we nu dezelfde wavelettransformatie toe als voorheen. Het verschil en het gemiddelde van twee willekeurige (dit betekent door het toeval bepaalde) getallen zijn natuurlijk opnieuw louter toevallig, en bovendien staat het gemiddelde van een paar getallen volledig los van het gemiddelde van het volgende paar, want we nemen geen overlappende paren. Figuur 2.19 laat zien hoe de ruis zich zo over alle waveletcoëfficiënten gelijkmatig verspreidt. We krijgen dus een gelijkaardig model voor de waveletcoëfficiënten met ruis:

$$\boldsymbol{w} = \boldsymbol{v} + \boldsymbol{\omega},$$

waar $\boldsymbol{v}$ de vector is van ruisvrije coëfficiënten, $\boldsymbol{\omega}$ de ruis bevat en $\boldsymbol{w}$ de coëfficiënten met ruis voorstelt. De kleine coëfficiënten zinken nu weg in de ruis, maar voor de grote coëfficiënten, die de meeste informatie dragen, is de ruis relatief onbelangrijk. Tussen de ruis zijn de pieken, afkomstig van het ruisvrije signaal, nog duidelijk herkenbaar.

Onder milde omstandigheden gelden deze vaststellingen ook voor andere, ingewikkeldere wavelettransformaties (de transformatie moet enkel orthogonaal zijn). Als we alle coëfficiënten onder een goed gekozen drempelwaarde λ vervangen door nul, elimineren we dus een groot deel van de ruis en blijven de belangrijkste kenmerken van het signaal bewaard: de informatie daarover zit immers in de grote coëfficiënten. Het voorbeeld in figuur 2.20 illustreert dit. Een groot deel van dit proefschrift handelt over deze methode om ruis te verwijderen. Ze staat bekend als *wavelet thresholding*, threshold is het Engelse woord voor drempel. In zijn meest eenvoudige vorm, zoals net uitgelegd, steunt deze methode vooral op het *decorrelerend* vermogen van een wavelettransformatie: enkele grote waveletcoëfficiënten dragen bijna alle informatie, alle andere ruisvrije coëfficiënten zijn zo goed als nul. Later bespreken we hoe het multischaalkarakter van een wavelettransformatie van pas komt bij meer algemene types van ruis en breiden we de procedure uit.

De coëfficiënten die groter zijn dan grenswaarde kunnen we gewoon laten staan of ook 'bewerken'. Veel algoritmen trekken van die coëfficiënten de drempelwaarde af. Dit heet in het Engels *soft-thresholding*. Figuur 2.21(b) toont hoe groot de coëfficiënt na de drempeloperatie w_λ is in functie van zijn waarde w bij het begin. Op het eerste zicht lijkt het misschien vreemd ook de grote coëfficiënten kleiner te maken, maar op die manier zorgt het algoritme wel voor een geleidelijke overgang tussen kleine en grote coëfficiënten. Het gebeurt namelijk dat een coëfficiënt met weinig informatie en extra veel ruis toch net boven de drempel uitkomt. Als we die helemaal behouden te midden van nulwaarden, zal die ene achterliggende basisfunctie als een piek verschijnen in de reconstructie. *Soft-thresholding* tempert dit effect. Bovendien is de geleidelijke overgang een wiskundige noodzaak voor de goede werking van sommige algoritmen. De werkwijze die hoofdstuk 4 belicht, is daar een voorbeeld van.

De centrale vraag in ieder drempelalgoritme luidt: hoe vinden we een goede waarde voor de drempel? Die vraag beheerst de volgende twee hoofdstukken van dit proefschrift. In hoofdstuk 3 maken we duidelijk wat we precies verstaan onder een goede drempelwaarde en onderzoeken we hoe zulk een drempel zich gedraagt. Die kennis gebruiken we in hoofdstuk 4 waar we een methode voorstellen om in praktische gevallen snel een betrouwbare schatting te maken van een goede drempelwaarde.

3 De drempel met de kleinste kwadratische fout

3.1 De fout van het resultaat

We zoeken de drempelwaarde λ die het resultaat $\boldsymbol{y_\lambda}$ zo dicht mogelijk bij de ongekende ruisvrije gegevens $\boldsymbol{f}$ brengt. De uitvoerfout moet dus zo klein mogelijk zijn. Als definitie voor de fout van het resultaat kiezen we de gemiddelde kwadratische afwijking, die we noteren met R of met MSE, een afkorting van het Engels *Mean Square Error*. Voor een signaal met N punten is die fout:

$$R(\lambda) = \frac{1}{N}\sum_{i=1}^{N}(y_{\lambda i} - f_i)^2.$$

We noteren $R(\lambda)$ om aan te geven dat de fout een functie is van de drempelwaarde λ. De precieze waarde van $R(\lambda)$ hangt natuurlijk af van de optredende storing. Die is niet juist te voorspellen, en daarom werkt de theorie meestal met de *verwachte waarde* van de fout, die we met $\mathrm{E}R(\lambda)$ noteren. (E staat voor het Engelse *expectation*). De verwachte waarde van de fout heet in het Engels kortweg *Risk*-functie, (risico) hetgeen het gebruik van de letter R verklaart. Deze functie heeft een kenmerkend verloop, dat geschetst wordt in figuur 3.1. Voor kleine drempelwaarden heeft de drempel niet veel invloed. Er blijft dus nog veel ruis over. Ruis is iets onvoorspelbaars en wordt dus gekenmerkt door zijn *variantie* (variance in het Engels) σ^2. Naarmate we de drempel verhogen, zullen almaar meer coëfficiënten op nul komen. De bijdrage van die coëfficiënten tot de totale variantie is klein, want iets dat zo goed als zeker op nul staat is niet erg onvoorspelbaar (varieert niet sterk). De hoeveelheid ruis, of anders gezegd, de totale variantie, daalt dus, en dat doet de fout als geheel ook dalen. Coëfficiënten door nul vervangen betekent ook ruisvrije informatie verwaarlozen. Bij lage drempels is dit niet zo erg, want veruit de meeste informatie is geconcentreerd in de grote coëfficiënten. Als de drempel groeit, wordt dit effect wel belangrijk. Het signaal is dan *vertekend*. Vertekening heet in het Engels '*bias*'. De verwachte fout is dus een som van twee effecten:

$$\mathrm{Risk} \qquad = \qquad \mathrm{vertekening} \qquad + \qquad \mathrm{variantie}.$$

Vanaf een zekere drempelwaarde neemt de vertekening de bovenhand, en als de drempel dan nog groter wordt, groeit ook de verwachte fout weer aan.

Een drempel vermindert dus de hoeveelheid ruis, maar vervormt (vertekent) het ruisvrije signaal. De *optimale* drempel is het beste vergelijk tussen vertekening en ruis.

3.2 Model voor asymptotische benadering

In praktijk is het onmogelijk om de *optimale* drempel exact te berekenen. Daartoe zouden we immers de fout van het resultaat moeten minimaliseren, maar omdat we het ruisvrije signaal niet kennen, kunnen we die fout niet eens uitrekenen.

We zullen de foutencurve schatten. In het volgend hoofdstuk stellen we een schatting voor op basis van *veralgemeende kruisvalidatie* (generalized cross validation). We onderzoeken dan ook de kwaliteit van die schatter, zowel theoretisch als experimenteel. Zoals zo vaak in statistische methoden, zal de schatting beter zijn naarmate het aantal meetpunten N van het signaal groter wordt. Daarom bestuderen we eerst het *asymptotisch* gedrag van de optimale drempel, dit is het gedrag als $N \to \infty$.

We veronderstellen dat de aan ruis onderhevige metingen afkomstig zijn van een tijdscontinu signaal. Het aantal waarnemingen N laten toenemen betekent meer monsters nemen van *hetzelfde* signaal, meer informatie over een signaal binnen een *vast* interval. Als men de bemonsteringsperiode constant houdt, en het signaal over een langere tijd beschouwt, neemt het totaal aantal monsters ook toe. Voor die situatie geldt onze analyse niet, omdat we niet meer gegevens krijgen van eenzelfde (stuk) functie.

De tijdscontinue functie waarvan de invoer afkomstig is, moet bovendien *stuksgewijs zacht verlopend* zijn. Dit betekent dat de functie op een begrensd interval zacht moet verlopen, behalve eventueel in een eindig aantal punten met sprongen of knikken (discontinuïteiten in de functie of één van zijn afgeleiden). Eendimensionale doorsneden van beelden en vele signalen voldoen precies aan deze voorwaarden. We moeten ook nog de notie ‘zacht verlopend’ nauwkeuriger omschrijven. Dat bekijken we nu in twee stappen.

3.3 Stuksgewijze veeltermen

Zacht verlopende functies zijn veeltermachtig. Het loont dus de moeite eerst na te gaan hoe de optimale drempel evolueert voor stuksgewijze veeltermen. Als de waveletbasis aan een bepaalde voorwaarde voldoet (met name voldoende nulmomenten heeft; zie (2.14) voor een definitie), dan zijn alle coëfficiënten in de waveletontbinding exact nul, behalve waar de bijhorende basisfunctie in aanraking komt met één van de singuliere punten (sprong of knik). Een eerste belangrijk resultaat van dit proefschrift zegt dat bij een toenemend aantal monsters N, de drempel λ^* met minimale verwachte kwadratische fout (risk) zich dan gedraagt als (zie bewijs in paragraaf 3.3.3):

$$\lambda^* \sim \sqrt{2 \log N}\sigma \tag{1a}$$

Op het eerste zicht mag het vreemd lijken dat de optimale drempel groter wordt als we meer stalen nemen van het tijdscontinu signaal. Er is nochtans een intuïtieve verklaring:

1. Wanneer we het aantal metingen N opvoeren, liggen de opeenvolgende monsters dichter bij elkaar, we werken dus op fijnere schaal. Het aantal basisfuncties dat op fijne schaal in contact komt met één van de singulariteiten

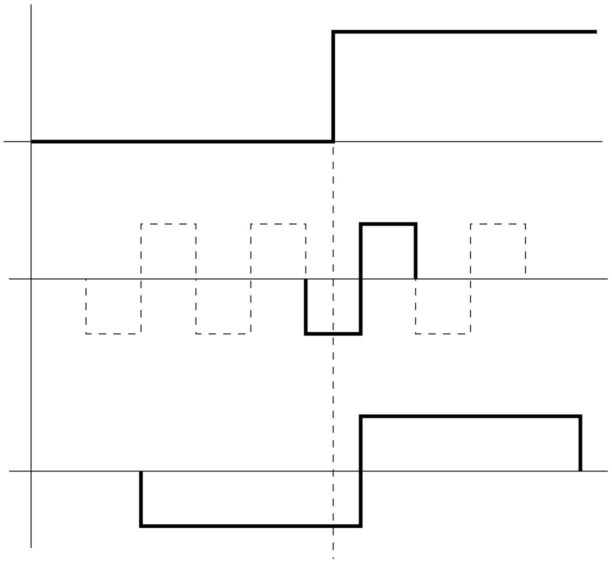

Figuur 1: Op de bovenste as staat een eenvoudige functie met een sprong. Op de tweede as staan basisfuncties getekend op een fijne schaal. Slechts één basisfunctie (in het vet) 'ziet' de sprong. De andere blokgolven op die schaal dragen niet bij tot de singulariteit: hun coëfficiënten zijn dus nul. Op een grovere schaal (onderste as) hebben we even goed precies één bijdrage. Het punt van singulariteit heeft immers geen afmetingen. Bij gevolg zijn er op fijne schalen relatief meer coëfficiënten nul.

is even groot als op een grove schaal. Figuur 1 illustreert deze vaststelling voor een Haar-basis: hier ziet op iedere schaal ten hoogste één basisfunctie de singulariteit. De basisfuncties die met de singulariteit niet overlappen, hoeven er ook niet aan bij te dragen. Hun coëfficiënten zijn dus nul. Op fijne schalen is een groter aandeel van de coëfficiënten gelijk aan nul. Als het aantal stalen en dus ook het aantal coëfficiënten N oneindig groot wordt, daalt het percentage niet-nulcoëfficiënten tot nul. Meer bepaald is dit percentage van grootte-orde $\log N/N$.

Dit kan men ook zo zien: als we meer stalen nemen van het tijdscontinue signaal, krijgen we almaar meer overbodige informatie: er zit steeds minder nieuws in de jongste verfijning van de schaal. Dus is het logisch dat de voorstelling van die gegevens steeds ijler kan.

2. Stel nu dat de drempel niet verandert bij een toenemend aantal coëfficiënten. Op een kleine minderheid na, zijn alle N coëfficiënten puur ruis. Die hebben allemaal een zekere kans p om groter te zijn dan de drempel. Omdat de drempel niet verandert, blijft ook die kans dezelfde. Die kans is tevens

het verwachte percentage coëfficiënten dat inderdaad groter is dan de drempel. Het aandeel coëfficiënten die enkel ruis bevatten en toch de drempel overleven, is dus bijna p en blijft ongeveer constant.

3. Terwijl het aantal informatiedragers relatief afneemt, blijft de procentuele hoeveelheid niet verwijderde ruis constant. Dus bevat het eindresultaat almaar meer ruis. Om dit tegen te gaan, moet de drempel dus groter worden.

4. De groei van de drempel in functie van het aantal punten $\sqrt{2 \log N}\sigma$ is zeer zwak. Men kan aantonen (3.19) dat deze groei net volstaat om te garanderen dat alle coëfficiënten met enkel ruis *op termijn* (dit wil zeggen voor een oneindig aantal coëfficiënten) met kans 1 onder de drempel blijven en dus verwijderd worden. De optimale drempel zorgt er dus voor dat op termijn eerst en vooral alle ruis verdwijnt, en bekommert zich blijkbaar niet om de coëfficiënten die de informatie dragen. In het geval van stuksgewijze veeltermen blijkt dit niet nodig, omdat het aantal informatiedragers een orde kleiner is dan het aantal coëfficiënten gedomineerd door ruis. Als de drempel niet sneller toeneemt dan strikt nodig om de ruis te verwijderen, blijft de vertekening beperkt.

In tabel 3.1 en figuur 3.5 stellen we vast dat in een concreet geval de optimale drempel weliswaar even snel *groeit* als de formule aangeeft, maar dat de eigenlijke *waarde* nog een constante waarde onder de voorspelde ligt. Dat constante verschil is voor een oneindig aantal punten (met oneindig grote drempels) niet belangrijk, maar voor eindige waarden natuurlijk wel. Voor het vervolg is het belangrijkste dat de optimale drempel groeit.

3.4 Universele drempel

De drempel met minimale verwachte fout verloopt dus *asymptotisch* als $\sqrt{2 \log N}\sigma$, en dan nog enkel voor stuksgewijze veeltermen. Nochtans komt de waarde

$$\lambda_{\mathrm{UNIV}} = \sqrt{2 \log N}\sigma$$

ook in veel algoritmen voor als daadwerkelijk toegepaste drempel. De vergelijking in figuur 3.5 illustreert dat deze waarde te groot is als schatting voor de minimum-risk-drempel. In sommige toepassingen is een zacht verlopend resultaat echter belangrijker: terwijl de minimum-risk-waarde een vergelijk zoekt tussen het verminderen van de ruis en het vrijwaren van het signaal, elimineert deze grote drempel met meer zekerheid resterende ruispiekjes.

Deze keuze staat bekend als de ‘universele drempel’ (universal threshold). Die naam verwijst naar de eenvoud van zijn formule: de waarde is voor alle signalen met gegeven lengte dezelfde. Als het signaal tot een functieklasse behoort met zekere eigenschappen wat betreft zacht verloop, dan garandeert deze drempel met grote waarschijnlijkheid dat de uitvoer minstens even zacht is.

Deze keuze biedt nog andere statistisch interessante eigenschappen, die we kort bespreken in paragraaf 3.4. In paragraaf 3.4.6 stellen we vast dat deze drempel niet geschikt is voor toepassing op beelden.

3.5 Voorbij de stuksgewijze veeltermen

In werkelijkheid is vrijwel geen enkel signaal of beeld exact een stuksgewijze veelterm. Daarom bestuderen we ook wat er gebeurt voor algemeen stuksgewijs zacht verlopende functies. De mate waarin een functie zacht verloopt kan men kwantificeren met een zogenaamde Lipschitz- of Hölder-coëfficiënt α. Definitie 3.2 geeft een precieze omschrijving.

Nu zijn ook de coëfficiënten die niks met een singulariteit in het signaal te maken hebben, niet exact nul. Natuurlijk zijn die coëfficiënten wel erg klein, maar omdat ze zo talrijk zijn, moet de drempel met extra vertekening rekening houden. De optimale drempel is dus iets kleiner dan bij de stuksgewijze veeltermen. Onder milde omstandigheden bekomen we als resultaat:

$$\lambda^* \sim \sqrt{\frac{2\alpha}{2\alpha+1}}\,\sqrt{2\log N}\sigma. \tag{1b}$$

4 Het schatten van de optimale drempel

4.1 Kruisvalidatie (cross validation)

Zoals we eerder hebben aangehaald, kennen we in praktische toepassingen het ruisvrije signaal niet, anders zou de vraag van ruisverwijdering zich uiteraard niet eens stellen. Bijgevolg kunnen we de fout van het resultaat niet exact berekenen, laat staan minimaliseren.

Het verloop van de fout als functie van de drempelwaarde zullen we schatten op basis van de informatie die we hebben. Die informatie bestaat uit invoer met ruis. De methode van *kruisvalidatie* (Cross Validation) laat bij gegeven drempelwaarde één (of enkele) invoerwaarden onbenut en voert het algoritme uit met de overblijvende waarden. De mate waarin die onvolledige uitvoer de weggelaten waarde kan voorspellen is dan een aanwijzing voor de kwaliteit van de procedure en meer in het bijzonder van de gekozen drempelwaarde. Het voorspellen van een stuk weggelaten invoer berust impliciet op een aanname dat het signaal in zekere zin zacht verloopt. In de formele verantwoording van de methode zullen we dus opnieuw de ijlheid van een waveletvoorstelling gebruiken. We herhalen dit “leaving-out-one” voor alle invoergetallen om zo een gemiddelde kwaliteitsmaat te bekomen.

Deze werkwijze is nogal omslachtig, en dus zoeken we naar een vereenvoudiging. Door een formalisering en een veralgemening, komen we uit op volgende formule als kwaliteitsmaat voor een gegeven drempelwaarde (4.15):

$$GCV(\lambda) = \frac{\frac{1}{N}\sum_{i=1}^{N}(y_{\lambda i} - y_i)^2}{\left(\frac{N_0(\lambda)}{N}\right)^2}.$$

In deze formule staat y_i voor een invoerwaarde en $y_{\lambda i}$ voor de bijhorende uitvoer. $N_0(\lambda)$ het aantal coëfficiënten dat bij een gegeven drempelwaarde λ op nul komt, en N is nog steeds het totaal aantal gegevens.

Deze uitdrukking staat bekend als de *veralgemeende kruisvalidatie* (generalized cross validation), afgekort als GCV. Ze bestaat al langer (in iets andere vorm) voor spline-smoothing-procedures [148]. In het kader van een waveletdrempelalgoritme duikt ze voor het eerst op in 1994 [149], echter zonder theoretische verantwoording. Het bewijs in hoofdstuk 4 is een tweede belangrijk resultaat van dit proefschrift.

4.2 Kenmerken van de GCV-procedure

1. $GCV(\lambda)$ is een functie van de drempelwaarde die voorts enkel afhangt van gekende grootheden. Er is zelfs geen waarde of een schatting nodig voor de *hoeveelheid ruis* σ. De grootte van de ruis schat de procedure impliciet op basis van de invoer. In die zin is GCV dus een *volautomatische* methode om de optimale drempel te schatten.

2. De methode is *snel*. We moeten de GCV-functie minimaliseren. Voor een vooropgestelde relatieve nauwkeurigheid volstaat een vast aantal functie-evaluaties met elk een hoeveelheid rekenwerk die lineair toeneemt met de lengte N van de coëfficiëntenvector. Bovendien kunnen we de minimalisering ook doorvoeren in termen van waveletcoëfficiënten. Enkel voor orthogonale transformaties is dit volledig equivalent met een minimalisering op de oorspronkelijke gegevens, maar de numerieke stabiliteit van een wavelettransformatie garandeert een zinvol resultaat voor biorthogonale transformaties.

   Alles bij elkaar vormt de GCV-procedure geen flessenhals tegenover de toch ook al snelle wavelettransformatie.

3. De methode is *asymptotisch optimaal*. Als de invoer lang genoeg is, heeft de GCV-curve bijna dezelfde vorm als de kwadratisch gemiddelde fout, zoals in figuur 4.1. Dit houdt in dat de kwaliteit van het resultaat over het algemeen beter wordt naarmate de invoer meer gegevens bevat. In praktijk lijkt een

duizendtal monsters een minimum om een goede werking te verzekeren. Bij kleinere datasets bestaat de mogelijkheid dat de procedure misloopt.

4. Zoals we dadelijk nader bekijken, treden problemen vooral op bij kleine drempelwaarden. Als het aantal punten groot genoeg is, bevindt de optimale drempel zich buiten deze gevarenzone en is een GCV-minimalisering dus mogelijk.

4.3 Asymptotisch optimaal

Het gebruik van de GCV-procedure steunt dus op een asymptotisch argument. Bekijken we de definitie van de GCV-functie van naderbij, dan valt het op dat de noemer het relatief aantal coëfficiënten onder de drempel telt. Dit aantal gaat natuurlijk in sprongen omhoog als de drempel groeit. Omdat de meeste coëfficiënten klein zijn, en nagenoeg alleen ruis bevatten, vertaalt dit zich vooral bij kleine drempelwaarden in een onregelmatig gedrag van de GCV-functie. Dit is te zien aan de linkerkant van figuur 4.3. Dit verklaart ook waarom we willen dat de optimale drempel toeneemt als de invoer langer wordt: het minimum van de kwadratisch gemiddelde fout komt dan in een gebied waar de GCV-functie relatief zacht verloopt.

We bewijzen *niet* dat de drempel met minimale GCV voor grote N ongeveer *samenvalt* met de minimum-risk-drempel, enkel dat GCV minimaliseren een drempel oplevert met gelijke kwaliteit: het enige dat telt, is een drempel met een resultaat dat de ruisvrije gegevens (ongeveer) even goed schat als de drempel met de kleinste verwachte fout. Als die foutenfunctie meer dan één minimum heeft, of een zeer uitgestrekt interval met ongeveer dezelfde minimale waarden, dan speelt het geen rol welke drempel de GCV-procedure daarbinnen precies selecteert. Als het aantal punten groeit, daalt de fout op het resultaat bij optimale drempel naar nul. Dan volstaat het het *niet* dat de drempel met minimale GCV eveneens een dalende fout oplevert bij langer wordende invoer: de *relatieve* kwaliteit van het GCV-resultaat moet die van de optimale drempel benaderen. Meer bepaald bewijzen we de volgende stelling (zie paragraaf 4.3.2):

Stelling 4.1 *Als λ^* de verwachte kwadratisch gemiddelde fout $\mathrm{E}R(\lambda)$ minimaliseert en $\hat{\lambda}$ minimaliseert de verwachte waarde van de GCV-functie, dan geldt voor een toenemend aantal invoerpunten $N \to \infty$:*

$$\frac{\mathrm{E}R(\hat{\lambda})}{\mathrm{E}R(\lambda^*)} \to 1, \tag{2a}$$

en in de omgeving van de optimale drempel λ^* is de GCV-functie ongeveer een verticaal verschoven kopie van de kwadratisch gemiddelde fout:

$$\mathrm{E}GCV(\lambda) \approx \mathrm{E}R(\lambda) + \sigma^2. \tag{2b}$$

Het bewijs van de stelling volgt de grote lijnen van de argumentatie voor een GCV-schatting van de vereffeningsparameter in een spline-smoothing-algoritme [148]. Die spline-smoothing is een *lineaire* werkwijze: men kan ze voorstellen met een matrix. Drempels voor waveletcoëfficiënten leiden tot een typisch niet-lineair algoritme: we houden namelijk de *grootste* coëfficiënten over, en het hangt af van het concreet signaal welke coëfficiënten dat zullen zijn. Omdat we vooraf niet weten op welke plaats de nullen gaan komen, kunnen we ook geen operatiematrix opstellen.

Die niet-lineariteit maakt het wat moeilijker te rekenen met *verwachte waarden*. Bovendien zorgt die niet-lineariteit er ook voor dat in de definitie van GCV zowel teller als noemer toevalsveranderlijken zijn. De noemer telt het aantal coëfficiënten onder de drempel. Dit aantal vertelt iets over de drempeloperatie, maar ze hangt ook af van de ruis, en dus van het toeval. Bij spline-smoothing komt de overeenkomstige grootheid rechtstreeks uit de operatiematrix, en die hangt niet af van de ruis. Werken met een quotiënt van twee toevalsveranderlijken ligt niet zo voor de hand.

Om het bewijs te leveren, steunen we op een aantal veronderstellingen:

1. De ruisvrije informatie moet afkomstig zijn van een stuksgewijs zacht verlopende functie, met een ijle waveletontbinding .

2. De ruis op de waveletcoëfficiënten moet stationair zijn. Anders kan één enkele drempel sowieso moeilijk alle coëfficiënten tegelijk en degelijk aanpakken. De drempel met minimaal kwadratische fout presteert dus slecht en bovendien kunnen we die met GCV niet vinden: het bewijs voor GCV maakt op zijn beurt nogmaals gebruik van die aanname van stationariteit. Deze voorwaarde houdt in dat

   (a) de invoerruis stationair is,

   (b) de invoerruis niet gecorreleerd is (ook gekend als *niet-gekleurde* of *witte* ruis),

   (c) de wavelettransformatie orthogonaal is.

3. De ruis moet verwachte waarde nul hebben en Gaussiaans zijn. Deze laatste voorwaarde is eerder technisch en stelt in de praktijk geen grote problemen.

4. Het algoritme *moet soft*-thresholding gebruiken. Als we de grote coëfficiënten willen behouden, werkt de GCV-procedure niet.

Hoofdstuk 4 eindigt met een bespreking van enkele praktische problemen en belangrijke speciale gevallen: hoe reageert de procedure op een invoer die enkel uit ruis bestaat? Het blijkt dat de GCV-functie dit inderdaad opmerkt en een hoge drempel kiest. Hoe reageert de procedure op een invoer zonder ruis? Ook dit detecteert de methode en de drempel is verwaarloosbaar klein. Tenslotte bedenken we dat de GCV-procedure de drempel schat die de kwadratisch gemiddelde fout minimaliseert. De GCV-drempel vertoont dan ook dezelfde gebreken als die ‘optimale’ waarde: sporadisch ontsnapt een coëfficiënt met enkel ruis aan de drempel en dit resulteert in storende piekjes in het resultaat. Het wegwerken van die effecten is één van de opdrachten voor het volgend hoofdstuk.

5 Waveletdrempels en GCV in praktijk

Tot hier toe hebben we vooral het *decorrelerend* vermogen van een wavelettransformatie benut: dat zorgt voor een *ijle voorstelling* van ruisvrije gegevens. Niet gecorreleerde ruis kan de transformatie natuurlijk niet verder decorreleren, dus de ruis verandert niet van aard door de transformatie. Deze vaststellingen verantwoorden het zetten van een drempel.

Het *multiresolutie*-karakter van een waveletvoorstelling hebben we nog niet gebruikt. Dat gebeurt in hoofdstuk 5, waar we ook enkele andere eenvoudige aanpassingen voorstellen: alle dragen ze bij tot een voorzichtiger aanpak, met minder bruuske effecten dan een gewone drempel. Sommige van de aangehaalde verbeteringen zijn ook elders beschreven (met name de redundante wavelettransformatie en schaalafhankelijke drempels) of zijn geïnspireerd door voorstellen van andere auteurs (boomgestructureerde drempelmethodes). Wel is de inbreng van de GCV-procedure overal origineel, en de voordelen van de GCV-aanpak komen soms goed van pas. Deze haalbaarheidsstudie voor praktische gevallen vormt dan ook een derde component van dit onderzoek.

5.1 Schaalafhankelijke drempels

Gekleurde ruis

Het bewijs voor de asymptotische optimaliteit van de GCV-aanpak verantwoordt niet alleen deze werkwijze, maar verschaft ook inzicht in de werking ervan. In praktijk zijn ruiscomponenten dikwijls gecorreleerd: ze zijn afkomstig van dezelfde storingsbron (bv. bewolking die ruis veroorzaakt in een beeld). GCV werkt niet voor signalen met gecorreleerde (gekleurde) ruis. Een analyse van het bewijs leert dat niet de correlatie op zich een probleem is, maar wel het feit dat de wavelettransformatie van zulke ruis geen *stationaire* ruis meer is.

Als de invoerruis zelf wel stationair is, blijkt wel dat de ruis op de waveletcoëfficiënten stationair is *binnen iedere resolutielaag*. In zekere zin kunnen we dit verwachten: correlaties treden op binnen een zekere afstand, het zijn fenomenen met een zekere schaal. Bijgevolg zal de ruis zich meer concentreren op de ene schaal dan op de andere, maar binnen een schaal blijft het een stationair verschijnsel.

Deze vaststellingen verantwoorden drempels en GCV-schattingen per schaal afzonderlijk. Hier speelt het voordeel van GCV als volautomatische schatting een belangrijke rol. Zo goed als alle andere methoden hebben op zijn minst een waarde nodig voor de hoeveelheid ruis σ. Als de ruis over alle resolutielagen constant is, kan men die waarde gemakkelijk schatten op de fijnste schaal, omdat daar het aandeel coëfficiënten met belangrijke signaalinformatie bijzonder laag ligt. Dit wordt veel moeilijker als men op iedere schaal een aparte waarde voor σ nodig heeft. Op grove schalen zijn dikwijls wel te weinig coëfficiënten voor handen om een asymptotische methode zoals GCV goed te laten werken.

Niet-orthogonale transformaties

Gelijkaardige argumenten gelden voor niet-orthogonale transformaties. Een bijkomend probleem is hier dat minimalisatie in termen van waveletcoëfficiënten niet volledig overeenkomt met minimalisatie van de fout op het uiteindelijke resultaat. Bij het minimaliseren van de GCV van het resultaat zouden we dus bij elke functie-evaluatie eerst een inverse wavelettransformatie doorvoeren: dat vergt veel werk. De (Riesz-)stabiliteit van een wavelettransformatie garandeert echter een redelijke benadering van optimale kwaliteit en bovendien is de kwadratisch gemiddelde fout ook geen absoluut criterium: een definitie van een fout gebaseerd op een meerschalen-voorstelling van een beeld is misschien zelfs beter dan een definitie gebaseerd op beeldpunten. Wij zien het beeld wel in de beeldpuntvoorstelling, maar onze ogen nemen het beeld niet op die manier waar.

Adaptiviteit

De optimale drempel is altijd een vergelijk tussen ruis en signaal. Zelfs indien de ruis op elke schaal even sterk aanwezig is (orthogonale transformatie en witte ruis), is een schaalafhankelijke drempel nog aangewezen: de meeste signalen vertonen andere kenmerken op verschillende schalen. Op fijne schalen is weinig informatie aanwezig, daar mag de drempel iets groter zijn. Op die manier krijgt men ook gemakkelijker de vreemde piekjes weg die ontstaan als een coëfficiënt met extra veel ruis toevallig toch de drempel overleeft.

5.2 Boomgestructureerde aanpak

We kunnen ook bij één enkele drempel blijven en achteraf nagaan of bepaalde coëfficiënten niet ten onrechte behouden zijn. Echte signaalsprongen zijn geen kortstondige storingen maar hebben een wijd bereik en vertonen daarom grote coëfficiënten op verschillende schalen. Een wavelettransformatie decorreleert dus niet volledig: coëfficiënten op verschillende schalen en op dezelfde locatie blijven gecorreleerd. Als nu een coëfficiënt op fijne schaal de drempel heeft overleefd, loont het de moeite om na te gaan of op naburige schalen op die plaats ook grote coëfficiënten voorkomen. Zoniet is die ene coëfficiënt wellicht een toevalstreffer, veroorzaakt door de ruis, en kan die beter alsnog verdwijnen. Met deze gerichte aanpak werkt men de nadelen van een drempel met minimale kwadratische fout enigszins weg: men verwijdert sporadische piekjes zonder al te veel vertekening te veroorzaken, zoals de universele drempel.

Andere methoden [152] gebruiken de correlaties tussen opeenvolgende schalen rechtstreeks als maat voor het belang van de coëfficiënten: niet de grootte van een coëfficiënt bepaalt of hij bewaard blijft bij de reconstructie, wel de aanwezigheid van grote coëfficiënten op de betrokken schaal én naburige schalen.

5.3 Niet-gedecimeerde wavelettransformaties

De niet-gedecimeerde of redundante wavelet transformatie is een alternatief voor de klassieke wavelettransformatie, dat meer coëfficiënten voortbrengt dan strikt noodzakelijk om de invoer te reconstrueren. De vector van waveletcoëfficiënten is dus langer dan de invoervector, het is een redundante voorstelling van de informatie. In feite is het een bundeling van N ineengevlochte wavelettransformaties.

Hoewel deze transformatie iets meer rekenwerk en geheugenruimte vraagt dan de snelle wavelettransformatie ($\mathcal{O}(N \log N)$ i.p.v. $\mathcal{O}(N)$), biedt deze vorm allerlei voordelen:

1. Op iedere schaal zijn evenveel coëfficiënten, dus moet GCV op iedere schaal in principe even goed werken als men opteert voor schaalafhankelijke drempels. Op grove schalen is de voorstelling dikwijls niet zo ijl, wat dit voordeel dan weer enigszins teniet doet. Ijlheid is noodzakelijk voor een goede werking van de GCV-procedure.

2. Stationaire ruis blijft ook hier stationair binnen iedere resolutielaag.

3. Veel gemakkelijker dan bij de snelle wavelettransformatie kan men de transformatie toepassen op signalen waarvan de lengte niet precies een macht van twee is.

4. De transformatie is translatie-invariant: als de invoer verschuift, verschuiven de coëfficiënten mee, zonder totaal te veranderen. Een gedecimeerde wavelettransformatie kan totaal andere coëfficiënten opleveren als de invoer een beetje verschoven is. We hebben natuurlijk liever niet dat de kwaliteit van het resultaat afhangt van een eventuele verschuiving.

5. Het belangrijkste voor deze bespreking is de redundantie zelf: als een drempel de coëfficiënten wijzigt, zal het resultaat daarvan allicht niet exact de redundante wavelettransformatie van een of ander signaal zijn. Als we het signaal reconstrueren vanuit een (voldoende groot) deel van de coëfficiënten, krijgen we een ander resultaat dan voor een ander deel van de coëfficiënten. Door een soort gemiddelde te nemen van alle mogelijke reconstructies, verwijderen we een deel van de restruis: toevallige piekjes vlakken wat af.

5.4 Gehele-getallen-transformatie

Er bestaat een variant van de klassieke wavelettransformatie die gehele getallen afbeeldt op gehele getallen. Deze transformatie blijft bovendien perfect omkeerbaar. Het werkingsprincipe staat uitgelegd in paragraaf 2.4.2 en in figuur 2.17. Deze variant is interessant voor sommige toepassingen, zoals beelden, waar de invoer bestaat uit gehele getallen. Als de transformatie dan ook uitsluitend met gehele getallen werkt, besparen we rekenwerk: het is voor een computer gemakkelijker te rekenen met gehele getallen dan met (bewegende) komma-getallen.

Deze gehele variant is echter geen lineaire transformatie. Theoretisch gezien maakt dat de resultaten van hiervoor ongeldig. Waveletdrempels introduceren weliswaar een niet-lineair algoritme, maar we maken wel gebruik van de lineariteit van de wavelettransformatie om iets te zeggen over het gedrag van de ruis op de waveletcoëfficiënten.

Onze experimenten hebben aangetoond dat die niet-lineariteit in de praktijk weinig problemen stelt: een gehele-getallen-transformatie benadert dus wel zijn klassieke variant, en laat tegelijk toe de hele ruisverwijderingsoperatie uit te voeren zonder over te gaan op bewegende komma-voorstelling.

6 Bayesiaanse correctie met ruimtelijke a priori modellen voor het verwijderen van ruis uit beelden

Een waveletontbinding is een ijle gegevensvoorstelling. Dat vormde de basis voor drempelmethoden. Wavelets zijn de natuurlijke invulling van het begrip multiresolutie: dat leidde naar enkele interessante aanpassingen van de algoritmen. We zijn nu bij een derde uitbreiding aanbeland: wat verandert er als we van ééndimensionale signalen overschakelen op (tweedimensionale) beelden?

6.1 Probleemstelling (vanuit benaderingstheorie)

Waveletdrempelmethodes zijn in eerste instantie gebaseerd op het decorrelerend vermogen van een wavelettransformatie. Zoals in één dimensie de wavelet-basisfuncties maar op een beperkt interval verschillen van nul, zo is dat in twee dimensies op een vierkantje. Figuur 6.4 toont het ‘grondplan’ van de tweedimensionale Haar-functies. Die localiteit in ruimte of tijd zorgt ervoor dat slechts een beperkt aantal coëfficiënten met de singulariteit te maken krijgen, en dus zijn de andere coëfficiënten zo goed als nul. Nochtans bestaat er een fundamenteel verschil tussen het één- en tweedimensionale geval. Singulariteiten in ééndimensionale signalen zijn punten met een sprong of knik, zoals in figuur 6.1. Dat punt heeft geen afmetingen: op iedere schaal komt maar een vast aantal basisfuncties dit punt tegen. Bij toenemende verfijning neemt het aantal schaalfuncties op singuliere punten dus niet toe. In twee dimensies krijgen we te maken met *lijn*singulariteiten, bv.

randen in een beeld. Figuur 6.2 toont een eenvoudig voorbeeld. Een lijn heeft een *lengte*. Bij toenemende verfijning zijn steeds meer schaalfuncties (en dus ook waveletfuncties) nodig om de hele singulariteit te 'bedekken'. De nul-coëfficiënten maken nog altijd de overgrote meerderheid uit, maar lijnsingulariteiten, onbekend in één dimensie, maken het werk toch ingewikkelder.

Grote coëfficiënten zijn nu geconcentreerd in de buurt van randen, en hun aantal neemt toe (niet relatief, maar wel absoluut) op fijnere schalen. In feite is het niet ideaal dat één singulariteit door een hele lijn van coëfficiënten moet worden opgevangen. De zoektocht naar betere basisfuncties voor beelden is een boeiende uitdaging [27].

In hoofdstuk 6 aanvaarden we dat grote coëfficiënten voorkomen als clusters op de plaats van randen in het beeld. We proberen de selectie van een drempelalgoritme te verbeteren, zodat die clusters beter tot hun recht komen en tussenliggende toevallig grote coëfficiënten verdwijnen.

6.2 Maskers en uitgezuiverde selecties

De selectie die een drempel- of andere methode maakt, kunnen we visualiseren als een binair beeld: zwarte puntjes geven de coëfficiënten aan die behouden blijven, wit komt overeen met coëfficiënten die nul worden. Figuur 6.5(b) toont zulk een *masker* voor GCV-drempels op één bepaalde schaal van de redundante wavelettransformatie van een beeld. De ruis is hier kunstmatig aangebracht, en daarom kunnen we ook het masker laten zien van de drempel met minimale kwadratische fout: dit is figuur 6.5(a). We zien dat de geselecteerde coëfficiënten zich hoofdzakelijk in de buurt van de randen in het beeld bevinden, en dat daarbuiten enkele geïsoleerde selecties voorkomen, die horen bij grote ruiswaarden.

Twee verbeteringen willen we nu tegelijk aanbrengen:

1. De sporadisch onterecht geselecteerde coëfficiënten willen we weren.

2. Terzelfder tijd willen we andere coëfficiënten behouden, ook al liggen ze onder de drempel: vooral de randstructuren moeten beter tot hun recht komen.

Op die manier hopen we de *ideale* selectie van coëfficiënten te benaderen. Men kan argumenteren dat die ideale selectie volgt als we alle coëfficiënten met ruisvrije waarde boven het ruisniveau σ handhaven. Omdat we de ruisvrije waarde niet kennen, is die ideale selectie in praktijk niet haalbaar. Figuur 6.6(b) toont het masker van de ideale selectie voor het voorbeeld met kunstmatige ruis.

In eerste instantie kunnen we het selectiemasker van een drempelmethode als een binair beeld bekijken en er eenvoudige operaties op uitvoeren om een meer geclusterde selectie te bekomen: alle geïsoleerde punten verwijderen, of een mediaanfilter toepassen. Twee voorbeelden van wat zulke methoden opleveren staan in figuur 6.8. Het resultaat is niet zo goed, omdat de binaire beeldverbetering geen rekening houdt met de achtergrond van het masker: een zwart punt betekent een belangrijke coëfficiënt. Het is beter om bij het corrigeren van de initiële selectie die betekenis in acht te nemen.

6.3 Bayesiaanse aanpak

Met de regel van Bayes kunnen we het selectiemasker verbeteren op grond van het algemeen idee dat grote coëfficiënten gegroepeerd voorkomen, en tegelijk de betekenis van het masker laten meespelen. Voor deze methode vertrekken we vanuit een volledig stochastisch model:

$$\boldsymbol{W} = \boldsymbol{V} + \boldsymbol{N}.$$

Ook de ruisvrije coëfficiënten $\boldsymbol{V}$ bekijken we nu als een toevalsvector. Dat moet zo omdat we willen uitdrukken dat we clusters van grote coëfficiënten *verwachten*: het gaat dus om een experiment met onzekere uitslag.

We noemen $\boldsymbol{M}$ de maat die voor iedere coëfficiënt aangeeft hoe belangrijk hij is. Bij de correctie van een eenvoudig drempelalgoritme is die maat gewoon de absolute waarde. Met $\boldsymbol{X}$ duiden we het masker van de uiteindelijke classificatie aan. Bij een gewoon drempelalgoritme is die classificatie een eenvoudige functie van de $\boldsymbol{M}$: is de maat groter dan de drempel, dan is de classificatie één en anders is ze nul. Omdat we nu het selectie van de drempel willen verbeteren, is het verband tussen $\boldsymbol{M}$ en $\boldsymbol{X}$ niet meer eenduidig, maar is het beïnvloed door omgevingsfactoren.

We stellen dat *a priori* configuraties met clusters van belangrijke coëfficiënten waarschijnlijk zijn. Dit leidt tot een a priori model voor het masker:

$$\mathrm{P}(\boldsymbol{X} = \boldsymbol{x}).$$

Dit is een *ruimtelijk* model omdat het interacties beschrijft tussen naburige coëfficiënten. We gebruiken de theorie van Gibbs-distributies en Markov Random Velden (MRF) voor de opbouw van dit model.

Daarnaast voeren we ook een conditioneel model in. Dit model beschrijft welke waarden we kunnen verwachten als de classificatie in een punt nul resp. één is. Dit model legt dus het (nu toevalsafhankelijke) verband tussen classificatie $\boldsymbol{X}$ en de mate van belangrijkheid $\boldsymbol{M}$. Dit verband kunnen we voor iedere coëfficiënt afzonderlijk leggen, het model is daarom het product van locale voorwaardelijke dichtheden:

$$f_{\mathbf{M}|\mathbf{X}}(\boldsymbol{m}|\boldsymbol{x}) = \prod_{s \in S} f_{M_s|X_s}(m_s|x_s).$$

Een voorbeeld van een dergelijk locaal verband tussen classificatie en coëfficiëntenwaarde staat in figuur 6.10.

De regel van Bayes levert dan een *a posteriori* kansfunctie voor het classificatiemasker $\boldsymbol{X}$, gegeven de waarnemingen $\boldsymbol{W}$ en $\boldsymbol{M}$:

$$\mathrm{P}(\boldsymbol{X} = \boldsymbol{x}|\boldsymbol{M} = \boldsymbol{m}) = \frac{\mathrm{P}(\boldsymbol{X} = \boldsymbol{x}) f_{\mathrm{M}|\mathbf{X}}(\boldsymbol{m}|\boldsymbol{x})}{f_{\mathrm{M}}(\boldsymbol{m})}$$

De noemer $f_{\mathrm{M}}(\boldsymbol{m})$ moet men bekijken als een evenredigheidsconstante: bij gegeven waarneming $\boldsymbol{M}$ is die voor alle maskers gelijk.

In principe kunnen we nu van elk mogelijk masker de *a posteriori* kans berekenen, en zo kunnen we het masker zoeken met de *maximale a posteriori* kans, of we kunnen de marginale kansfunctie voor iedere coëfficiënt afzonderlijk uitrekenen:

$$\mathrm{P}(X_s = 1|\boldsymbol{M} = \boldsymbol{m}) = \sum_{\boldsymbol{x}} x_s \mathrm{P}(\boldsymbol{X} = \boldsymbol{x}|\boldsymbol{M} = \boldsymbol{m}),$$

Beide gevallen vereisen de berekening van de kansen van alle mogelijke maskers. Omdat het hier gaat over enorme aantallen is dit praktisch niet haalbaar. De marginale kansfuncties kunnen we schatten met behulp van *Markov-keten-Monte-Carlo-technieken*. Een voorbeeld van een dergelijke bemonsteringsmethode is het algoritme van Metropolis.

6.4 Parameterschatting

Het voorgestelde model bevat een aantal parameters. De parameters die voorkomen in het conditioneel gedeelte kunnen we invullen op basis van hun betekenis.

In het ruimtelijk a priori model komt een parameter τ voor die de stijfheid uitdrukt: hoe groter τ, des te sterker de neiging om clusters te vormen. Als τ te groot is, heeft het conditioneel model geen vat meer op de uiteindelijke selectie. Om deze parameter te bepalen, gebruiken we een *pseudo-aannemelijkheidsfunctie* (pseudo likelihood), toegepast op het masker van een GCV-drempel.

6.5 Resultaten

In enkele experimenten stellen we vast dat de selectie van coëfficiënten door de inbreng van het a priori model inderdaad gestructureerder verloopt, en zich meer concentreert op de randen. Voorlopig is de verbetering van de kwaliteit van het eindresultaat eerder beperkt, althans in termen van signaal-ruis-verhouding. We moeten daarbij opmerken dat de klassieke definitie van signaal-ruis-verhouding (3.2) weinig aandacht besteedt aan goed contrast in de randen, en precies daar beoogt de Bayesiaanse aanpak een verbetering.

7 Het vereffenen van meetgegevens op onregelmatige roosters met drempels voor tweede-generatie-coëfficiënten

De wavelettransformatie zoals we die tot nu toe besproken hebben, veronderstelt dat de invoer afkomstig is van een regelmatig bemonsterd signaal. In veel toepassingen beschikken we echter enkel over stalen op onregelmatige tijdstippen of op onregelmatige afstand van elkaar. Als we daarop een klassieke wavelettransformatie toepassen en de coëfficiënten wijzigen, dan verschijnen de onregelmatigheden van het rooster in het resultaat. De klassieke wavelettransformatie werkt immers met basisfuncties die zacht verlopen op een regelmatig rooster.

Het *liftingschema* is een alternatieve procedure om wavelettransformaties uit te rekenen. Alle klassieke transformaties passen in dit schema. Bovendien leent het schema zich tot uitbreiding tot het geval van onregelmatige roosters. De basisfuncties die hiermee overeenkomen staan bekend als wavelets van de tweede generatie. Overigens is ook de gehele-getallen-transformatie op dit schema gebaseerd.

De theorie van het liftingschema garandeert een zacht verlopende reconstructie. In hoofdstuk 7 onderzoeken we of en wanneer die reconstructie ook nauw aansluit bij de invoer of bij de ruisvrije gegevens. Experimenten wijzen namelijk uit dat de transformatie geen waarborg geeft voor stabiliteit. Dat betekent dat kleine acties op de waveletcoëfficiënten onverwacht grote gevolgen kunnen hebben na reconstructie.

Alle bestaande waveletalgoritmen voor ruisverwijdering op onregelmatige roosters herleiden het probleem op één of andere manier tot een regelmatig rooster. Hierin verschilt onze opzet dus fundamenteel van alle voorgaande.

7.1 De werkwijze

Omdat de transformatie nu rekening houdt met de structuur van het rooster waarop de gegevens liggen, verliest ze — behalve bij een Haar-transformatie — de orthogonaliteit. De transformatie van stationaire ruis is zelfs niet meer stationair binnen één resolutieniveau, omdat de schaal binnen één niveau niet meer constant is: die hangt af van de onderlinge afstand tussen de invoercomponenten. Mits een goede organisatie van het rekenwerk kunnen we wel met een lineaire complexiteit de variantie van de ruis op de waveletcoëfficiënten vinden, op voorwaarde dat correlatiematrix van de invoer een bandstructuur heeft. De waarden van die matrix moeten bovendien bekend zijn, eventueel op een constante factor na. De uitdrukking (2.20) levert dan de gevraagde varianties van de waveletcoëfficiënten.

We normaliseren iedere coëfficiënt met de vierkantswortel van zijn variantie en zoeken voor die genormaliseerde waarden de optimale drempel met de GCV-methode.

Twee voorbeelden illustreren dat het resultaat veel zachter verloopt dan wanneer men de structuur van het rooster verwaarloost en de klassieke transformatie toepast. Bij het tweede voorbeeld in figuur 7.3 vertoont de uitvoer van de tweede-generatie-procedure een onaanvaardbare vertekening, terwijl de klassiek aanpak, met voorts dezelfde parameterinstellingen, bevredigende resultaten oplevert, afgezien van de onregelmatigheden vanwege het rooster.

7.2 De vertekening

De vertekening komt doordat de transformatie niet altijd goed geconditioneerd is. Dit betekent dat we werken met een basis die “ver van orthogonaal” is, en kleine operaties op de coëfficiënten in zulke basis kunnen een belangrijk effect hebben bij de wedersamenstelling (synthese). De eenvoudige veronderstelling dat de grote coëfficiënten de belangrijke zijn en dat de kleintjes zonder problemen door nul kunnen vervangen worden, gaat hier ook niet zonder meer op.

De precieze oorzaak van deze slechte conditie is tot op heden niet gekend. Blijkbaar gaat het om samenspel van verschillende factoren:

1. Een liftingschema bestaat uit liftingstappen die voorkomen in twee soorten: duale lifting of voorspelling (prediction) en primale lifting of bijsturing (update). Wellicht kunnen stabiliteitsproblemen in beide stappen optreden, kunnen beide stappen elkaars effect versterken of gedeeltelijk opheffen.

2. De belangrijkste problemen schijnen zich voor te doen bij de eindpunten van het interval. Een tweede-generatie-algoritme past zijn basisfuncties daar aan. Nochtans treden er veel minder problemen op als we met dezelfde aanpassing op een regelmatig rooster opereren. Dus ook de onregelmatigheid van het rooster speelt een rol.

3. In feite negeert de liftingaanpak de notie van schaal volledig: als een groot gat in de metingen volgt op een stuk met veel gegevens, dan verwerkt het liftingschema die gegevens over het gat heen in één stap. Verschijnselen die zich voordoen op grote schaal worden zo verwerkt samen met verschijnselen op fijne schaal. We zouden de transformatie kunnen herordenen, maar dat lijkt bij nader toezien niet vanzelfsprekend.

7.3 Oplossen of omzeilen

Het is moeilijk na te gaan welke basisfuncties samen verantwoordelijk zijn voor slechte conditie. Verschillende functies die twee aan twee bijna loodrecht staan kunnen samen toch een slechte basis vormen. Zulk een basis heeft soms zeer grote coëfficiënten nodig om een kleine ruiswaarde voor te stellen. Als we één van die coëfficiënten door nul vervangen, komen de andere plots te voorschijn als grote componenten, en veroorzaken zo een grote vertekening. We zouden liever alle betrokken coëfficiënten verwijderen.

Daartoe hebben we een betrouwbare schatting van het ruisvrije signaal nodig. Deze schatting moet niet per se zacht verlopen, daar zorgt de tweede-generatie-transformatie wel voor. We gebruiken hiervoor de oplossing van de klassieke aanpak, die geen rekening houdt met het rooster. Van dit resultaat berekenen we de tweede-generatie-transformatie. De intervallen waarop dit resultaat sterk afwijkt van de reconstructie na toepassing van drempels op tweede-generatie-coëfficiënten, markeren we als intervallen met vertekend resultaat. We onderzoeken welke coëfficiënten horen bij basisfuncties die met deze intervallen te maken hebben. Binnen deze verzameling van coëfficiënten gaan we na waar de ruwe, eerste schatting ver afwijkt van de vertekende oplossing die de tweede generatie levert. Het blijkt dat we een zachte, mooi aansluitende schatting vinden als we minder dan één procent van de coëfficiënten in de vertekende oplossing vervangen door de waarde van de overeenkomstige coëfficiënt van de ruwe oplossing.

8 Besluiten en toekomstig onderzoek

Dit proefschrift behandelt een aantal aspecten van drempels voor waveletcoëfficiënten:

1. De optimale drempel verloopt asymptotisch (ongeveer) zoals de universele drempel van Donoho en Johnstone.

2. Veralgemeende kruisvalidatie (GCV) is een snelle en asymptotisch optimale methode om de optimale drempel te schatten.

3. De multiresolutie-achtergrond van een waveletontbinding verschaft de mogelijkheid om het drempelalgoritme te verbeteren, bijvoorbeeld door de operaties schaalafhankelijk te maken. Bij dit alles blijft GCV een interessante werkwijze om drempelwaarden in te vullen.

4. Randen in beelden kan een waveletvoorstelling als dusdanig niet herkennen. Om hieraan te verhelpen voeren we een ruimtelijk a priori model in, dat we combineren met het drempelalgoritme in een Bayesiaanse aanpak. De randen krijgen hierdoor extra aandacht.

5. Stabiliteitsproblemen maken dat drempels voor wavelets op onregelmatige roosters veel minder voor de hand liggen. We doen een beroep op de klassieke ontbinding, zonder onregelmatig rooster, om de problemen te omzeilen.

Dit zijn alle originele bijdragen. De eerste twee vormen zeker afgeronde geheel. Met het multiresolutie-karakter van een wavelettransformatie kunnen we verder experimenteren om goed werkende procedures te vinden in allerhande praktijkvoorbeelden. Voor de Bayesiaanse procedure speelt de uitvoeringstijd een cruciale rol: enerzijds kunnen we proberen die naar omlaag te halen zonder aan kwaliteit in te boeten, anderzijds moeten we bij verdere verfijningen aan het model de complexiteit in het oog houden. We stellen vast dat de Bayesiaanse aanpak structuur brengt in de selectie van waveletcoëfficiënten. Het eindresultaat vertoont echter geen grote verbetering in signaal-ruis-verhouding. Misschien is signaal-ruis-verhouding geen goede maat om contrastverbetering aan de randen te meten. Een nauwkeurigere maat voor dit contrast moet hierover uitsluitsel brengen, en als de randen nog niet voldoende bewaard zijn, kan een beter a priori of conditioneel model dan soelaas brengen? Verreweg de meeste vragen blijven er bij de toepassing op onregelmatige roosters. Hier is zowel theoretisch als praktisch nog heel wat werk. Momenteel werken we op het departement nog volop aan verklaringen en goede oplossingen voor het stabiliteitsprobleem. In plaats van het probleem te omzeilen met enkele extra wavelettransformaties, willen we het voorkomen. Hiertoe bestuderen we de transformatie en proberen we de oorzaken van instabiliteit te isoleren en op te lossen.

Contents

Notations and Abbreviations

List of Symbols

Symbol	:	Description	Page
$\mathbf{0}$	:	zero vector	93
$\sim$	:	asymptotic equivalence	53
∞	:	infinity	
$\lfloor x \rfloor$	:	integer part of real number x	72
$\lceil x \rceil$	:	smallest integer equal or larger than real number x	131
$\oplus$	:	direct sum of two subspaces	12
$\langle \cdot, \cdot \rangle$	:	Scalar product in unitary space	2
$\|\| \cdot \|\|$	:	norm in a general vector space	2
$\|\|f\|\|_p$	:	L_p-norm	2
$\|f\|_{B^{\alpha}_{p,q}}$	:	Besov semi-norm of f	75
$\overline{V}$	:	colsure of set V	12
∂s	:	set of neighboring sites of a site s	141
A	:	Jacobian matrix of $\boldsymbol{y}_{\boldsymbol{\lambda}}$ as function of $\boldsymbol{y}$	82
C	:	clique in a neighboring system	142
$\mathcal{C}$	:	set of all cliques in a neighboring system	142
C^{α}	:	space of Lipschitz (Hölder) α-continuous functions	70
E	:	expected value	32
$\mathrm{E}R$	:	Risk = expected mean square error	46
D	:	Delay (inverse shift) operator	4
$\mathcal{E}$	:	entropy	37
$F(\omega)$	:	Fourier transform of $f(x)$	3
$\boldsymbol{f}$	:	Noise-free digital signal	1
$f_X(x)$	:	Density function of random variable X	171
$F_X(x)$	:	Distribution function of random variable X	62
$\mathcal{F}$	:	Fourier transform operator	3

$\mathcal{F}$	:	General function space	61
$\boldsymbol{g}$, g_k	:	highpass filter in filter bank; coefficients in wavelet equation (primal)	14
$\boldsymbol{h}$, h_k	:	lowpass filter in filter bank; coefficients in dilation equation (primal)	14
$h(\lambda)$	:	help function in upperbound GCV error	86
$H(\boldsymbol{x})$	:	energy function in a Gibbs distribution	141
$\mathcal{H}$	:	Digital filter	4
I	:	unity matrix	155
I_0	:	set of noise-free wavelet coefficients exactly zero	55
I_1	:	set of noise-free wavelet coefficients not exactly zero	55
J	:	Highest resolution level in a MRA (level of approximation or sampling)	12, 130
L	:	Lowest resolution level in a MRA	12
$\mathrm{L}(\tau)$	:	Likelihood of parameter value τ	148
$L_2[0,1]$	:	Hilbert space of square integrable functions on $[0,1]$	2
$L_p[0,1]$	:	Banach space of p-th power integrable functions on $[0,1]$	2
$\ell_2(\mathbb{Z})$	:	Hilbert space of square summable sequences	1
$\boldsymbol{M}$	:	Measure of significance in Bayesian model	136
M_0	:	number of noise-free wavelet coefficients exactly zero	55
M_1	:	number of noise-free wavelet coefficients not exactly zero	55
$\boldsymbol{N}$	:	noise vector in Bayesian approach	39
N	:	number of data points in a discrete, finite signal	32
N_0	:	number of noisy wavelet coefficients below a threshold	82
$\mathcal{O}$	:	Landau big "O" symbol (order of magnitude)	17
$\mathrm{P}(A)$	:	Probability of event A	59
p	:	number of vanishing moments	20
p	:	smoothness parameter in Besov spaces	75
$\mathrm{PL}(\tau)$	:	Pseudo-likelihood of parameter value τ	148
Q	:	covariance matrix of input noise	32
R	:	Mean Square Error (= MSE)	46
$r(v,\lambda)$	:	contribution of coefficient w to the total risk function	49
$\mathbb{R}$	:	set of real numbers	1
s	:	'two-dimensional' index of coefficient in two-dimensional wavelet transform: $s=(k,l)$	136
S	:	covariance matrix of wavelet coefficients	33
$s_{j,k}$	:	scaling coefficient (level j, position k)	136
T_J	:	diagonal matrix containing the squared norms of the scaling function at the initial, fine resolution	162
$\mathrm{Tr}(D)$	:	trace of matrix D	81
$\boldsymbol{v}$, v_i	:	noise-free wavelet coefficients (general index i)	33
$v_{j,k}$	:	noise-free wavelet coefficient at level j, position k	55
$\boldsymbol{V}$	:	vector of noise-free wavelet coefficients in Bayesian approach	39

V_j	:	primal multiresolution space at level j	12
$\tilde{V}_j$	:	dual multiresolution space at level j	13
$\tilde{W}$	:	forward wavelet transform matrix	23
W	:	inverse wavelet transform matrix	162
$\boldsymbol{w}$, w_i	:	noisy wavelet coefficients (general index i)	33
$w_{j,k}$	:	noisy wavelet coefficient at level j, position k	55
$\boldsymbol{W}$	:	vector of noisy wavelet coefficients in Bayesian approach	39
$\boldsymbol{w_\lambda}$, $w_{\lambda i}$	:	wavelet coefficients after thresholding	47
W_j	:	primal detail subspace at level j	12
$\tilde{W}_j$	:	dual detail subspace at level j	13
W_s	:	noisy wavelet coefficient in Bayesian model (also see s)	136
$\boldsymbol{x}$, x_i	:	vector of grid positions for nonequispaced data	154
$\boldsymbol{X}$, X_s	:	vector of classification labels (mask) in Bayesian model	136
$\boldsymbol{y}$, y_i	:	noisy input	32
$\tilde{\boldsymbol{y}}$	:	modified output for cross validation	84
$\boldsymbol{y_\lambda}$, $y_{\lambda i}$	:	output of threshold algorithm	46
Z	:	partition function in a Gibbs distribution	141
$\mathbb{Z}$	:	set of integers	1
α	:	significance level	59
α	:	smoothness parameter for C^α (Lipschitz α), or in Besov spaces	61,75
δ_n, δ_0	:	Kronecker delta (discrete Dirac impulse in n or 0)	4
ϵ	:	error of approximation	130
ε	:	arbitrarily small real number	88
$\boldsymbol{\eta}$	:	vector of input zero mean noise	32
κ	:	parameter in Laplacian distribution	145
$\boldsymbol{\eta_\lambda}$	:	vector of output noise	46
λ	:	smoothing parameter, in particular a threshold	37,34
λ^*	:	minimum risk threshold	54
$\hat{\lambda}$	:	minimum expected GCV threshold	86
λ_{mM}	:	minimax threshold	61
λ_{UNIV}	:	universal threshold	60
μ_1, $\mu_1(\lambda)$	:	help function for $\mathrm{E}GCV$: $\mu_1 = 1 - \mathrm{E}N_0/N$	81
τ	:	Rigidity parameter in a Gibbs distribution	142
$\varphi(x)$	:	primal (synthesis) scaling (father) function	10
$\tilde{\varphi}(x)$	:	dual (analysis) scaling (father) function	13
$\phi(x)$	:	normal density function	49
$\phi_1(x)$	:	standard normal density function	66
$\Phi(x)$	:	normal distribution function	49
$\Phi_1(x)$	:	standard normal distribution function	66
$\psi(x)$	:	primal (synthesis) wavelet (mother) function	12
$\tilde{\psi}(x)$	:	dual (analysis) wavelet (mother) function	14
ω	:	pulsation of a sinusoid	15

ω	:	wavelet coefficients of input noise	33
ω_λ	:	wavelet coefficients of output noise	47

List of Abbreviations

1D	:	one-dimensional	23
2D	:	two-dimensional	33
CDF	:	Cohen-Daubechies-Feauveau (wavelets)	21
CPRESS	:	Complexity-penalized residual sum of squares	108
CT	:	Computed Tomography	6
CWT	:	Continuous wavelet transform	23
DSA	:	Digital Subtraction Angiography	123
DTFT	:	Discrete Time Fourier Transform	4
DWT	:	Discrete Wavelet Transform	23
FDR	:	False Discovery Rate	59
FIR	:	Finite Impulse Response (filter)	17
FFT	:	Fast Fourier Transform	4
FWT	:	Fast Wavelet Transform	17
GCV	:	Generalized cross validation	85
GIS	:	Geographical information system	6
HVS	:	Human Visual System	6
MAD	:	Median Absolute Deviation	116
MAP	:	Maximum A Posteriori	145
MCMC	:	Markov Chain Monte Carlo	146
MDL	:	Minimum Description Length	35
MLE	:	Maximum Likelihood Estimation	148
MMP	:	Maximal Marginal Posterior	145
MPLE	:	Maximum Pseudo-Likelihood Estimation	148
MRA	:	Multiresolution analysis	12
MRF	:	Markov Random Field	135
MRI	:	Magnetic Resonance Imaging	6
MSE	:	Mean Square Error	46
PSNR	:	Peak signal-to-noise ratio	47
SNR	:	Signal-to-noise ratio	46
SURE	:	Stein's Unbiased Risk Estimate	80
a.s.	:	almost sure(ly) (with probability one)	92
i.i.d.	:	independent, identically distributed noise	33
dB	:	deciBel	47

List of Figures

List of Tables

Chapter 1

Introduction and overview

"Lies keine Oden,
lies die Fahrpläne:
die sind genauer,
die lügen nicht."
—Hans Magnus Enzensberger, *(1929 –).*

Thanks to the combination of a nice theoretical foundation and the promising applications, wavelets have become a popular tool in many research domains. In fact, wavelet theory combines many existing concepts into a global framework. This new theoretical basis reveals new insights and throws a new light on several domains of applications.

This thesis lies on the bridge between two or three domains of application: on one side, we have statistics, on the other side there are the domains of digital signal- and image processing. From time to time, we encounter notions from approximation theory too.

1.1 Notions and notations

Before actually describing wavelets and their applications in the next chapter, we first introduce some concepts and notations from the various fields.

1.1.1 Mathematical preliminaries

A real, digital signal $\boldsymbol{f}$ is nothing but a sequence of real numbers: $f_i \in \mathbb{R}$. In this thesis, we suppose them to be square summable: $\boldsymbol{f} \in \ell_2(\mathbb{Z})$, where $\mathbb{Z}$ denotes the set of integers. In most practical applications, the signals have a finite number N of non-zero elements. With a slight abuse of notation, we could say that $\boldsymbol{f} \in \mathbb{R}^N \subset \ell_2(\mathbb{Z})$, $\mathbb{R}$ being the set of real numbers.

In a way that we explain immediately, such a discrete input can be associated with a function defined on the interval $[0,1]$. This function is square integrable, *das heißt*:

$$f(x) \in L_2[0,1] \Leftrightarrow \int_{[0,1]} f^2(x)dx < \infty.$$

Strictly speaking, this integral should be taken in the sense of *Lebesgue*, although the Riemann construction suffices to understand what follows. The space of all square integrable functions is a Hilbert space. This means that it is a unitary space, *id est* a complete vector space with a definition of a *scalar product* (inner product or dot product):

$$\langle f, g \rangle = \int_{[0,1]} f(x)g(x)dx.$$

Such an inner product allows for the notion of orthogonality: two elements (functions) are said to be orthogonal if their inner product equals zero. An inner product also induces a *norm*:

$$\|f\| = \sqrt{\langle f, f \rangle}.$$

A Hilbert space must also be complete, *cioè*, all Cauchy sequences must converge within the Hilbert space and with respect to its norm. A Cauchy sequence is a sequence of functions the elements of which come arbitrarily close to each other, with respect to the given norm.

Square integrability can be generalized:

$$f(x) \in L_p[0,1] \Leftrightarrow \int_{[0,1]} |f(x)|^p dx < \infty,$$

but for $p \neq 2$, there is no scalar product which induces the norm

$$\|f\|_p = \int_{[0,1]} |f(x)|^p dx.$$

The function spaces $L_p[0,1]$ with $p \geq 1$ are examples of Banach spaces, complete vector spaces with a norm, but not necessarily an inner product.

A *basis* $\varphi_k, k \in \mathbb{Z}$ is a free set of functions (*c'est-à-dire* a set of linearly independent functions) that generates the entire space. Since we are dealing with infinite dimensional spaces, we should we careful about the word *generate*: we are dealing with infinite sums and convergence issues are involved [46]: if there exists for every function $f \in L_p[0,1]$ a unique sequence $s_i, i \in \mathbb{Z}$ so that $f(x) = \sum_i s_i \varphi_i(x)$, then we have a *Schauder basis*. This uniqueness is the guarantee for linear independence of the basis functions, but convergence in such a basis may depend on the ordening of the components. A basis is called *unconditional* if $\sum_i |s_i|\varphi_i(x) \in L_p[0,1]$ for all $\sum_i s_i\varphi_i(x) \in L_p[0,1]$ and *vice versa*. As a consequence, the sum $\sum_i s_i\varphi_i(x)$ converges independent of the order of summation. Unconditional basis means that the coefficient *magnitude* only determines whether or not a function belongs to a Banach space: the phase of the coefficients (in real analysis this is the sign only) is of no importance.

In the Hilbert space $L_2[0,1]$, an unconditional basis is called a *Riesz* basis if it is *almost normalized*. This means that there exist real, positive, non-zero constants m and M so that:

$$0 < m \leq \|\varphi_i\| \leq M < \infty.$$

A Riesz basis is characterized by two Riesz *constants* A and B, so that for all $f = \sum_i s_i\varphi_i \in L_2[0,1]$:

$$A^2\|f\|^2 \leq \sum_{i\in\mathbb{Z}} s_i^2 \leq B^2\|f\|^2.$$

A Riesz basis is also called a *stable* basis. It is essentially the second best type of basis after orthonormal bases.

1.1.2 Fourier analysis and digital signals

Functions in $L_2[0,1]$ can be decomposed into a basis of waves $\mathrm{e}^{i2\pi kx}$:

$$f(x) = \sum_{k\in\mathbb{Z}} c_k \mathrm{e}^{i2\pi kx}.$$

This is a Fourier series expansion. Since these waves constitute an orthogonal basis, the coefficients are easy to find:

$$c_k = \frac{1}{2\pi}\int_0^1 f(x)\mathrm{e}^{-i2\pi kx}.$$

The minus sign in the exponent appears because the basis functions are complex, and the proper definition of a scalar product for complex functions uses complex conjugates. The basis functions are of course not limited to the interval $[0,1]$: they are periodic. The Fourier series is also valid for a periodic extension of $f \in L_2[0,1]$ to the entire real axis.

General functions in $L_2(\mathbb{R})$ are not periodic nor can they be periodically extended. Frequency analysis now goes by a *Fourier transform*, defined as:

$$F(\omega) = \mathcal{F}\left\{f(x)\right\} = \frac{1}{\sqrt{2\pi}}\int_{-\infty}^{\infty} f(x)\mathrm{e}^{-i\omega x}dx.$$

The inverse of this transform is given by:

$$f(x) = \frac{1}{\sqrt{2\pi}} \int_{-\infty}^{\infty} F(\omega) \mathrm{e}^{i\omega x} d\omega.$$

Since most of this text is about discrete signals (samples), we are also investigating the frequency contents of this kind of signals. This is given by the inner product of a discrete signal $\boldsymbol{f}$ with a wave $\{\mathrm{e}^{i\omega k}\}$:

$$F(\omega) = \sum_{k \in \mathbb{Z}} f_k \mathrm{e}^{-i\omega k}.$$

This is the Discrete Time Fourier Transform (DTFT). By a substitution $\omega = -2\pi x$, we see that f_k is nothing but the Fourier series expansion of $F(\omega)$. $F(\omega)$ is 2π-periodic and the inverse of a DTFT is a Fourier series expansion. Discretizing the frequency parameter ω in a DTFT leads to a (fully) discrete Fourier transform (DFT), for which exists a fast algorithm, the Fast Fourier Transform (FFT) .

A DTFT gives the frequency *contents* of a discrete signal, but, as the next chapter illustrates, it is also the formula for the frequency *response* of a linear, time-invariant filter. A digital *filter* $\mathcal{H}$ is any system operating on a digital signal. Linear filters satisfy:

$$\mathcal{H}(\alpha \boldsymbol{f} + \beta \boldsymbol{g}) = \alpha \mathcal{H}(\boldsymbol{f}) + \beta \mathcal{H}(\boldsymbol{g})$$

and time-invariance (or shift-invariance) means that: $\mathcal{H} D = D \mathcal{H}$, where D is the delay (inverse shift) operator:

$$\boldsymbol{y} = D\boldsymbol{x} \Leftrightarrow y_k = x_{k-1}, \forall k \in \mathbb{Z}.$$

A time-invariant filter is characterized by its *impulse response* $\boldsymbol{h}$:

$$\boldsymbol{h} = \mathcal{H}(\boldsymbol{\delta_0}),$$

where $\boldsymbol{\delta_0} = \{\ldots, 0, 0, 1, 0, 0, \ldots\}$ is a Kronecker delta (discrete Dirac impulse) signal. $\boldsymbol{h}$ by itself is a signal. If the filter is linear, its response to an arbitrary signal $\boldsymbol{x}$ equals:

$$\boldsymbol{y} = \mathcal{H}(\sum_{k=-\infty}^{\infty} x_k \boldsymbol{\delta_k}) = \sum_{k=-\infty}^{\infty} x_k \mathcal{H}(D^k \boldsymbol{\delta_0}) = \sum_{k=-\infty}^{\infty} x_k D^k \boldsymbol{h}.$$

and so:

$$y_n = \sum_{k=-\infty}^{\infty} h_{n-k} x_k.$$

This expression is called a *convolution sum*.

The next chapter illustrates with an example how a filter modifies the frequency contents of a signal.

1.1.3 A note on images

A digital image can be seen as a matrix of pixels. Digital image *processing* is everything *beyond* a matrix of pixels. It deals with all the operations you can perform on the image by considering the image *not* just as a matrix. To distinguish an image, which is basically a specially structured data *vector* from a linear operation matrix we use bold lower case letters to denote an image, except when this image is a random variable.

So $\boldsymbol{x}$ is the normal notation for an image, $\boldsymbol{X}$ emphasizes that this image is a matrix of random variables and X may denote a random variable or a linear operation matrix.

1.2 Outline of this thesis

This thesis is about noise reduction or non-parametric regression, using wavelets. It focuses on the technique of wavelet thresholding. This method is simple and fast. Chapter 2 explains the essentials about wavelets and wavelet based noise reduction. It introduces the idea of wavelet thresholding and addresses the problems involved with this method.

The next two chapters belong together. Chapter 3 studies the asymptotic behavior of the threshold that minimizes the expected mean square error of the result. The mean square error is of course not the only possible objective function for a noise reduction algorithm nor does it yield the best output in all circumstances. In spite of its shortcomings, it is often used, because of its mathematical tractability and fair results in a wide range of applications. Since the noise-free data are unknown in practical situations, we cannot compute and minimize the mean square error of the output exactly. Therefore, Chapter 4 presents an estimation of this error function, based on the method of generalized cross validation. This leads to fast procedure, which tend to be optimal in mean square error sense if the number of data grows to infinity. To prove this asymptotic optimality, we use what we know about the behavior of minimum error threshold for large data sets.

After these two chapters of motivation, we investigate the applicability of our method in less conventional situations. This includes colored (correlated) noise, non-orthogonal transforms, integer transforms, which are interesting for fast and lossless algorithms in applications like image processing. Whereas Chapters 3 and 4 mainly rely on the *sparsity* of a wavelet transform, Chapter 5 also uses the concept of *multiresolution*, naturally supported by wavelet theory.

Chapter 6 concentrates on *image* noise reduction. It explains what additional problems occur when extending wavelet transforms to two-dimensional inputs. We take a Bayesian approach, where the prior model is inspired by the two-dimensional character of the input.

Chapter 7 takes a look at a domain that has only recently been discovered and explored by the wavelet community: reduction of noise in data on irregular grids. Our experience is that thresholding is not obvious in some extreme circumstances, and therefore we carefully design an algorithm combining stability of classical wavelet transforms and smoothness of the new transforms, developed specifically for non-equidistant data.

1.3 Motivation

Initially, this project was inspired by previous research by M. Malfait [106] and the applications in image processing in his thesis. Images play an important role, both in daily life applications and in areas of research and technology. We mention geographical information systems (GIS), astronomical and medical images. It is true that image acquisition techniques, like cameras, microscopes and various types of scanners (CT - computed tomography, MRI - magnetic resonance imaging) have had important developments in the last years and that images carry much less noise than before. On the other hand, the requisites for the desired applications are often stronger too. Nowadays, a medical image may have 2048 grey levels instead of the classical 256. This is more than what our human visual system (HVS) can distinguish. Typically, only a small part of this dynamical range is important. For the application, contrast in this part is enhanced so that this interesting piece covers the entire range from black to white. All other grey levels in the original image are mapped to perfect white or black. This contrast enhancement blows up the present noise. So, even if in the first instance the noise is quasi invisible, it may be important to reduce it, in the light of the further use of these data.

Imaging remains an important application of the noise reduction algorithms described in this dissertation. Nevertheless, we realized that nearly all the material in this text has a wider range of applications. Since this research was not performed in an image processing laboratory, but in a division of applied mathematics, we chose not to concentrate on this specific domain of application, but rather formulate more general algorithms. The method of Chapter 6 is more image-oriented, but yet, this may serve for other two-dimensionally structured data too. We want too stress this generality also on another point: the procedure of generalized cross validation for non-linear smoothing, as described in Chapter 4 is not limited to wavelets. It should also work for other types of sparse data representations. We discuss in Chapter 6 why wavelets might not be the ultimate way for representing images, but generalized cross validation remains interesting, even beyond the classical wavelets.

Section 2.8 contains a more complete list of wavelet applications. These are not limited to the problem of noise reduction.

Chapter 2

Wavelets and wavelet thresholding

"Bencio," mi disse poi Guglielmo, "è vittima di una grande lussuria, che non è quella di Barengario né quella del cellario. Come molti studiosi, ha la lussuria del sapere. Del sapere per se stesso. Escluso da una parte di questo sapere, voleva impadronirsene. Ora se ne è impadronito. Malachia conosceva il suo uomo e ha usato il mezzo migliore per riavere il libro e suggellare la labbra di Bencio. Tu mi chiederai a che pro controllare tanta riserva di sapere se si accetta di non metterlo a disposizione di tutti gli altri. Ma proprio per questo ho parlato di lussuria. Non era lussuria la sete di conoscenza di Ruggiero Bacone, che voleva impiegare la scienza per rendere più felice il popolo di Dio e quindi non cercava il sapere per il sapere. Quella di Bencio è solo curiosità insaziabile, orgoglio dell' intelletto, un modo come un altro, per un monaco, di trasformare e pacificare le voglie dei propri lombi, o l'ardore che fa di un altro un guerriero della fede, o dell' eresia. Non c'è solo la lussuria della carne."
—Umberto Eco, *Il Nome della Rosa, quinto giorno, vespri.*

For those who do not understand Italian, I found this wisdom on the internet:

"A man who has not been in Italy is always conscious of an inferiority."
—Samuel Johnson, *1776.*

Every theory starts from an idea. The wavelet idea is simple and clear. At a first confrontation, the mathematics that work out this idea might appear strange and difficult. Nevertheless, after a while, this theory leads to insight in the mechanism in wavelet based algorithms in a variety of applications.

This chapter discusses the wavelet idea and explains the wavelet slogans. For the mathematics, we refer to the numerous publications. Comprehensive introductions to the field include [133, 24, 19, 121]. Other, sometimes more application oriented or more theoretical treatments can be found in [113, 46, 138, 103, 127, 93, 5, 91].

Although this chapter does not go far into mathematical details, readers interested in wavelets but without a strong mathematical background, may wish to skip the definitions and equations. Reading Sections 2.1.1, 2.1.2 (until Definition 2.1), 2.4, 2.5.3, 2.5.4, 2.5.5, and 2.8 should give an idea about wavelets without struggling through mathematical symbols.

2.1 Exploiting sample correlations

2.1.1 The input problem: sparsity

Suppose we are given a *discrete* signal f. In practice, this signal is often digital, i.e. quantized and possibly transformed into a binary form. Figure 2.1 shows how these discrete data can be represented on a continuous line as a piecewise constant function. This piecewise constant is of course not the only possible continuous representation.

Typically, adjacent points show strong correlations. Only at a few points, we find large jumps. Storing all these values separately seems a waste of storage capacity. Therefore, we take a pair of neighbors f_1 and f_2 and compute average and difference coefficients:

$$\begin{aligned} a_1 &= \frac{f_1 + f_2}{2} \\ d_1 &= \frac{f_1 - f_2}{2} \end{aligned}$$

In the figure, the averages are represented on the second line as a piecewise constant, just like the input, but the difference coefficients appear as two opposite blocks: every pair of two opposite blocks is one coefficient. This coefficient tells how far the first data point was under the average of the pair and at the same time, how much the second data point was above this average. ‘Adding’ the left plot and the right one returns the input on top. This ‘adding’ is indeed the inverse operation:

$$\begin{aligned} f_1 &= a_1 + d_1 \\ f_2 &= a_1 - d_1 \end{aligned}$$

The average signal is somehow a blurred version of the input. We can repeat the same procedure on the averages again. Eventually, this operation decomposes the input into one global average *plus* difference signal at several locations on the axis and with different widths, *scales* , or *resolutions*. Since each step is invertible, the whole transform satisfies the *perfect reconstruction* property. This is called the *Haar*-transform, after Alfred Haar, who was the first to study it in 1910, long before the actual wavelet history began [71].

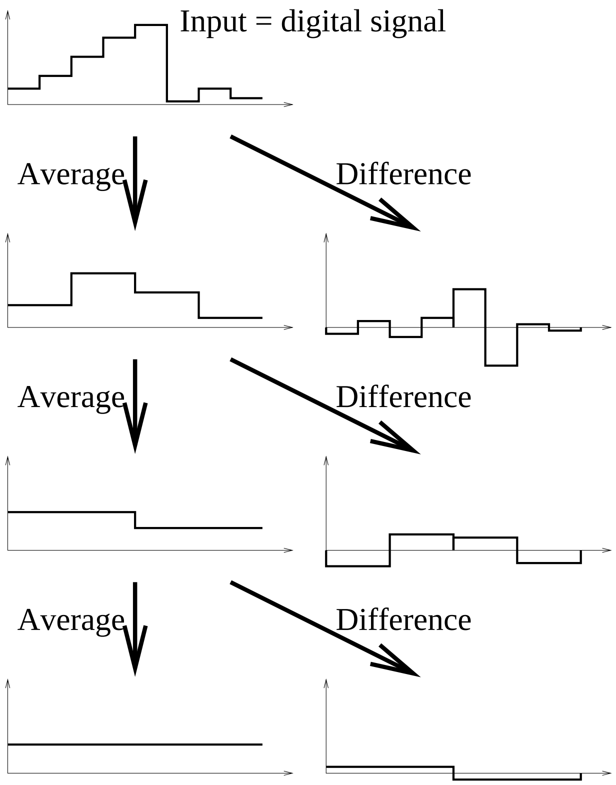

Figure 2.1: Using correlations between neighboring samples leads to a sparse representation of the input. This is the Haar wavelet transform.

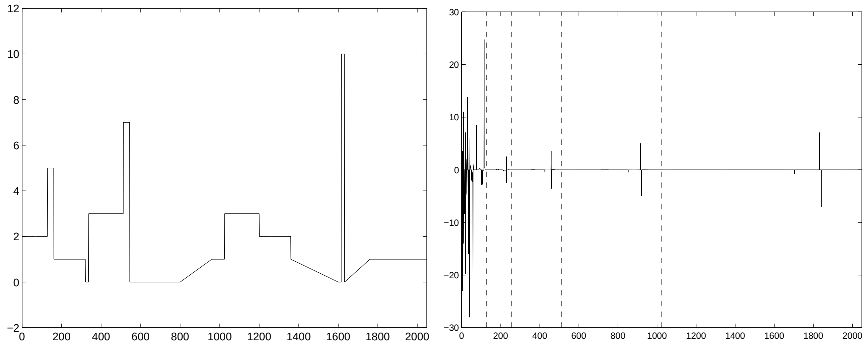

Figure 2.2: Test signal (Left) and Haar transform (Right): all coefficients are plotted on one line. Dashed lines indicate the boundaries between scales.

As the Figure 2.1 illustrates, most of the difference coefficients are small. The largest coefficient appears at the location of the biggest ‘jump’ in the input signal. This is even more striking in the more realistic example of Figure 2.2. In this picture, all coefficients are plotted on one line. Dashed lines indicate the boundaries between scales. Only a few coefficients are significant. They indicate the singularities (jumps) in the input. This *sparsity* is a common characteristic for all wavelet transforms. Wavelet transforms are said to have a *decorrelating property*.

2.1.2 Basis functions and multiresolution

The input vector $\boldsymbol{f}$ can be seen as coefficients for a basis of characteristic functions (‘block’ functions), as shown on top of Figure 2.3: i.e. we can write the continuous representation $f(x)$ of the discrete input $\boldsymbol{f}$ as a linear combination of these basis functions, which we call $\varphi_k(x)$:

$$f(x) = \sum_k f_k \varphi_k(x).$$

All these functions are translates of one *father* function, they are called *scaling* functions. The differences, computed during the algorithm, correspond to the basis functions on the next rows in Figure 2.3. All these functions are translations (shifts) *and* dilations (stretches) of one *mother* function. Because these functions have block-wave-form, vanishing outside a small interval, they are called ‘short waves’ or wave-lets.

The decomposition from a function in a scaling basis into a wavelet basis is an example of a *multiresolution* analysis. In image processing, the scaling function basis correspond roughly to the classical pixel representation. Not only is this redundant, our visual system does not look at images that way. The wavelet representation, i.e. a set of details at different locations and different scales, is said to

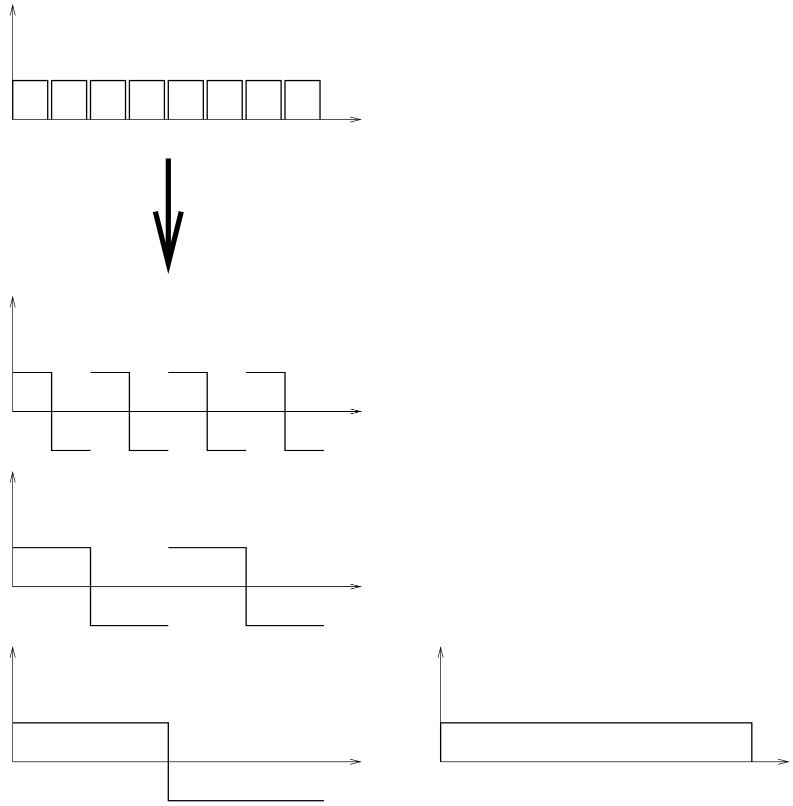

Figure 2.3: Basis functions in a wavelet decomposition. The line on top shows the basis functions of the original representation: any linear combination of these characteristic functions leads to a piecewise constant. Piecewise constants can also be built in a block-wavelet-basis: these basis functions have a short waveform, all have a certain scale and are situated at different locations.

be closer to the way we look at images: at a first sight, we see general features, at a closer inspection, we discover the details.

Instead of just taking averages and differences, one could of course think of more complex tricks to exploit inter-sample coherence. This corresponds to less trivial ‘continuous representations of discrete data’ than just blocks and blocky wave-lets: this is the way we can build more complex wavelets. While doing so, we have to take care not to lose basic properties, like transform invertibility, and several convergence issues. To this end, we start with a formal definition of the notion of multiresolution:

Definition 2.1 *A sequence of nested, closed subspaces* $V_j \subset L_2[0,1]$, $j = L, \ldots, J$ *is called a* multiresolution analysis *(MRA) if*

$$\forall j \in \mathbb{Z} : V_j \subset V_{j+1}, \tag{2.1}$$

$$\overline{\lim_{j \to \infty} V_j} = \overline{\bigcup_{j \in \mathbb{Z}} V_j} = L_2[0,1], \tag{2.2}$$

$$\lim_{j \to -\infty} V_j = \bigcap_{j \in \mathbb{Z}} V_j = \{0\}, \tag{2.3}$$

$$f(x) \in V_j \Leftrightarrow f(2x) \in V_{n+1}, j \in \mathbb{Z}, \quad \textit{(scale invariance)} \tag{2.4}$$

$$f(x) \in V_0 \Leftrightarrow f(x+k) \in V_0, k \in \mathbb{Z}, \quad \textit{(shift invariance)} \tag{2.5}$$

$$\exists \varphi(x) \in V_0 : \{\varphi(x-k)\}_{k \in \mathbb{Z}} \quad \textit{is a } \text{stable } \textit{basis for } V_0 \tag{2.6}$$

The function $\varphi(x)$ plays the role of father function: all basis functions of V_0 are shifted versions of this function. Trivialiter, $2^{j/2}\varphi(2^j x - k)$ then is a (normalized) basis for V_j. V_1 contains functions that are not included in V_0. To generate all elements in the finer scale V_1, starting from the basis of the coarser scale V_0, we need additional basis functions. These basis functions generate a space W_0 of detail functions. W_0 is not unique: it maybe the orthogonal or an oblique complement, but it holds that all functions in V_1 can be decomposed in the union of the basis of V_0 and the basis of W_0:

$$V_{j+1} = V_j \oplus W_j.$$

Theorem 2.1 *[46, 64] If* $\{\varphi(x-k)\}_{k \in \mathbb{Z}}$ *constitute an orthogonal basis for* V_0*, then there exists one function* $\psi(x)$ *such that* $\{\psi(x-k)\}_{k \in \mathbb{Z}}$ *forms an orthogonal basis for the orthogonal complement* W_0 *of* V_0 *in* V_1*. Furthermore,* $\{\psi(2^j x - k)\}_{k \in \mathbb{Z}}$ *constitutes an orthogonal basis for the orthogonal complement* W_j *of* V_j *in* V_{j+1}*. And we have that:*

$$\forall L \in \mathbb{Z} : \overline{V_L \oplus \left(\bigoplus_{j=L}^{\infty} W_j \right)} = L_2[0,1]. \tag{2.7}$$

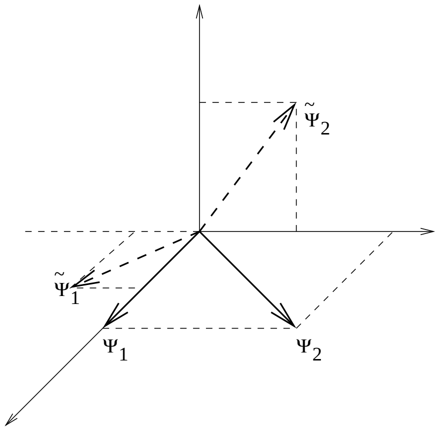

Figure 2.4: A pair of biorthogonal bases in $\mathbb{R}^3$.

This function $\psi(x)$ is called the *mother* function or *wavelet* function. It takes care of the detail information at different scales in the signal.

A general MRA has no orthogonality. In this case, we look for a *dual* father function $\tilde{\varphi}(x)$, so that:

$$\langle \tilde{\varphi}(x), \varphi(x-l) \rangle = \delta_l .$$

This pair of bases is called *biorthogonal*. Figure 2.4 illustrates this notion in $\mathbb{R}^3$. The coefficients $\boldsymbol{f}$ in the expansion

$$f(x) = \sum_{k \in \mathbb{Z}} f_k \varphi(x-k)$$

are then:

$$f_k = \langle f(x), \tilde{\varphi}(x-l) \rangle$$

This expression shows that projection in a biorthogonal setting is still simple and stable.

The dual father function generates a dual MRA $\tilde{V}_j$, $j \in \mathbb{Z}$ and the primal wavelet function now also has its dual $\tilde{\psi}(x) \in \tilde{W}_0$, so that:

$$V_j \perp \tilde{W}_j \ \text{ and } \ \tilde{V}_j \perp W_j ,$$

which implies:

$$W_j \perp \tilde{W}_i \ \text{ for } \ i \neq j$$

This also implies biorthogonality of the basis functions:

$$\langle \tilde{\varphi}(x), \psi(x-k) \rangle = 0 \text{ and } \langle \tilde{\psi}(x), \varphi(x-k) \rangle = 0,$$

and we also have

$$\langle \tilde{\psi}(x), \psi(2^j x - k) \rangle = \delta_j \delta_k.$$

2.1.3 The dilation equation

Wavelet theory, like most interesting branches in mathematics or physics, has a central equation. It is called the *dilation equation*, *two-scale equation*, or *refinement equation*. It follows from the fact that $\varphi(x) \in V_0 \subset V_1$, so the father function is a linear combination of the basis in V_1:

$$\exists \boldsymbol{h} \in \ell_2(\mathbb{Z}) : \varphi(x) = \sqrt{2} \sum_{k \in \mathbb{Z}} h_k \varphi(2x - k). \tag{2.8}$$

A similar argument holds for the mother function:

$$\exists \boldsymbol{g} \in \ell_2(\mathbb{Z}) : \psi(x) = \sqrt{2} \sum_{k \in \mathbb{Z}} g_k \varphi(2x - k). \tag{2.9}$$

This is the *wavelet equation* . In the case of a biorthogonal basis, there are of course a dual $\tilde{\boldsymbol{h}}$ and a dual $\tilde{\boldsymbol{g}}$. There is a one-to-one relation between these *filters* and the basis functions. Given the filters, the corresponding basis follows by solving dilation and wavelet equation. Solving techniques appear in books like [133].

We use the following notations for the normalized basis functions:

$$\varphi_{j,k}(x) = 2^{j/2} \varphi(2^j x - k), \tag{2.10}$$

and similarly for $\tilde{\varphi}_{j,k}(x), \psi_{j,k}(x), \tilde{\psi}_{j,k}(x)$. We assume that the two father and the two mother functions are normalized.

2.1.4 (Fast) Wavelet Transforms and Filter Banks

Suppose we want to decompose a signal in a scaling function basis at a given scale into detail coefficients and scaling coefficients at the next, coarser scale:

$$f_{j+1}(x) = \sum_{k \in \mathbb{Z}} s_{j+1,k} \varphi_{j+1,k}(x) = \sum_{k \in \mathbb{Z}} s_{j,k} \varphi_{j,k}(x) + \sum_{k \in \mathbb{Z}} w_{j,k} \psi_{j,k}(x).$$

Computing $s_{j,k}$ and $w_{j,k}$ from $s_{j+1,k}$ is one step in a *Forward Wavelet Transform*. Clearly

$$\begin{aligned} w_{j,k} &= \langle f_{j+1}, \tilde{\psi}_{j,k} \rangle \\ &= \langle f_{j+1}, \sum_{l \in \mathbb{Z}} \tilde{g}_l \tilde{\varphi}_{j+1,2k+l} \rangle \\ &= \sum_{l \in \mathbb{Z}} \tilde{g}_{l-2k} s_{j+1,l}. \end{aligned} \tag{2.11}$$

Similarly

$$s_{j,k} = \sum_{l \in \mathbb{Z}} \tilde{h}_{l-2k} s_{j+1,l}. \tag{2.12}$$

The inverse step is easy to find, if we use primal dilation and wavelet equation:

$$\begin{aligned} \sum_{l \in \mathbb{Z}} s_{j+1,l} \varphi_{j+1,l} &= \sum_{k \in \mathbb{Z}} s_{j,k} \varphi_{j,k} + \sum_{k \in \mathbb{Z}} w_{j,k} \psi_{j,k} \\ &= \sum_{k \in \mathbb{Z}} s_{j,k} \sum_{l \in \mathbb{Z}} h_l \varphi_{j+1,2k+l} + \sum_{k \in \mathbb{Z}} w_{j,k} \sum_{l \in \mathbb{Z}} g_l \varphi_{j+1,2k+l} \\ &= \sum_{l \in \mathbb{Z}} \varphi_{j+1,l} \left(\sum_{k \in \mathbb{Z}} h_{l-2k} s_{j,k} + \sum_{k \in \mathbb{Z}} g_{l-2k} w_{j,k} \right), \end{aligned}$$

from which:

$$s_{j+1,l} = \sum_{k \in \mathbb{Z}} h_{l-2k} s_{j,k} + \sum_{k \in \mathbb{Z}} g_{l-2k} w_{j,k}. \tag{2.13}$$

Forward and inverse transform can be seen as convolution sums, in which (parts of) the dual respectively primal filters appear. It is not a mere convolution. In the reconstruction formula, we only use half of the filter coefficients for the computation of a scaling coefficient: the sum goes over index k, which appears in the expression as $2k$: this is up-sampling: we could artificially add zeros between every input scaling or wavelet coefficients and then perform a plain convolution. In the decomposition formula, the sum goes over index l, and k is fixed. This is as if we drop half of the results from a plain convolution. This is *down-sampling*. Putting all this together in a scheme, we get a *filter bank* [145], as in Figure 2.5.

As the symbols HP en LP in the figure indicate, the wavelet filters are typically high pass: they enhance details, whereas the scaling filters are low pass: they have a smoothing effect, eliminate high frequencies. The Haar filters illustrate this: $\boldsymbol{h} = \tilde{\boldsymbol{h}} = \{1/2, 1/2\}$ and $\boldsymbol{g} = \tilde{\boldsymbol{g}} = \{1/2, -1/2\}$. If the input is a pure wave with pulsation ω , i.e.

$$f_k = \mathrm{e}^{i\omega k},$$

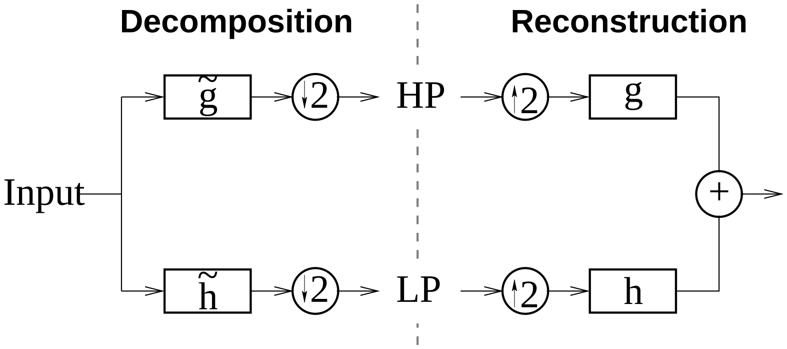

Figure 2.5: One step of a wavelet decomposition and its reconstruction. This is a filter bank: The input is filtered and down-sampled to get a low pass signal LP and a high pass signal HP. Reconstruction starts with up-sampling by introducing zeroes between every pair of points in LP and HP.

convolving with $\boldsymbol{h}$ yields an output $\boldsymbol{y} = \boldsymbol{h} * \boldsymbol{f}$, which in general terms equals:

$$y_k = \sum_{l \in \mathbb{Z}} h_l f_{k-l} = \sum_{l \in \mathbb{Z}} h_l \mathrm{e}^{i\omega(k-l)} \mathrm{e}^{i\omega k} \sum_{l \in \mathbb{Z}} h_l \mathrm{e}^{-i\omega l} = f_k H(\omega).$$

The output is again a pure wave, with the same frequency, but different amplitude and phase. The amplitude depends on the *frequency* ω by (the modulus of) the *frequency response function*

$$H(\omega) = \sum_{l \in \mathbb{Z}} h_l \mathrm{e}^{-i\omega l}.$$

This expression is known as the *Discrete Time Fourier Transform* (DTFT). It is actually the inverse of a Fourier series expansion: the function $H(\omega)$ is 2π-periodic. For the Haar scaling function, this becomes:

$$H(\omega) = \frac{1}{2} + \frac{1}{2}\mathrm{e}^{-i\omega} = \frac{\mathrm{e}^{i\omega/2} + \mathrm{e}^{-i\omega/2}}{2}\mathrm{e}^{-i\omega/2} = \cos(\frac{\omega}{2})\mathrm{e}^{-i\omega/2},$$

for which the amplitude (modulus) $|H(\omega)|$ is plotted on top in Figure 2.6 (Left). This shows that waves with low frequencies ($\omega \approx 0$) are better preserved than high frequencies. Indeed, averaging the strongly oscillating signal

$$\{\ldots, 1, -1, 1, -1, 1, -1, \ldots\},$$

would leave us with a zero output. The situation is different for the detail filter $\boldsymbol{g}$:

$$G(\omega) = \frac{1}{2} - \frac{1}{2}\mathrm{e}^{-i\omega} = \frac{\mathrm{e}^{i\omega/2} - \mathrm{e}^{-i\omega/2}}{2}\mathrm{e}^{-i\omega/2} = \sin(\frac{\omega}{2})i\mathrm{e}^{-i\omega/2},$$

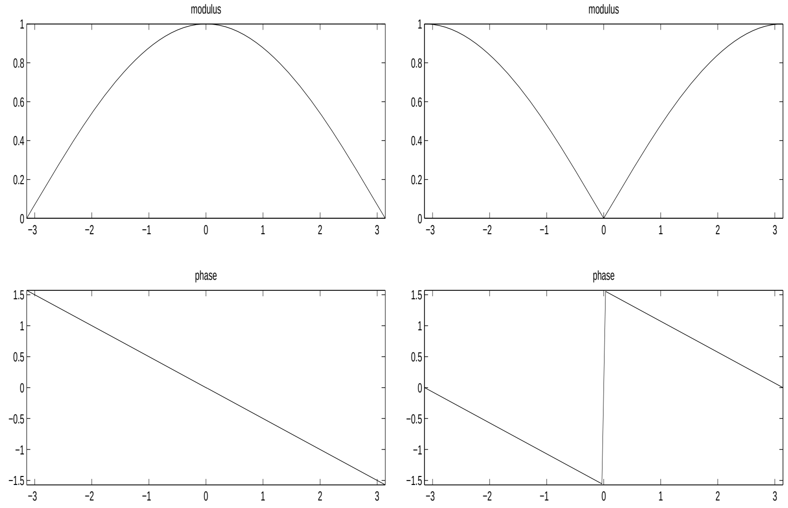

Figure 2.6: Modulus (amplitude) and phase of the frequency response function for the *moving average filter* (Haar low pass filter) $\boldsymbol{h} = \{1/2, 1/2\}$ (Left) and for the *moving difference filter* (Haar high pass filter) $\boldsymbol{g} = \{1/2, -1/2\}$ (Right). Convolution with $\boldsymbol{h}$ suppresses high frequencies, convolution with $\boldsymbol{g}$ suppresses frequencies near to zero.

and the amplitude plot in Figure 2.6 (Top right) illustrates that low frequencies are being suppressed. A non-oscillating signal, like $\{\ldots, 1, 1, 1, \ldots\}$ has no differences at all: a difference filter shows a zero response to this signal.

Figure 2.7 is a schematic overview of a complete wavelet transform of an input signal. In real applications, signals have a finite number N of samples, and also the transform filters have a finite number of taps. Such filters are referred to as *Finite Impulse Response* (FIR) filters. We call $F_{\tilde{h}}$ and $F_{\tilde{g}}$ the length of these filters. From the figure, we conclude that a complete wavelet transform of N data points requires $N-1$ convolutions with $\tilde{\boldsymbol{h}}$ and $N-1$ convolutions with $\tilde{\boldsymbol{g}}$. A convolution with a filter of length F requires F multiplications and $F-1$ additions. The total complexity of the transform is:

$$(N-1)(2F_{\tilde{h}} - 1) + (N-1)(2F_{\tilde{g}} - 1) \sim 2(F_{\tilde{h}} + F_{\tilde{g}})N.$$

A wavelet transform can be computed with a linear amount of flops. Since a general linear transform has square complexity, this is called the *Fast Wavelet Transform* (FWT) [112]. The Fast Fourier Transform (FFT) has complexity $\mathcal{O}(N \log N)$, which is a bit slower than FWT.

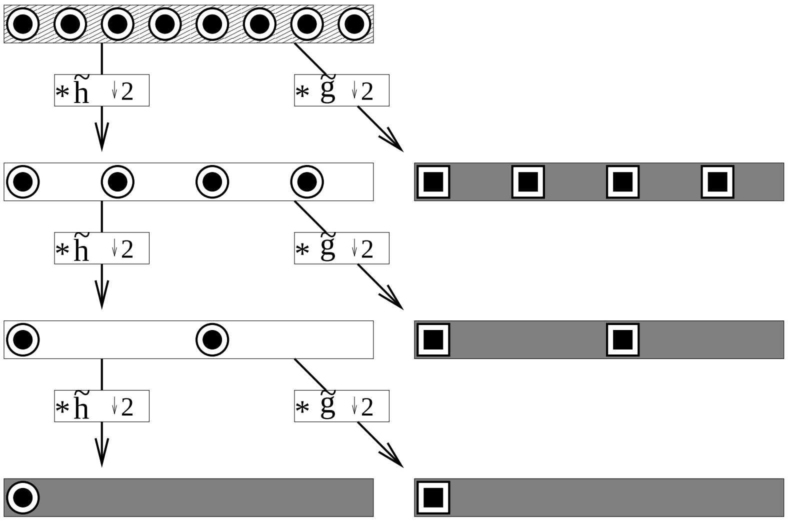

Figure 2.7: Scheme of a Fast Wavelet Transform (FWT). It is computed scale after scale. At each scale, a number of filter operations are needed. Because of subsampling, the number of coefficients to be computed decreases with scale, and this causes the transform to be linear.

2.1.5 Locality

Wavelet basis functions are localized in space (or time, depending on the actual problem being a signal in time or in space, like images) and are scaled versions of one mother function. A wavelet coefficient tells how much of the corresponding wavelet basis function 'is present' in the total signal: a high coefficient means that at the given location and scale there is an important contribution of a singularity. This information is local in *space* (or time) and in *frequency* (frequency is approximately the inverse of scale): it says where the singularity (jump in the input) is and how far it ranges, i.e. how large its scale is.

A pixel representation of an image carries no direct scale information: one pixel value gives no information about neighboring pixels, and so there is no notion of scale. The basis functions corresponding to this representation are *Dirac* impulses, like in Figure 2.9 (a). On the other hand, a Fourier transform uses pure waves (sines and cosines) as basis functions. It displays a complete frequency spectrum of the image or signal but destroys all space or time information. A coefficient with a never ending wave cannot tell anything about the location of one singularity.

No basis function can give exact information on frequency and localization at the same time. Formalizing the notion of *frequency uncertainty* and *space/time*

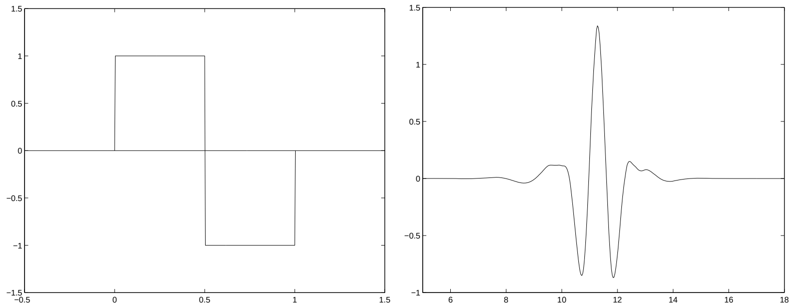

Figure 2.8: Wavelet basis functions for two types of wavelets (Haar and coiflets): these functions live at a specific location and have a specific scale. The coefficient in a signal decomposition that corresponds to this basis function tells how much of this function contributes to the total signal. This information is *local* in space/time *and* frequency.

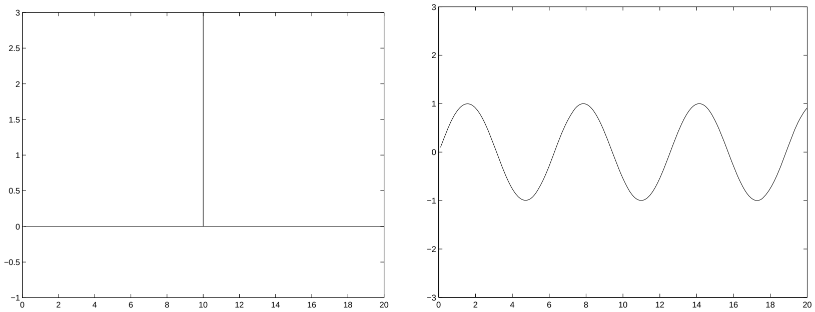

(a) (b)

Figure 2.9: (a) A Dirac impulse is the basis function behind the classical sample representation of a signal or the pixel representation of an image. One coefficient (sample or pixel) gives the exact information on the function value at this location, but tells nothing about the *range* or *scale* of phenomena happening in the image or signal. (b) A sine has a sharp frequency but is not able to capture any information on the localization of singularities.

uncertainty leads to lower bound on the product of both. More precisely, define:

$$\begin{aligned}\overline{x}_\psi &= \frac{\displaystyle\int_{-\infty}^{\infty} |\psi(x)|^2 x dx}{\displaystyle\int_{-\infty}^{\infty} |\psi(x)|^2 dx} \\ \Delta x_\psi{}^2 &= \frac{\displaystyle\int_{-\infty}^{\infty} |\psi(x)|^2 (t-\overline{x}_\psi)^2 dx}{\displaystyle\int_{-\infty}^{\infty} |\psi(x)|^2 dx}\end{aligned}$$

and let $\overline{\omega}_\Psi$ and $\Delta\omega_\Psi{}^2$ be similar entities in the Fourier domain, then:

$$\Delta x_\psi \Delta\omega_\Psi \geq \frac{1}{2} \text{ or } \Delta x_\psi{}^2 \Delta\omega_\Psi{}^2 \geq \frac{1}{4}.$$

This is Heisenberg's uncertainty principle, mainly known from physics, but actually a purely mathematical inequality [133].

Not only a wavelet coefficient carries local *information*, manipulating it causes a local *effect*, both in space and in frequency. Signal or image processing by operating on wavelet coefficients permits good control on what the algorithm is actually doing.

The idea of locality in time *and* frequency is far from new. The notes of a music score for instance indicate which tone (frequency) should sound at a given moment (time). One could phrase that the score is an approximate wavelet transform of the music signal. This inspires people looking for applications of wavelet theory in music [50].

2.1.6 Vanishing moments

Not surprisingly, the sparsity property plays an important role in wavelet compression algorithms. As we explain in Section 2.5, it is also the basis for noise reduction by wavelet coefficient thresholding. To create a really sparse representation, we try to make coefficients that live between points of singularities as small as possible. In these intervals of smooth behavior, the signal can be locally well approximated by a polynomial. Therefore, we are interested in polynomials having zero coefficients. If all monomials up to a degree $p-1$ satisfy

$$\langle x^n, \tilde{\psi}\rangle = 0,\ n = 0, \ldots, p-1, \tag{2.14}$$

we are sure that the first p terms in a Taylor approximation of an analytic function do not contribute to the wavelet coefficient, provided that there is no singularity in the support of the corresponding dual wavelet. The highest p for which (2.14) holds, is called the (dual) *number of vanishing moments*. For $n < p$, this implies

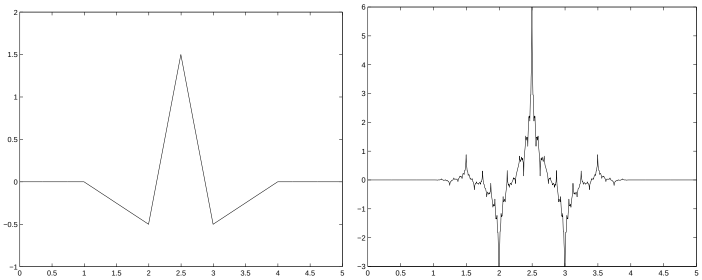

Figure 2.10: Primal and dual wavelet function with two vanishing moments from the Cohen-Daubechies-Feauveau family. The smoother function is preferably used as synthesis (primal) wavelet, and the other one then serves as dual or analysis wavelet.

that $x^n \in V_j, \forall j \in \mathbb{Z}$: all polynomials up to a degree equal to the *dual* number of vanishing moments rest within the scaling spaces V_j of the *primal* MRA. Indeed, all detail (wavelet) coefficients of these functions are zero. Each vanishing moment imposes a condition on $\tilde{\psi}$, and so on the wavelet filter $\tilde{\boldsymbol{g}}$. More equations lead to longer filters, and longer filters correspond to basis functions with larger support [133]. This is why we cannot increase the number of vanishing moments *ad infinitum*: the price to pay is loss of locality, the basis functions grow wider and have more chance to get in touch with some of the singularities.

Primal vanishing moments are less important for signal processing applications. We do however prefer at least one vanishing moment, i.e. a zero mean wavelet: this allows for better control of the impact on the output energy of coefficient manipulations. Primal wavelets should be as smooth as possible: each manipulation of a coefficient (for instance thresholding) is actually making a difference between output and input coefficient. After reconstruction, this corresponds to subtracting the corresponding wavelet from the original signal. A non-smooth wavelet shows up in this reconstruction. Vanishing moments are an indication of smoothness, but no guarantee, as illustrates the plot of two biorthogonal wavelets from the Cohen-Daubechies-Feauveau (CDF) [38] family in Figure 2.10. Both primal and dual wavelet have two vanishing moments, but they are clearly not equally smooth. The smoother one is the best candidate for the role of primal (syntheses) wavelet. The other one serves as analysis wavelet.

2.1.7 Two-dimensional wavelet transforms

In applications like digital image processing, we need a two-dimensional transform. Although much effort has been and is still being devoted to general, non-separable 2D wavelets [131, 98, 97, 141], this discussion limits itself to separable

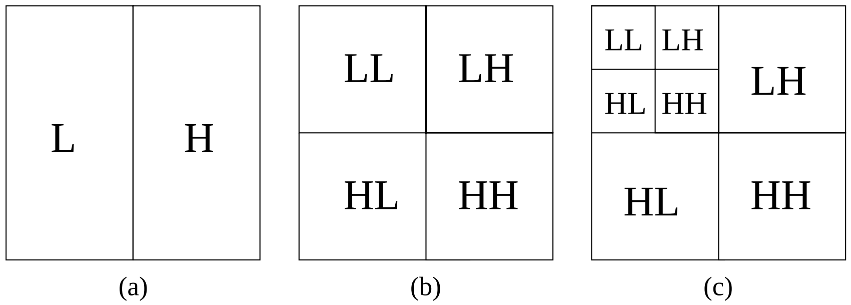

Figure 2.11: A two-dimensional wavelet transform. First we apply one step of the one dimensional transform to all rows (a). Then, we repeat the same for all columns (b). In the next step, we proceed with the coefficients that result from a convolution with $\tilde{\boldsymbol{h}}$ in both directions (c).

2D transforms, i.e. consecutive one-dimensional operations on columns and rows of the pixel matrix. We have two constructions of separable transforms:

1. the square wavelet transform
   The square wavelet transform first performs one step of the transform on all rows, yielding a matrix where the left side contains down-sampled lowpass coefficients of each row, and the right contains the highpass coefficients, as illustrated in Figure 2.11 (a). Next, we apply one step to all columns, this results in four types of coefficients:

   (a) coefficients that result from a convolution with $\tilde{\boldsymbol{g}}$ in both directions (HH) represent diagonal features of the image.

   (b) coefficients that result from a convolution with $\tilde{\boldsymbol{g}}$ on the columns after a convolution with $\tilde{\boldsymbol{h}}$ on the rows (HL) correspond to horizontal structures.

   (c) coefficients from highpass filtering on the rows, followed by lowpass filtering of the columns (LH) reflect vertical information.

   (d) the coefficients from lowpass filtering in both directions are further processed in the next step.

   At each level, we have three *components*, *orientations*, or *subbands*: vertical, horizontal and diagonal. If we start with:

$$f(x,y) = \sum_{k\in\mathbb{Z}} \sum_{l\in\mathbb{Z}} s_{J,k,l}\varphi_{J,k}(x)\varphi_{J,l}(y)$$

the transform decomposes this into:

$$\begin{aligned} f(x,y) &= \sum_{k\in\mathbb{Z}}\sum_{l\in\mathbb{Z}} s_{L,k,l}\varphi_{L,k}(x)\varphi_{L,l}(y) \\ &+ \sum_{j=L}^{J-1}\sum_{k\in\mathbb{Z}}\sum_{l\in\mathbb{Z}} w_{j,k,l}^{\mathrm{HH}}\psi_{j,k}(x)\psi_{j,l}(y) \\ &\qquad\qquad +w_{j,k,l}^{\mathrm{LH}}\psi_{j,k}(x)\varphi_{j,l}(y) \\ &\qquad\qquad +w_{j,k,l}^{\mathrm{HL}}\varphi_{j,k}(x)\psi_{j,l}(y) \end{aligned}$$

2. The rectangular wavelet transform

   Instead of proceeding with the LL-coefficients of the previous step only, we could also further transform all rows and all columns in each step. This leads to the *rectangular* two-dimensional wavelet transform, illustrated in Figure 2.12.

   If $\boldsymbol{w} = \tilde{W}\boldsymbol{y}$ is the matrix representation of a 1D wavelet transform, then the rectangular transform, applied to an image $\boldsymbol{I}$ is:

   $$\tilde{W}\boldsymbol{I}\tilde{W}^T$$

   The basis corresponding to this decomposition contains functions that are tensor products of wavelets at *different* scales:

   $$\psi_{j,k}(x)\psi_{i,l}(y)$$

   Such functions do not appear in the basis of a square wavelet transform.

   This alternative not only requires more computation, it is also less useful in applications: in the *square* wavelet transform, the HL and LH components contain more specific information on horizontal or vertical structures.

2.2 Continuous wavelet transform

So far, this text has been discussing the *Discrete Wavelet Transform* (DWT). In many applications, also in image analysis and even image processing [10, 9], the *continuous* wavelet transform (CWT) plays an important role. Although both are related to a certain degree, the CWT starts from a quite different point of view. There is no multiresolution analysis here, at least not in the sense of the mathematical definition, nor is there any father function involved. The theory immediately introduces a wavelet function $\tilde{\psi}(x)$ and a corresponding wavelet transform $F(a,b)$ of a function $f(x) \in L_2[0,1]$:

$$F(a,b) = \langle f, \tilde{\psi}_{a,b}\rangle, \qquad (2.15)$$

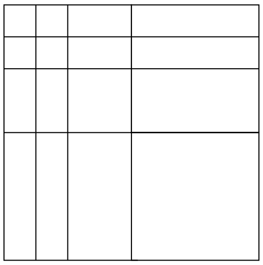

Figure 2.12: Graphical representation of wavelet coefficients after three steps of the rectangular wavelet transform: in each step all rows and all columns are completely further transformed.

where $a \in \mathbb{R}_0^+, b \in \mathbb{R}$ and

$$\tilde{\psi}_{a,b}(x) = \frac{1}{\sqrt{a}}\tilde{\psi}\left(\frac{x-b}{a}\right).$$

The notion of scale enters into this transform through the *continuous* parameter a.

In principle, we allow all function $\tilde{\psi}(x)$ to play the role of wavelet, provided they guarantee a reconstruction of the input signal through:

$$f(x) = \frac{1}{C_{\tilde{\psi}}}\int_{-\infty}^{\infty}\int_{-\infty}^{\infty} F(a,b)\tilde{\psi}_{a,b}(x)\frac{dadb}{a^2}. \tag{2.16}$$

So, for invertibility, we need the constant $C_{\tilde{\psi}}$ to be finite. This is the admissibility condition:

$$C_{\tilde{\psi}} = \int_{-\infty}^{\infty}\frac{\tilde{\Psi}(\omega)}{\omega}d\omega < \infty.$$

In this expression, $\tilde{\Psi}(\omega)$ stands for the Fourier transform of $\tilde{\psi}(x)$. In most cases, the admissibility condition is satisfied if the pole in the integrand is neutralized by a zero of $\tilde{\Psi}(\omega)$, this is:

$$\tilde{\Psi}(0) = \int_{-\infty}^{\infty}\tilde{\psi}(x)dx = 0.$$

Functions $\tilde{\psi}(x)$ with zero integral typically show a oscillating behavior, hence the name wavelets.

No other condition rests on the wavelets in a continuous transform. All wavelets from the DWT-theory remain good candidates here, other important functions do not fit into a MRA, but are often used in CWT. Examples are the Morlet wavelet:

$$\tilde{\psi}(x) = \mathrm{e}^{i\omega_0 x}\mathrm{e}^{-x^2/2\sigma_0^2},$$

and the Mexican hat wavelet:

$$\tilde{\psi}(x) = (1 - x^2)\mathrm{e}^{-x^2/2}.$$

This is the second derivative of a Gaussian.

The CWT is highly redundant: it maps a 1D signal into a bivariate function. Obviously, this transform has other applications than the DWT. Whereas the latter appears in fast algorithms for signal- and image *processing* (reconstruction, synthesis), a continuous transform is mainly useful for the *characterization* of signals (analysis). The evolution of $F(a,b)$ as a function of a gives information about smoothness at location b. Loosely spoken, if at location b, the value of $F(a,b)$ increases for small scales, we may expect a short range singularity, such as noise. Large values at coarse scales indicate a long range singularity, typically an important signal feature. A singularity at position b also affects a neighborhood. The evolution of this *cone of influence* across scales a is another regularity indicator. A CWT distinguishes different types of signal singularities, including oscillating singularities [12], and noise. *Uniform* regularity is reflected by the decay of the Fourier transform, but a CWT is able to detect *local* regularity [113, 109]. Section 3.5.4 discusses how a DWT is the appropriate tool for functions with *global* but *piecewise* regularity properties.

2.3 Non-decimated wavelet transforms and frames

Historically, the continuous wavelet transform came first. The link with filter banks and multiresolution only became clear at the end of the eighties [112]. If the wavelet function $\tilde{\psi}(x)$ fits into a MRA, discretizing the continuous wavelet transform by:

$$a = 2^{-j}k \text{ and } b = 2^{-j}$$

leads to the DWT. If there is no MRA however, associated with the wavelet function, this discretization scheme does not allow for a simple reconstruction.

When performing a CWT on a computer, it is common to discretize the location parameter a at sample frequency, this is:

$$a_{j,k} = 2^{-j}k,$$

independent from scale j. This yields the same number of

$$w_{j,k} = F(a_{j,k}, b_j) = \langle f, \tilde{\psi}_{a_{j,k},b_j} \rangle$$

at each scale. Therefore, this is an overcomplete data representation. The functions $\tilde{\psi}_{a_{j,k},b_j}$ do not possibly constitute a basis, because of the oversampling of a. For

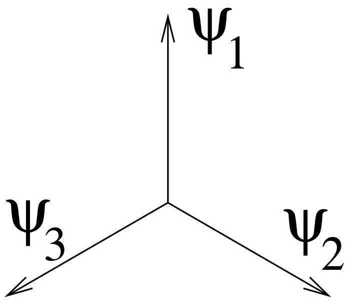

Figure 2.13: An example of a *tight* frame in $\mathbb{R}^2$. It holds for all vectors $\boldsymbol{f} \in \mathbb{R}$ that: $\boldsymbol{f} = \sum_{i=1}^{3} \langle f, \psi_i \rangle \psi_i$.

ease of notation, we write $\tilde{\psi}_{j,k}$ from now on. This set of functions is called a *frame* if

$$\exists A, B \in \mathbb{R}_0^+, \forall f \in L_2[0,1] : A\|f\|^2 \leq \sum_{j,k \in \mathbb{Z}} \langle f, \tilde{\psi}_{j,k} \rangle \leq B\|f\|^2. \qquad (2.17)$$

In that case, we can find functions $\psi_{j,k}$ and reconstruct the input as:

$$f(x) = \sum_{j,k \in \mathbb{Z}} \langle f, \tilde{\psi}_{j,k} \rangle \psi_{j,k} = \sum_{j,k \in \mathbb{Z}} w_{j,k} \psi_{j,k}.$$

The set $\{\psi_{j,k}, j, k \in \mathbb{Z}\}$ shows of course the same degree of redundancy. Figure 2.13 contains a frame in $\mathbb{R}^2$. In this case, the sets $\{\psi_{j,k}\}$ and $\{\tilde{\psi}_{j,k}\}$ coincide. This is called a *tight* frame; in terms of the frame constants, this situation corresponds to the case $A = B$.

A typical example of a wavelet frame follows from a dyadic discretization of the scale parameter *b*:

$$b = 2^{-j}, j = L, \ldots, J-1.$$

The frame consists of translations and dyadic dilations of one mother function:

$$\tilde{\psi}_{j,k}(x) = \tilde{\psi}(2^j x - 2^{j-J} k).$$

If the mother wavelet fits into a MRA, the frame coefficients follow from a multiscale filter algorithm, very similar to the fast wavelet transform algorithm, using filter banks. More precisely, as Figure 2.14 explains, this transform results from omitting the sub-sampling step in a classical wavelet algorithm. Thinking of this transform as an extension of the FWT, we want of course this overcomplete representation to be *consistent* with the decimated version, in the sense that all the

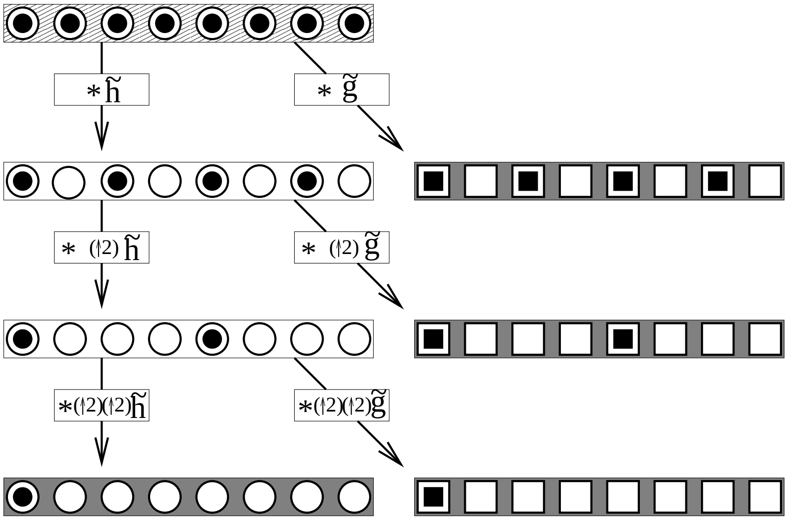
$* \tilde{h}$
$* \tilde{g}$
$* (\uparrow 2) \tilde{h}$
$* (\uparrow 2) \tilde{g}$
$*(\uparrow 2)(\uparrow 2)\tilde{h}$
$*(\uparrow 2)(\uparrow 2)\tilde{g}$

Figure 2.14: The redundant wavelet transform. The points with a black center represent coefficients that also appear in the decimated transform. To be consistent with this decimated transform, we should make sure that we only combine intermediate results from the original transform in our computation of coefficients "with a black center". To this end, we insert at each level, new zero elements between the filter coefficients of the previous step. This up-sampling operation is represented by $(\uparrow 2)$.

decimated coefficients re-appear in our new transform. To compute, for instance, the wavelet coefficients on the one but finest resolution level, we cannot, like in the decimated case, just convolve the scaling coefficients of the previous step with the high frequency filter $\tilde{\boldsymbol{g}}$. If we want to get the original coefficients among our redundant set, we have to skip the extra coefficients of the previous step before the actual convolution. Of course these extra coefficients serve in their turn to complete the redundant set of wavelet coefficients at the given resolution level. A similar procedure is necessary for the computation of the scaling coefficients at the next level. At each level, the number of coefficients to skip, increases as a power of two minus one. As a matter of fact, instead of sub-sampling the coefficients, this alternative introduces up-sampling of the filters $\tilde{\boldsymbol{h}}$ and $\tilde{\boldsymbol{g}}$. Indeed, the wavelet and scaling coefficients at a certain resolution level can be seen as the result of a convolution with filters that are obtained by inserting zeros between the filter coefficients of the previous step. This adaptation preserves the multiresolution character of the wavelet transform: the synthesis frame functions are now:

$$\psi_{j,k}(x) = \psi(2^j x - 2^{j-J} k).$$

Orthogonal wavelet transforms have that $\tilde{\psi}(x) = \psi(x)$. In this redundant scheme, we get a tight frame. This does not mean that all tight frames are built up from an orthogonal transform, as Figure 2.13 illustrates. But the properties of a tight frame are similar to those of an orthogonal basis, just as a general frame recalls the properties of a Riesz basis.

For obvious reasons, the scheme in Figure 2.14 is known as *Non-decimated wavelet transform*, or *Redundant Wavelet Transform*. Other nomenclature includes *Stationary Wavelet Transform*, referring to the translation invariance property. This transform appears in several papers [100, 101, 117, 126, 108], for various reasons, some of which we mention in Section 5.3, while discussing the applicability of this oversampled analysis in noise reduction.

2.4 Lifting and second generation wavelets

2.4.1 The idea behind lifting

Beside the extension of the *Haar* transform to a filter bank algorithm, there exists another way of generalizing the exploration of intersample correlations: the lifting scheme [138, 135, 136]. Figure 2.15 illustrates the idea. First the data are split into even and odd samples. Both parts are highly correlated. The scheme then *predicts* the odd samples using the information from the even ones. A typical example is an interpolating polynomial . Figure 2.16 shows a cubic interpolating prediction. This prediction is called *dual lifting* for reasons explained below. Subtracting this prediction from the actual odd values leads to the detail or wavelet coefficients. Dual lifting for a Haar transform is particularly simple: an odd sample is predicted

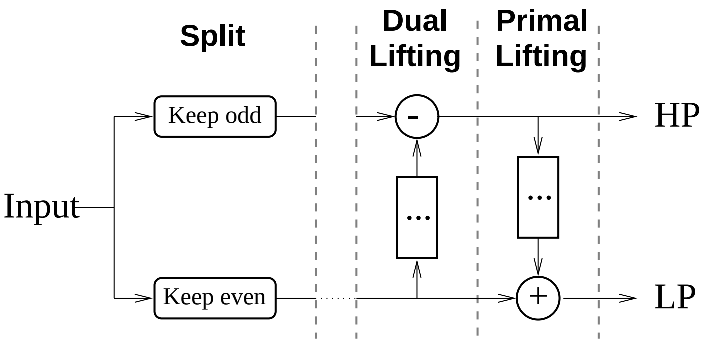

Figure 2.15: Decomposition of a filter bank into lifting steps. The first type of lifting is called *dual lifting* or a *prediction step*. The other type is *primal lifting* or *update*.

by the value of its left even neighbor, the difference between them is the wavelet coefficient. As in the filter bank algorithm, these detail coefficients are typically small on intervals of smooth signal behavior. Staying with this one prediction step is however not sufficient to build all types of wavelet transforms. Concentrating on the Haar case, for instance, we see that we did not compute the *average* of the two subsequent samples, only the difference. As a consequence, the *meaning* of the coefficients is different, i.e. the basis functions are not those of Figure 2.3. Indeed, the detail coefficient does not indicate how far two input data are below and above the common mean value, but rather how far the second, odd point is from the first, even one. The corresponding detail basis function is a single block, not a block wave. Therefore, we want to *update* the *meaning* (interpretation) of the detail coefficient without changing its *value*. We replace the *even* sample by the average of the two consecutive values. Since

$$\mathrm{average} = \frac{\mathrm{even} + \mathrm{odd}}{2} = \mathrm{even} - \frac{\mathrm{even} - \mathrm{odd}}{2} = \mathrm{even} - \frac{\mathrm{difference}}{2},$$

we compute this average by adding an *update* based on the detail coefficients to the even samples. Because this lifting step changes the synthesis or primal wavelet basis function (the ‘interpretation’ of the coefficient), it is called the primal lifting step. This primal lifting step may be followed by a new dual step and so on. Each step adds more properties — for instance more vanishing moments — to the overall transform: it is a gradual increase in complexity, hence the name lifting. All classical filter bank algorithms can be decomposed into an alternating sequence of primal and dual lifting steps [49]. This decomposition has several advantages: it generally saves computations, although the order of complexity obviously cannot be better than $\mathcal{O}(N)$ as for the classical FWT. Figure 2.15 learns that the result of each dual and primal filtering step with input from one branch is simply added

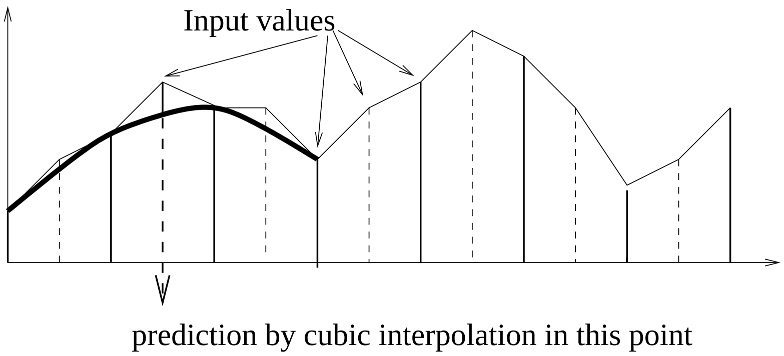

Figure 2.16: A cubic interpolation as a prediction operator. The thin, piecewise linear line links the input data. The bold line is an example of a cubic polynomial, interpolating 4 successive points with even index.

to the other branch. The result of this addition may be stored immediately at the place of the output branch coefficients. The transform is *in place* (computation), it requires no additional working memory. The inverse transform is easy to construct: it uses the same filters in the opposite order and subtracts the result that had been added in the forward transform and vice versa. In the classical filterbank setting, complicated biorthogonality conditions for perfect reconstruction rest on the filter coefficients: these are solved using Fourier techniques. The most important property of lifting is its generality: the dual and primal lifting steps are by no means limited to the classical, linear filter operations. This opens the way to a new, 'second generation' of wavelets. The next sections discuss two examples of these new wavelets.

2.4.2 The integer wavelet transform

In many applications, like digital image processing, the input data are integer numbers. The filters of a wavelet transform are mostly fractions or even irrational numbers, and so is then the output. Performing the transform requires floating point computation *and* storage. The lifting scheme *an sich* does not bring any remedy to this: the coefficients remain the same, regardless of the way of computing, but Figure 2.17 shows that rounding the filter outputs creates a transform that maps integers to integers, called the *Integer Wavelet Transform* [26]. Rounding is not possible in a classical filterbank scheme, since this would destroy perfect reconstruction. In the lifting scheme, the input of each filter operation remains available after this step has been concluded. Going back is always possible by recomputing the filter result.

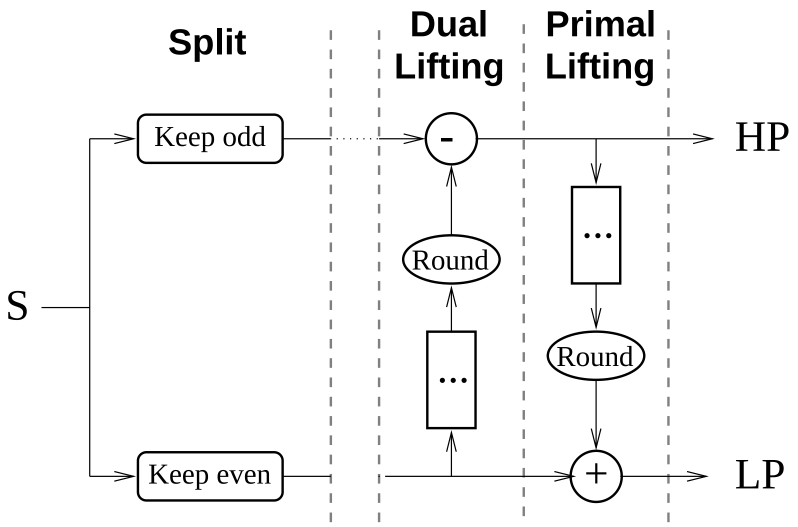

Figure 2.17: Integer wavelet transform.

2.4.3 Non-equidistant data

The lifting philosophy is by no means limited to equidistant samples [137]. The idea of interpolation, for instance, can be extended to an irregular grid, as shows Fig. 2.18 in the case of linear interpolation. Of course, one could forget about the grid where the input data live on, just treat these points as if they were regular and apply a classical wavelet transform. This does not correspond to reality. For instance, if there is large gap in the measurements, there may be an important difference in signal values in the two end points of this gap, just because they are so far away from each other. If we consider them as samples at uniform distances, it looks as if there is an important singularity at this place. This is obviously a wrong

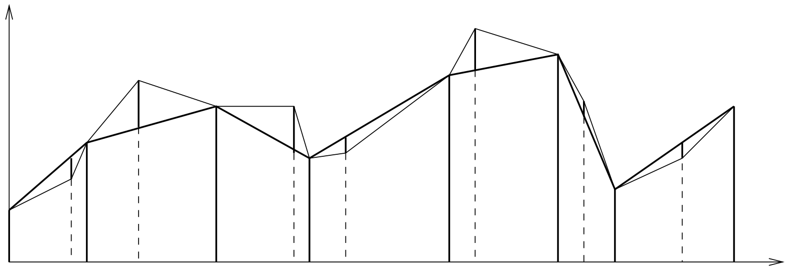

Figure 2.18: Linear prediction operator on an irregular grid.

analysis. On the synthesis side we have basis functions with a given smoothness on a regular grid. If we stretch the sample points to fit within the irregular grid, this smoothness is lost. In other words, if we process the wavelet coefficients, the grid irregularity shows up in the result after reconstruction. A scheme that takes into account the grid structure guarantees a smooth reconstruction on this grid [48].

2.5 Noise reduction by thresholding wavelet coefficients

2.5.1 Noise model and definitions

Most noise reduction algorithms start from the following additive model of a discrete signal $\boldsymbol{f}$ of N data points corrupted with noise $\boldsymbol{\eta}$:

$$\boldsymbol{y} = \boldsymbol{f} + \boldsymbol{\eta}. \tag{2.18}$$

The vector $\boldsymbol{y}$ represents the input signal. The noise is a vector of random variables, while the untouched values $\boldsymbol{f}$ are a purely deterministic signal. We call N the length of these vectors. Some descriptions start from a full stochastic model, letting the uncorrupted values be an instance from a random distribution. This leads to Bayesian estimators, as we explain later.

We suppose that the noise has zero mean, i.e. $\mathrm{E}\boldsymbol{\eta} = \mathbf{0}$ and define

$$Q = \mathrm{E}[(\boldsymbol{\eta} - \mathrm{E}\boldsymbol{\eta})(\boldsymbol{\eta} - \mathrm{E}\boldsymbol{\eta})^T] = \mathrm{E}\boldsymbol{\eta}\boldsymbol{\eta}^T$$

the covariance matrix of $\boldsymbol{\eta}$. On the diagonal we find the variances $\sigma_i^2 = \mathrm{E}\eta_i^2$. If this matrix is diagonal, i.e. if $\mathrm{E}\eta_i\eta_j = 0$ for $i \neq j$, the noise is called *white* or *uncorrelated*. If all the data points come from the same probability density, we say that the points are *identically distributed*. This implies of course

$$\sigma_i^2 = \sigma^2, \forall i = 1 \ldots N.$$

Noise with constant variance is called *homoscedastic*. Non-homoscedastic noise is heteroscedastic. Homoscadastic, white noise has a simple covariance matrix:

$$Q = \sigma^2 I.$$

Stationarity also involves the correlation between successive observations: the distance between two observations only determines whether and how much these data are mutually dependent. In the special case of second order stationarity, the covariance between two data points only depends on the distance between these two observations. This text mostly assumes second order stationary data. This always includes homoscedasticity.

An important density model is the joint Gaussian:

$$\phi_{\boldsymbol{\eta}}(\boldsymbol{\eta}) = \frac{1}{(2\pi)^{N/2}\sqrt{\det Q}}\ \mathrm{e}^{-\frac{1}{2}\boldsymbol{\eta}^T Q^{-1}\boldsymbol{\eta}}.$$

If Gaussian noise variables are uncorrelated, they are also *independent*. The reverse implication holds for all densities. A classical assumption in regression theory is that of independent, identically distributed noise (i.i.d.). For Gaussian variables this is equivalent with supposing stationary and white noise.

2.5.2 The wavelet transform of a signal with noise

The linearity of a wavelet transform leaves the additivity of model (2.18) unchanged. We get:

$$\boldsymbol{w} = \boldsymbol{v} + \boldsymbol{\omega}, \tag{2.19}$$

where $\boldsymbol{v}$ is the vector of uncorrupted (untouched, noise-free) wavelet coefficients, $\boldsymbol{\omega}$ contains the wavelet transform of the noise and $\boldsymbol{w}$ are the observed wavelet coefficients:

$$\begin{array}{rcl} \boldsymbol{w} & = & \tilde{W}\boldsymbol{y}, \\ \boldsymbol{v} & = & \tilde{W}\boldsymbol{f}, \\ \boldsymbol{\omega} & = & \tilde{W}\boldsymbol{\eta}. \end{array}$$

As before, $\tilde{W}$ is the forward wavelet transform matrix.

With these definitions, it is easy to prove that the covariance matrix of the noise in the wavelet domain $S = \mathrm{E}\boldsymbol{\omega}\boldsymbol{\omega}^T$ equals:

$$S = \tilde{W}Q\tilde{W}^T. \tag{2.20}$$

This equality holds for a general linear transform $\tilde{W}$.

If $\tilde{W}$ is a one-dimensional wavelet transform, this can be interpreted as the *rectangular* wavelet transform of the correlation matrix of the data vector. This should not be confused with the fact that we use a square wavelet transform for the decomposition of 2D data, like images.

If $\tilde{W}$ is orthogonal and $Q = \sigma^2 I$, then we have that $S = \sigma^2 I$. This means that:

Observation 2.1 *An* orthogonal *wavelet transform of* stationary *AND* white *noise is* stationary *AND* white.

A wavelet transform decorrelates a signal with structures. It leaves uncorrelated noise uncorrelated. Figure 2.19 illustrates what this means for the wavelet transform of a signal with noise. The noise is spread out evenly over all coefficients,

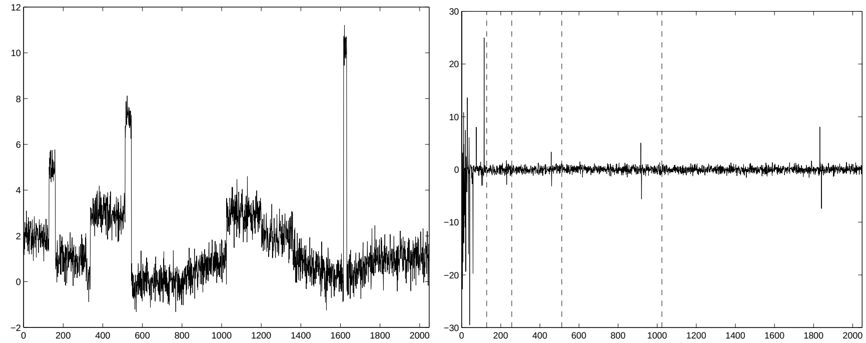

Figure 2.19: Test signal with stationary and white noise (Left) and Haar transform (Right): this is an orthogonal wavelet transform. The noise is spread out equally over all the coefficients, and the important signal singularities are still distinguishable from this noisy coefficients.

and the important signal singularities are still distinguishable from this noisy coefficients. The situation becomes slightly more complicated in the case of non-orthogonal transforms or correlated noise. Chapter 5 discusses these cases. For this and the next two chapters, we work with stationary, white noise and orthogonal transforms.

2.5.3 Wavelet thresholding, motivation

The plot of wavelet coefficients in Figure 2.19 suggests that small coefficients are dominated by noise, while coefficients with a large absolute value carry more signal information than noise. Replacing the smallest, noisy coefficients by zero and a backwards wavelet transform on the result may lead to a reconstruction with the essential signal characteristics and with less noise. More precisely, we motivate this idea by three observations and assumptions:

1. The decorrelating property of a wavelet transform creates a sparse signal: most untouched coefficients are zero or close to zero.

2. Noise is spread out equally over all coefficients.

3. The noise level is not *too* high, so that we can recognize the signal and the signal wavelet coefficients.

If we replace all coefficients in Figure 2.19 with magnitude below a well chosen *threshold* $\lambda = 1$, we get wavelet coefficients as in Figure 2.20. The Figure also shows the corresponding reconstructed signal, which is indeed less noisy than the input. Wavelet thresholding combines simplicity and efficiency and therefore it is

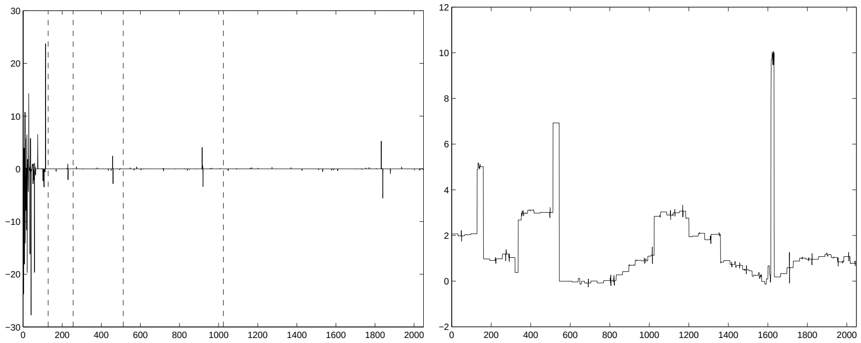

Figure 2.20: Wavelet coefficients after soft-thresholding with threshold $\lambda = 1$ (Left) and reconstruction by inverse Haar transform (Right).

an extensively investigated noise reduction method [55, 60, 56, 32]. The sparsity of representation also motivates the use of wavelets for compression applications and so there are links between compression and noise reduction: wavelet compression techniques show a noise suppressing effect [140] and thresholding based on the technique of context modeling [31, 30] or on the principle of Minimum Description Length (MDL) [77] allows for simultaneous noise reduction and compression.

2.5.4 Hard- and soft-thresholding, shrinking

Until now we have suggested a procedure in which small coefficients are removed, while the others are left untouched. This ‘keep-or-kill’ procedure is called *hard-thresholding*. Figure 2.21(a) plots the output coefficient versus the input. An alternative for this scheme is soft-thresholding, illustrated in Figure 2.21(b): coefficients above the threshold are shrunk in absolute value. The amount of shrinking equals the threshold value, so that the input-output plot becomes continuous. While at first sight hard-thresholding may seem a more natural approach, the continuity of the soft-thresholding operation has important advantages. In the analysis of algorithms it may be mathematically more tractable. Some algorithms even do not work in combination with hard-thresholding. This is the case for the GCV procedure of Chapter 4. As becomes clear through the next chapters, pure noise coefficients may pass a threshold. In the hard-thresholding scheme, they appear in the output as annoying, spurious ‘blips’. Soft-thresholding shrinks these false structures.

A compromise is a more continuous approach as in Figure 2.21(c). It preserves the highest coefficients and has a smooth transition from noisy to important coefficients. Several functions have been proposed [23, 65]. Some of these depend on

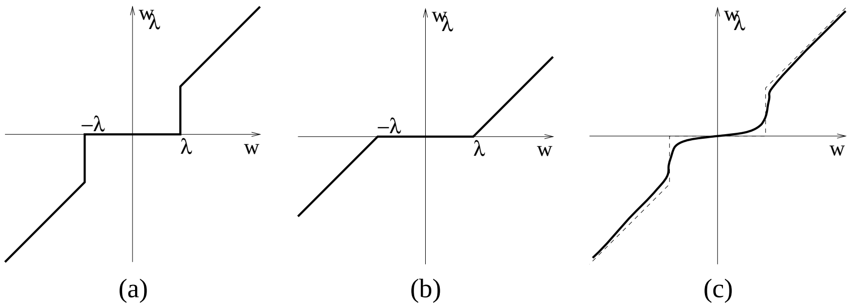

Figure 2.21: Noise reduction by wavelet shrinking. (a) Hard-thresholding: a wavelet coefficient w with an absolute value below the threshold λ is replaced by 0. Coefficients with an absolute value above the threshold are kept. (b) Soft-thresholding: Coefficients with magnitude above the threshold are shrunk. (c) a more sophisticated shrinking function.

more than one threshold parameter, others do not introduce any threshold explicitly. An important class of these methods result from a Bayesian modeling of the noise-reduction problem, as we discuss in Section 2.6. In general, these sophisticated shrinking schemes are computationally more intensive. Soft-thresholding is a trade-off between a fast and straightforward method and a continuous approach.

2.5.5 Threshold assessment

A central question in many threshold procedures is how to choose the threshold. As we explain in Chapter 3, a threshold is a trade-off between closeness of fit and smoothness. A small threshold yields a result close to the input, but this result may still be noisy. A large threshold on the other hand, produces a signal with a lot of zero wavelet coefficients. This sparsity is a sort of smoothness: the output has a simple, smooth representation in the chosen basis. Paying too much attention to smoothness however destroys some of the signal singularities, in image processing, it may cause blur and artifacts.

Literature contains a bunch of papers devoted to this problem of threshold selection. The next two chapters describe a method that looks for the minimum mean square error threshold: this threshold minimizes the error of the result as compared with the noise-free data. Since these data are unknown, the error cannot be computed or minimized exactly. Estimating the minimum is a topic in some papers [61, 89, 116, 115].

The *universal threshold* [56, 62] pays attention to smoothness rather than to minimizing the mean square error. We discuss this well known threshold in Chapter 3. This threshold comes close to the minimax threshold, i.e. the threshold that minimizes the worst case mean square error in a typical function space [59].

Other methods consider wavelet coefficient selection as an example of (multiple) hypothesis testing [2, 125, 124].

2.5.6 Thresholding as non-linear smoothing

There is a formal way to demonstrate that thresholding is a particular example of a more general class of smoothing algorithms. These algorithms typically look for a compromise between closeness of fit and smoothness. Smoothness, or sparsity, can be expressed by some measure of 'entropy', which should be minimized. On the other hand, for closeness of fit, the algorithms use an error 'energy' term, mostly the norm of the difference between input and output. A smoothing parameter λ takes care of the compromise between these two and the algorithm minimizes:

$$\|\boldsymbol{w}_{\boldsymbol{\lambda}} - \boldsymbol{w}\|^2 + \lambda \mathcal{E}(\boldsymbol{w}_{\boldsymbol{\lambda}}), \tag{2.21}$$

where $\mathcal{E}(\boldsymbol{w}_{\boldsymbol{\lambda}})$ is the entropy of the output.

For this entropy there exist many expressions.

1. Using the ℓ_2 norm

   $$\mathcal{E}(\boldsymbol{w}_{\boldsymbol{\lambda}}) = \|\boldsymbol{w}_{\boldsymbol{\lambda}}\|^2$$

   leads to a linear shrinking operation:

   $$\boldsymbol{w}_{\boldsymbol{\lambda}} = \frac{1}{1+\lambda}\boldsymbol{w}.$$

   By linearity of the wavelet transform, this would correspond to shrinking the untransformed data, unless we leave the scaling coefficients untouched, but even then, this operation does not make so much sense: the ℓ_2 norm is measure of energy, not sparsity or entropy.

   We could make the contributions level-dependent:

   $$\mathcal{E}(\boldsymbol{w}_{\boldsymbol{\lambda}}) = \sum_{j=L}^{J-1} \gamma_j \|\boldsymbol{w}_{\boldsymbol{\lambda},\boldsymbol{j}}\|^2,$$

   Taking $\lambda_j = \lambda\gamma_j$, we see this is equivalent to a level-dependent shrinking:

   $$\boldsymbol{w}_{\boldsymbol{\lambda},\boldsymbol{j}} = \frac{1}{1+\lambda_j}\boldsymbol{w}_{\boldsymbol{j}}.$$

   The smoothing parameters could be chosen to optimize the mean square error of the result, although in practical applications, this error cannot be computed exactly. We could limit the possibilities *a priori* to:

   $$\begin{aligned} \lambda_j &= 0 \quad \text{for} \quad j = L, \ldots, K-1, \\ \lambda_j &= \infty \quad \text{for} \quad j = K, \ldots, J-1 \end{aligned}$$

This means: keep the first coefficients, in this case the coefficients at low resolution levels, and throw away the next ones at finer scales. Keeping the *first* is always a linear operation. Now K is acting as smoothing parameter.

2. Keeping the *largest* coefficients is a *non-linear* operation, it corresponds to minimizing:

$$\sum_{i=1}^{N}\left(|w_{\lambda i}-w_i|^k+\lambda^k x(w_{\lambda i})\right).$$

In this expression the *label* $x(w)$ is zero if the output $w_{\lambda i}$ is exactly zero, and one in all other cases. For all k, this leads to hard-thresholding:

$$\begin{aligned} w_{\lambda i} = w_i \quad & \text{if} \quad |w_i| \geq \lambda \\ w_{\lambda i} = 0 \quad & \text{if} \quad |w_i| < \lambda \end{aligned}$$

For $k = 2$, this reduces to the form of (2.21), where the entropy is the number of non-zero coefficients:

$$\mathcal{E}(\boldsymbol{w_\lambda}) = N_1 = \#\{i = 1, \ldots, N | w_{\lambda i} \neq 0\},$$

and of course we use λ^2 instead of λ in (2.21), but this is only a matter of notation.

3. Soft-thresholding follows if we use the ℓ_1 norm as measure of sparsity. We minimize

$$\sum_{i=1}^{N}\left((w_{\lambda i}-w_i)^2+2\lambda|w_{\lambda i}|\right),$$

this means that the entropy in (2.21) equals:

$$\mathcal{E}(\boldsymbol{w_\lambda}) = 2\sum_{i=1}^{N}|w_{\lambda i}|.$$

2.6 Other coefficient selection principles

Coefficient thresholding is only one example of a wider class of algorithms, which proceed in three steps:

1. Wavelet transform of the input.
2. *Manipulation* of the *empirical* wavelet coefficients.
3. Inverse wavelet transform of the modified coefficients.

Most important and characteristic is of course the second step. The manipulation aims at a noise reduction, without losing too much signal information. In most algorithms, this manipulation depends on a *classification* of a coefficient, which is often binary: a coefficient is either *noisy* or *relatively noise-free* and important. To distinguish between these classes, we need a *criterion*, a sort of threshold on a measure of *regularity*. There are essentially two types of models on which this measure of regularity is based: Bayesian and non-Bayesian models.

The former type thinks of the uncorrupted coefficients $\boldsymbol{V}$ as an instance from a density function $f_{\boldsymbol{V}}(\boldsymbol{v})$, so we get a fully random model:

$$\boldsymbol{W} = \boldsymbol{V} + \boldsymbol{N},$$

where $\boldsymbol{N}$ is the noise. In principle, these methods compute the posterior density for the noise-free coefficients from Bayes' rule:

$$f_{\mathbf{V}|\mathbf{W}}(\boldsymbol{v}|\boldsymbol{w}) = \frac{f_{\mathbf{V}}(\boldsymbol{v}) f_{\mathbf{W}|\mathbf{V}}(\boldsymbol{w}|\boldsymbol{v})}{f_{\mathbf{W}}(\boldsymbol{w})}, \tag{2.22}$$

which allows, for instance, to estimate the underlying 'true' coefficients by the posterior mean:

$$\hat{\boldsymbol{v}} = \mathrm{E}(\boldsymbol{V}|\boldsymbol{W}).$$

Depending on the chosen density functions $f_{\mathbf{V}}(\boldsymbol{v})$ and $f_{\mathbf{W}|\mathbf{V}}(\boldsymbol{w}|\boldsymbol{v})$, this mostly leads to shrinking rules [35, 37, 44, 128, 146, 3, 130, 85]. Chapter 6 discusses an example of such a method.

The other type of classification considers the noise-free signal as a deterministic member of a smooth function space. These methods try to understand how signal regularity can be observed from wavelet coefficients:

1. As seen before, coefficients with a large magnitude are important. This is however not the only possible measure of regularity.

2. Simple thresholding is a very local approach: each coefficient is classified independent from its neighbors. It does not take into account the correlations between different coefficients, especially across scales. Other methods [152] are based on the assumption that regular signal or image features show correlated coefficients at different scales, whereas irregularities due to noise do not. These algorithms compute the *correlation* between coefficients at successive scales.

3. A third class of methods is based on the characterization of the Lipschitz or Hölder regularity of a function by its (continuous) wavelet transform [109, 111]. These methods look at the *evolution* of the coefficients across the different scales to distinguish regular from noisy contributions. As mentioned before, a regular image or signal singularity has a long-term range and

therefore the corresponding wavelet coefficients at coarse scales are large. Noise on the contrary, is local and therefore its singularities have larger coefficients at finer scales.

At first sight, these methods may seem more heuristic, but they avoid the possibly extensive use of hyperparameters in a Bayesian approach. Those parameters have to be chosen, often on a heuristic basis.

The algorithms based on Lipschitz characterization actually use a continuous wavelet transform, or a sampled version of it, i.e. some sort of non-decimated transform. This is a overcomplete data representation. The essential signal information is captured by the local coefficient extrema on each scale. The evolution through scales allows to distinguish signal extrema from noise extrema. These local extrema suffice to reconstruct the input signal, apart from some pathological cases [109, 111]. The reconstruction scheme, proposed by Mallat and collaborators is a time-consuming iterative process. Carmona [28] introduced a direct procedure, but a master's thesis at our department [144] seem to indicate that this method shows some instability problems.

2.7 Basis selection methods

Wavelet coefficient manipulation methods proceed within one wavelet basis, or one pair of dual bases. More adaptive methods build up the basis in which the given signal or image is processed. The objective is to make the signal fit as well as possible into this self-constructed basis. The method uses an overcomplete set of functions φ_i, in the sense that a given signal can be expressed as a linear combination of more than one subset of these 'library' or 'dictionary' of functions. Well structured libraries lead to fast algorithms (typically order $\mathcal{O}(N \log N)$) for best basis selection, i.e. finding the basis in which the coefficients $\boldsymbol{a}$ in the decomposition

$$\boldsymbol{f} = \sum_i a_i \phi_i$$

has minimal entropy. As in Section 2.5.6, the concept of entropy has several possible definitions. The ℓ_1-norm is one of these, and another well known example is:

$$\mathcal{E}(\boldsymbol{a}) = \sum_i \frac{-|a_i|}{\|\boldsymbol{a}\|_2} \log \frac{|a_i|}{\|\boldsymbol{a}\|_2}.$$

The wavelet packet transform belongs to this methods of best basis selection [41]. Other methods use different types of functions, like local trigonometric functions [39].

If the input data $\boldsymbol{y}$ are noisy, the noise can be eliminated by a decomposition

$$\boldsymbol{y} = \sum_{i=1}^{m} a_i \phi_i + R^{(m)},$$

so that:

$$\frac{1}{2}\|R^{(m)}\|_2^2 + \lambda \mathcal{E}(\boldsymbol{a}) \tag{2.23}$$

is as small as possible. The result is a trade-off between a close approximation of the input and a sparse representation. In this objective function, λ plays the role of smoothing parameter. The idea is that noise cannot be sparsely represented in any basis from the library. Some variants include:

1. *Basis pursuit* [34] uses the ℓ_1-norm as entropy. The objective function (2.23) then reduces to the form of a linear programming problem. Moreover, this expression has the same form as the one leading to soft-thresholding in the fixed basis setting. This motivates a choice of the smoothing parameter λ similar to the universal threshold.

2. *Matching pursuit* [110] is a greedy algorithm. In each step, it looks for the function from the library with the highest correlation with the residual after the previous step.

3. *Best Orthogonal Basis* [42] is limited to orthogonal bases. Extensions are in [40, 39].

2.8 Wavelets in other domains of application

Noise reduction by wavelet thresholding is an example of *non-parametric regression*. Similar techniques are used for *density estimation*, but the settings for this problem are different, as we briefly discuss in Section 8.2.1. Apparently, the wavelet world gets more and more penetrated with statisticians. Other applications in statistics [1] include time series analysis (stochastic processes) [118, 119, 120], change point analysis [125, 124], and inverse problems [94, 4, 57].

Other operations from signal processing [139] and more general system theory as well as identification problems belong to popular subjects of investigation for wavelet methods. The input may come from various domains, like geology, geography, or financial data.

Among all possible fields of application for wavelet based methods, digital image processing is probably the most visible or visual one. Most problems and solutions from one-dimensional signal processing have an equivalent in image processing, but the real challenge in this field is of course developing algorithms which are not mere more-dimensional versions of classical digital signal processing operations.

Not only wavelet based noise reduction schemes are applicable to images. The analysis of wavelet extrema by Mallat and collaborators, discussed in the previous section, also opens the way to multiresolution image contrast enhancement methods [104, 99, 122] and the decorrelating properties of a wavelet transform (the sparsity properties) are the basis for many image and video compression applications. Compression is closely related to image processing and can be seen as an example of approximation. Approximation theory is another field of application and, as becomes clear from subsequent chapters, its results may be interesting to explain wavelet based smoothing algorithms.

The flexibility of the lifting scheme for the construction on all types of lattices turns out to be useful in computer graphics and geometrical modeling [47, 138].

Another important domain of application is numerical analysis [134]. For the solution of partial differential equations, for instance, wavelet methods may serve as preconditioners [45, 69, 70].

A domain which is at first sight a bit further away from the material in this thesis is theoretical and mathematical physics.

2.9 Summary and concluding remarks

Wavelet theory combines the following properties:

1. A wavelet transform has a *decorrelating* property. A wavelet decomposition leads to a *sparse* representation. This is useful in compression applications and is a basis for noise reduction algorithms by wavelet thresholding.

2. Wavelet theory naturally supports the idea of *multiresolution*. Since a lot of phenomena in nature have a multiscale character, the ability to analyze and process data level-dependent is interesting in many applications. Images are a typical example of multiscale data: they contain information, objects of different scales.

3. Wavelet basis functions are *local* in time/space and frequency (scale). Manipulating the corresponding coefficients has a local effect: this allows good control on the effect of these manipulations.

4. A wavelet decomposition is a linear transform with linear complexity. This allows fast algorithms.

5. Orthogonality or bi-orthogonality in a Riesz-basis guarantee numerically well conditioned transforms.

6. The variety of wavelet basis functions and corresponding filters allows for each application an ideal choice of working basis.

7. Wavelet methods are based on a sometimes difficult, but nice mathematical background.

The next two chapters concentrate on the *sparsity* and *locality* to motivate wavelet thresholding for noise reduction. In Chapter 5, the *multiresolution* character of the transform turns out to be useful when dealing with less standard, academic situations of noisy signals. If the data live on an irregular grid, the lifting scheme comes in. This happens in Chapter 7. This lifting scheme has the following properties:

1. The lifting scheme for performing a wavelet transform speeds up computations, although the general order of complexity remains of course linear. Moreover, all computations are in place.

2. The basic ideas are easier to understand and implement: it is a more intuitive approach and does not require any Fourier techniques.

3. The inverse transform is trivial to construct from the data flow picture.

4. The lifting approach is more generic. It allows for extensions to non-equispaced samples and integer transforms. In the former case, lifting guarantees a smooth reconstruction. Stability however, does not seem to be guaranteed, as Chapter 7 points out.

Chapter 3

The minimum mean squared error threshold

"Du aber wanderst auf und ab
Aus Ostens Wieg' in Westens Grab,
Wallst Länder ein und Länder aus,
Und bist doch, wo du bist, zu Haus.
(...)
O glücklich, wer, wohin er geht,
Doch auf der Heimat Boden steht"
—Johann Gabriel Seidl, *(1804–1875), Der Wanderer an den Mond, set to music by* Franz Schubert *(1797–1828), D. 870.*

"Wie was deze eenzame zwerver, die zo kort op aarde was, en die zulke raadselachtige mooie muziek schreef en zulke vrolijke liederen over de last van het bestaan? Schubert was zijn naam."
—TV-uitzending over Franz Schubert, *VRT (BRTN), 1997.*

This chapter investigates the mean squared error as a criterion for selecting an optimal soft threshold. In applications like image processing, it is often objected that this expression of the error does not always correspond to a more subjective experience of quality. Our visual system, for instance, is much more sensitive to contrast than is expressed by a mean squared error. Nevertheless, even in the image processing world, definitions of signal-to-noise ratio, based on mean squared errors, are commonly used.

On the other hand, the material of this chapter is not limited to a specific application. Moreover, the ideas can easily be extended to representations, different from wavelet bases. The only thing we need, is a data set where a few coefficients carry a large proportion of the information, so that an algorithm can "throw away" an important part of the data without losing substantial information. The decorrelating property of a wavelet transform provides us with this sparsity . This chapter is therefore based on this decorrelation.

In the first section, we introduce the mean square error as a function of the threshold value, and examine its typical shape. Next, we focus on the threshold that minimizes this this objective function. We try to understand how it behaves asymptotically, i.e. if the number of data N tends to infinity. We operate in two steps: first we study piecewise polynomials, and second we turn to the general piecewise smooth function case. The outcome of this study reveals an interesting similarity to the well-known *universal threshold*. Section 3.4 resumes the principal properties of this often used threshold. The mean square error has been analyzed in other works too [29, 73, 75, 74]. Apart from Section 3.4, the analysis in this chapter is original material.

3.1 Mean square error and Risk function

3.1.1 Definitions

In the previous chapter, we already learnt that a threshold can be seen as a smoothing parameter: it controls the compromise between goodness of fit and smoothness of approximation. In this context, smoothness should be interpreted as sparsity: we try to find a sparse data set, close to the noisy input.

The ultimate objective is of course an approximation of the noise-free data. While balancing between closeness of fit and sparsity, the *best* compromise minimizes the error of the result as compared with these unknown, uncorrupted data.

If $\boldsymbol{y_\lambda}$ is the output of the threshold algorithm with some threshold value λ and $\boldsymbol{f}$ is the vector of untouched data, the remaining noise on this result equals $\boldsymbol{\eta_\lambda} = \boldsymbol{y_\lambda} - \boldsymbol{f}$, and the mean squared error (MSE) is then defined as:

$$R(\lambda) = \mathrm{MSE}(\lambda) = \frac{1}{N}\|\boldsymbol{\eta_\lambda}\|^2. \tag{3.1}$$

As the notation indicates, the MSE, $\mathrm{R}(\lambda)$, is a function of the threshold value λ. It is also a random variable, because it depends on the noise. The expected value of this error is called the *risk*-function.

The main challenge with this MSE as an objective function is the fact that in real applications, it can never be computed exactly: its definition uses the value of the exact, unknown data $\boldsymbol{f}$. In practical situations, this MSE has to be estimated. As the next chapter discusses, GCV is such an estimator.

A common definition of signal-to-noise ratio (SNR) is based on this notion of MSE:

$$\mathrm{SNR}(\lambda) = 10 \cdot \log_{10} \frac{\|\boldsymbol{f}\|^2}{\|\boldsymbol{\eta_\lambda}\|^2} = 10 \cdot \log_{10} \frac{\|\boldsymbol{f}\|^2/N}{R(\lambda)}. \tag{3.2}$$

An alternative is the peak signal-to-noise ratio, which is equal to the previous one, up to constant, depending on the uncorrupted data:

$$\mathrm{PSNR}(\lambda) = 10 \cdot \log_{10} \frac{(\max \boldsymbol{f})^2/N}{R(\lambda)} = \mathrm{SNR}(\lambda) + 10 \cdot \log_{10} \frac{(\max \boldsymbol{f})^2}{\|\boldsymbol{f}\|^2}. \quad (3.3)$$

Both SNR and PSNR are expressed in deciBels (dB) .

An orthogonal wavelet transform $\tilde{W}$ preserves the ℓ_2-norm, and so:

$$R(\lambda) = \frac{1}{N}\|\boldsymbol{\omega}_{\boldsymbol{\lambda}}\|^2,$$

where $\boldsymbol{\omega}_{\boldsymbol{\lambda}} = \boldsymbol{w}_{\boldsymbol{\lambda}} - \boldsymbol{v} = \tilde{W}(\boldsymbol{y}_{\boldsymbol{\lambda}} - \boldsymbol{f})$. From now on, we do all our computations in the wavelet domain. If the transform is biorthogonal, there is no exact equivalence with the data domain. Nevertheless, computation and minimization in terms of wavelet coefficients seems to give satisfactory results, and several reasons could explain this: Riesz-bounds guarantee a nearly equivalent norm. Moreover, since MSE does not correspond exactly to a human perception of quality, the question arises whether MSE in the original data domain is always a better measure than MSE in the wavelet domain. In image processing applications, for instance, we view the image in the pixel domain, but we do not look at an image as a matrix of pixels. Since our visual system seems to work on a multiscale basis, a norm based on a multiresolution decomposition might be a better expression of visual quality. Further illustrations show that there is no need for expressing norms in the original data domain. This preserves us from applying an inverse wavelet transform every time we want to evaluate the quality of a result. An inverse wavelet transform is only necessary to compute the eventual output of the algorithm.

3.1.2 Variance and bias

The input wavelet coefficients are unbiased estimates of the noise-free coefficients:

$$\mathrm{E}\boldsymbol{w} = \mathrm{E}\tilde{W}\boldsymbol{y} = \tilde{W}\mathrm{E}\boldsymbol{y} = \tilde{W}\boldsymbol{f} = \boldsymbol{v}$$

but the variance of this "estimation" is too high. Replacing the smallest coefficients with zero reduces the variance, at the cost of an increasing bias:

$$\begin{aligned} \mathrm{bias}(\lambda) &= \frac{1}{N}\|\mathrm{E}\boldsymbol{w}_{\boldsymbol{\lambda}} - \boldsymbol{v}\|^2 && (3.4) \\ \mathrm{variance}(\lambda) &= \frac{1}{N}\mathrm{E}\|\boldsymbol{w}_{\boldsymbol{\lambda}} - \mathrm{E}\boldsymbol{w}_{\boldsymbol{\lambda}}\|^2. && (3.5) \end{aligned}$$

Then it holds that:

$$\begin{aligned} \mathrm{E}R(\lambda) &= \frac{1}{N}\|\mathrm{E}\boldsymbol{w}_{\boldsymbol{\lambda}} - \boldsymbol{v}\|^2 + \frac{1}{N}\mathrm{E}\|\boldsymbol{w}_{\boldsymbol{\lambda}} - \mathrm{E}\boldsymbol{w}_{\boldsymbol{\lambda}}\|^2 && (3.6) \\ \mathrm{Risk} &= \qquad \mathrm{bias} \qquad + \qquad \mathrm{variance} \end{aligned}$$

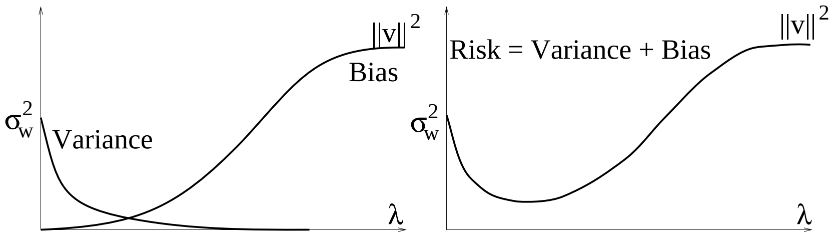

Figure 3.1: Typical behavior of bias and variance as a function of the threshold value. Thresholding introduces bias, but reduces variance. The best compromise minimizes the risk.

The most reliable method to remove *all* noise is just removing everything:

$$\lim_{\lambda \to \infty} \mathrm{variance}(\lambda) = 0.$$

If all coefficients are removed, there is no variance anymore, all the noise has gone, but so has the signal: the bias equals the total energy of the noise-free input:

$$\lim_{\lambda \to \infty} \mathrm{bias}(\lambda) = \|\boldsymbol{v}\|^2$$

Figure 3.1 shows a typical behavior of these functions. The minimum risk threshold is the best compromise (in ℓ_2) between variance and bias.

In Chapter 2, we motivated thresholding as a smoothing algorithm: our objective was to find a compromise between closeness of fit and smoothness. Next, we introduced the notion of MSE and Risk to define the *best* compromise. This risk function is a sum of two effects: variance and bias, and the minimum risk threshold is again the best compromise between these two. We already mentioned that the MSE or the risk function cannot be possibly computed in real applications. Unlike smoothness and closeness of fit, both variance and bias are unknown in practice, but a solution with small variances is probably smooth whereas a close fit generally shows little bias. This link is implicitly present when estimating the optimal threshold with cross validation, as becomes clear in the next chapter.

3.2 The risk contribution of each coefficient (Gaussian noise)

This section puts some elementary calculations together. The results are necessary for the next sections. From now on, we assume that the input noise is Gaussian and we call:

$$\begin{aligned}\phi(\omega) &= \frac{1}{\sqrt{2\pi}\sigma}\mathrm{e}^{\omega^2/2\sigma^2},\\ \Phi(\omega) &= \int_{-\infty}^{\omega}\phi(u)du.\end{aligned}$$

Every classical, linear wavelet transform preserves the normality of a density. If the input noise is not Gaussian, the density of the wavelet coefficients, if at all computable in practice, would depend on the type of wavelets being used.

Some of the following results also appear in different papers like [60]. A first lemma gives an expression for the bias of one coefficient $w = v + \omega$ (the notation omits the index of the coefficient).

Lemma 3.1

$$\begin{aligned}\mathrm{E}\omega_\lambda &= \sigma^2[\phi(\lambda - v) - \phi(\lambda + v)] + \lambda[\Phi(\lambda - v) - \Phi(\lambda + v)]\\ &\quad +v[1 - \Phi(\lambda - v) - \Phi(\lambda + v)]. \qquad (3.7)\end{aligned}$$

The proof is by simple calculations, using the fact that a Gaussian distribution satisfies the following differential equation:

$$\omega\phi(\omega) = -\sigma^2\phi'(\omega). \qquad (3.8)$$

We denote by

$$r(v, \lambda) = \mathrm{E}(w_\lambda - v)^2 \qquad (3.9)$$

the contribution of coefficient w to the total risk function. Using Equation (3.8) and partial integration leads to

$$\int \omega^2\phi(\omega)d\omega = -\omega\sigma^2\phi(\omega) + \sigma^2\int\phi(\omega)d\omega,$$

which allows to conclude, after some calculation, that:

Lemma 3.2

$$\begin{aligned}r(v, \lambda) &= \left[2(\sigma^2 + \lambda^2) - v^2\right] + \left[\Phi(\lambda - v) + \Phi(\lambda + v)\right](v^2 - \sigma^2 - \lambda^2)\\ &\quad -\sigma^2\left[(\lambda - v)\phi(\lambda + v) + (\lambda + v)\phi(\lambda - v)\right]. \qquad (3.10)\end{aligned}$$

Plots of this contribution as a function of the threshold λ for various values of v show that coefficients with little information ($v \approx 0$) are best served with large thresholds, whereas important coefficients (v large) prefer little thresholding. The overall optimal threshold is the best compromise between these two.

To find the minima, we compute the derivative. Again an trivial computation leads to:

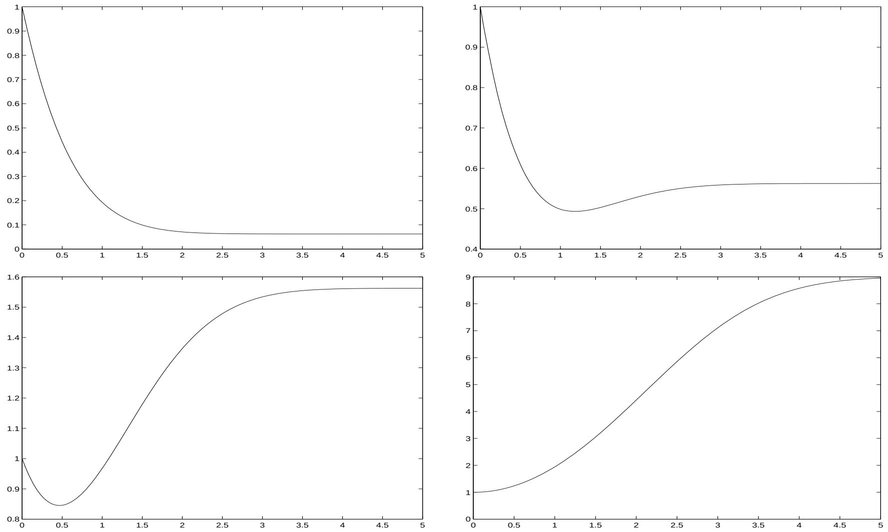

Figure 3.2: Contribution of individual coefficients to the total risk as a function of the threshold value. Small values of v (upper left) prefer large thresholds, because bias is small. Large values of v (lower right) would cause considerable bias if the threshold gets large.

Lemma 3.3

$$\frac{\partial r}{\partial \lambda}(v,\lambda) = 2\lambda\,[1+\Phi(-v-\lambda)-\Phi(-v+\lambda)] - 2\sigma^2\,[\phi(v+\lambda)+\phi(-v+\lambda)]. \tag{3.11}$$

The proof uses the fact that

$$\frac{\partial}{\partial \lambda}\mathrm{E}(w_\lambda - v)^2 = \mathrm{E}\frac{\partial}{\partial \lambda}(w_\lambda - v)^2.$$

An important case is that of a coefficient without any information. It turns out that if $v = 0$, the derivative $\frac{\partial r}{\partial \lambda}$ is always negative (see Figure 3.2, upper left). If $\lambda \to \infty$, the derivative approaches zero, but it remains negative. This means that the optimal threshold for this zero coefficient equals infinity. This is confirmed by the following asymptotic behavior:

Lemma 3.4

$$\frac{\partial r}{\partial \lambda}(0,\lambda) \sim -4\sigma^4\,\frac{\phi(\lambda)}{\lambda^2}. \tag{3.12}$$

Proof:
From the previous lemma, we see that:

$$\frac{\partial r}{\partial \lambda}(0,\lambda) = 4\lambda[1-\Phi(\lambda)] - 4\sigma^2\phi(\lambda).$$

Three times De L'Hôpital's rule shows that:

$$\lim_{\lambda\to\infty}\frac{\lambda[1-\Phi(\lambda)]-\sigma^2\phi(\lambda)}{\frac{\phi(\lambda)}{\lambda^2}} = \sigma^4.$$

□

To get an idea of how $\frac{\partial r}{\partial \lambda}$ behaves more generally, we compute the derivative of this expression with respect to the uncorrupted coefficient value v:

Lemma 3.5

$$\frac{\partial}{\partial v}\left(\frac{\partial r}{\partial \lambda}(v,\lambda)\right) = 2v\,[\phi(v+\lambda)+\phi(-v+\lambda)] \tag{3.13}$$

$$\begin{cases} \geq 0 & \textit{if}\ v \geq 0, \\ \leq 0 & \textit{if}\ v \leq 0. \end{cases} \tag{3.14}$$

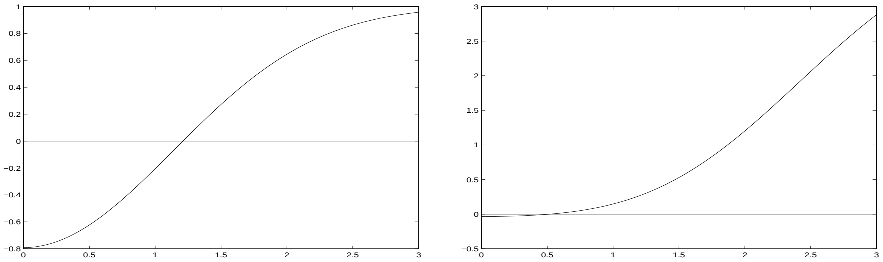

Figure 3.3: Derivative of the risk in a given coefficient with respect to the threshold value as a function of the noise-free coefficient value. Left: $\lambda = 0.5\,\sigma$. For coefficients approximately below $1.1\,\sigma$, this threshold is too low. Right: $\lambda = 2\sigma$. This threshold is too large for coefficients above $0.5\,\sigma$. The distribution of noise-free coefficients determines the optimal threshold.

Consequently, for a given threshold, $\frac{\partial r}{\partial \lambda}$ has a minimum for $v = 0$. Figure 3.3 shows $\frac{\partial r}{\partial \lambda}$ as a function of v for two different values of λ. The plot on the left-hand side corresponds to a threshold $\lambda = 0.5\,\sigma$. This threshold is too small for all coefficients smaller than approximately $1.1\,\sigma$. If we choose $\lambda = 2\sigma$, only coefficients below $0.5\,\sigma$ find this value too small. The value of the optimal threshold depends on how the noise-free coefficients are distributed: the sparser the representation is, the larger the optimal threshold will be. Indeed, if the proportion of small coefficients increases, the threshold should be large, because all these small coefficients prefer large thresholds. The next sections try to find an asymptotic behavior for this optimal threshold. We assume that generating more samples from a given signal on a continuous line, introduces more redundancy in the information. This causes more sparsity in the wavelet representation. We expect that the optimal threshold increases as the number of samples N grows.

3.3 The asymptotic behavior of the minimum risk threshold for piecewise polynomials

3.3.1 Motivation

The next chapter shows that, in minimum risk sense, the GCV-method asymptotically yields the optimal threshold. This property motivates the use of GCV in a threshold assessment procedure. For the proof of this asymptotic optimality, we need to know how the optimal threshold itself behaves if the number of samples $N \to \infty$. This section assumes that the samples come from a piecewise polynomial on $[0,1]$:

$$y_i = f(\Delta t \cdot i) + \eta_i,$$

where $f(t)$ is a piecewise polynomial and $t \in [0,1]$. No real signal is of course a perfect piecewise polynomial, but typical signals are piecewise smooth. Section 3.5 investigates how the threshold behaves in this more general case.

3.3.2 Asymptotic equivalence

Before studying the asymptotics of the minimum risk threshold, we recall the definition of asymptotic equivalence:

Definition 3.1 *Two functions $f(x)$ and $g(x)$ are said to be asymptotic equivalent for $x \to \infty$, i.e. $f(x) \sim g(x)$, if and only if*

$$\lim_{x\to\infty} \frac{f(x)}{g(x)} = 1.$$

The study of the asymptotics of the minimum risk threshold uses a couple of properties of this notion:

Lemma 3.6 *Let $x \to \infty$. If $f(x) \sim g(x)$, we have:*

1. $f(x)h(x) \sim g(x)h(x)$.
2. *If $f(x) \sim h(x)$, then $h(x) \sim g(x)$.*
3. *If $h(x) = o(f(x))$, then $f(x) \pm h(x) \sim g(x)$.*
4. *If*

   $$\lim_{x\to\infty} f(x) \neq 1 \neq \lim_{x\to\infty} g(x),$$

   and both functions are differentiable, then

   $$\log f(x) \sim \log g(x).$$

Proof:

1. Trivialiter
2. $\lim_{x\to\infty} \frac{h(x)}{g(x)} = \lim_{x\to\infty} \frac{h(x)}{f(x)} \frac{f(x)}{g(x)}$,

   and we may split the limit of this product, since both factors have a limit.

3. This is actually a special case of the previous statement.

$$\lim_{x\to\infty}\frac{f(x)\pm h(x)}{g(x)} = \lim_{x\to\infty}\frac{f(x)}{g(x)}\left(1+\frac{h(x)}{f(x)}\right) = \lim_{x\to\infty}\frac{f(x)}{g(x)}\cdot\lim_{x\to\infty}\left(1+\frac{h(x)}{f(x)}\right)$$

4. For $\lim_{x\to\infty} f(x)=\infty$, we use De L'Hôpital's rule:

$$\begin{aligned}\lim_{x\to\infty}\frac{\log f(x)}{\log g(x)} &= \lim_{x\to\infty}\frac{f'(x)/f(x)}{g'(x)/g(x)} = \lim_{x\to\infty}\frac{f'(x)}{g'(x)}\lim_{x\to\infty}\frac{g(x)}{f(x)} \\ &= \lim_{x\to\infty}\frac{f(x)}{g(x)}\lim_{x\to\infty}\frac{g(x)}{f(x)} = 1.\end{aligned}$$

For a finite limit, we do not need the differentiability:

$$\lim_{x\to\infty}\frac{\log f(x)}{\log g(x)} = \frac{\lim_{x\to\infty}\log f(x)}{\lim_{x\to\infty}\log g(x)} = \frac{\log\left(\lim_{x\to\infty} f(x)\right)}{\log\left(\lim_{x\to\infty} g(x)\right)} = 1$$

□

We remark that the inverse implication of the last statement definitely does not hold: if $\log f(x)\sim\log g(x)$, $f(x)$ and $g(x)$ may be not asymptotically equivalent. For instance, if $\log f(x) = x+\sqrt{x}$ and $\log g(x) = x$, then

$$\frac{f(x)}{g(x)} = \mathrm{e}^{\sqrt{x}} \not\to 1.$$

3.3.3 The asymptotic behavior

For the piecewise polynomial case, we assume that the wavelet analysis has more vanishing moments than the highest degree of the polynomials. As a consequence, wavelet coefficients are zero if they do not correspond to a basis function which interferes with a singularity . We assume that the number of singularities is finite on $[0,1]$.

We then have the following theorem for the asymptotic behavior of the minimum of $\mathrm{E}R(\lambda) = \mathrm{E}\|\boldsymbol{y_\lambda}-\boldsymbol{f}\|^2$:

Theorem 3.1 *Suppose $f(x)$ is a piecewise polynomial on $[0,1]$, $v_i := v_{j,k}, i = 2,\ldots N = 2^J, j = 0,\ldots, J-1, k = 1,\ldots, 2^j$ are the wavelet coefficients of the orthogonal projection of f on V_J. Call $w_i = v_i + \omega_i$ the noisy wavelet coefficients and $R(\lambda)$ the soft-threshold MSE-function as defined in (3.1). If λ^* minimizes $\mathrm{E}R(\lambda)$, then for $N\to\infty$:*

$$\lambda^* \sim \sqrt{2\log N}\sigma \tag{3.15}$$

Proof:
We suppose that the wavelet transform is orthogonal, so the problem model in the wavelet domain is the same as in the input (time or space) domain:

$$\boldsymbol{w} = \boldsymbol{v} + \boldsymbol{\omega},$$

where $\boldsymbol{\omega}$ is i.i.d. noise with variance σ^2. A wavelet coefficient v_i or w_i corresponds to a basis function $\psi_{j,k}$ at resolution level j and place k. Sometimes we use the double index notation for these coefficients: $v_i = v_{j,k}$ and $w_i = w_{j,k}$.

We call:

$$\begin{aligned} I_0 &= \{i = 1, \ldots, N | v_i = 0\} \\ I_1 &= \{i = 1, \ldots, N | v_i \neq 0\} \\ M_0 &= \# I_0 \\ M_1 &= \# I_1 \end{aligned}$$

M_0 and M_1 of course depend on N. Since $f(t)$ is a piecewise polynomial, at each level only a constant number of coefficients is not exactly zero. The total number of non-zero coefficients is proportional to the number of levels:

$$M_1 \sim \log N,$$

and so:

$$\frac{M_1}{N} \to 0.$$

Using the notation from the previous section, we may write:

$$\mathrm{E}R(\lambda) = \sum_{i=1}^{N} r(v_i, \lambda).$$

And so:

$$\mathrm{E}R'(\lambda) = M_0 \frac{\partial r}{\partial \lambda}(0, \lambda) + \sum_{i \in I_1} \frac{\partial r}{\partial \lambda}(v_i, \lambda).$$

Lemma 3.3 learns that $\frac{\partial r}{\partial \lambda}(0, \lambda) < 0$. Call $I_1' \subset I_1$ the indices of the non-zeros for which $\frac{\partial r}{\partial \lambda}(v_i, \lambda^*)$ is negative. These indices belong to the smaller coefficients. The indices of the large coefficients are in $I_1'' = I_1 \backslash I_1'$. We define

$$\begin{aligned} M_1' &= \# I_1' \\ M_1'' &= \# I_1''. \end{aligned}$$

We know that

$$v_i = v_{j,k} \approx \sqrt{N} \int_{\mathbb{R}} f(t)\psi_{j,k}(t)dt,$$

where the integral is a constant value which does not depend on N, so $v_i \sim \sqrt{N}$, and we are looking for a λ^* which does not increases faster. This means that M_1'' is a non-decreasing function of N: if $N \to \infty$, ever more coefficients are classified as large, since all non-zero coefficients grow at least as fast as the optimal threshold. On the other hand, $M_1'' \leq M_1$ does not increase too fast. We now write the equation for λ^*: $\mathrm{E}R'(\lambda^*) = 0$ or:

$$-M_0 \frac{\partial r}{\partial \lambda}(0, \lambda^*) - \sum_{i \in I_1'} \frac{\partial r}{\partial \lambda}(v_i, \lambda^*) = \sum_{i \in I_1''} \frac{\partial r}{\partial \lambda}(v_i, \lambda^*). \tag{3.16}$$

We consider this equation as an equality of two functions of N, and let $N \to \infty$. Both sides of this equation have all positive terms. Lemma 3.5 says that

$$\forall i \in I_1' : \left| \frac{\partial r}{\partial \lambda}(v_i, \lambda^*) \right| \leq \left| \frac{\partial r}{\partial \lambda}(0, \lambda^*) \right|.$$

Moreover $M_1' \leq M_1 \sim \log N$, so $\frac{M_1'}{M_0} \sim \frac{\log N}{N} \to 0$. From this, we may conclude that the sum $\sum_{i \in I_1'}$ in Equation (3.16) can be neglected.

If v_i grows faster than λ^* for increasing N, the right-hand side behaves like $M_1'' 2\lambda^*$, as follows from letting $v \to \infty$ in Lemma 3.3. We have:

$$\frac{M_0}{M_1''} \sim \frac{2\lambda^*}{-\frac{\partial r}{\partial \lambda}(0, \lambda^*)}.$$

If $N \to \infty$, the left-hand side grows like $N/\log N \to \infty$. The right-hand side is an increasing function of λ^*: it is easy to verify (from the proof of Lemma 3.4) that

$$-\frac{\partial^2 r}{\partial \lambda^2}(0, \lambda) = -4\left[1 - \Phi(\lambda)\right] \leq 0,$$

so the denominator is a positive, decreasing function, while the numerator is positive and increasing. To make this right-hand side grow to infinity, we need $\lambda^* \to \infty$. Therefore, we can use Lemma 3.4 and get the following asymptotic equation:

$$\begin{aligned} \frac{M_0}{M_1''} &\sim \frac{2\lambda^* \lambda^{*2}}{4\sigma^4 \phi(\lambda^*)}, \\ \frac{\sigma^3 M_0}{M_1''} &\sim \sqrt{\frac{\pi}{2}}\, e^{\lambda^{*2}/2\sigma^2} \lambda^{*3}, \\ 3\log\sigma + \log M_0 - \log M_1'' &\sim \frac{\lambda^{*2}}{2\sigma^2} + 3\log\lambda^* + \frac{1}{2}\log\frac{\pi}{2}. \end{aligned}$$

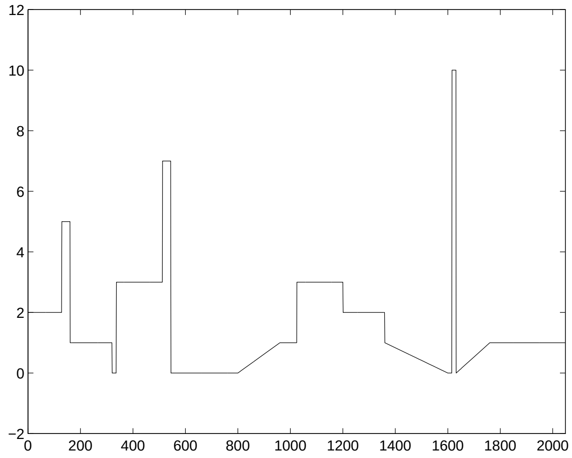

Figure 3.4: An example of a piecewise polynomial: in this case, all pieces are linear or constant.

The left-hand side depends on N, the right-hand side depends on λ^*. We keep the essential on both sides:

$$\begin{aligned}\log M_0 &\sim \frac{\lambda^{*2}}{2\sigma^2},\\ \log(N-M_1) &\sim \frac{\lambda^{*2}}{2\sigma^2},\\ 2\sigma^2\log N &\sim \lambda^{*2}.\end{aligned}$$

□

3.3.4 An example

Figure 3.4 shows the plot of a piecewise, linear polynomial. This function is sampled, and transformed into wavelet domain, using the orthogonal Daubechies wavelets with two vanishing moments. We then compute numerically the minimum of $\mathrm{E}R(\lambda)$ for different sample rates, and $\sigma = 1$. These values are listed in Table 3.1 and plotted in Figure 3.5.

Both table and figure illustrate that indeed

$$\lambda^* \approx K + \sqrt{2\log N}\sigma = K + \sqrt{2\log 2}\sqrt{J},$$

where K is constant and $2^J = N$.

J	$N = 2^J$	λ^*
7	128	1.00564887172677
8	256	1.12338708120546
9	512	1.25150560042977
10	1024	1.40212517387946
11	2048	1.55837014248141
12	4096	1.75818138547032
13	8192	1.94789562337191
14	16384	2.13051380127175
15	32768	2.30620858768226
16	65536	2.47521770450833
17	131072	2.63789870923179
18	262144	2.79627013633284
19	524288	2.95567796055755
20	1048576	3.11403413842011

Table 3.1: Minimum risk threshold for the piecewise polynomial in Figure 3.4 as a function of the number N of samples.

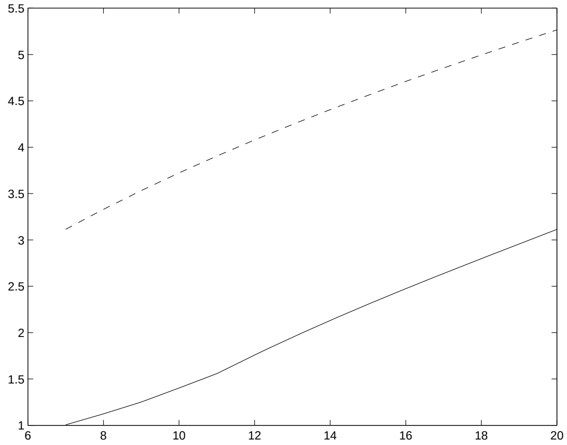

Figure 3.5: Plot of minimum risk threshold for the signal in Figure 3.4 as a function of the binary logarithm J of the number of samples (full line). De dashed line is a plot of the predicted equivalence: $\sqrt{2\log 2}\sqrt{J}$. The plot seems to confirm this asymptotic behavior.

3.3.5 Why does the threshold depend on the number of data points?

To engineers it might look strange that the optimal threshold depends on the number of data points. They object that the threshold should not change by putting two signals together?

First, this objection does not correspond to the philosophy behind this asymptotic analysis: we do not join two signals, but merely take more samples from one function on a given interval. Second, as Table 3.1 illustrates, we note that $\sqrt{2\log N}$ is only a very weak dependence.

And third, there is a comprehensive explanation for this behavior. Adding more samples enhances redundancy in the signal: there is less new information in new samples than there was in the first samples. In wavelet domain, this means that the number of important coefficients is hardly growing, and all information remains concentrated in a limited number of coefficients. If we suppose that the transform is normalized, the magnitude of these large coefficients should increase, since more samples mean a higher total energy (2-norm of the data vector) and this energy is preserved by the wavelet transform, while all nearly zero coefficients hardly take any of it. On the other hand, the noise variance in all coefficients remains σ^2 all the time. If the threshold would be independent of N, say $\lambda = k\sigma$, then the relative number of purely noise coefficients which passes the threshold would converge to $\mathrm{P}(|Z| > k)$, Z being a standard normal variable. So, the total number of noise coefficients would be proportional to N. Since the number of important coefficients is approximately a constant, the reconstruction would become noisier. Therefore, it is better to let the threshold increase slowly to catch all noise coefficients, while leaving the faster growing signal coefficients intact.

This observation is related to the notion of *False Discovery Rate* (FDR) in multiple hypothesis testing [16]: testing whether N values are 'significantly different from zero' with a fixed significance level α leads to an average of αN false rejections of the $H_{0,i}$ hypothesis: 'value i is essentially zero'. Defining the False Discovery Rate as

$$\mathrm{FDR} = \mathrm{E}\frac{N_{1,0}}{N_1},$$

where N_1 is the total number of discoveries and $N_{1,0}$ the number of false discoveries, more sophisticated testing guarantees the FDR to be lower than a chosen, global α. Applied to wavelet thresholding, discoveries correspond to wavelet coefficients with a magnitude essentially different from zero, i.e. above a threshold [2].

3.4 Universal Threshold

Of course, the formula of the asymptotic behavior of the minimum risk threshold does not tell everything about the actual, optimal threshold value. This actual value depends on all coefficients, while the asymptotic formula only depends on N and σ. We did not say that one should use this asymptotic formula as a real threshold. Nevertheless, the value

$$\lambda_{\mathrm{UNIV}} = \sqrt{2 \log N} \sigma \tag{3.17}$$

is well known in wavelet literature and it is used as a threshold value, not only as an asymptotic equivalence. This is the so-called *universal threshold*. This name reflects the idea that this threshold is "valid" for all signals with length N, provided that these signals are "sufficiently" smooth: it is a general threshold value. Donoho, Johnstone and collaborators have proven a lot of optimality properties for this choice. We briefly discuss some of these ideas.

3.4.1 Oracle mimicking

Wavelet coefficient shrinking, especially hard-thresholding, can be seen as an example of selective wavelet reconstruction, i.e. based on a given regularity *criterion* some of the coefficients are preserved and others are removed to reconstruct the signal. For thresholding, the measure of regularity is simply the coefficient magnitude. If the underlying uncorrupted coefficient were known, one could of course find the best possible selection. If the objective is to minimize the risk, it is easy to prove that one should select the coefficients for which $|v_i| > \sigma$ and omit the others. All this is of course a completely irrealistic situation: if we knew the untouched v_i, we would not even consider reconstruction by *noisy* coefficient selection. One could imagine an *oracle* telling us whether the uncorrupted coefficients are above σ but not the exact values. This remains an unrealistic dream, but can serve as a benchmark: it leads to the best possible selection. With respect to this, there are two important results [60]:

1. Within a logarithmic factor, (optimal) wavelet coefficient selection performs essentially as well as any piecewise polynomial and spline method: if SW stands for selective wavelet reconstruction, and PP for piecewise polynomial reconstruction, we have that

$$\mathrm{Risk}(\mathrm{SW}) \leq (A \log N + B)(\mathrm{Risk}(\mathrm{PP}))$$

2. Again within a logarithmic factor wavelet thresholding using the universal threshold performs as well as optimal selective wavelet reconstruction:

$$\mathrm{Risk}(\lambda_{\mathrm{UNIV}}) \leq (2 \log N + 1)(\mathrm{Risk}(\mathrm{SW}) + \frac{\sigma^2}{N})$$

3.4.2 Minimax properties

In a certain sense, the previous result also holds in the opposite direction: there is no threshold that in all cases essentially performs better than the universal threshold. More precisely, let λ_{mM} be the minimax threshold, i.e. the largest threshold that minimizes the maximum relative risk with respect to the optimal selection risk. Then it holds that this risk ratio also behaves like $2 \log N$ and the minimax threshold itself is asymptotically

$$\lambda_{\mathrm{mM}} \sim \sqrt{2 \log N}.$$

3.4.3 Adaptivity, optimality within function classes

The previous two results relate the performance of universal soft-thresholding to the ideal oracle coefficient selection. This is a relative result: basically it states that *if* optimal coefficient selection performs well, thresholding performs nearly as well. This leaves us with the question when selective wavelet reconstruction is a good method for noise reduction. Clearly, we may expect good performance for signals with a sparse wavelet representation. These are typically piecewise smooth signals. To characterize this piecewise smoothness we cannot use the normal concept of C^{α} (Lipschitz or Hölder; see Definition 3.2) functions, since one singularity destroys the overall smoothness. On the other hand, the L_p spaces may be too general and contain really non-smooth functions. Section 3.5.4 introduces and briefly discusses the concept of Besov spaces. For the moment, we just mention that a Besov space $B^s_{p,q}$ contains piecewise smooth signals and the parameters p, q, s measure different aspects of this smoothness.

If a function f lies in such a space $\mathcal{F}$, the universal threshold risk is guaranteed to come within a logarithmic factor of the minimax risk, i.e. the risk of the estimator which minimizes the worst case risk within the function space:

$$\sup_{f \in \mathcal{F}} \mathrm{Risk}(\lambda_{\mathrm{UNIV}}) \leq C \log N \cdot \inf_{\hat{f}} \sup_{f \in \mathcal{F}} \mathrm{Risk}(\hat{f}), \tag{3.18}$$

where the infimum is taken over all possible estimators $\hat{f}$. The universal threshold comes that close without knowing the exact smoothness parameters p, q, s, whereas the optimal estimator clearly depends on these values. This is why the threshold procedure is called adaptive to unknown smoothness [56].

3.4.4 Smoothness

A Besov space is of course associated with a corresponding norm. This Besov norms measures the smoothness of a function, thereby being “flexible” with singularities: one isolated singularity poses no problem for Besov-smoothness. It turns out that the reconstruction using a universal threshold with high probability (tending to one if $N \to \infty$) is at least as smooth as the untouched signal [56].

This smoothness guarantee is not available for thresholds designed for minimum risk optimality, like SURE and GCV (see next chapter). The output of these algorithms indeed often shows noisy “blips”. In Chapter 5 we propose some modifications to the GCV-threshold algorithm to get rid of these annoying false structures.

3.4.5 Probabilistic Upper bound

Since $\|0\|_{\mathcal{F}} = 0$ in every smoothness space $\mathcal{F}$, the previous result implies that if $f = 0$, the reconstruction is the zero function with high probability. There is another way of explaining this constation. From classical extreme value theory we have the following theorem [56, 102]:

Theorem 3.2 *Let $\{X_k\}_{k\in\mathbb{N}}$ be an i.i.d. sequence with common distribution function $F_X(x)$ and let $M_N = \max\{X_k | k = 1, \ldots, N\}$, then for a real sequence λ_N:*

$$\lim_{N\to\infty} \mathrm{P}(M_N \leq \lambda_N) = \mathrm{e}^{-a} \quad \Leftrightarrow \quad \lim_{N\to\infty} N\left(1 - F_X(\lambda_N)\right) = a. \tag{3.19}$$

For $\lambda_N = \sqrt{2\log N}\sigma$ and $F_X(x) = \Phi(x)$, we can use

$$1 - \Phi(x) \sim \sigma^2\,\frac{\phi(x)}{x} \qquad x \to \infty, \tag{3.20}$$

to find that:

$$\lim_{N\to\infty} N\left(1 - \Phi(\sqrt{2\log N}\sigma)\right) = \lim_{N\to\infty} N\sigma^2\,\frac{1}{\sqrt{2\pi}\sigma}\,\frac{1}{N\sqrt{2\log N}\sigma} = 0.$$

and so:

$$\lim_{N\to\infty} \mathrm{P}(M_N \leq \sqrt{2\log N}\sigma) = 1.$$

This means that with probability increasing to one, the universal threshold λ_N removes all coefficients that are purely noise. On the other hand, suppose we have a slower growing threshold μ_N and call $\nu_N = \mu_N/\lambda_N$, so that

$$\lim_{N\to\infty} \nu_N < 1,$$

then

$$\begin{aligned}
\lim_{N\to\infty} N\left(1 - F_X(\mu_N)\right) &= \lim_{N\to\infty} \frac{\mathrm{e}^{\log N}\,\sigma^2\,\mathrm{e}^{-(\nu_N\lambda_N)^2/2\sigma^2}}{\sqrt{2\pi}\sigma\nu_N\lambda_N} \\
&= \lim_{N\to\infty} \frac{\mathrm{e}^{\log N}\mathrm{e}^{-\nu_N^2\log N}}{2\sqrt{\pi\log N}\nu_N} \\
&= \lim_{N\to\infty} \frac{N^{1-\nu_N^2}}{2\nu_N\sqrt{\pi\log N}} > 0
\end{aligned}$$

All slower growing thresholds lack this probabilistic upper bound property.

3.4.6 Universal threshold in practice

Figure 3.6 shows this universal threshold at work. We add artificial white noise ($\sigma = 0.2$) to test signal with $N = 2048$ data points. Only the finest five levels are thresholded. Using the universal threshold ($\lambda_{\mathrm{UNIV}} = 0.7810$) yields indeed a smoother result than the minimum MSE threshold ($\lambda_{\mathrm{MSE}} = 0.2656$).

In an image processing context, smoothness means blur. Figure 3.7 shows that the universal threshold, without further modifications to the algorithm, is certainly not appropriate for image de-noising. The minimum MSE threshold performs better, but still does not satisfy. Several further modifications to ameliorate this result are discussed in the subsequent chapters.

3.5 Beyond the piecewise polynomial case

Theorem 3.1 investigated the asymptotic behavior of the minimum risk threshold λ^* for piecewise polynomials. We would like to generalize this result to general piecewise smooth functions. The proof of the polynomial theorem introduced the idea that the optimal threshold is the best compromise between coefficients with a large uncorrupted value, for which this threshold is already beyond the optimum, ($\frac{\partial r}{\partial \lambda}(v_i, \lambda^*) > 0$) and small coefficients, for which the optimal threshold could be larger ($\frac{\partial r}{\partial \lambda}(v_i, \lambda^*) < 0$). This distinction implicitly divides the coefficients into two groups, but we did not compute the boundary v^* between them, because for piecewise polynomials, we can count on the important group of coefficients exactly equal to zero.

For general piecewise smooth functions, none of the coefficients is exactly zero, and therefore we want to have an idea for which and for how many coefficients a given threshold λ^* is too large or too small. This could give us an impression of the behavior of the optimal compromise.

3.5.1 For which coefficients is a given threshold too large/small?

From Lemma 3.3, we learn that:

$$\frac{\partial r}{\partial \lambda}(v, \lambda) = 0 \Leftrightarrow \frac{\sigma^2}{\lambda} = \frac{1 + \Phi(-v - \lambda) - \Phi(-v + \lambda)}{\phi(v + \lambda) + \phi(-v + \lambda)}. \tag{3.21}$$

We now consider this as an equation in v and look for a lower bound for its solution v^* as a function of λ. Lemma 3.5 says that for a fixed threshold value, $\frac{\partial r}{\partial \lambda}(v, \lambda)$ is a monotonically increasing function of v if $v > 0$, and this guarantees that Equation (3.21) has at most one solution.

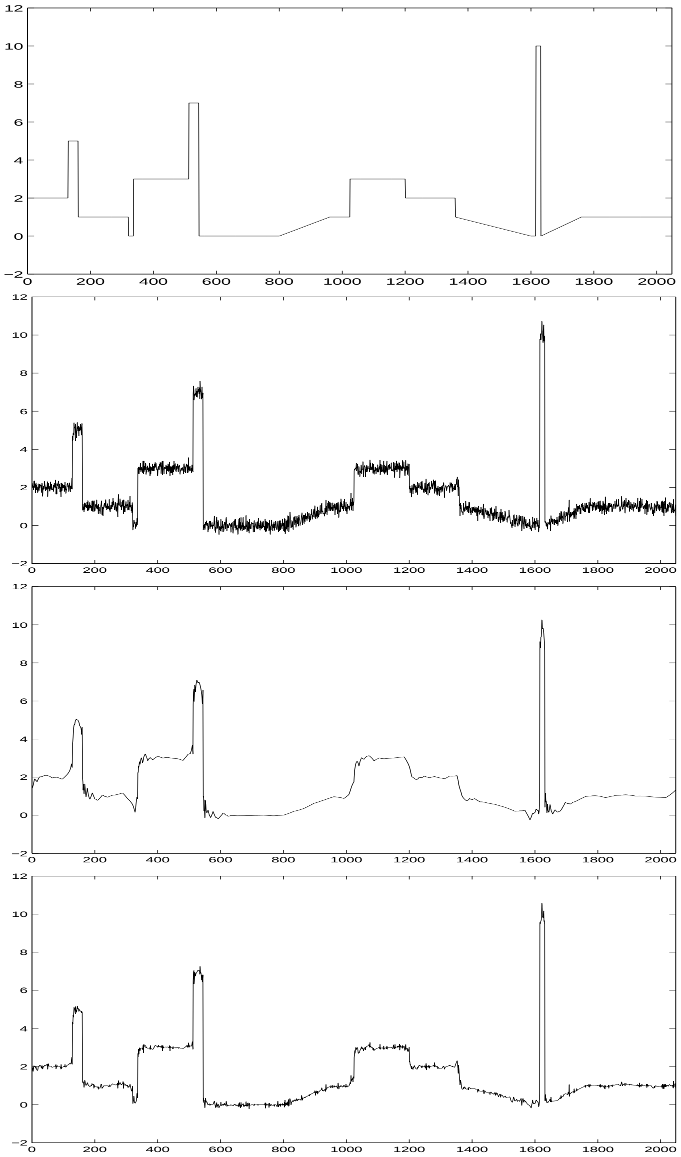

Figure 3.6: Universal threshold at work. The first plot shows a test signal. Next is the same signal with additive, Gaussian i.i.d. noise. The first reconstruction is by thresholding the finest five resolution levels, using a universal threshold ($\lambda_{\mathrm{UNIV}} = 0.7810$). The second reconstruction uses the minimum MSE threshold ($\lambda_{\mathrm{MSE}} = 0.2656$). The universal threshold is larger, and so creates a smoother reconstruction, but it also introduces more bias. We use orthogonal Daubechies wavelets with three vanishing moments here.

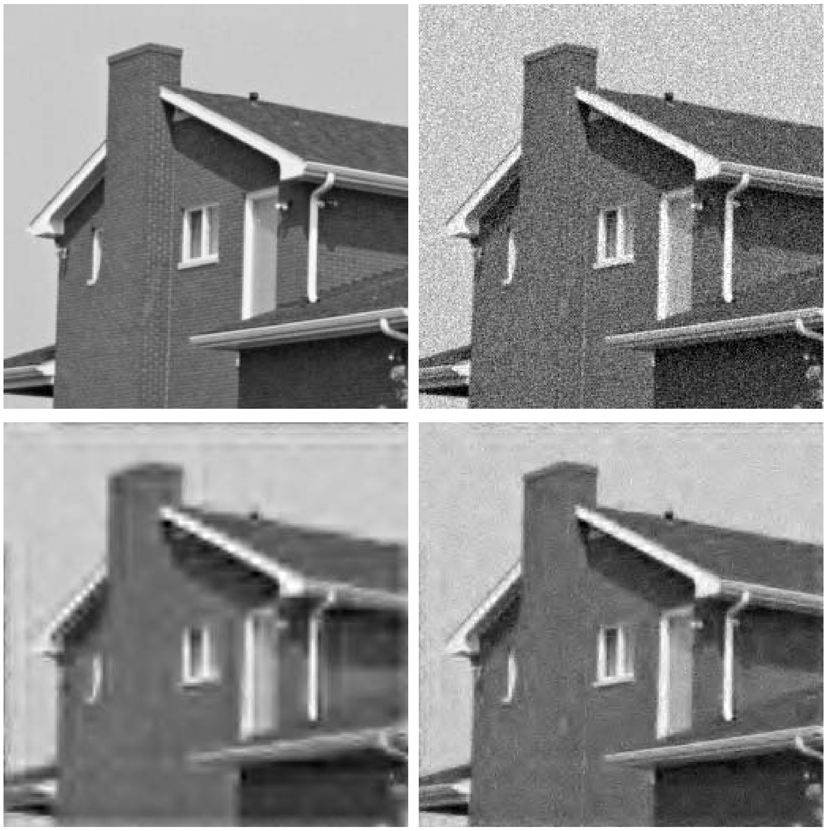

Figure 3.7: Thresholding for images. The image on lower left was obtained by the universal threshold. Smoothness means blur here. The minimum MSE threshold gives a better result (lower right). The wavelet basis is Daubechies' orthogonal one with three vanishing moments, and we process the three finest resolution levels only. The image has 256 by 256 pixels.

Let $G(v, \lambda)$ be the right-hand side of Equation (3.21):

$$G(v,\lambda) = \frac{1 + \Phi(-v-\lambda) - \Phi(-v+\lambda)}{\phi(v+\lambda) + \phi(-v+\lambda)}.$$

It is trivial to see that

$$\lim_{v\to\infty} G(v,\lambda) = \infty.$$

If we find a value v^0 for which $G(v^0, \lambda) \leq \frac{\sigma^2}{\lambda}$, we may conclude that the solution v^* of (3.21) satisfies $v^* \geq v^0$.

We evaluate

$$G\left(\frac{\sigma^2}{\lambda}, \lambda\right) = \sigma \; \frac{2 - \Phi_1(u+1/u) - \Phi_1(u-1/u)}{\phi_1(u+1/u) + \phi_1(u-1/u)},$$

in which $u = \lambda/\sigma$ and ϕ_1, Φ_1 are standard normal density and distribution:

$$\phi_1(x) = \frac{1}{\sqrt{2\pi}}\, \mathrm{e}^{-x^2/2}.$$

The next, technical section argues that:

$$u \; \frac{2 - \Phi_1(u+1/u) - \Phi_1(u-1/u)}{\phi_1(u+1/u) + \phi_1(u-1/u)} \leq 1 \qquad (3.22)$$

for all $u \geq 1.7815$, and so

$$G\left(\frac{\sigma^2}{\lambda}, \lambda\right) \leq \frac{\sigma^2}{\lambda}$$

if $\lambda \geq 1.7815\,\sigma$.

This allows us to formulate the following theorem:

Theorem 3.3 *If $\lambda \geq 1.7815\,\sigma$, and v^* satisfies*

$$\frac{\partial r}{\partial \lambda}(v^*, \lambda) = 0$$

then

$$v^* \geq \frac{\sigma^2}{\lambda}. \qquad (3.23)$$

Figure 3.8 shows a numerical computation of the curve $v^*(\lambda)$. It demonstrates that we have found a sharp lower bound.

In the upcoming analysis we need the fact that $\frac{\partial r}{\partial \lambda}(v, \lambda)$ is convex as a function of v for $|v| \leq \sigma^2/\lambda$. Therefore, we formulate an additional lemma:

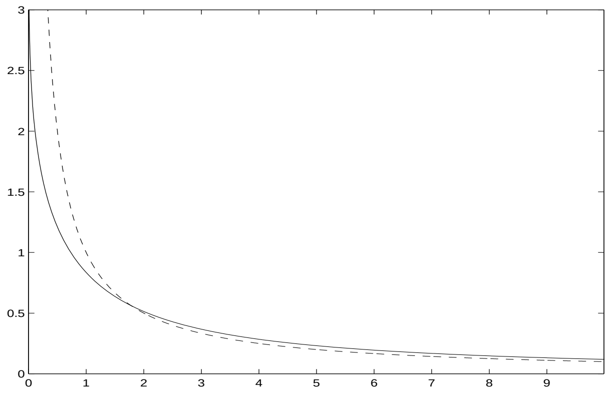

Figure 3.8: Full line: plot of v^* as a function of λ, where v^* satisfies $\frac{\partial r}{\partial \lambda}(v^*, \lambda) = 0$. Dashed line: plot of σ^2/λ. In this example we put $\sigma = 1$.

Lemma 3.7 *If $\lambda \geq \sigma$, we have for $v \leq \sigma^2/\lambda$:*

$$\frac{\partial^2}{\partial v^2}\left(\frac{\partial r}{\partial \lambda}\right) \geq 0. \tag{3.24}$$

Proof:
From Lemma 3.5 we compute

$$\frac{\partial^2}{\partial v^2}\left(\frac{\partial r}{\partial \lambda}\right) = 2\phi(v+\lambda)\left[1 - \frac{v(v+\lambda)}{\sigma^2}\right] + 2\phi(v-\lambda)\left[1 - \frac{v(v-\lambda)}{\sigma^2}\right]. \tag{3.25}$$

The factor

$$1 - \frac{v(v-\lambda)}{\sigma^2}$$

is positive on

$$\left[\frac{\lambda - \sqrt{\lambda^2 + 4\sigma^2}}{2}, \frac{\lambda + \sqrt{\lambda^2 + 4\sigma^2}}{2}\right],$$

which contains the interval $[0, \lambda]$.

Since $v \leq \sigma^2/\lambda$ and $\lambda \geq \sigma$ by assumption, we have $v \leq \lambda$, and so:

$$\begin{aligned} \frac{\partial^2}{\partial v^2}\left(\frac{\partial r}{\partial \lambda}\right) &\geq 2\phi(v+\lambda)\left[1 - \frac{v(v+\lambda)}{\sigma^2} + 1 - \frac{v(v-\lambda)}{\sigma^2}\right] \\ &= 4\phi(v+\lambda)\left[1 - \frac{v^2}{\sigma^2}\right]. \end{aligned}$$

From $v \leq \sigma^2/\lambda$ and $\lambda \geq \sigma$, it also follows that $v \leq \sigma$, and so we know that this expression is positive. □

Corollary 3.1 *For $\lambda \to \infty$,*

$$\frac{\partial r}{\partial \lambda}(\frac{\sigma^2}{2\lambda}, \lambda)$$

is negative and tends to 0, but not faster than

$$-2\sigma^4 \frac{\phi(\lambda)}{\lambda^2}$$

Proof:
This follows from the asymptotic behavior of $\frac{\partial r}{\partial \lambda}(0, \lambda)$ in Lemma 3.4, the fact that

$$\frac{\partial r}{\partial \lambda}(\frac{\sigma^2}{\lambda}, \lambda) \leq 0,$$

which follows from Theorem 3.3, and from the previous lemma, stating that $\frac{\partial r}{\partial \lambda}$ is convex between 0 and σ^2/λ. □

3.5.2 Intermediate results for the risk in one coefficient

This leaves us with the question to prove the inequality in (3.22). This section is purely technical, and may be skipped for understanding the rest of this chapter.

Call

$$H(u) = u \, \frac{2 - \Phi_1(u + 1/u) - \Phi_1(u - 1/u)}{\phi_1(u + 1/u) + \phi_1(u - 1/u)}. \tag{3.26}$$

The plot of this function in Figure 3.9 seems to confirm that indeed $H(u) < 1$ for $u > 1.7815$. To make sure that this remains true for higher values of u, we start with the following lemma:

Lemma 3.8 *The function*

$$H_0(x) = \frac{1 - \Phi_1(x)}{\phi_1(x)} \tag{3.27}$$

tends to zero for $x \to \infty$ and decreases monotonically for all positive x.

Proof:
The computation of $\lim_{x\to\infty} H_0(x)$ is straightforward, using De L'Hôpital's rule.

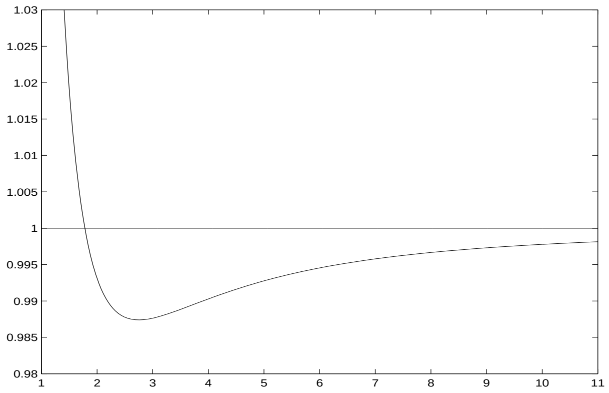

Figure 3.9: Plot of function $H(u)$, defined in (3.26). Important to note is that this function is smaller than 1 for $u > 1.7815$.

Next, it can be verified that $H_0(x)$ satisfies the first order differential equation:

$$H_0'(x) = xH_0(x) - 1,$$

and so

$$H_0''(x) = xH_0'(x) + H_0(x).$$

Suppose $H_0'(x) > 0$. Since $H_0(x) > 0$, this means that $H_0''(x) > 0$. So, $H_0'(x)$ would be positive and increasing. This conflicts with the limit of $H(x)$ to be zero. □

As a consequence of this lemma, and since it follows from $a/b \leq c/d$ that $a/b \leq (a+c)/(b+d) \leq c/d$, we have that for positive u:

$$u\,\frac{1-\Phi_1(u+\frac{1}{u})}{\phi_1(u+\frac{1}{u})} \leq u\,\frac{\left(1-\Phi_1(u+\frac{1}{u})\right)+\left(1-\Phi_1(u-\frac{1}{u})\right)}{\phi_1(u+\frac{1}{u})+\phi_1(u-\frac{1}{u})} \leq u\,\frac{1-\Phi_1(u-\frac{1}{u})}{\phi_1(u-\frac{1}{u})}.$$

It is easy to verify that both the left and the right-of this inequalities tend to one if $u \to \infty$, and so, we may conclude that

$$\lim_{u\to\infty} H(u) = 1. \tag{3.28}$$

We now use the fact that

$$\phi_1(u-\frac{1}{u}) = \mathrm{e}^2\,\phi_1(u+\frac{1}{u})$$

to rewrite $H(u)$ as:

$$H(u) = \frac{u}{\mathrm{e}^2+1}\,\frac{2-\Phi_1(u+\frac{1}{u})-\Phi_1(u-\frac{1}{u})}{\phi_1(u+\frac{1}{u})}.$$

From this expression we calculate:

$$H'(u) = -u - \frac{\mathrm{e}^2-1}{\mathrm{e}^2+1}\frac{1}{u} + \left(u + \frac{1}{u} - \frac{1}{u^3}\right) H(u).$$

This allows us to prove that:

Lemma 3.9 *The function $H(u)$, as defined in Equation (3.26), satisfies:*

$$H(u) \leq 1, \quad \forall u \geq \sqrt{\frac{\mathrm{e}^2+1}{2}} \approx 2.048. \tag{3.29}$$

Proof:
Suppose $H(u) \geq 1$, then

$$H'(u) \geq \frac{\mathrm{e}^2+1}{2}\frac{1}{u} - \frac{1}{u^3}.$$

This expression is positive for $u \geq \sqrt{\frac{\mathrm{e}^2+1}{2}}$, which means that $H(u)$ would increase and its limit could never become one. □

3.5.3 Piecewise smooth functions

If the noise-free signal is an exact polynomial, and if the multiresolution analysis has sufficiently many vanishing moments, the signal can be written as a linear combination of scaling functions at an arbitrary resolution. This means that all detail coefficients, i.e., the wavelet coefficients, are exactly zero. We used this property to describe what happens with *piecewise* polynomials. To investigate piecewise smooth functions, we follow the same way: we start with properties for wavelet coefficients of functions with a certain degree of smoothness. Of course, these coefficients will not be exactly zero, but smooth functions can be approximated by polynomials and this approximation guarantees that wavelet coefficients are “sufficiently” small. All this motivates the following definition of *Lipschitz continuity* as a measure of smoothness:

Definition 3.2 *A function f is called (uniformly) Lipschitz α over an interval $[a, b]$ if for all $x \in [a, b]$ there exists a polynomial $p_x(t)$, and there exists a constant K, independent of x, so that*

$$\forall t \in [a, b] : |f(t) - p_x(t)| \leq K|t - x|^\alpha. \tag{3.30}$$

A Lipschitz continuous function can be locally approximated by a polynomial. The effect on the wavelet coefficients of such a function is described by the following theorem, due to Jaffard [81, 113]:

Theorem 3.4 *If a function f is uniformly Lipschitz α over $[a,b]$ and if the wavelet function ψ has p vanishing moments with $p \geq \alpha$, then*

$$\exists C \in \mathbb{R}^+, \forall j \in \mathbb{Z}, \forall i = 1 \ldots 2^j : |\langle f, \psi_{j,k} \rangle| \leq C 2^{-j\left(\alpha + \frac{1}{2}\right)}. \tag{3.31}$$

We now have all the elements to study the asymptotic behavior of the minimum MSE threshold λ^* for piecewise Lipschitz α signals, corrupted by white, stationary and Gaussian noise. We work on the bounded interval $[0,1]$ and assume that the number of singularities is finite and that the function $f(x)$ is bounded. As in the piecewise polynomial case, we call I_0 the set of coefficients corresponding to basis functions not interfering with one the singularities and I_1 all the other coefficients. The cardinal numbers of these sets are respectively M_0 and M_1.

We call v^* the critical untouched coefficient value, corresponding to the minimum MSE threshold λ^*: for noise-free coefficients below this value, λ^* is too small, for coefficients with larger magnitude, the threshold is too large. The minimum MSE threshold is the best compromise between these two groups and in Section 3.5.1, Equation 3.23 we found a lower bound for the critical coefficient value: $v^* \geq \sigma^2/\lambda^* \geq \sigma^2/2\lambda^*$. This means that if we call

$$F_0 = \{i = 1, \ldots, N \mid |v_i| \leq v^* \},$$

and

$$F_L = \{i = 1, \ldots, N : |v_i| \leq \sigma^2/2\lambda^*\},$$

then we know that

$$F_L \subset F_0.$$

We call $K_0 = \#F_0$ the number of coefficients beneath the critical value and $K_1 = N - K_0$ the number of coefficients above this value. It is important to note that

$$v_i \in F_0 \Leftrightarrow \frac{\partial r}{\partial \lambda}(v_i, \lambda^*) \leq 0,$$

and so, we can write the equation

$$\mathrm{E}R'(\lambda^*) = 0$$

as

$$-\sum_{i \in F_0} \frac{\partial r}{\partial \lambda}(v_i, \lambda^*) = \sum_{i \in F_1} \frac{\partial r}{\partial \lambda}(v_i, \lambda^*), \tag{3.32}$$

and both sides in this equation have only positive terms.

We suppose that the coefficients are computed from a direct projection of the continuous signal:

$$v_{j,k} = \sqrt{N}\langle f, \psi_{j,k}\rangle = 2^{J/2}\langle f, \psi_{j,k}\rangle.$$

In practice, these values are approximated by a Fast Wavelet Transform on sample values, or pre-filtered sample values.

To have an idea of the asymptotic behavior of the sums in Equation (3.32), we count the number of terms on the left-hand side:

$$K_0 = \#F_0 \geq \#(F_0 \cap I_0) \geq \#(F_L \cap I_0).$$

The coefficients at the jth resolution level in I_0 satisfy $v_i \leq C2^{J/2}2^{-j(\alpha+1/2)}$. So, if a given resolution level j satisfies

$$C2^{(J-2j\alpha-j)/2} \leq \sigma^2/2\lambda^*,$$

we are sure that all I_0-coefficients at that level are in $F_L \subset F_0$. This condition on j can be worked out as:

$$j \geq \frac{J - \frac{2}{\log 2}\log\sigma^2 + \frac{2}{\log 2}\log\lambda^* + \frac{2}{\log 2}\log 2C}{2\alpha+1}.$$

In the expression on the right-hand side λ^* is expected to depend on J, but we assume that $\log\lambda^*$ can be neglected with respect to J. If this is not the case, this means that the optimal threshold would increase at least linearly with N. This would not pose any problem to our further analysis, but it is rather unlikely to happen, apart from some pathological cases (a zero signal, for instance). We also drop the constant terms in this right-hand side and we express that $K_1 = N - K_0$ must be smaller than the total number of coefficients at scales j not satisfying this condition *plus* the total number of coefficients in I_1:

$$\begin{aligned} K_1 &\leq M_1 + \sum_{j=0}^{\lfloor J/(2\alpha+1)\rfloor} 2^j \\ &\approx M_1 + \frac{2^{J/(2\alpha+1)+1}-1}{2-1} \\ &\sim 2\cdot 2^{J/(2\alpha+1)} \\ &= 2N^{1/(2\alpha+1)}. \end{aligned}$$

So: $$\frac{K_1}{N} \sim 2N^{1/(2\alpha+1)-1} = 2N^{-2\alpha/(2\alpha+1)}.$$

Taking the logarithm of these asymptotics gives:

$$\begin{aligned} \log K_1 &\sim \frac{\log N}{2\alpha+1}, \\ \log K_0 &= \log(N-K_1) = \log N + \log\left(1 - \frac{K_1}{N}\right) \sim \log N - \frac{K_1}{N} \sim \log N. \end{aligned}$$

Actually, we have started from a lower bound for K_0 to find this behavior. Obviously $\log K_0$ cannot grow faster than $\log N$, since $K_0 \leq N$. On the other hand, the behavior of $\log K_1$ is based on an upper bound. Theoretically, $\log K_1$ may grow slower than $\log N/(2\alpha+1)$. Following the analysis below, it would turn out that in that case, the minimum MSE threshold would grow (a little) faster. The asymptotic behavior that we will find is a minimal one. Since our primary concern for the next chapter is to demonstrate that the threshold does increase to infinity with N, our result is sufficient for further usage.

We are now ready to fill in both sides of Equation (3.32). For the right-hand side, we assume that λ^* increases slower than v_i, and from Lemma 3.3 it then follows that this side behaves like $K_1 2\lambda^*$. For the left-hand side, we use lower bounds, both for the number of coefficients in F_0 as for their asymptotic behavior. We only consider the coefficients in $F_L \subset F_0$ for which Corollary 3.1 gives a lower bound on the asymptotic behavior.

$$\begin{aligned}
K_0 2\sigma^4 \frac{\phi(\lambda)}{\lambda^2} &\sim K_1 2\lambda \\
\sigma^4 \frac{\phi(\lambda)}{\lambda^3} &\sim \frac{K_1}{N-K_1} \\
\sigma^4 \frac{\phi(\lambda)}{\lambda^3} &\sim \frac{1}{\frac{N}{K_1}-1} \\
\sigma^4 \frac{\phi(\lambda)}{\lambda^3} &\sim \frac{1}{\frac{1}{2}N^{2\alpha/(2\alpha+1)}-1} \\
\sigma^4 \frac{\mathrm{e}^{-\lambda^2/2\sigma^2}}{\sqrt{2\pi}\sigma\lambda^3} &\sim 2N^{-2\alpha/(2\alpha+1)}.
\end{aligned}$$

Taking the logarithm on both sides leads to the following theorem:

Theorem 3.5 *If a function f is Lipschitz α on $[0,1]$, except in a finite number of points and the wavelet analysis has p vanishing moments with $p \geq \alpha$, then the minimum MSE-threshold λ^* for de-noising the corrupted observation*

$$y_i = f(i/N) + \eta_i \qquad i = 1, \ldots, N$$

behaves asymptotically as

$$\lambda^* \sim \sqrt{\frac{2\alpha}{2\alpha+1}}\ \sqrt{2\log N}\sigma, \tag{3.33}$$

if the number of observations N increases.

The factor

$$\sqrt{\frac{2\alpha}{2\alpha+1}}$$

comes from the fact that for piecewise smooth functions, coefficients with no interaction with the singularities are not exactly zero. In our analysis, when estimating the number of coefficients K_1 above the critical value v^*, we even neglected the singularity coefficients, compared to these non-zero coefficients with no singularity interaction: the same behavior would appear (as a lower bound) for signals with no singularity at all.

3.5.4 Function spaces

Lipschitz continuity is *in se* a local, pointwise description of regularity. A function which is Lipschitz-1-continuous in x is also continuous in this point, but not necessarily differentiable. The notion of uniform Lipschitz regularity extends this regularity to an interval. For $\alpha = 1$, for instance, this measurement of regularity is stronger than pointwise continuity and even uniform continuity is a weaker statement. The uniform Lipschitz idea is based on a minimax principle, which is definitely to restrictive for the type of signals we want to describe. As a matter of fact, the functions that we have in mind typically have *no* uniform behavior, they are *piecewise* smooth . These functions can be approximated arbitrarily well by uniformly Lipschitz functions in the sense of mean square loss. The sequence of approximations converges, so it is a Cauchy sequence, which means that two elements from the sequence can come arbitrarily close. A Cauchy sequence with all elements being Lipschitz α does not necessarily converge in mean square error to a Lipschitz α function. This is serious shortcoming from the approximation theoretic point of view. The Hölder space of uniformly Lipschitz functions $C^{\alpha}[0,1]$ is said to be *not complete* with respect to the quadratic distance.

The well known Lebesgue spaces $L_p[0,1]$ ($p \geq 1$), equipped with the corresponding norm

$$\|f\|_{L_p[0,1]} = \left(\int_{[0,1]} |f(x)|^p dx \right)^{\frac{1}{p}}$$

are complete, they allow for singularities, but these spaces provide little smoothness guarantee.

Sobolev spaces $W_p^k[0,1]$ [22] are a sort of complete extensions of $C^k[0,1]$ functions in $L_p[0,1]$. The Sobolev norm is defined as:

$$\|f\|_{W_p^k} = \left(\sum_{n=0}^{k} \|f^{(n)}\|_{L_p[0,1]}^p \right)^p ,$$

For $1 \leq p < \infty$, and

$$\|f\|_{W_\infty^k} = \max_{0 \leq n \leq k} \|f^{(n)}\|_{L_\infty[0,1]}.$$

In this definition $f^{(n)}$ stands for (a weak version of) the nth derivative of f. $W_2^k[0,1]$ spaces are often notated as $H^k[0,1]$.

A further generalization leads to Besov spaces [54, 52, 53, 56]. The definition is quite complicated, and involves a couple of additional concepts:
The r-th difference of a function $f \in L_p[0,1]$ is defined by

$$\Delta_h^{(r)} f(x) = \sum_{k=0}^{r} (-1)^k \left(\begin{array}{c} r \\ k \end{array} \right) f(x+kh), \tag{3.34}$$

and call

$$\nu_{r,p}(f;t) = \sup_{h \leq t} \|\Delta_h^{(r)} f\|_{L_p[0,1-rh]} \tag{3.35}$$

the r-th *modulus of smoothness* of f in $L_p[0,1]$. Then for $r > s$, and $1 \leq p, q < \infty$,

$$|f|_{B_{p,q}^{\alpha}} = \left[\int_{[0,1]} \left(\frac{\nu_{r,p}(f;u)}{u^{\alpha}} \right)^q \frac{du}{u} \right]^{\frac{1}{q}} \tag{3.36}$$

is the Besov semi-norm of f. A semi-norm may be zero for an essentially non-zero function. To eliminate this unwanted situation, we define the Besov norm of $f \in L_p[0,1]$ as:

$$\|f\|_{B_{p,q}^{\alpha}} = \|f\|_{L_p[0,1]} + |f|_{B_{p,q}^{\alpha}}. \tag{3.37}$$

For $q = \infty$, the semi-norm becomes:

$$|f|_{B_{p,\infty}^{\alpha}} = \sup_{0<t<1} \frac{\nu_{r,p}(f;t)}{t^{\alpha}}. \tag{3.38}$$

A Besov space is a set functions with finite Besov norm. To understand what kind of functions belong to a given Besov space, it is interesting to look at the wavelet expansion of these functions. Since all Besov spaces are in $L_p[0,1]$ and

$$\lim_{j \to \infty} V_j = V_L \oplus \left(\bigoplus_{j=L}^{\infty} W_j \right)$$

is dense in $L_2[0,1]$, the wavelet expansion

$$f(x) = \sum_{k=1}^{2^L} s_{L,k} \varphi_{L,k}(x) + \sum_{j=L}^{\infty} \sum_{k=1}^{2^j} w_{j,k} \psi_{j,k}(x)$$

converges in $L_p[0,1]$ sense. Indeed, $L_q[0,1] \subset L_p[0,1]$ for $q \geq p$. So, for $p > 2$, we have that $L_p[0,1] \subset L_2[0,1]$. Suppose that the mother function $\psi \in L_p[0,1]$, then all elements of the expansion as well as the limit function are in $L_p[0,1]$. The error then converges in $L_p[0,1]$-norm. On the other hand, it is straightforward to see that $L_2[0,1]$ is a dense subset of $L_p[0,1]$ with respect to the $L_p[0,1]$-norm if $1 \leq p < 2$. V_∞ is dense in $L_2[0,1]$, with respect to the $L_2[0,1]$-norm, and the Hölder inequality learns that for $p < 2$ (i.e. $2/p > 1$) and q satisfying $p/2 + 1/q = 1$:

$$\begin{aligned}\left[\int_{[0,1]} |f(u)|^p du\right]^{\frac{1}{p}} &\leq \left[\left(\int_{[0,1]} (|f(u)|^p)^{\frac{2}{p}} du\right)^{\frac{p}{2}} \left(\int_{[0,1]} 1^q du\right)^{\frac{1}{q}}\right]^{\frac{1}{p}} \\ &= \left(\int_{[0,1]} |f(u)|^2\right)^{\frac{1}{2}}.\end{aligned}$$

So all approximations that converge with respect to the $L_2[0,1]$-norm, do so for the $L_p[0,1]$-norm as well, provided $1 \leq p \leq 2$. Hence, V_∞ is dense in $L_2[0,1]$, with respect to the $L_p[0,1]$-norm. All elements together lead to the conclusion that V_∞ is dense in $L_p[0,1]$, with respect to the $L_p[0,1]$-norm: a function in $L_p[0,1]$ has a converging wavelet expansion.

It turns out that both an upper bound and a lower bound for the Besov norm of a function in $L_p[0,1]$ can be expressed in terms of this expansion. Call the Besov sequence space:

$$\|\boldsymbol{w}\|_{b^\alpha_{p,q}} = \left[\sum_{j=L}^{\infty} 2^{j\beta q} \left(\sum_{k=1}^{2^j} |w_{j,k}|^p\right)^{\frac{q}{p}}\right]^{\frac{1}{q}}, \tag{3.39}$$

with $\beta = \alpha + 1/2 - 1/p$. For $q = \infty$, this is:

$$\|\boldsymbol{w}\|_{b^\alpha_{p,\infty}} = \sup_{j \geq L} \left[2^{j\beta} \left(\sum_{k=1}^{2^j} |w_{j,k}|^p\right)^{\frac{1}{p}}\right]. \tag{3.40}$$

Then there exist constants c and C, not depending on f so that:

$$c\|f\|_{B^\alpha_{p,q}} \leq \|\boldsymbol{w}\|_{b^\alpha_{p,q}} \leq C\|f\|_{B^\alpha_{p,q}}. \tag{3.41}$$

The wavelet basis is an *unconditional* basis for the Besov space, since the absolute values of the coefficients suffice to check whether a function belongs to the space or not.

This norm equivalence also allows for a characterization of functions in Besov spaces: the wavelet coefficients should decay sufficiently fast to have an expansion with finite Besov sequence norm, and hence a finite Besov function norm.

Piecewise smooth functions with a finite number of singularities are among these functions [113]. More thorough interpretations are in [3, 36].

It would be interesting to check whether the minimum risk threshold for functions in Besov spaces has a similar behavior as in Theorem 3.5.

3.6 Conclusion

We have proven that the minimum risk threshold is slowly growing if the sample size increases. For piecewise polynomials, the minimum risk threshold asymptotically coincides with the universal threshold, for general piecewise smoothness, the minimum risk threshold is lower, but it comes close to the universal threshold within a constant factor.

We are now ready to motivate an estimation procedure for this minimum risk threshold. The following chapter introduce a generalized cross validation approach and proves that it has asymptotically optimal quality.

Chapter 4

Estimating the minimum MSE threshold

“Nel mezzo del cammin di nostra vita
mi ritrovai per una selva oscura,
che la diritta via era smarrita.
Ahi quanto a dir qual era ‘e cosa dura
esta selva selvaggia e aspra e forte
che nel pensier rinova la paura!”
—Dante Alighieri, *La Divina Commedia, Inferno: Canto I.*

The previous chapter has investigated the behavior of the minimum risk threshold. In practical problems, the mean square error function can never be evaluated exactly, because the uncorrupted coefficients are necessary to compute the error of the output. Therefore, we need to estimate this MSE function.

This chapter examines a generalized cross validation (GCV) procedure and shows that this leads to an estimate of the MSE-function, the so called GCV-function. So, like MSE, GCV is a function of the threshold value, but evaluation of this function only requires input data and yet its expected value is asymptotically a vertical translation of the risk function. Hence the minimum of this GCV can serve as an estimate for the minimum MSE threshold.

The optimality of GCV is only an asymptotic one. The behavior of GCV for finite data, discussed in Section 4.4, explains why we cannot expect more. To prove this asymptotic properties, we use the knowledge about the asymptotics of the minimum risk threshold from the previous chapter.

GCV is an asymptotically optimal threshold estimator. Speed is a second property: the GCV procedure finds and applies a threshold with less operations than necessary for a wavelet transform. Third, this procedure only uses input data: no additional knowledge or estimations are needed, even not on the amount of noise (the input variance).

Cross Validation is a widely used method for evaluating the optimality of a smoothing parameter. Applications in wavelet based smoothing appear in diverse algorithms [116, 123, 149, 150].

GCV in threshold applications is based on Stein's Unbiased Risk Estimation (SURE). Section 4.1 explains the basics of this threshold estimation method. What follows, is an original investigation of the GCV method. The theoretical argument is illustrated by several test examples.

Like the previous one, this chapter is based on the idea of sparsity in a wavelet representation.

4.1 SURE, a first estimator for the MSE

4.1.1 The effect of the threshold operation

We are looking for an estimator for $R(\lambda)$, which is based on known variables. Therefore we first investigate the effect of the threshold operation on the input data.

Define

$$F(\lambda) = \frac{\sum_{i=1}^{N}(w_{\lambda i} - w_i)^2}{N} = \frac{1}{N}\|\boldsymbol{w_\lambda} - \boldsymbol{w}\|^2. \tag{4.1}$$

For the expectation of this function, we can write:

$$\begin{aligned} \mathrm{E}F(\lambda) &= \mathrm{E}\frac{1}{N}\left(\|\boldsymbol{w} - \boldsymbol{v}\|^2 + \|\boldsymbol{v} - \boldsymbol{w_\lambda}\|^2 + 2 \cdot \langle(\boldsymbol{w} - \boldsymbol{v}), (\boldsymbol{v} - \boldsymbol{w_\lambda})\rangle\right) \\ &= \sigma^2 + \mathrm{E}R(\lambda) - \frac{2}{N}\mathrm{E}\langle\boldsymbol{\omega}, \boldsymbol{\omega_\lambda}\rangle \end{aligned} \tag{4.2}$$

The following lemma leads to an alternative expression for the third term on the right hand side:

Lemma 4.1 *If the density $\phi(\omega_i)$ is Gaussian, then for* soft-*thresholding:*

$$\mathrm{E}[\omega_i \omega_{\lambda i}] = \sigma^2 \mathrm{P}(|w_i| > \lambda). \tag{4.3}$$

Proof:
The Gaussian density function satisfies a first order differential equation:

$$\omega_i \phi(\omega_i) = -\sigma^2 \phi'(\omega_i),$$

which allows to write:

$$\begin{aligned}
\mathrm{E}[\omega_i \omega_{\lambda i}] &= \int_{-\infty}^{\infty} \omega_{\lambda i}\, \omega_i\, \phi(\omega_i)\, d\omega_i \\
&= -\sigma^2 \int_{-\infty}^{\infty} \omega_{\lambda i}\, \phi'(\omega_i)\, d\omega_i \\
&= -\sigma^2 \omega_{\lambda i}\, \phi(\omega_i)\big|_{-\infty}^{\infty} + \sigma^2 \int_{-\infty}^{\infty} \frac{\partial \omega_{\lambda i}}{\partial \omega_i}\, \phi(\omega_i)\, d\omega_i .
\end{aligned}$$

Integration by parts is allowed since $\omega_{\lambda i}(\omega_i)$ is a continuous function, at least if we use soft-thresholding.
It is easy to see that:

$$\frac{\partial \omega_{\lambda i}}{\partial \omega_i} = \begin{cases} 0 & \text{if } |w_i| < \lambda, \\ 1 & \text{otherwise,} \end{cases}$$

from which (4.3) follows. □

This lemma is in fact a special case of more general results by Hudson [79] and Stein [132].

With respect to the third term in (4.2), and for further use, we define

$$\mu_1(\lambda) = \frac{\sum_{i=1}^{N} \mathrm{E}[\omega_i \omega_{\lambda i}]}{N\sigma^2}. \tag{4.4}$$

The lemma says that:

$$\mu_1(\lambda) = \frac{1}{N} \sum_{i=1}^{N} \mathrm{P}(|w_i| > \lambda). \tag{4.5}$$

4.1.2 Counting the number of coefficients below the threshold

We now introduce a matrix:

$$D_{ij} = \frac{\partial w_{\lambda i}}{\partial w_j}. \tag{4.6}$$

Note that if $i \neq j$, then $D_{ij} = 0$.For $i = j$ we have

$$D_{ii} = \begin{cases} 0 & \text{if } |w_i| < \lambda, \\ 1 & \text{otherwise.} \end{cases}$$

Thus, if $\mathrm{Tr}(D)$ is the trace of D, then

$$\mathrm{Tr}(D) = \#\{i \mid w_{\lambda i} \neq 0\} = N - N_0,$$

where

$$N_0 = \#\{i | w_{\lambda i} = 0\} \tag{4.7}$$

Furthermore we consider the Jacobian matrix A with entries

$$A_{ij} = \frac{\partial y_{\lambda i}}{\partial y_j}. \tag{4.8}$$

Then it is easy to see that

$$A = \tilde{W}^{-1} \cdot D \cdot \tilde{W}, \tag{4.9}$$

where $\tilde{W}$ is the forward wavelet transform matrix. If the transform is orthogonal and $W = \tilde{W}^{-1}$ is the inverse transform matrix, we can write A as the rectangular two-dimensional inverse transform of D:

$$A = WDW^T.$$

Since $\tilde{W}$ is non-singular,

$$\mathrm{Tr}(A) = \mathrm{Tr}(D).$$

With these notations, and since for a Bernoulli variable

$$\mathrm{E}D_{ii} = \mathrm{P}(D_{ii} = 1), \tag{4.10}$$

we can rewrite μ_1 as:

$$\begin{aligned}
\mu_1(\lambda) &= \frac{1}{N}\sum_{i=1}^{N} \mathrm{P}(D_{ii} = 1) \\
&= \frac{1}{N}\sum_{i=1}^{N} \mathrm{E}D_{ii} \\
&= \frac{\mathrm{Tr}(\mathrm{E}A)}{N}.
\end{aligned} \tag{4.11}$$

Starting from $\langle \boldsymbol{\omega}, \boldsymbol{\omega_\lambda} \rangle$, which is not computable in practice, we end up with $\sigma^2 \mathrm{Tr}(A)$, which is easy to find while both have the same expectation. Thus, from (4.2), (4.4), and (4.5) we can construct

$$\mathrm{SURE}(\lambda) = F(\lambda) - \sigma^2 + 2\sigma^2 \cdot \frac{\mathrm{Tr}(A)}{N} \tag{4.12}$$

as an approximation for $R(\lambda)$. Application of Stein's Unbiased Risk Estimator [132] leads to the same result [61]. The unbiasedness of this estimator is not an asymptotic property, as it is the case for GCV-optimality (see further). The number of coefficients plays no role, at least not for the expected value.

The estimator can be computed in the original data domain, but since

$$\mathrm{Tr}(A) = \mathrm{Tr}(D) = N - N_0,$$

it is easier to count the number of zero coefficients in the wavelet domain.

4.1.3 SURE is adaptive

Unlike the universal threshold

$$\lambda_{\text{UNIV}} = \sqrt{2\log N}\sigma,$$

the SURE-threshold does depend directly on the given input signal, not just through a data based estimation of the noise variance σ^2. We may expect a more adaptive threshold choice. Donoho and Johnstone explain how a minimum SURE procedure adapts itself automatically to the smoothness class (Besov space) in which the uncorrupted signal probably lies: the method attains asymptotically the minimax behavior within a constant factor, and it does so simultaneously for all spaces taken from a *scale* of Besov spaces [61]. This means that if the uncorrupted function lies in a Besov smoothness space $\mathcal{F} = B^s_{p,q}$, the SURE-algorithm acts as a near-minimax procedure, i.e. it is nearly the estimator that minimizes the worst case risk within the function space:

$$\sup_{f\in\mathcal{F}} \text{Risk}(SURE) \leq C \cdot \inf_{\hat{f}} \sup_{f\in\mathcal{F}} \text{Risk}(\hat{f}), \tag{4.13}$$

where the infimum is taken over all possible estimators $\hat{f}$.

The constant C depends on the smoothness parameters p, q, s of the Besov space, but the result holds simultaneously for all spaces in a scale. This is why the procedure automatically adapts itself to the smoothness class of the uncorrupted signal. Actually, this constant C is not due to the SURE-estimate, but rather to the threshold procedure itself. As a matter of fact, SURE performs asymptotically as well as the minimax threshold on a given Besov space: threshold procedures do not need additional knowledge about the smoothness of the underlying signal to find the (nearly) best threshold.

With respect to this near-minimaxity the performance of SURE is better than that of the universal threshold by a logarithmic factor: compare (4.13) with (3.18).

4.2 Ordinary Cross Validation

This section introduces the idea of Cross Validation in an informal way. Our aim is to minimize the error function based on an unknown exact signal. We therefore try to find a good compromise between goodness of fit and smoothness. We assume that the original signal is *regular* to some extent, which means that the value f_i can be approximated by an linear combination of its neighbors. So, by considering $\tilde{y}_i$, a combination of y_j, not depending on y_i itself, we can eliminate the noise in this particular component. Since we replace it by a weighted average of its neighbors, noise in these components is smoothed, and so we end up with a relatively clean, noise-independent value. This value can be used in the computation of an approximation for $R(\lambda)$.

To investigate the closeness of fit, we compute the result of the threshold operation Λ for the modified signal $\tilde{\boldsymbol{y}}$, in which the i–th component y_i was replaced by $\tilde{y}_i$, i.e.,

$$\tilde{\boldsymbol{y}} = \Lambda\left([y_1, \dots, y_{i-1}, \tilde{y}_i, y_{i+1}, \dots, y_N]^T\right).$$

We then consider the ability of $\tilde{y}_{\lambda i}$ to "predict" the value y_i as a measure for the optimality of the choice of the threshold [43].

For (too) small values of λ the difference $y_i - \tilde{y}_{\lambda i}$ is dominated by noise, while for large values of λ the signal itself is too much deformed. We repeat the same procedure for all components and compute

$$OCV = \frac{1}{N}\sum_{i=1}^{N}(y_i - \tilde{y}_{\lambda i})^2 \tag{4.14}$$

to express the compromise. This function is called "(Leaving-out-one) Ordinary Cross Validation". This name indicates that we use the values of the *other* components in the calculation for one point. Every function evaluation of (4.14) implies N complete threshold procedures, forward and inverse transform included.

Many combination formulas are possible for $\tilde{y}_i$. Most obvious is to take $\tilde{y}_i = \frac{1}{2}\cdot(y_{i-1} + y_{i+1})$. [115, 116] But taking $\tilde{y}_i$ so that $\tilde{y}_{\lambda i} = \tilde{y}_i$ turns out to be an interesting choice: it leads to an approximating formula for OCV. This value always exists, since the threshold algorithm has a levelling effect. Indeed, taking $\tilde{y}_{\lambda i} = \max_i y_i$, we obtain $\tilde{y}_{\lambda i} \leq \tilde{y}_i$, while the opposite is true for $\tilde{y}_{\lambda i} = \min_i y_i$. So, by continuity arguments, one can expect such a value to exist.

For this last choice of $\tilde{y}_i$ we can write:

$$y_i - \tilde{y}_{\lambda i} = \frac{y_i - y_{\lambda i}}{1 - a_i^*},$$

with:

$$a_i^* = \frac{y_{\lambda i} - \tilde{y}_{\lambda i}}{y_i - \tilde{y}_{\lambda i}} = \frac{y_{\lambda i} - \tilde{y}_{\lambda i}}{y_i - \tilde{y}_i} \approx \frac{\partial y_{\lambda i}}{\partial y_i} = A_{ii}.$$

So we have:

$$OCV \approx \frac{1}{N}\sum_{i=1}^{N}\alpha_i^2(\lambda)(y_i - y_{\lambda i})^2,$$

with:

$$\alpha_i(\lambda) = \frac{1}{(1 - A_{ii})}.$$

This expression cannot be evaluated in the wavelet domain and the computation of the matrix A using (4.9) is still cumbersome. We have to minimize the function, and so for each evaluation we need an inverse wavelet transform to compute $\boldsymbol{y_\lambda}$ as well as the computation of A. Moreover, our experiments indicate that the evaluation is an ill-posed problem, especially for small threshold values, when most of the A_{ii} are close to one. To speed up computations, we can use a kind of an average value for $\alpha_i(\lambda)$:

$$\alpha_i(\lambda) = \alpha(\lambda) = \frac{1}{\frac{1}{N}\sum_{i=1}^{N}(1 - A_{ii})} = \frac{1}{\frac{1}{N}(\mathrm{Tr}(I - A))} = \frac{1}{\frac{1}{N}(\mathrm{Tr}(I - D))}.$$

This gives us the formula of the so called “Generalized Cross Validation” [43, 148, 149, 150]. It turns out that this function can be evaluated and minimized in the wavelet domain. The next section also gives a more mathematical basis for this estimator.

4.3 Generalized Cross Validation

4.3.1 Definition

Generalized Cross Validation is a function of the threshold value:

Definition 4.1

$$GCV(\lambda) = \frac{\frac{1}{N} \cdot \|\boldsymbol{y} - \boldsymbol{y_\lambda}\|^2}{[\frac{\mathrm{Tr}(I-A)}{N}]^2} = \frac{F(\lambda)}{\left(\frac{N_0(\lambda)}{N}\right)^2}, \tag{4.15}$$

with $F(\lambda)$ as in (4.2) and $N_0(\lambda)$ as in (4.7).

With this definition, $GCV(\lambda)$ would become infinite if $N_0 = 0$. For signals in the presence of Gaussian noise this is of course extremely unlikely to happen if $\lambda > 0$, but yet $\mathrm{P}(N_0 = 0) \neq 0$, as long as N is finite. This would cause problems for $\mathrm{E}GCV(\lambda)$. Therefore we explicitly set $GCV(\lambda) = 0$ if $N_0 = 0$. Another value but zero is of course also possible: since $\mathrm{P}(N_0 = 0)$ is close to zero, this has little influence on $\mathrm{E}GCV(\lambda)$.

If the wavelet transform is orthogonal, the same formula can be used, mutatis mutandis, in the wavelet domain.

$$GCV(\lambda) = \frac{\frac{1}{N} \cdot \|\boldsymbol{w} - \boldsymbol{w_\lambda}\|^2}{\left(\frac{N_0(\lambda)}{N}\right)^2}.$$

Minimizing this function can be done in the wavelet domain. The denominator is extremely easy to find: just count the number of coefficients below the threshold.

4.3.2 Asymptotic behavior

In this paragraph we prove that if $\lambda^* = arg \min R(\lambda)$ and $\hat{\lambda} = arg \min GCV(\lambda)$, then for $N \to \infty$, both minimizers yield a result of the same quality:

$$\frac{\mathrm{E}R(\hat{\lambda})}{\mathrm{E}R(\lambda^*)} \downarrow 1. \tag{4.16}$$

The first difficulty is due to the fact that, unlike in the spline case, or other linear smoothing procedures [7, 6, 72], $GCV(\lambda)$ is a quotient of two variables both depending on the input signal. Next, we compare the result obtained by the minimal GCV-threshold $\hat{\lambda}$ with the result for the optimal threshold λ^*. We give an upper bound for the ratio $\frac{R(\hat{\lambda})}{R(\lambda^*)}$. Finally we show that this upper bound tends to one.

A quotient of two random variables

$GCV(\lambda)$ is a ratio of two random, mutually dependent, variables. We therefore use asymptotic arguments [14] to obtain that for $N \to \infty$:

$$\begin{aligned}
\frac{\mathrm{E}R(\lambda) - (\mathrm{E}GCV(\lambda) - \sigma^2)}{\mathrm{E}R(\lambda)} &= 1 - \frac{\mathrm{E}GCV(\lambda)}{\mathrm{E}R(\lambda)} + \frac{\sigma^2}{\mathrm{E}R(\lambda)} \\
&\approx 1 - \frac{\mathrm{E}R + \sigma^2 - 2\sigma^2\mu_1}{(1-\mu_1)^2 \cdot \mathrm{E}R} + \frac{\sigma^2}{\mathrm{E}R} \\
&= (1 - \frac{1}{(1-\mu_1)^2}) + \frac{\sigma^2}{\mathrm{E}R} \cdot [\frac{-1+2\mu_1}{(1-\mu_1)^2} + 1] \\
&= \frac{-\mu_1(2-\mu_1)}{(1-\mu_1)^2} + \frac{\sigma^2}{\mathrm{E}R} \cdot \frac{\mu_1^2}{(1-\mu_1)^2}.
\end{aligned}$$

Because $\mu_1 \leq 1$, we have $2\mu_1 \geq \mu_1^2$, and so:

$$\begin{aligned}
\left| \frac{\mathrm{E}R(\lambda) - (\mathrm{E}GCV(\lambda) - \sigma^2)}{\mathrm{E}R(\lambda)} \right| &\leq \frac{1}{(1-\mu_1)^2} \left(|-2\mu_1 + \mu_1^2| + \left| \frac{\sigma^2\mu_1^2}{\mathrm{E}R} \right| \right) \\
&= \frac{1}{(1-\mu_1)^2} \left(2\mu_1 - \mu_1^2 + \frac{\sigma^2\mu_1^2}{\mathrm{E}R} \right) \\
&\leq \frac{1}{(1-\mu_1)^2} \left(2\mu_1 + \frac{\sigma^2\mu_1^2}{\mathrm{E}R} \right) =: h(\lambda).
\end{aligned}$$

If $\mathrm{E}GCV(\hat{\lambda}) = \min_\lambda \mathrm{E}GCV(\lambda)$ and $\mathrm{E}R(\lambda^*) = \min_\lambda \mathrm{E}R(\lambda)$, then:

$$[1 - h(\hat{\lambda})]\mathrm{E}R(\hat{\lambda}) \leq \mathrm{E}GCV(\hat{\lambda}) - \sigma^2 \leq \mathrm{E}GCV(\lambda^*) - \sigma^2 \leq [1 + h(\lambda^*)]\mathrm{E}R(\lambda^*),$$

or:

$$1 \leq \frac{\mathrm{E}R(\hat{\lambda})}{\mathrm{E}R(\lambda^*)} \leq \frac{1+h(\lambda^*)}{1-h(\hat{\lambda})}. \tag{4.17}$$

Limit behavior of the upper bound

If $h(\lambda) \to 0$, then $\mathrm{E}R(\hat{\lambda}) \to \mathrm{E}R(\lambda^*)$. This means that the GCV procedure asymptotically yields a minimum risk threshold. To this end, it is sufficient that $\mu_1(\lambda) \to 0$ and $\frac{\mu_1^2(\lambda)}{\mathrm{E}R(\lambda)} \to 0$.

Like in the previous chapter, we first consider the piecewise polynomial case. We call again:

$$\begin{aligned} I_0 &= \{i = 1, \ldots, N | v_i = 0\} \\ I_1 &= \{i = 1, \ldots, N | v_i \neq 0\} \\ M_0 &= \# I_0 \\ M_1 &= \# I_1 \end{aligned}$$

We find for $\mu_1(\lambda^*)$:

$$\begin{aligned} \mu_1(\lambda^*) &= \frac{1}{N} \sum_{i=1}^{N} \mathrm{P}(|w_i| > \lambda^*) \\ &\leq \frac{\sum_{i \in I_1} 1 + \sum_{i \in I_0} \mathrm{P}(|\omega_i| > \lambda^*)}{N} \\ &\sim \frac{M_1}{N} + \frac{M_0}{N} \frac{1}{\sqrt{\pi} N \sqrt{\log N}}, \end{aligned}$$

where we used the asymptotic equivalence for the cumulative Gaussian (3.20) and filled in $\lambda^* \sim \sqrt{2 \log N} \sigma$, which indeed tends to infinity.

So, if $N \to \infty$, we know that $\mu_1(\lambda) \to 0$ in the neighborhood of $\lambda = \lambda^*$:

$$\mu_1(\lambda^*) = \mathcal{O}\left(\frac{\log N}{N} + \frac{1}{N\sqrt{\log N}}\right) \to 0.$$

To show that $\frac{\mu_1^2(\lambda^*)}{\mathrm{E}R(\lambda^*)} \to 0$, we use the fact that for positive a, b, c, d:

$$\frac{a}{b} < \frac{c}{d} \Rightarrow \frac{a}{b} < \frac{a+c}{b+d} < \frac{c}{d}.$$

Using the notation $r(v, \lambda)$ from (3.9), we have:

$$\frac{\sigma^2 \mu_1}{\mathrm{E}R} = \frac{\sum_{i=1}^N \mathrm{E}(\omega_i \omega_{\lambda i})}{\sum_{i=1}^N r(v_i, \lambda)} \leq \max_{i=1\ldots N} \frac{\mathrm{E}(\omega_i \omega_{\lambda i})}{r(v_i, \lambda)}.$$

If $v_i \neq 0$, we have:

$$\lim_{\lambda \to \infty} \frac{\mathrm{E}(\omega_i \omega_{\lambda i})}{r(v_i, \lambda)} = \frac{\lim_{\lambda \to \infty} \sigma^2 \mathrm{P}(|w_i| > \lambda)}{\lim_{\lambda \to \infty} r(v_i, \lambda)} = \frac{0}{v_i^2} = 0$$

We concentrate on the case $v_i = 0$, and use Lemma 3.2 (expression (3.10) for $v = 0$):

$$\sigma^2 \frac{\mathrm{P}(|\omega_i| > \lambda)}{r(0, \lambda)} = \frac{2\sigma^2 \left[1 - \Phi(\lambda)\right]}{2(\sigma^2 + \lambda^2)\left[1 - \Phi(\lambda)\right] - 2\sigma^2 \lambda \phi(\lambda)}.$$

A long but trivial calculation shows that

$$\frac{\sigma^2 \left[1 - \Phi(\lambda)\right]}{(\sigma^2 + \lambda^2)\left[1 - \Phi(\lambda)\right] - \sigma^2 \lambda \phi(\lambda)} \sim \frac{\lambda^2}{2\sigma^2} \qquad \lambda \to \infty. \tag{4.18}$$

For the minimum risk threshold $\lambda^* \sim \sqrt{2 \log N} \sigma$, this means that:

$$\frac{\sigma^2 \mu_1^2(\lambda^*)}{\mathrm{E}R(\lambda^*)} = \mu_1(\lambda^*) \frac{\sigma^2 \mu_1(\lambda^*)}{\mathrm{E}R(\lambda^*)} = \mathcal{O}\left(\frac{\log^2 N}{N}\right) \to 0.$$

General piecewise smooth signals

We now turn to the non-polynomial case. Probably none of the uncorrupted coefficients will be exactly zero, so we define:

$$\begin{aligned} I_0^\varepsilon &= \{i = 1, \ldots, N \mid |v_i| \leq \varepsilon \lambda^*\} \\ I_1^\varepsilon &= \{i = 1, \ldots, N \mid |v_i| > \varepsilon \lambda^*\} \\ M_0^\varepsilon &= \# I_0^\varepsilon \\ M_1^\varepsilon &= \# I_1^\varepsilon, \end{aligned}$$

where $0 < \varepsilon < 1$ is some arbitrarily small value . We seek an upper bound for M_1^ε. To this end, we determine all levels j where coefficients are certainly below $\varepsilon\lambda^*$ if the corresponding basis function does not interfere with one of the singularities. A similar argument as in Section 3.5.3 leads to:

$$j \geq \frac{J - \frac{\log J}{\log 2} - \frac{2 \log \varepsilon}{\log 2} + \frac{2 \log C}{\log 2} - 1 - \frac{\log \log 2}{\log 2}}{2\alpha + 1},$$

where C and α are the same smoothness parameters as in Section 3.5.3, and J is the finest resolution level ($N = 2^J$). We still follow the same argument as in Section 3.5.3 to find:

$$\begin{aligned} M_1^\varepsilon &\leq M_1 + \sum_{j=0}^{\lfloor J/(2\alpha+1) \rfloor} 2^j \\ &\sim 2N^{1/(2\alpha+1)}. \end{aligned}$$

For the coefficients in the I_0^ε-class, we can write

$$\mathrm{P}(|w_i| > \lambda^*) \leq \mathrm{P}\left(|\omega_i| > (1-\varepsilon)\lambda^*\right),$$

and so we find, using the asymptotics of Theorem 3.5:

$$\begin{aligned} \mu_1(\lambda^*) &\sim \frac{M_1^\varepsilon}{N} + \frac{M_0^\varepsilon}{N} \frac{\sqrt{2\alpha+1}}{\sqrt{2\alpha\pi}(1-\varepsilon)N^{2\alpha(1-\varepsilon)^2/(2\alpha+1)}\sqrt{\log N}} \\ &= \mathcal{O}\left(\frac{1}{N^{2\alpha/(2\alpha+1)}} + \frac{1}{N^{2\alpha(1-\varepsilon)^2/(2\alpha+1)}\sqrt{\log N}} \right) \to 0. \end{aligned}$$

And also

$$\frac{\sigma^2 \mu_1^2(\lambda^*)}{\mathrm{E}R(\lambda^*)} \to 0,$$

as in the piecewise polynomial case.

Conclusion

In the neighborhood of λ^*, $\mathrm{E}GCV(\lambda)$ tends to be a vertical translation of $\mathrm{E}R(\lambda)$ and the relative error of $\mathrm{E}GCV(\lambda) - \sigma^2$ has a vanishing upper bound. This leads to the following theorem:

Theorem 4.1 *If* $\mathrm{E}R(\lambda^*) = \min_\lambda \mathrm{E}R(\lambda)$ *and* $\mathrm{E}GCV(\hat{\lambda}) = \min_\lambda \mathrm{E}GCV(\lambda)$, *then for* $N \to \infty$*:*

$$\frac{\mathrm{E}R(\hat{\lambda})}{\mathrm{E}R(\lambda^*)} \downarrow 1, \tag{4.19}$$

and in the neighborhood of λ^**:*

$$\mathrm{E}GCV(\lambda) \approx \mathrm{E}R(\lambda) + \sigma^2. \tag{4.20}$$

Figure 4.1 compares both functions $R(\lambda)$ and $GCV(\lambda)$ for a typical case. The noise variance is 1.1925, the number of data N equals 2048, from which 1984 wavelet coefficients and 64 scaling coefficients, which are not being thresholded.

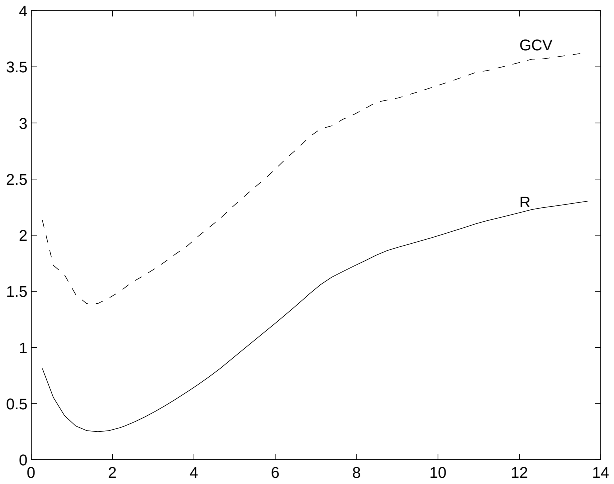

Figure 4.1: GCV and mean square error of the result in function of the threshold λ .

4.4 GCV for a finite number of data

Asymptotic optimality ensures good behavior in most cases, provided that the number of data N is sufficiently large. For signal de-noising applications, our experience is that $N = 1000$ seems to be a minimum for successful application. To illustrate this, we subsample the signal of Figure 3.4, add i.i.d. Gaussian noise ($\sigma = 0.2$) and plot the corresponding GCV and MSE in Figure 4.2. From this example we see that the quality of GCV as an estimator clearly deteriorates for smaller N, although in this case, the minimum GCV threshold remains a reasonable estimate for the minimum MSE-threshold. This is not always the case for small values of N.

4.4.1 The minimization procedure

For the moment being, we assume that $GCV(\lambda)$ is a convex function, and we use a Fibonacci minimization procedure [63]. Because $GCV(\lambda)$ is an approximation itself, it is not useful to compute its minimum very precisely. Moreover, in most cases this is not necessary either, due to the smooth curve of $R(\lambda)$ in the neighborhood of its minimum. A relative accuracy of 10^{-4} will do. The Fibonacci procedure attains this error after approximately 20 function evaluations.

Computation of $GCV(\lambda)$ can be performed completely in the wavelet domain. Only at the beginning of the minimization procedure a wavelet transform is needed. As we said before, the denominator in the definition (4.15) counts the

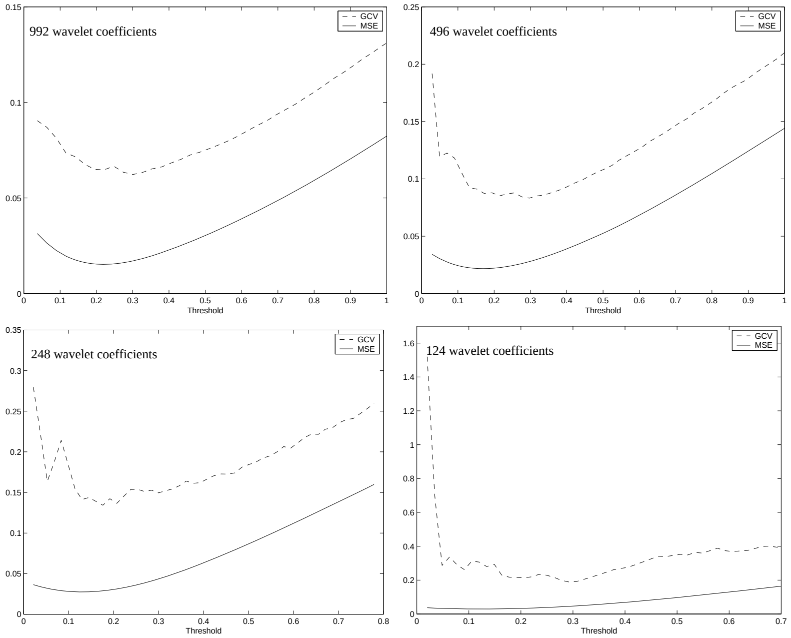

Figure 4.2: GCV and mean square error of the result in function of the threshold λ for different numbers of coefficients.

number of coefficients that are set to zero. This does not require any floating point operation. Computation of the numerator can be done with $2N$ floating point operations. So 20 function evaluations lead to some $40N$ floating point operations.

For a fast wavelet transform we need $2F2N$ flops, where F is the number of filter coefficients. For $F = 4$, we have $16N$ flops. To reconstruct the signal after the operation with optimal λ, we need an inverse transform too. This makes the minimization procedure not too expensive, as compared with the wavelet transform.

4.4.2 Convexity and continuity

Fibonacci minimization works fine and fast for convex functions. Figure 4.2 however illustrates that $GCV(\lambda)$ is certainly not always strictly convex. As a matter of fact, it is neither continuous: the number of discontinuities almost surely (a.s.) equals the number of data points N. In these points, the right limit is always lower than the left limit, since the denominator increases with one, and between two points of discontinuity the function is a local, increasing parabola:

$$GCV(\lambda) = \frac{N}{N_0^2}\left[\sum_{|w_i|<\lambda} w_i^2 + (N - N_0)\lambda^2\right].$$

The expected value of this GCV function is continuous:

Theorem 4.2 *If the noise has a non-degenerated Gaussian distribution,* $\mathrm{E}\,GCV(\lambda)$ *is continuous.*

Proof:

$$\mathrm{E}\,GCV(\lambda) = \sum_{I\subset\{1,\ldots,N\}} \mathrm{E}\left[GCV(\lambda) \mid |w_i| > \lambda \Leftrightarrow i \in I\right] \mathrm{P}(|w_i| > \lambda \Leftrightarrow i \in I)$$

The second factor in each term is clearly a continuous function of λ, depending of course on the unknown noise-free coefficient values. The first factor equals:

$$\mathrm{E}\left[GCV(\lambda) \mid |w_i| > \lambda \Leftrightarrow i \in I\right] = N\frac{\sum_{i\notin I} \mathrm{E}(w_i^2 \mid |w_i| < \lambda) + \#I \cdot \lambda^2}{(N - \#I)^2},$$

which is also continuous □

Convexity is not guaranteed, even not in the expected value. Fortunately, the overall curve is "close to convex" so that we do not experience too many problems in minimizing the function.

4.4.3 Behavior for large thresholds and problems near the origin

We examine this function and its singularities at a higher resolution. Figure 4.3 shows a GCV-function, evaluated in 5000 threshold values, instead of 50 as before. We see that most of the discontinuities appear near the origin. This is to be expected, since the major part of the wavelet coefficients are close to zero. Every coefficient value causes a change in the denominator. Actually, this is precisely the mechanism how GCV works: as long as coefficient magnitudes succeed each other at a high rate, many discontinuities appear on a small threshold range. Every discontinuity means a decrease, and the GCV-function has little possibility to 'recover' in between these singularity points. The procedure assumes that this behavior corresponds to the zone of noisy coefficients. The important, large coefficients are far less numerous, and so, from a certain threshold value, the GCV function is able to grow without being 'disturbed' by discontinuities. So, for large threshold values, the function is smoother, and moreover:

$$\lim_{\lambda\to\infty} GCV(\lambda) = \frac{\frac{1}{N}\|\mathbf{0}-\boldsymbol{w}\|^2}{\left(\frac{N}{N}\right)^2} = \frac{1}{N}\|\boldsymbol{w}\|^2.$$

And so:

$$\begin{aligned}\lim_{\lambda\to\infty} \mathrm{E}GCV(\lambda) &= \frac{1}{N}\mathrm{E}\|\boldsymbol{v}+\boldsymbol{\eta}\|^2 = \frac{1}{N}\|\boldsymbol{v}\|^2 + \frac{1}{N}\mathrm{E}\|\boldsymbol{\eta}\|^2 \\ &= \lim_{\lambda\to\infty} \mathrm{E}R(\lambda) + \sigma^2. \qquad (4.21)\end{aligned}$$

For large thresholds and finite N, $\mathrm{E}GCV(\lambda)$ behaves like it does asymptotically. This is why we want the minimum risk threshold to increase: the difficulties at the origin persist for $N \to \infty$, while for $\lambda \to \infty$ we get the requested behavior. Since discontinuities happen mainly for typical magnitudes of the numerous noisy coefficients, we may expect success as soon as the minimum risk threshold gets away from the noise level σ. Table 3.1, where $\sigma = 1$, illustrates that this happens for $N \approx 1000$. This corresponds to our experimental findings: for typical signals, we need approximately thousand samples to guarantee a successful GCV procedure.

For small values of λ, we have that

$$\lim_{\lambda\to 0} N_0(\lambda) = 0 \qquad a.s.,$$

and in Section 4.3.1 we mentioned that the GCV-definition should treat the case $N_0 = 0$ separately. We could use this opportunity to define

$$GCV(\lambda, N_0 = 0) = 2\sigma^2,$$

so that

$$\lim_{\lambda\to 0} GCV(\lambda) = \sigma^2 + \sigma^2 = \lim_{\lambda\to 0} \mathrm{E}R(0) + \sigma^2 \qquad a.s.,$$

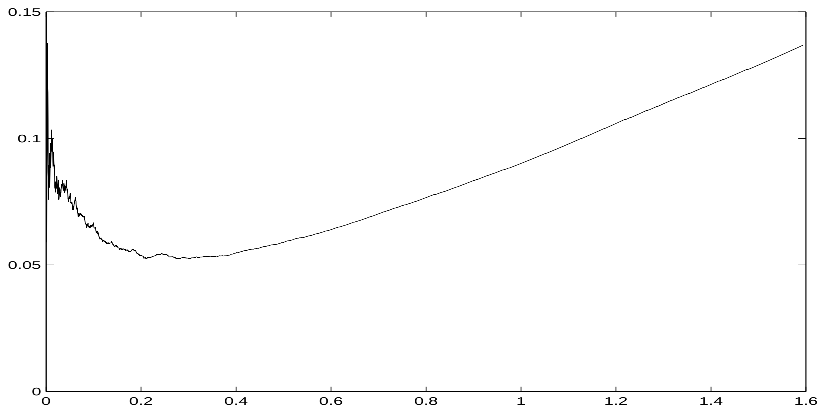

Figure 4.3: $GCV(\lambda)$ at high resolution (5000 function evaluations).

but of course this does not change the difficulties in the neighborhood of the origin, nor has it much influence on the curve of $\mathrm{E}GCV(\lambda)$, as the example in the next Section makes clear. Moreover, in practical cases the value of σ is unknown.

4.4.4 GCV in absence of signal and in absence of noise

Two important cases are pure noise and noise-free signals.

In the former case, we can compute $\mathrm{E}GCV(\lambda)$ analytically starting from

$$\mathrm{E}GCV(\lambda) = \sum_{n=0}^{N} \mathrm{E}\left[GCV(\lambda)|N_0 = n\right] \mathrm{P}(N_0 = n).$$

After some calculations we find:

$$\begin{aligned} \mathrm{E}GCV(\lambda) &= 2^N \left[1 - \Phi(\lambda)\right]^N \; GCV(0) \\ &+ \sum_{n=1}^{N} \frac{N}{n^2} \left(\begin{array}{c} N \\ n \end{array} \right) 2^{N-n} \left[1 - \Phi(\lambda)\right]^{N-n} \left[2\Phi(\lambda) - 1\right]^n \\ & \left[n\sigma^2 \left(1 - \frac{\lambda\phi(\lambda)}{2\Phi(\lambda) - 1}\right) + (N-n)\lambda^2 \right] \end{aligned}$$

If we choose $GCV(0) = 2\sigma^2$, we get the plot in Figure 4.5 for $\sigma = 1$. We know that $\lambda^* = \infty$ is the minimum risk threshold. It is also a local minimum of $\mathrm{E}GCV(\lambda)$, but there is an extra minimum in the immediate neighborhood of the origin.

If the input signal is noise-free, the minimum risk threshold is of course zero. With our experience of difficulties near the origin, we expect a troublesome application of GCV. Of course, the performance depends on the signal characteristics.

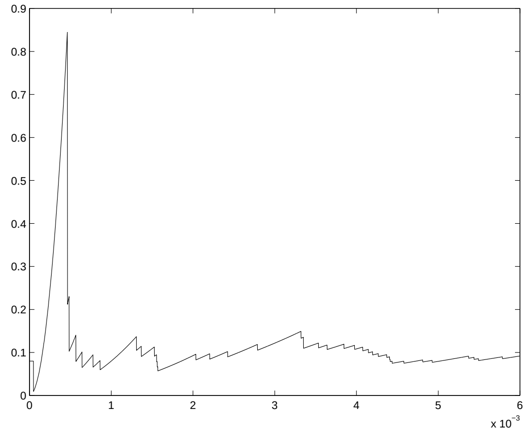

Figure 4.4: $GCV(\lambda)$ for small threshold values. This plot is a detail of the previous one.

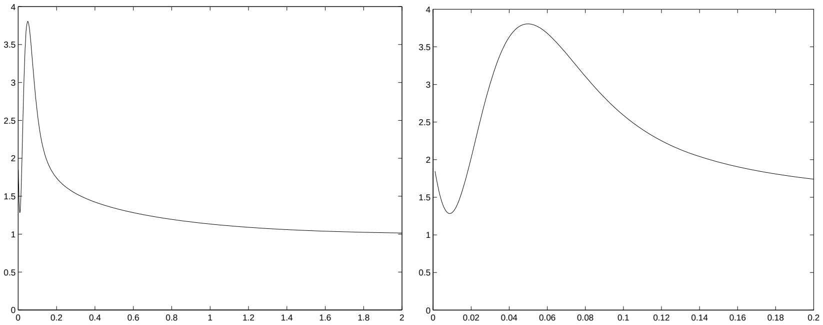

Figure 4.5: $\mathrm{E}GCV(\lambda)$ for $\boldsymbol{f} = \mathbf{0}$. The minimum risk threshold is $\lambda = \infty$. This is also the minimum of $\mathrm{E}GCV(\lambda)$, if we neglect the minimum near the origin. The right plot is a detail of the left one.

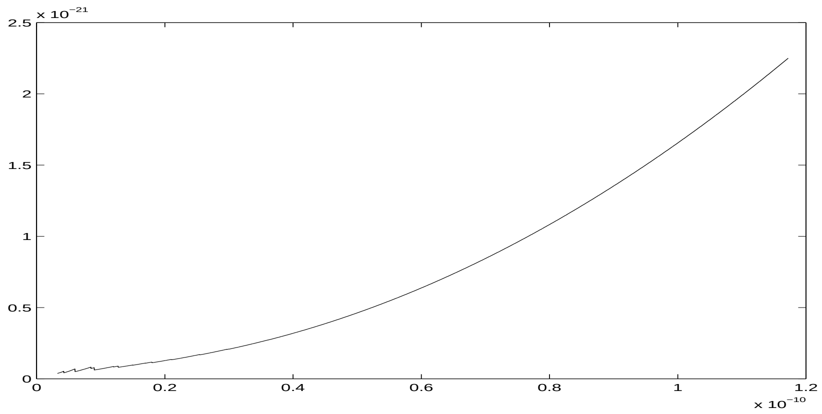

Figure 4.6: $GCV(\lambda)$ for $\boldsymbol{\eta} = \mathbf{0}, \sigma = 0$. Pay attention to the abscis values: even for extremely small threshold values, GCV performs almost perfectly.

If the signal looks irregular, almost like noise, GCV cannot detect this as a real signal. But for typical piecewise smooth signals, the procedure does a pretty good job. We have that:

$$\mathrm{E}GCV(\lambda) = GCV(\lambda) = \frac{\frac{1}{N}\|\boldsymbol{w}_{\boldsymbol{\lambda}} - \boldsymbol{w}\|^2}{\left(\frac{N_0}{N}\right)^2} = \frac{\frac{1}{N}\|\boldsymbol{v}_{\boldsymbol{\lambda}} - \boldsymbol{v}\|^2}{\left(\frac{N_0}{N}\right)^2} = \frac{R(\lambda)}{\left(\frac{N_0}{N}\right)^2}.$$

The problems occur in the region where many coefficient values succeed each other. If the coefficients are affected by noise, this interval stretches from the origin to σ say. But if the signal has no noise, $\sigma = 0$, most of the coefficients are much closer to zero. Even if GCV would fail on this tiny interval, this would hardly affect the result. Figure 4.6 plots $GCV(\lambda)$ for the wavelet coefficients of the test signal in Figure 3.4.

4.4.5 Absolute and relative error

We know that

$$\left| \frac{\mathrm{E}R(\lambda) - (\mathrm{E}GCV(\lambda) - \sigma^2)}{\mathrm{E}R(\lambda)} \right| \leq h(\lambda).$$

This is an upper bound on the relative error of $\mathrm{E}GCV(\lambda) - \sigma^2$ as an approximation of $R(\lambda)$. The question arises whether it would not be easier to start from the asymptotic behavior of the minimum risk threshold $\lambda^* \sim \sqrt{2 \log N}\sigma$ and to use the fact that for increasing threshold values, the *absolute* approximation error (4.21) tends to zero.

At least two reasons make this a bad idea. The first is of course that increasing N not only causes λ^* to grow, but also adds more data, and so changes the entire GCV-curve. It is not clear how to use a asymptotic result for a fixed curve in a situation of a simultaneous change of curve and abscis point.

Second, both $\mathrm{E}GCV(\lambda^*) - \sigma^2$ and $R(\lambda^*)$ tend to zero for large N. Proving that the absolute difference between these two vanishes, gives little information on the real quality of the GCV-procedure as an estimate.

4.4.6 Which is better: GCV or universal?

We have proven that the quality of the minimum GCV-threshold $\hat{\lambda}$ tends to be optimal for large data sets:

$$\frac{\mathrm{E}R(\hat{\lambda})}{\mathrm{E}R(\lambda^*)} \downarrow 1.$$

Strictly spoken, this gives no certainty about the asymptotics of $\hat{\lambda}$ itself, and as a matter of fact, we do not need to know how it behaves: if we can count on its *quality* in terms of risk, we have all we want.

Nevertheless, we may *expect* that $\hat{\lambda}$ has the same behavior as λ^*. In the piecewise polynomial case, this coincides with the universal threshold, in the piecewise smooth case, it coincides up to a constant.

This does not mean that the GCV-threshold has the same properties as the universal threshold. For signals with finite length, we may expect that the GCV-procedure, like SURE, is more adaptive to the signal than the universal threshold: GCV uses all data, and not just through an estimate of the noise level σ. (GCV does not need a value at all for σ.)

Moreover, a similar asymptotic behavior is no guarantee for a similar asymptotic quality. The following — hypothetic — example illustrates this. Suppose the risk is given by the expression:

$$\mathrm{E}R(\lambda) = (\lambda - \sqrt{2\log N} + 1/N)^2 + 1/N^3,$$

so we see that the minimum risk threshold would be $\lambda^* = \sqrt{2\log N} - 1/N$. And assume that GCV finds $\hat{\lambda} = \sqrt{2\log N} - 1/N + 1/N^2$ and the noise variance equals 1, so the universal threshold is simply $\sqrt{2\log N}$. These three thresholds all have the same asymptotic behavior. We see that, like in Theorem 4.1

$$\frac{\mathrm{E}R(\hat{\lambda})}{\mathrm{E}R(\lambda^*)} = \frac{1}{N} + 1 \rightarrow 1,$$

but the universal threshold does not attain this quality, in terms of minimum risk:

$$\frac{\mathrm{E}R(\lambda_{\mathrm{UNIV}})}{\mathrm{E}R(\lambda^*)} = \frac{(1/N)^2 + (1/N)^3}{(1/N)^3} = N + 1 \rightarrow \infty.$$

The GCV threshold, being an estimator for the minimum risk threshold, of course shows the same disadvantages. In particular, it tends to leave too much noisy coefficients at finer scales, which causes unwanted ‘blips’ in the output. The next chapter explains where this problem comes from and gives several possible remedies.

4.5 Concluding remarks

This chapter has introduced and motivated the use of a *generalized cross validation* procedure for finding a good threshold for wavelet coefficients. This method shows the following properties:

1. Minimizing the GCV-function is a fast method: it is not a bottleneck in a wavelet threshold procedure.

2. The method needs no explicit estimation for the noise level σ (or its variance σ^2). This advantage becomes particularly useful when the amount of noise depends on the resolution level. Next chapter illustrates that this is the case if the input noise is correlated.

3. The method is asymptotically optimal.

4. For finite data, the GCV function shows a difficult behavior near the origin, but this is a unimportant region: it contains threshold values below the noise level σ.

To prove the asymptotic optimality, we had to make several assumptions. Our experiments show that most of these conditions are crucial: if the noise or the wavelet transform does not satisfy one of them, the algorithm does not work as expected:

1. The untouched signal should be *smooth* in the sense that it can be represented sparsely by taking a wavelet transform. In fact, this assumption justifies the use of wavelets, since the decorrelating properties of wavelet transform guarantee such a sparse representation for most noise-free signals and images.

2. The noise in wavelet domain should be homoscedastic. As the following chapter explains, this is because GCV is based on SURE, and we need one σ for a successful application of SURE. To this end, we need:

   (a) the input noise to be second order stationary,

   (b) the input noise to be uncorrelated,

   (c) the wavelet transform to be orthogonal.

The next chapter goes deeper into this condition and also proposes a relaxation.

3. The noise should be Gaussian with zero mean. Experiments showed that, in practice, the GCV-method performs well for other zero mean stationary distributions of the noise.

4. The algorithm should use *soft*-thresholding. Minimizing GCV, while using hard-thresholding for the output mostly leads to a threshold equal to zero.

We also remark that the ideas of this chapter are not strictly limited to *wavelet* thresholding. The GCV procedure is based on the *sparsity* of this representation, and the proofs can probably easily be adapted to other kinds of sparse representations. This chapter shows that the idea of generalized cross validation, well-known in the framework of linear smoothing (like splines) is also applicable to non-linear methods.

Chapter 5

Thresholding and GCV applicability in more realistic situations

> *"E spesso il passo tra visione estatica e frenesia di pecato è minimo (...) Quello che volevo dire è che c'è poca differenza tra l'ardore dei Serafini e l'ardore di Lucifero, perché nascono sempre da un'ascensione estrema della volontà." "Oh, la differenza c'è, e io la so!" disse ispirato Ubertino. "Tu vuoi dire che tra volere il bene e volere il male c'è un piccolo passo, perché si tratta sempre di dirigere la stessa volontà. Questo è vero. Ma la differenza è nel oggetto, e l'oggetto è riconoscibile limpidamente. Di qui Dio, di là il diavolo."*
>
> —Umberto Eco, *Il Nome della Rosa,primo giorno, sesta.*

We have exploited the sparsity of a wavelet representation to motivate thresholding as a curve fitting method and to find GCV as an asymptotically optimal threshold assessment procedure. We explained that sparsity is a sort of smoothness and explained that wavelets are well suited to measure this concept of piecewise smoothness.

Until now, we have not used another important wavelet characteristic, which is the natural way wavelets support the idea of multiresolution . A wavelet decomposition is not only a sparse representation, it is also a multiscale data representation.

Most of this chapter emphasizes this aspect of a wavelet decomposition. Multiresolution and sparsity together create more possibilities. First, signals mostly have different characteristics at different scales. Indeed, scale can be seen as the approximate inverse of frequency. Just as in signal or image processing lots of operations are based on frequency analysis, we can use the multiscale character of the wavelet transform to make operations more adaptive. Not only should the operations be scale-dependent, but it is also useful to look across scales and handle one scale taking into account the information at adjacent resolutions.

Second, if the noise is correlated instead of white, also the noise behavior depends on the resolution. Clearly, one threshold cannot remove noise decently if the amount of noise σ depends on the resolution level. Scale-dependent thresholds are a solution for correlated noise, and are more adaptive to signal characteristics.

Other modifications to the classical settings are less related to multiresolution. The non-decimated wavelet transform causes additional smoothing, at the price of an $N \log N$ algorithm instead of a linear complexity. The integer wavelet transform avoids the use of floating point numbers, thereby speeding up computations, and eliminating rounding errors.

5.1 Scale dependent thresholding

5.1.1 Correlated noise

To generate correlated or colored noise, we apply a FIR-highpass-filter to white noise. A FIR or finite impulse response filter has a finite number of taps (filter coefficients), for the example of Figure 5.1 we convolve with 100 coefficients. If we add this noise to the test signal in Figure 3.4, we get a picture on top of Figure 5.1 which at first sight does not show any difference from the classical setting. A plot of the GCV and MSE function in Figure 5.2 however indicates that GCV is not able to find an approximation for the minimum risk threshold. The reason for this becomes clear if we plot the wavelet coefficients of the noise in Figure 5.1, middle. This noise is clearly not stationary, and therefore we have a coefficient-depending σ in Lemma 4.1 (4.3). As a consequence, a SURE-formula as in (4.12) is no longer valid. Since the GCV-asymptotic properties are based on this unbiased estimator, we cannot guarantee a successful application of GCV anymore.

From the analysis of the correlation matrix of the noisy wavelet coefficients, we observed that uncorrelated, stationary noise remains stationary after an orthogonal transform. If the noise is not stationary or not white, the wavelet transform could be neither white nor stationary.

To prove that GCV yields the optimal threshold if the number of wavelet coefficients tends to infinity, we do not need uncorrelated wavelet coefficients at any moment, but for the motivation of the SURE-threshold, we do need stationary noise in the wavelet domain.

Even if we would find the minimum MSE threshold, it would not be that useful. Indeed, intuition says that the more the coefficients are affected by noise, the higher the threshold should be. The universal threshold states this explicitly: $\lambda_{\mathrm{UNIV}} \sim \sigma$, but also the minimum risk threshold is approximately proportional to the amount of noise. If the amount of noise depends on the coefficient, it is hard to remove it by only one threshold. The reconstruction on the bottom of Figure 5.1 comes from

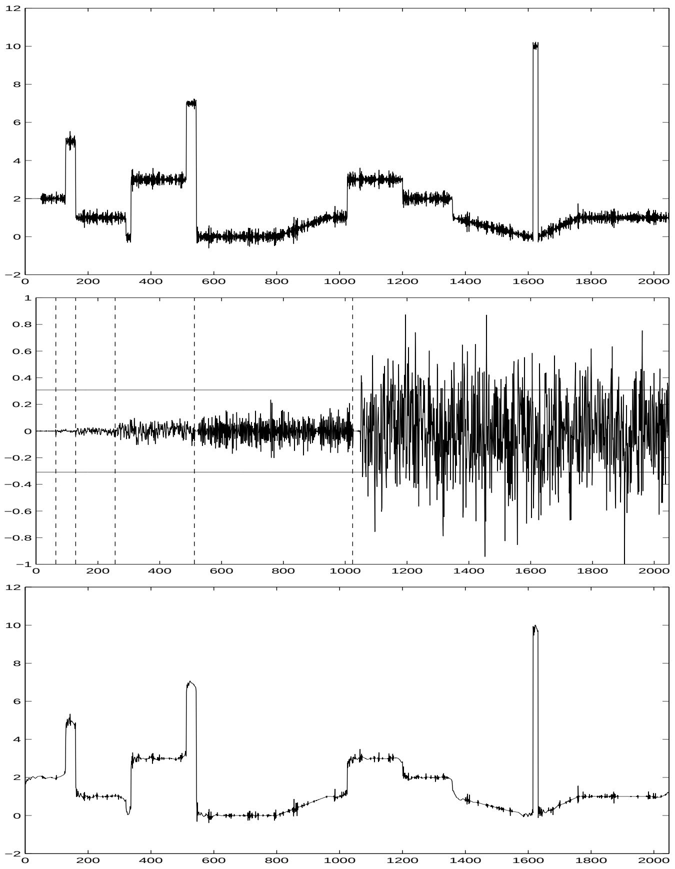

Figure 5.1: A signal with correlated, stationary noise ($\sigma = 0.2$). This noise was generated by convolution of white noise with a FIR-highpass-filter. In the middle: the wavelet transform of the noise. The dashed line indicates the boundaries between successive resolution levels. The two horizontal lines are at $\pm\lambda_{\mathrm{MSE}}$. One threshold, even the minimum MSE threshold, cannot remove noise with different σ simultaneously and decently. The bottom plot shows the reconstruction after applying the minimum MSE threshold: lots of noisy structures from the finest scale have survived the noise reduction.

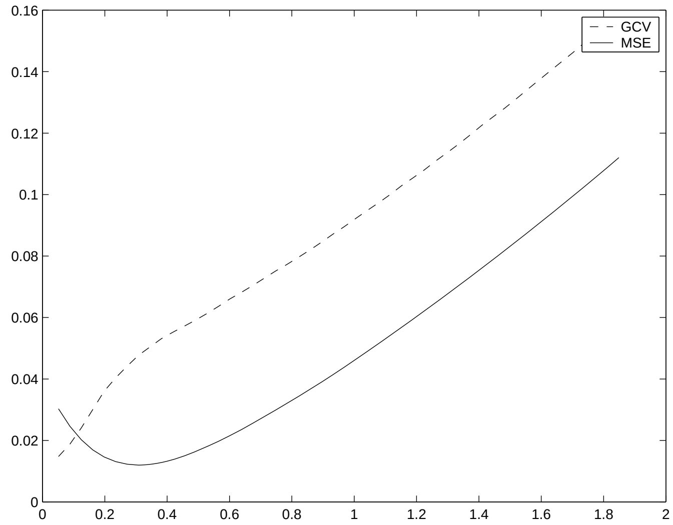

Figure 5.2: GCV and mean square error for the signal with correlated noise in Figure 5.1. GCV fails as an estimator of the optimal threshold.

a minimum MSE threshold. This threshold is clearly too small to remove the noise at the finest scale: most of the noise is concentrated at this resolution. This is not surprising, since the noise was generated by a highpass-filter and high frequencies correspond to fine scales.

If we happen to know the covariance structure of the input noise, i.e. if we know the covariance matrix up to a constant factor, then we can compute the covariance structure S in wavelet domain, using (2.20), and normalize the wavelet coefficients as:

$$w_i^{\mathrm{norm}} = w_i / \sqrt{S_{ii}}, \tag{5.1}$$

where, as usual, index i stands for j, k, j indicating scale and k indicating location. Unfortunately, normaliter we do not know the correlation structure of the input, and therefore we count upon the multiresolution character of wavelet transform.

We suppose that the original noise is stationary and more precisely that the correlation between two points only depends on the distance between them. This means that the correlation matrix Q is a (symmetric) Toeplitz matrix. If this is true, the multiresolution structure of a wavelet transform allows to prove that:

Lemma 5.1 *If $\omega_{j,k}$ represents a wavelet coefficient of a stationary random vector $\boldsymbol{\eta}$ at location k, and resolution level j (scale 2^{-j}), then the variance of this coefficient,* $\mathrm{E}(\omega_{j,k})^2$*, only depends on the resolution level j.*

This lemma explains why we denote the noise deviation at level j as σ_j.

Proof:

Since the correlation matrix is symmetric Toeplitz, we have that $Q_{u,v} = q_{|u-v|}$.

The wavelet coefficients at the finest resolution level $J-1$ (where $N = 2^J$) are then:

$$\begin{aligned} \mathrm{E}\omega_{J-1,k}\omega_{J-1,l} &= \sum_u \sum_v \tilde{g}_{u-2k}\tilde{g}_{v-2l}\mathrm{E}\eta_u\eta_v \\ &= \sum_u \sum_v \tilde{g}_{u-2k}\tilde{g}_{v-2l}q_{|u-v|}. \end{aligned}$$

Substitutions $m = u - 2k$ and $n = v - 2l$ then yield that:

$$\mathrm{E}\omega_{J-1,k}\omega_{J-1,l} = \sum_m \sum_n \tilde{g}_m\tilde{g}_n q_{|2(k-l)+m-n|}.$$

From this formula, it follows immediately that for all integer r:

$$\mathrm{E}\omega_{J-1,k+r}\omega_{J-1,l+r} = \mathrm{E}\omega_{J-1,k}\omega_{J-1,l}.$$

In particular, we have that:

$$\mathrm{E}\omega_{J-1,k+r}^2 = \mathrm{E}\omega_{J-1,k}^2 =: \sigma_{J-1}^2.$$

A similar argument holds for the scaling coefficients at resolution level $J-1$. We can thus repeat the same procedure for the wavelet coefficients at coarser levels, thereby completing the proof. □

For a two-dimensional wavelet transform, the noise level also depends on the orientation (vertical, horizontal, diagonal) of the coefficient [87].

We have proven that the wavelet transform of stationary correlated noise is stationary within each resolution level. Since stationarity is a condition for a successful GCV-estimation of the optimal threshold, this result suggests choosing a different threshold for each resolution level.

The mean square error now becomes a function of a vector of thresholds $\boldsymbol{\lambda}$. If $\boldsymbol{w_j^c}$ denotes the vector of wavelet coefficients at resolution level j, and component (orientation) c, then we can write:

$$R(\boldsymbol{\lambda}) = \sum_{j,c} \frac{N_j^c}{N} R_j^c(\lambda_j^c), \tag{5.2}$$

where N_j^c represents the number of wavelet coefficients on level j and component c, and

$$R_j^c(\lambda_j^c) = \frac{1}{N_j^c} \|\boldsymbol{w_{j,\lambda}^c} - \boldsymbol{v_j^c}\|^2. \tag{5.3}$$

Since all terms in (5.2) are positive, minimization of $R(\boldsymbol{\lambda})$ is equivalent to successive one dimensional minimizations of $R_j^c(\lambda_j^c)$ for all j and c. A similar argument as in Chapter 4 leads to an estimation [92]:

$$\mathrm{SURE}_j^c(\lambda_j^c) = F_j^c(\lambda_j^c) + (\sigma_j^c)^2 \cdot \frac{2N_j^c - N_{j0}^c}{N_j^c}, \tag{5.4}$$

with:

$$F_j^c(\lambda_j^c) = \frac{1}{N_j^c} \|\boldsymbol{w_{j,\lambda}^c} - \boldsymbol{w_j^c}\|^2,$$

and this leads to an adaptive estimation of the underlying signal, just like in the white noise case.

Based on this estimator, we can construct:

$$GCV_j^c(\lambda_j^c) = \frac{\frac{1}{N_j^c}\|\boldsymbol{w_j^c} - \boldsymbol{w_{j,\lambda}^c}\|^2}{\left(\frac{N_{j0}^c}{N_j^c}\right)^2}, \tag{5.5}$$

and the minimizer of this function is an asymptotically optimal estimator for the minimum risk threshold for level j and component c.

The reason for this straightforward application of the GCV procedure to data with correlated noise lies in the fact that the properties of GCV are not corrupted by correlated noise directly. Correlated noise only affects the algorithm through the heteroscedasticy of the wavelet coefficients. Fortunately, the multiresolution structure of a wavelet transform assures the noise to remain homoscedastic within one scale. The situation is different for some properties of the *universal* threshold. The ‘probabilistic upper bound’ from Section 3.4.5, for instance, is no longer preserved in the case of correlated data. This is a reason for using an updated expression in the case of correlated noise [17].

The fact that GCV needs no explicit estimation for σ_j^c becomes particularly advantageous here: in the white noise case, the noise level is equal at all scales, and it can be easily estimated from the coefficients at the finest scale, since this resolution level generally contains little important coefficients. If the noise is colored or the transform is non-orthogonal, however, we need an estimate at each scale and for each component. At coarser scales, this may be a problem, since relatively many large coefficients with information are present here. On the other hand, the same phenomenon also deteriorates the quality of the GCV-estimation, but we believe that the one-stage GCV-estimation better resists than a procedure in which noise estimation and noise reduction are separated.

5.1.2 Non-orthogonal transforms

If the input noise is uncorrelated and stationary, but we use a biorthogonal wavelet transform, Equation (2.20) learns that the wavelet coefficients are correlated and not stationary. In this case, we have all the information to normalize the coefficients like in (5.1), but we can also apply level-dependent thresholds. Level dependency has the advantage of signal-adaptivity as we explain in the following section and it still works if the noise is colored.

Another problem rises from the fact that non-orthogonal transforms do not preserve ℓ_2-norms. Stricto sensu, we cannot minimize MSE or GCV in the wavelet domain. Riesz bounds however guarantee a quasi-equivalence of norms. Moreover, as explained in Section 3.1, there seems to be no reason why pixel-MSE corresponds better to visual quality than multiscale-MSE.

5.1.3 Scale-adaptivity

Even for white noise and orthogonal transform, level-dependent thresholding may be interesting. Indeed, the optimal threshold not only depends on the noise level, but of course also on the signal characteristics. These characteristics may differ at different levels. Typically, coarse levels show a larger proportion of important signal features. The presence of large coefficients forces the optimal threshold to smaller values: the curves of the one-coefficient-risk in Figure 3.2 illustrate that large uncorrupted values prefer small thresholds. Although the noise level may be a constant across scales, minimum risk thresholds at coarser scales tend to be smaller. If the algorithm seeks one global threshold, this has to be a trade-off: for the finest scale, it is probably too small, and this shows up in the output as noisy ‘blips’. Scale-dependent thresholding is a way of reducing these spurious structures.

5.2 Tree-structured thresholding

If $N \to \infty$, we know that the minimum risk threshold behaves (approximately) like $\lambda^* \sim \sqrt{2 \log N}\sigma$. For general piecewise smooth functions, we are not sure that λ^* increases that fast, but the correction term $\sqrt{2\alpha/(2\alpha+1)}$ acts as a sort of ‘asymptotic lower bound’: the proof of Theorem 3.5 shows that λ^* may increase faster. So, for the moment we assume that the minimum risk threshold behaves asymptotically like the universal threshold, which means that for $N \to \infty$ a pure noise coefficients has no chance of passing the threshold.

For finite N, however, this probability is positive, even for the universal threshold, and the minimum risk threshold is still smaller. Level-dependent thresholding does not change this, and so there is always a proportion of noisy coefficients surviving the threshold.

Another problem for level-dependent thresholding comes from the fact that the GCV procedure needs sufficiently many coefficients to work well. Coarser resolution levels may lack this number of coefficients to find a separate threshold.

To further reduce these spurious output structures, we therefore return to one threshold, but appeal to another heuristic about wavelet transforms: if a coefficient at a given scale and location has a large value because it carries signal information, we may expect that the coefficient at the same location and coarser scale also has a large magnitude. This is because signal features typically have a wide range: a signal singularity therefore causes important coefficients at different scales. Noise, on the other hand, is a local phenomenon: a noise singularity does not show up at different scales.

This idea has been used in different alternatives for the classical thresholding. The algorithm by Xu, Weaver, Healy, and Lu [152] selects coefficients on a basis of interscale coefficient correlation instead of simple magnitudes. Other methods [13, 58] select *trees* of wavelet coefficients. A *tree* is a set of wavelet coefficients so that for each element, except one (called the *root*), the coefficient at the same location and at the next, coarser scale also belongs to the tree. Since two different fine scale coefficient share one single ‘parent’ coefficient, the multiscale representation of this set has a branched structure [13], hence it is called a tree.

Just as for minimum risk thresholding, the optimal tree is the best trade-off between sparsity and closeness of fit. To estimate this ‘best tree’ $\boldsymbol{w_T}$, the procedure minimizes a ‘complexity-penalized residual sum of squares’:

$$CPRESS(\boldsymbol{w_T}) = \|\boldsymbol{w_T} - \boldsymbol{w}\|^2 + \lambda^2(N - N_0),$$

where, as usual, N_0 indicates the number of coefficients in $\boldsymbol{w_T}$ that are exactly zero. In this expression, λ is a smoothing parameter that can be tuned to find a good compromise between smoothness and closeness of fit. When minimizing $CPRESS(\boldsymbol{w_T})$, we impose two constraints:

1. *Keep or kill*: every coefficient $w_{T,i}$ equals w_i or zero.

2. *Tree*: If a coefficient $w_{T,i} = 0$, then all coefficients at finer scales at the same location must be zero. So, we get a zero-subtree.

Actually, we are minimizing over a binary *label* vector $\boldsymbol{x} \in \{0,1\}^N$:

$$CPRESS(\boldsymbol{x}) = \sum_{i=1}^{N} (w_i x_i - w_i)^2 - \lambda^2 x_i \tag{5.6}$$

under the constraint that $\{x_i | x_i = 1\}$ must be a tree. This minimization problem can be solved in $\mathcal{O}(N)$ computations, using a dynamic programming algorithm [58, 21]. If we do not impose this tree structure, minimizing (5.6) would lead to a simple hard-thresholding, with threshold λ. Donoho proposes to choose he smoothing parameter as $\lambda \approx \sqrt{2 \log N}\sigma$.

The form of (5.6) is less general than the objective function that leads to hard-thresholding in Chapter 2. To our knowledge, there exists no immediate alternative for (5.6), leading to a sort of soft-thresholding, and allowing for a fast procedure. An algorithm may keep or kill coefficients in a tree, regardless of their magnitude, but it is impossible to shrink coefficients in a tree with a certain value, without actually killing some of them, if there is no *a priori* lower bound on the magnitude of the coefficients in the tree. Since the GCV-procedure is based on the idea of a *continuous* operation like soft-thresholding, it appears to be difficult to incorporate a GCV choice of the smoothing parameter in this tree-structured algorithm.

Nevertheless, we can use the idea that noise is local and only causes accidental values with no correlation across scales. After the threshold operation, we are suspicious of surviving coefficients at fine scales and we check whether the corresponding coefficient at coarser scales also have passed the threshold.

5.3 Non-decimated wavelet transforms

The discussion in Section 2.3 and Figure 2.14 show that the non-decimated wavelet transform has order of complexity $\mathcal{O}(N \log N)$, both for memory as for computations. This is a factor $\log N$ more expensive than the fast wavelet transform.

On the other hand, this redundant transform has some advantages, especially for noise reduction:

1. The non-decimated wavelet transform generates an equal number of coefficients at all resolution levels. In principle, this facilitates the use of an asymptotic method like GCV at coarse scales. The proportion of noise-free coefficients however remains the same: at coarse scales, these are quite numerous, and so, there is not really a sparse representation here, coefficients are highly correlated. This effect partially undoes the benefit from the extra coefficients. Therefore, we still leave the coarsest scales untouched.

2. It is easy to prove that a redundant wavelet transform of stationary noise is still stationary within each scale.

3. This redundant transform is immediately extensible for cases where the number of data is not a power of two.

4. Unlike the decimated transform, this redundant transform is translation invariant. As a matter of fact, the non-decimated wavelet transform is an interleaving rearrangement of all fast wavelet transforms of shifted versions of the input. More precisely, let the input $\boldsymbol{y}$ contain N data points and define the shift operator S as:

$$\boldsymbol{z} = S\boldsymbol{y} \Leftrightarrow \left\{ \begin{array}{lcl} z_i & = & y_{i-1} \text{ for } i = 2, \ldots, N \\ z_1 & = & y_N . \end{array} \right. \tag{5.7}$$

Then the redundant wavelet transform contains all coefficients from

$$\boldsymbol{w}_n = \tilde{W} S^n \boldsymbol{y}, \qquad n = 1, \dots N, \tag{5.8}$$

where $\tilde{W}$ is the non-redundant transform matrix. In principle, there are $N \times N = N^2$ of these coefficients, but the redundant transform eliminates doubles and rearranges the $N \log N$ remaining coefficients.

5. In each step of the inverse transform, we could omit one half of the (wavelet and scaling) coefficients before reconstruction of the scaling coefficients at the previous level. This means that these coefficients can be reconstructed in two independent ways. If we manipulate the wavelet coefficients, for instance to remove noise, then the result will probably not be an exact redundant wavelet transform of any signal at all. As a consequence the two possible reconstruction schemes at each level generate two different scaling coefficients at the previous level. Experiments show that taking a linear combination of these two possibilities causes an extra smoothing.

   It is not hard to understand that taking the simple mean of the two reconstruction schemes in each step corresponds to averaging the reconstructions from all fast wavelet transforms of shifted versions of the input. This is:

$$\boldsymbol{y}_{\mathrm{recon}} = \frac{1}{N} \sum_{n=1}^{N} S^{-n} W \boldsymbol{w}_n, \tag{5.9}$$

   where $W = \tilde{W}^{-1}$ is the inverse wavelet transform and $\boldsymbol{w}_n$ has been defined in (5.8).

   For manipulated $\boldsymbol{w}_n$, all terms in (5.9) are different, and averaging causes smoothing. In the case of orthogonal transforms $W = \tilde{W}^T$, $\boldsymbol{y}_{\mathrm{recon}}$ is the least squares solution to the overdetermined problem:

$$\tilde{W}_{\mathrm{redun}} \boldsymbol{y} = \boldsymbol{w}_{\mathrm{redun}}.$$

   Simple Matlab$^{\mathrm{TM}}$ testing shows that this least square interpretation does not hold for biorthogonal transforms. Anyway, the reconstruction from thresholded non-decimated coefficients is smoother, as experiments in Section 5.4 illustrate.

5.4 Test examples and comparison of different methods

We now discuss a couple of test examples.

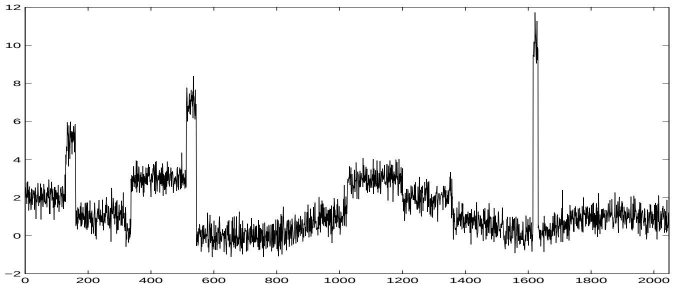

Figure 5.3: Noisy test signal. SNR = 10 dB.

simple GCV	tree-structured	level-dependent	non-decimated, level-dependent
16.81 dB	17.10 dB	17.06 dB	18.12 dB

Table 5.1: Output SNR-values for different methods of Figure 5.4.

5.4.1 Orthogonal transform, white noise

The first example is the signal from Figure 3.4, sampled at $N = 2048$ equidistant points. We add white noise in a signal-to-noise ratio of 10 decibels. This leads to the noisy signal in Figure 5.3. Figure 5.4 compares the output from different algorithms, all using Daubechies' orthogonal wavelets with 3 vanishing moments. Table 5.1 has the corresponding output SNR-values. Four levels are processed, all other, coarser scale coefficients are left untouched. Table and figure illustrate that signal-to-noise ratio and visual quality do not always coincide. The tree-structured method succeeds best in removing unwanted blips, but the redundant transform achieves a better SNR-value. The next figures contain the GCV-plots. Figure 5.5 shows the global threshold selection, used in the first two outputs. Figure 5.6 shows the four GCV-plots used in the level-dependent threshold algorithm. Even at the coarsest scale with only $N_j = 128$ data points, GCV does a good job, although the corresponding GCV-function for non-decimated coefficients in Figure 5.7 is clearly smoother. This function is based on $N_j = 2048$ coefficients.

A second example is Donoho's and Johnstone's ‘HeaviSine’ signal [61]:

$$f(x) = 4\sin(4\pi x) - \mathrm{sign}(x - 0.3) - \mathrm{sign}(0.72 - x),$$

sampled at $N = 1024$ equidistant points and corrupted by white, stationary noise with $\sigma = 0.5$. Again we use Daubechies wavelets with three vanishing moments, and this time we process six scales. This leads to the same test conditions as in [13]. Figure 5.8 has the noise-free data and the noisy input. The following figure and Table 5.2 summarize the results. Comparison of the different algorithms

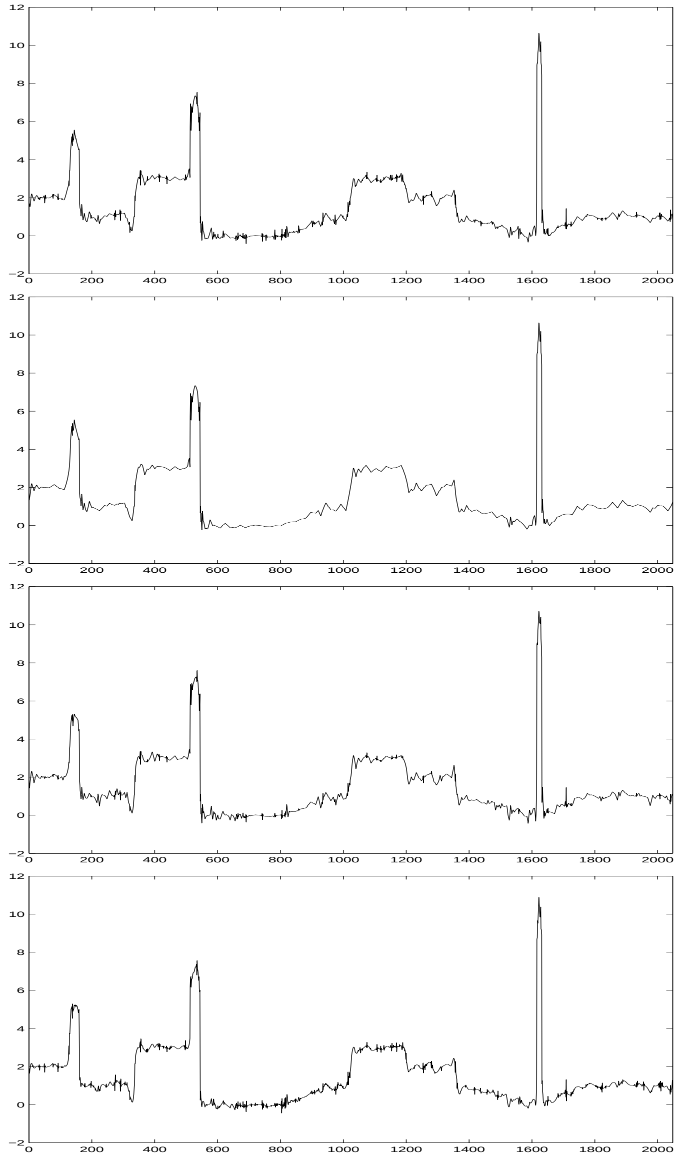

Figure 5.4: Outputs for different schemes, based on GCV threshold estimation. On top: simple, global thresholding the finest four scales. Second plot, tree-structured thresholding as explained in Section 5.2 yields a smoother result. The third plot is the output from a level-dependent threshold selection. The fourth one adds to this the use of the non-decimated wavelet transform. All outputs come from an orthogonal Daubechies wavelet transform with three vanishing moments.

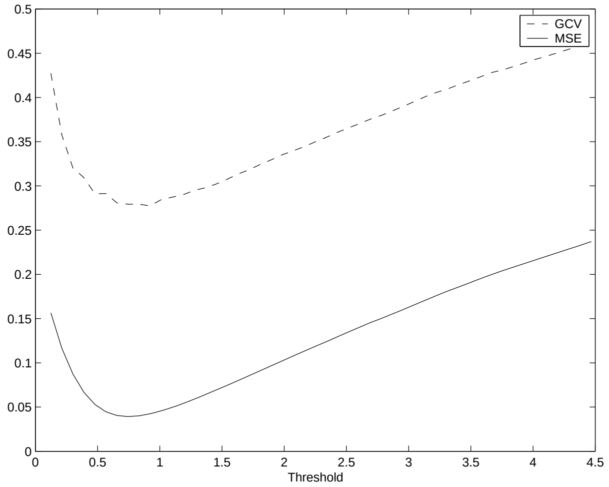

Figure 5.5: GCV and mean square error of the result in function of the threshold λ. This is the selection of one, global threshold for four resolution levels. This threshold is used to produce the first two outputs in Figure 5.4.

simple GCV	tree-structured	level-dependent	non-decimated, level-dependent
25.60 dB	27.17 dB	25.31 dB	27.95 dB

Table 5.2: Output SNR-values for different methods of Figure 5.9.

leads to similar results. We note that the underlying signal is smoother than in the previous example. Using a smooth wavelet basis, like the Daubechies basis with three vanishing moments, performs better in such cases than in the rather blocky signal of the previous example.

The two examples illustrate that level-dependent thresholding for decimated wavelet coefficients is not always that useful: the signal characteristics do not depend too much on scale in these examples. Conclusions may be different for other signals, and certainly for data with correlated noise. In that case, level-dependent thresholding is absolutely necessary and it acts as a whitening filter. This is illustrated in two examples with images.

5.4.2 Biorthogonal transform, colored noise

To the image of Figure 3.7 we add artificial colored noise. This noise was the result of a convolution of white noise with a FIR-highpass-filter. The signal-to-noise

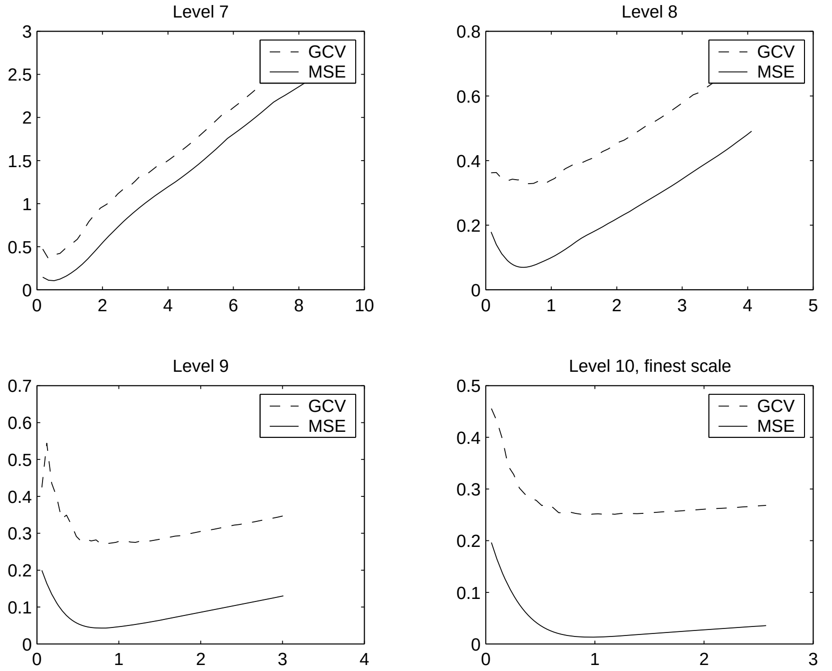

Figure 5.6: GCV_j and mean square error for level-dependent thresholds and a fast wavelet transform. This leads to the third output in Figure 5.4.

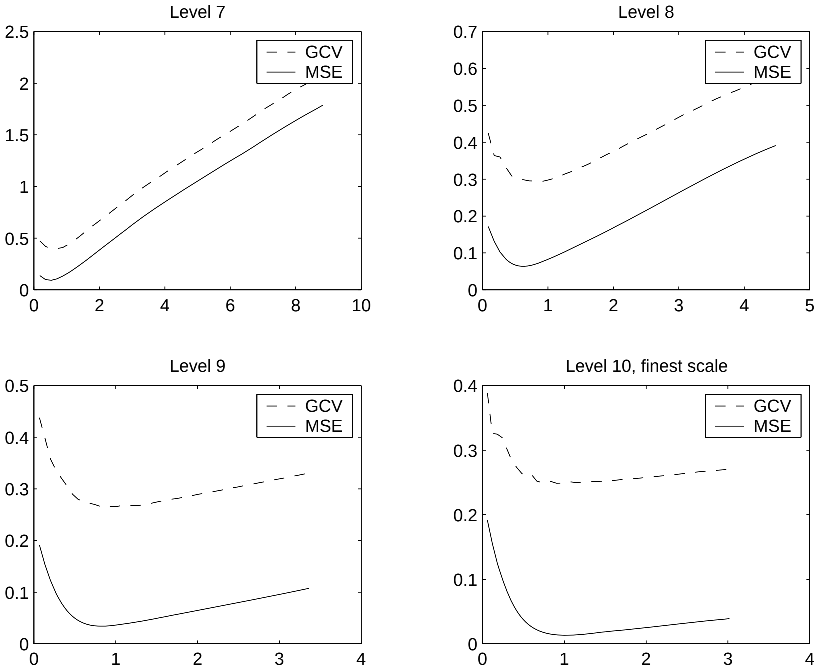

Figure 5.7: GCV_j and mean square error for level-dependent thresholds and a non-decimated wavelet transform. This leads to the bottom plot in Figure 5.4.

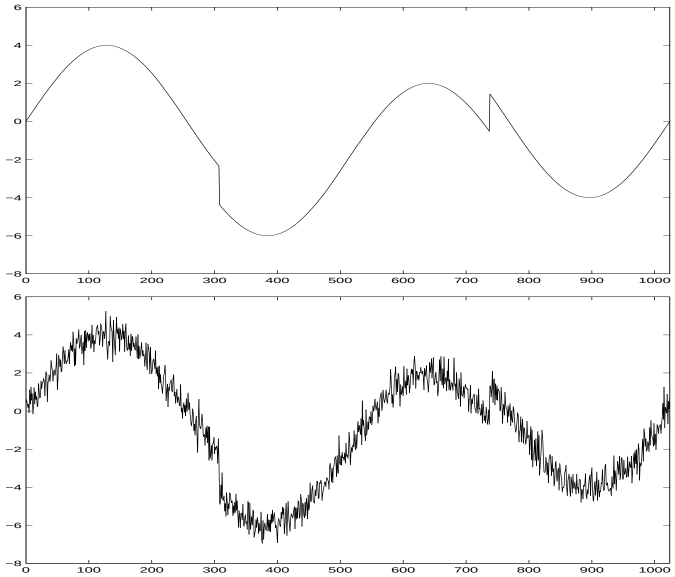

Figure 5.8: ‘HeaviSine’ test signal and noisy version SNR = 15.47 dB.

ratio is 4.97 dB. As wavelet filter, we use the variation on the CDF-(spline)-filters “with less dissimilar lengths” [38, 11]. We choose a basis with four primal and four dual vanishing moments. Figure 5.10 shows that the algorithm achieves a signal-to-noise ratio of 16.83 dB. Figure 5.11 plots the GCV-function and the mean square error for the vertical component at the one but finest resolution level. Table 5.3 compares the thresholds for different procedures. The first column contains the results for level-dependent GCV. This has to be compared with the thresholds minimizing the mean square error (MSE) in terms of wavelet coefficients. For an orthogonal transform, the corresponding SNR-value would have been the absolute maximum. Since we work with non-orthogonal transforms, and maximize in the wavelet domain, the value of 17.00 dB is only an approximative maximum. We add the results for SURE and universal thresholding. These algorithms need an explicit variance estimator. We use $\hat{\sigma}_j = \mathrm{MAD}(w_{j,k}, k = 1 \ldots 2^j)/0.6745$, where MAD is the median absolute deviation. If we suppose full knowledge of the noise energy in each component and at each level, the SURE-procedure rises from 16.24 dB to 16.94 dB, which is slightly better than the GCV based method. Both the GCV and the SURE procedure remove all coefficients at the finest scale ($j = 7$): the thresholds are equal to the largest coefficient. We remark that the universal threshold can be seen as a “statistical upper bound”: if $N \to \infty$, it is almost sure that a pure noise coefficient is removed. As discussed in Section 3.4.6, this over-smoothing threshold is not appropriate for image processing. We also note

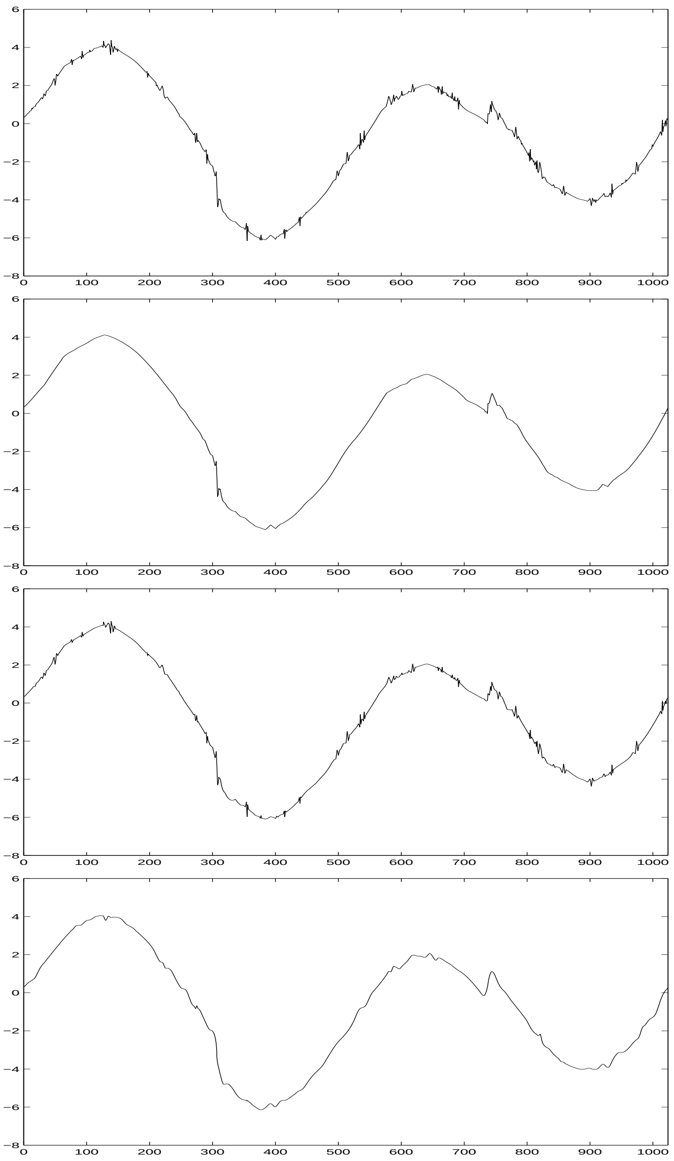

Figure 5.9: Outputs of different algorithms for the noisy signal in Figure 5.8. From top to bottom: (1) global thresholding the finest six scales. (2) tree-structured thresholding. (3) output from a level-dependent approach. (4) level-dependent thresholds for a non-decimated wavelet transform. All outputs come from an orthogonal Daubechies wavelet transform with three vanishing moments.

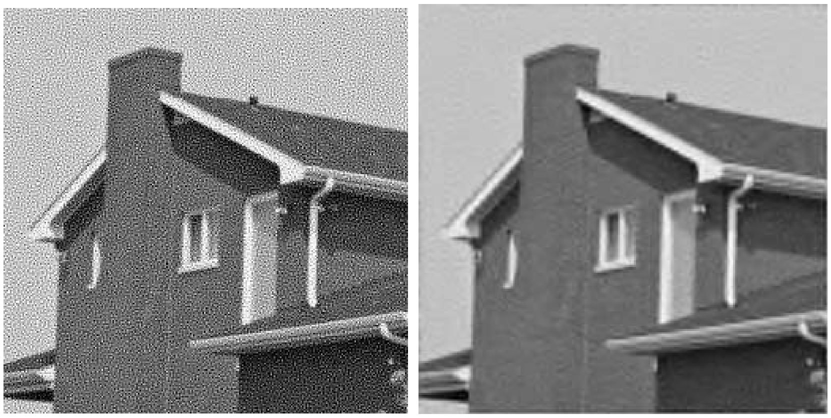

Figure 5.10: Left: an image with artificial, correlated noise. The noise is the result of a convolution of white noise with FIR highpass filter. Right: the result after level-dependent wavelet thresholding. We use biorthogonal filters with four primal and four dual vanishing moments and filter lengths 7 and 9. Signal-to-noise ratio rises from 4.97 dB to 16.83 dB.

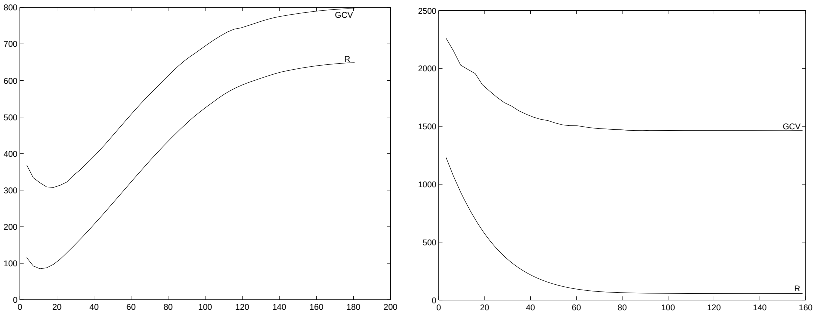

Figure 5.11: Mean square error and Generalized Cross Validation for vertical component coefficients at the one but finest resolution level (Left) and at the finest resolution level (Right).

	GCV	MSE	SURE	universal
$\lambda_{7,\mathrm{hor}}$	143.7	92.51	143.7	171.9
$\lambda_{7,\mathrm{ver}}$	148.6	118.7	148.6	168.0
$\lambda_{7,\mathrm{diag}}$	125.4	156.7	125.4	171.5
$\lambda_{6,\mathrm{hor}}$	10.21	10.40	22.89	72.82
$\lambda_{6,\mathrm{ver}}$	15.98	11.53	19.67	66.93
$\lambda_{6,\mathrm{diag}}$	63.72	63.58	63.72	116.7
$\lambda_{5,\mathrm{hor}}$	0.7780	1.677	18.66	85.82
$\lambda_{5,\mathrm{ver}}$	7.465	2.026	13.78	63.92
$\lambda_{5,\mathrm{diag}}$	13.13	5.282	15.90	52.16
SNR	16.83	17.00	16.24	12.64

Table 5.3: Comparison of thresholds for different procedures. The first column contains the results for level-dependent GCV. This is to compare with the thresholds minimizing the mean square error (MSE) in terms of wavelet coefficients. We add the results for SURE and universal thresholding.

that we only threshold coefficients at the three finest resolution levels. Coarse levels contain more important image information and thresholding these coefficients may cause a considerable bias and introduce visual artefacts. Figure 5.12 illustrates the smoothing effect of the redundant transform: the reconstruction from the overcomplete data representation reduces visual artefacts. Signal-to-noise ratio is now 18.02 dB.

We now apply the method to a realistic image. Figure 5.13 represents an aerial photograph of 340×350 pixels. We use the same biorthogonal filters with four primal and four dual vanishing moments as in the previous example. Table 5.4 compares the different thresholds of GCV with SURE. In contrast to the previous, artificial example, the threshold values are quite different at coarse levels. The SURE-thresholds are too high, probably because the MAD-estimator fails for this example.

Figure 5.14 contains the result for the GCV-procedure. The four finest resolution levels are thresholded. As can be expected, the algorithm does not distinguish real noise from the apparently noisy texture in the foliage of the trees.

5.5 Integer wavelet transforms

In applications like digital image processing, the input data are often integers. Section 2.4.2 explains that an integer wavelet transform avoids floating point operations and storage. If the input is affected by noise, but still integer, this noise cannot take an arbitrary real value and so its distribution cannot be Gaussian. Moreover, the integer wavelet transform is non-linear and so it does not preserve additivity

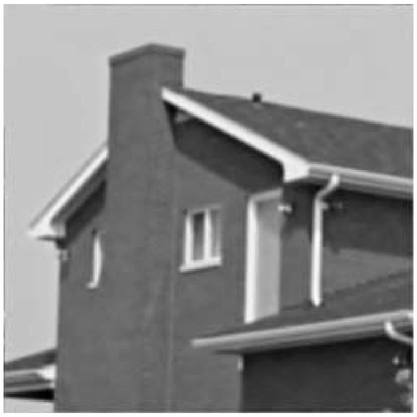

Figure 5.12: Result of level dependent wavelet thresholding on the redundant wavelet transform of the image with noise in Figure 5.10. We use the same wavelet filters. Signal-to-noise ratio is now 18.02 dB.

	GCV	SURE		GCV	SURE
$\lambda_{8,\mathrm{hor}}$	11.06	11.83	$\lambda_{6,\mathrm{hor}}$	10.79	26.37
$\lambda_{8,\mathrm{ver}}$	14.13	14.93	$\lambda_{6,\mathrm{ver}}$	12.07	19.56
$\lambda_{8,\mathrm{diag}}$	10.44	10.44	$\lambda_{6,\mathrm{diag}}$	12.32	19.90
$\lambda_{7,\mathrm{hor}}$	9.22	14.65	$\lambda_{5,\mathrm{hor}}$	12.34	75.59
$\lambda_{7,\mathrm{ver}}$	12.41	15.43	$\lambda_{5,\mathrm{ver}}$	12.36	37.32
$\lambda_{7,\mathrm{diag}}$	16.94	16.94	$\lambda_{5,\mathrm{diag}}$	13.81	41.84

Table 5.4: Comparison of different threshold values for GCV and SURE, applied on coefficients at four scales of the image in Figure 5.13. We call $j = 8$ the finest scale. Both methods show quite different thresholds at coarse scales. The SURE-thresholds are too high, probably because the variance estimator fails. This illustrates the advantage of an automatic threshold estimator.

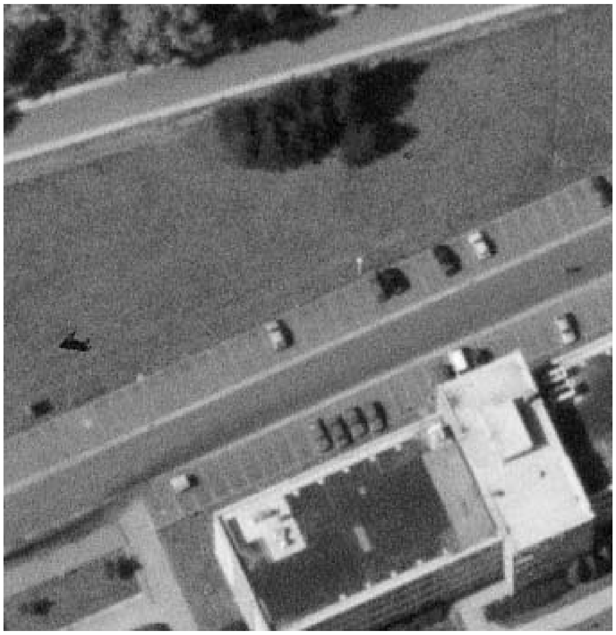

Figure 5.13: Aerial photograph with noise (340×350 pixels).

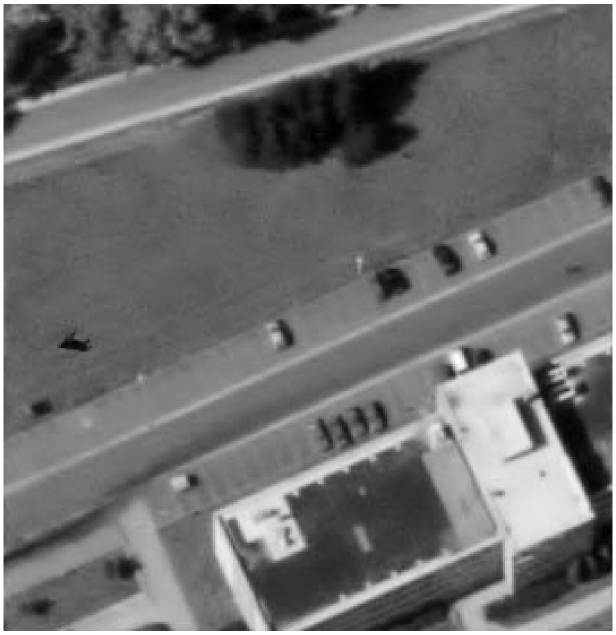

Figure 5.14: Result of level-dependent wavelet thresholding for the aerial photograph.

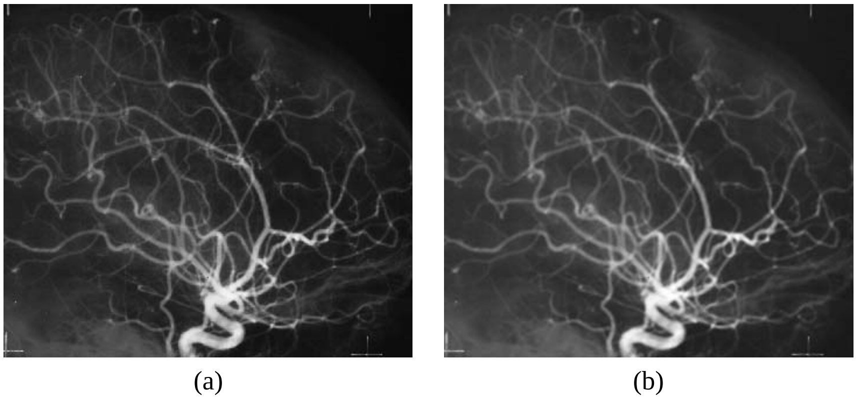

(a) (b)

Figure 5.15: An artificial test example. (a) a noise-free DSA test image. (b) The same image with artificial, additive and correlated noise. The noise is the result of a convolution of white noise with a FIR high pass filter. Signal-to-noise ratio is 10 dB.

nor stationarity. Al these conditions are stricto sensu necessary for a correct use of a GCV-threshold estimation.

Nevertheless, an artificial test example illustrates that, in practice, these conditions do not pose serious problems. Figure 5.15(a) shows a noise-free DSA (Digital Subtraction Angiography) test image. In Figure 5.15(b) we add artificial, colored noise. This noise was the result of a convolution of white noise with a FIR high pass-filter. The signal-to-noise ratio is 10 dB.

We compute the redundant, integer wavelet transform of the noisy and the noise-free image and estimate the optimal threshold at each resolution level and for each component by the GCV-procedure. Since we know the noise-free wavelet coefficients, we can compare the GCV-function with the mean square error as a function of the threshold. Figure 5.16(a) shows this comparison for the vertical component at the finest resolution level. Both $GCV_j^c(\lambda)$ and $R_j^c(\lambda)$ have about the same minimum. Figure 5.16(b) compares both functions at the one but finest resolution level. The optimal threshold at this level is close to zero. This is not surprising: we have added high-frequency noise which mainly manifests at fine scales. As Figure 5.17b shows, thresholding at this level causes considerable blur and artefacts and loss of important details: small blood-vessels become very unclear or even completely disappear. We get a better result if we only apply the algorithm at the finest resolution level. Figure 5.17a shows this reconstruction: signal-to-noise ratio is now 19.94 dB, compared to 17.27 dB for a threshold at two levels.

Table 5.5 compares the integer GCV procedure with other, classical threshold

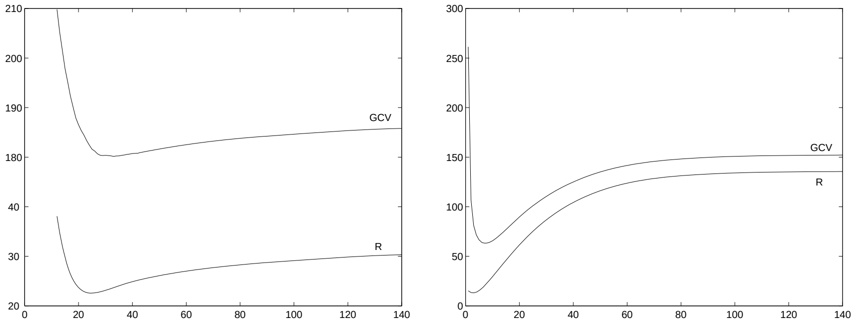

(a) (b)

Figure 5.16: An artificial test example: a comparison of $GCV_j^c(\lambda)$ and $R_j^c(\lambda)$ for the vertical component at the (a) finest resolution level and (b) one but finest resolution level. Both $GCV_j^c(\lambda)$ and $R_j^c(\lambda)$ have about the same minimum. At the one but finest level, the optimal threshold is close to zero, which indicates that the noise at this level is neglectable.

integer GCV	classical GCV	SURE	universal
19.94	19.88	19.26	18.72

Table 5.5: Comparison of different threshold procedures, applied to the finest scale of the coefficients of Figure 5.15. In all cases, we used a redundant transform with Cohen-Daubechies-Feauveau (2,2)-filters.

methods. It shows that, at least for this example, using the integer transform instead of the classical, linear transform poses no problem. (In this case, there is even a slight improvement.) The table also illustrates that the GCV-method performs at least as well as other threshold selection procedures, although GCV does not use information on the amount of noise (the deviation σ_j^c). The SURE- and universal procedures do need the values of σ_j^c. For the values in this table, we used the exact σ_j^c.

Our last example is an MRI image with 'natural' (no artificial) noise. This image has 128 by 128 pixels and shows a human knee. The input is in Figure 5.18(a). Figure 5.18(b) contains the result of the de-noising algorithm for a fast wavelet transform. Figure 5.18(c) is the result for a non-decimated transform. Figures 5.18(d) and 5.18(e) show the results if one uses universal thresholds. This illustrates, once more, that the universal threshold is in fact not appropriate for image de-noising.

We used biorthogonal CDF(2,2)-wavelet filters [38]. This is one of the popular filters for image processing. Its decomposition into lifting steps is particularly easy

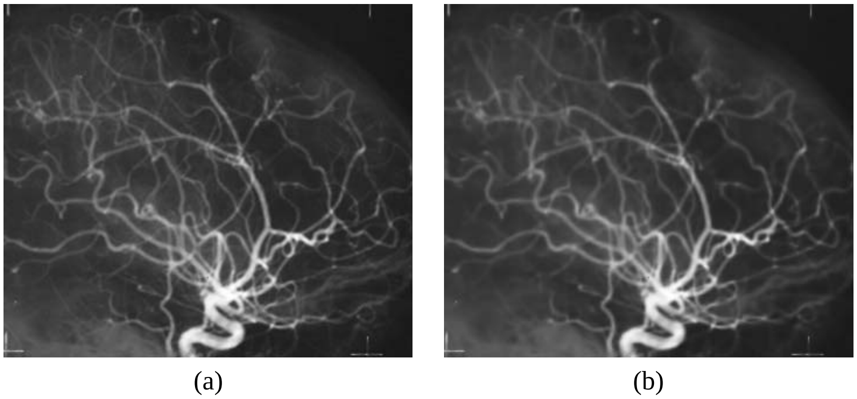
(a) (b)

Figure 5.17: An artificial test example: reconstruction by inverse redundant transform after removing small coefficients at (a) the finest resolution level only (Signal-to-noise ratio is 19.94 dB.), and (b) the two finest resolution levels. Signal-to-noise ratio is 17.27 dB. Thresholding at coarse levels introduces more visible artefacts.

[138]. In principle, the success of GCV in estimating the optimal threshold does not depend on the choice of a wavelet basis. Figure 5.19 shows the GCV-functions of the first (finest) and second resolution level of the fast wavelet transform. The corresponding plots for the redundant wavelet transform are in 5.20.

Another doctoral dissertation [140] from our department contains an extensive discussion about the fast integer wavelet transform for images and focusses on large-scale image processing. The use of GCV in the context of this fast integer transform is further investigated from the practical point of view. A GCV minimization is also a built-in procedure of the software library WAILI [142], developed in the framework of this doctoral dissertation.

“ La vita dei semplici, Abbone, non è illuminata dalla sapienza e dal senso vigile delle distinzioni che ci fa saggi. Ed è ossessionata dalla malattia, della povertà, fatta balbuziente dall’ignoranza. Spesso per molti di essi l’adesione a un gruppo eretico è solo un modo come un altro di gridare la propria disperazione. Si può bruciare la casa di un cardinale sia perché si vuole perfezionare la vita del clero, sia perché si ritiene che l’inferno, che lui predica, non esista. Lo si fa sempre perché esiste l’inferno terreno. ”

—Umberto Eco, *Il Nome della Rosa, secondo giorno, nona.*

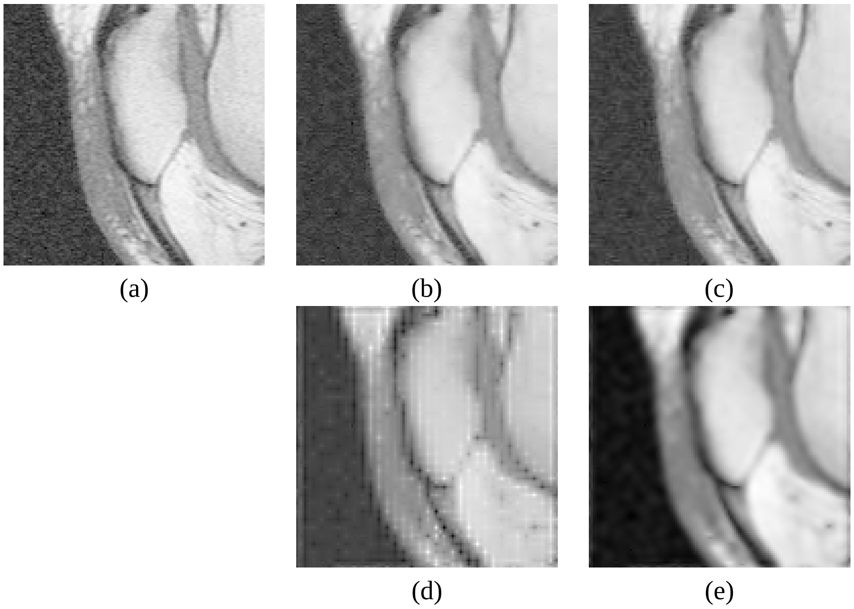

(a) (b) (c)

(d) (e)

Figure 5.18: An example. (a) The input image, an MRI image (128 × 128 pixels) with noise. (b) Result after thresholding the fast wavelet coefficients at the first and second resolution level, using GCV-thresholds. (c) Result after thresholding the redundant wavelet coefficients at the first and second resolution level, using GCV-thresholds. (d) Result after thresholding the fast wavelet coefficients at the first and second resolution level, using universal thresholds. (e) Result after thresholding the redundant wavelet coefficients at the first and second resolution level, using universal thresholds.

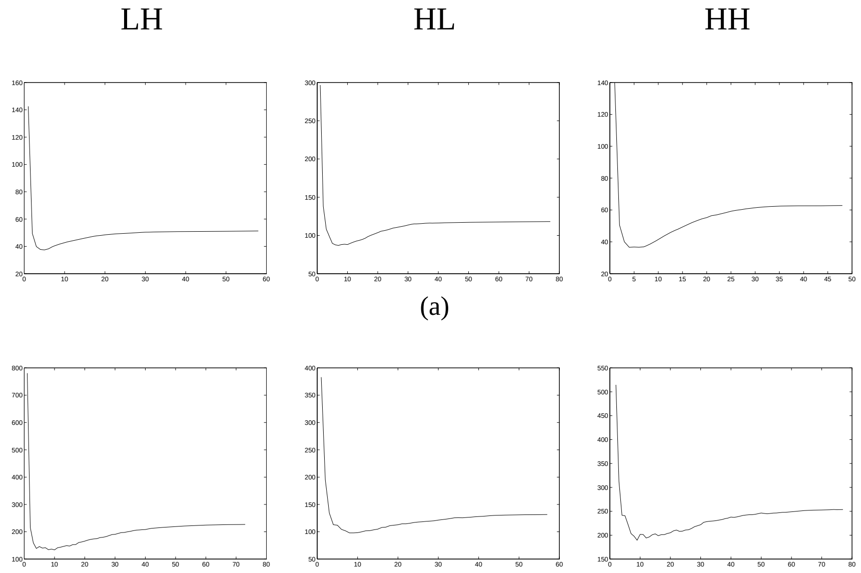

(a)

(b)

Figure 5.19: GCV-functions for a fast wavelet transform of MRI-image of figure 5.18. (a) The three components at the finest resolution level. (b) The three components at the second resolution level.

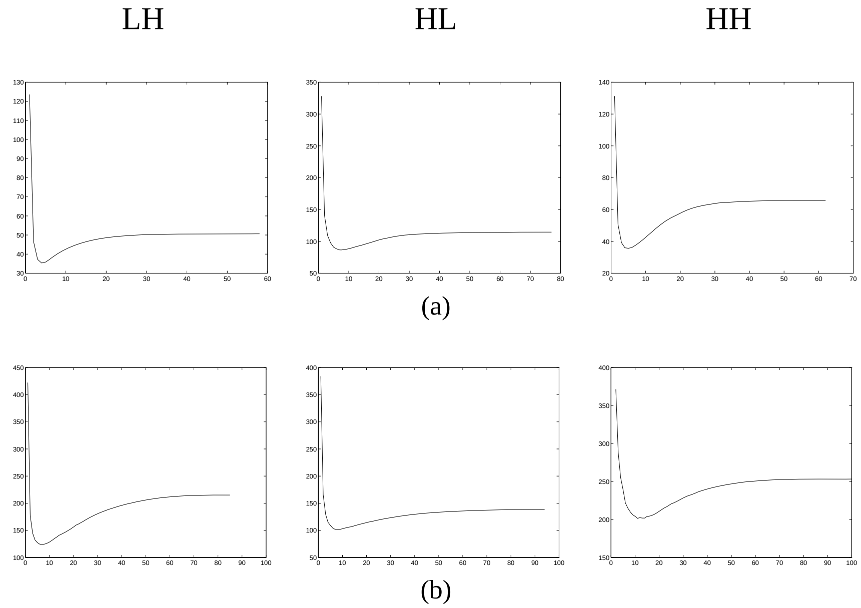

(a)

(b)

Figure 5.20: GCV-functions for a redundant wavelet transform of MRI-image of figure 5.18. (a) The three components at the finest resolution level. (b) The three components at the second resolution level.

Chapter 6

Bayesian correction with geometrical priors for image noise reduction

6.1 An approximation theoretic point of view

Image processing is not merely a two-dimensional translation of traditional signal processing techniques. The two-dimensional character has some important consequences, such as the existence of line singularities, manifesting as edges. The observations explained in this section also provide the basis for the development of new types of basis functions, such as ridgelets [27].

6.1.1 Step function approximation in one dimension

Suppose we want to approximate the step function of Figure 6.1. A periodic extension of this function can be decomposed into a Fourier series:

$$f(x) = \sum_{k \in \mathbb{Z}} a_k \mathrm{e}^{-i2\pi kx}.$$

The equation sign indicates convergence, both pointwise as in $L_2[0,1]$-norm. The coefficients a_k depend of course on the precise position of the singularity, but they behave like:

$$a_k = \mathcal{O}\left(\frac{1}{|k|}\right).$$

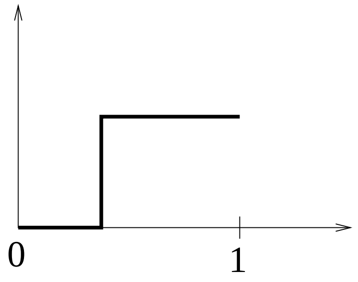

Figure 6.1: Step function.

We use this Fourier expansion to *approximate* the step function by taking the $2n+1$ harmonics with index $k = -n, \ldots, n$:

$$f_{2n+1}(x) = \sum_{k=-n}^{n} a_k \mathrm{e}^{-i2\pi kx}.$$

Since the coefficients decrease for $|k| \to \infty$, this *linear* approach happens to coincide with taking the largest contributions. This Fourier basis is orthonormal, so the approximation error satisfies

$$\begin{aligned}\|\epsilon_{2n+1}\|^2_{L_2[0,1]} &= \|f - f_{2n+1}\|^2_{L_2[0,1]} = \sum_{|k|\geq n+1} |a_k|^2 \\ &= \mathcal{O}\left(2\sum_{k=n+1}^{\infty} \frac{1}{k^2}\right) = \mathcal{O}(n^{-1}).\end{aligned}$$

We may conclude that a one dimensional Fourier decomposition performs as:

$$\|\epsilon_n\| = \mathcal{O}(n^{-1/2}).$$

This bad approximation of piecewise smooth signals is a well known drawback of the Fourier decomposition. The reason is of course that all basis functions cover the entire interval, and so all of them get in touch with the singularity, all of them have a contribution to it.

This is not the case in a wavelet decomposition, where at each scale only a constant number of coefficients are non-zero. For the Haar transform, there is only one function, say ψ_{j,k_j} with a non zero coefficient w_{j,k_j}. By orthogonality, the approximation error of the orthogonal projection f_J of f on V_J equals:

$$\|\epsilon_J\|^2_{L_2[0,1]} = \|f - f_J\|^2_{L_2[0,1]} = \sum_{j=J+1}^{\infty} w^2_{j,k_j}.$$

If $|f(x)| \leq 1$, we have

$$|w_{j,k_j}| \leq \int_0^1 |\psi_{j,k_j}(x)|\, dx = 2^{-j}\, 2^{j/2}.$$

Hence

$$\|\epsilon_J\|^2_{L_2[0,1]} = \mathcal{O}\left(\sum_{j=J+1}^{\infty} 2^{-j} \right) = \mathcal{O}(2^{-J}).$$

This expresses that a wavelet basis indeed captures isolated singularities much more efficiently than does a Fourier basis. We do not know in advance which coefficients are going to be non-zero: this depends on the input signal and more precisely on the exact position of the jump. Therefore, keeping the non-zero wavelet coefficients is a *non-linear* approximation.

If we have a superposition of this step function f and a C^{α} smooth function g, none of the wavelet coefficients of $h = f + g$ is exactly zero. The smooth part g is best approximated with a linear approach: take all coefficients up to scale J. If the number of vanishing moments $p \geq \alpha$, the approximation error satisfies [113]:

$$\|\epsilon_{g,J}\| = \|g - g_J\| = \mathcal{O}(2^{-J\alpha}).$$

This approximation uses 2^{J+1} coefficients. If we want the same order of precision for the non-smooth component, we add $\lceil J\alpha \rceil$ coefficients of f in the non-linear way, and the overall approximation error $\epsilon_h(x) = \epsilon_f(x) + \epsilon_g(x)$ is then bounded by:

$$\|\epsilon_h\| \leq \|\epsilon_f\| + \|\epsilon_g\| = \mathcal{O}(2^{-J\alpha}).$$

This approximation uses $2^{J+1} + \lceil J\alpha \rceil = \mathcal{O}(2^J)$ coefficients. If we call this number n, we conclude that the error of a one-dimensional wavelet approximation behaves as

$$\|\epsilon_n\| = \mathcal{O}(n^{-\alpha}),$$

for smooth as well as for piecewise smooth functions. Isolated singularities have no influence on the asymptotic approximation error.

6.1.2 Approximations in two dimensions

Now suppose we are given a two-dimensional function $f(x, y) \in L_2[0,1]^2$, which is 0 in one part of the square and 1 in the other part. The boundary between these two parts is a simple line, as in Figure 6.2. The coefficients of the Fourier

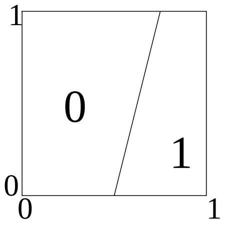

Figure 6.2: Two-dimensional step function.

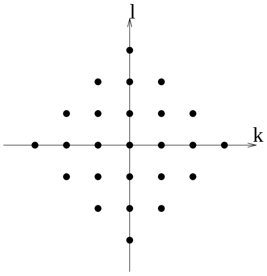

Figure 6.3: Position of indices in $\mathbb{Z}^2$ corresponding to coefficients in a linear Fourier approximation.

expansion of this function

$$f(x,y) = \sum_{k\in\mathbb{Z}} \sum_{l\in\mathbb{Z}} a_{k,l}\, \mathrm{e}^{i2\pi kx} e^{i2\pi ly}$$

can be found as:

$$\begin{aligned} a_{k,l} &= \int_0^1 \int_0^1 f(x,y)\, \mathrm{e}^{-i2\pi kx} e^{-i2\pi ly}\, dxdy \\ &= \mathcal{O}\left(\frac{1}{|kl|}\right). \end{aligned}$$

A linear approximation keeps all coefficients with indices k and l such that $|k| + |l| \leq m$, for a given m. Figure 6.3 shows the position of these indices in $\mathbb{Z}^2$ for $m = 3$. The approximation error satisfies:

$$\|\epsilon_n\|^2 = \sum_{k\in\mathbb{Z}} \sum_{l:|k|+|l|\geq m+1} |a_{k,l}|^2 = \mathcal{O}(m^{-1})$$

Since $n = (2m+1)^2$, we have

$$\|\epsilon_n\| = \mathcal{O}(n^{-1/4}).$$

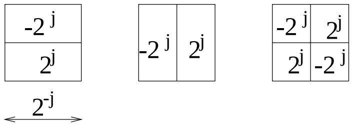

Figure 6.4: Two-dimensional Haar basis functions.

This says that for an equal order of magnitude of the error as in the one-dimensional case, we need the square of the number of coefficients.

We now proceed to a (Haar) wavelet expansion. The basis contains three types of functions: horizontally oriented, vertically oriented and diagonally oriented functions as depicted in Figure 6.4. At each scale we have $K2^j$ non-zero coefficients with all three types of basis functions. The exact value of the constant $K \geq 1$ depends on the length of the singularity, i.e. its orientation in the image. If $|f(x,y)| \leq 1$, the coefficients satisfy:

$$|w^{\mathrm{HH}}_{j,k,l}| \leq \int_0^1 \int_0^1 |\psi^{\mathrm{HH}}_{j,k,l}(x,y)|\, dxdy = 2^j\ 2^{-j} \times 2^{-j},$$

and similarly for horizontal and diagonal subbands. The approximation error becomes:

$$||f - f_J||^2 \leq 3 \sum_{j=J+1}^{\infty} K 2^j 2^{-j2} = \mathcal{O}(2^{-J}).$$

This is the same order of approximation as in the 1D-case, we now need

$$n = \sum_{j=0}^{J} K 2^j = \mathcal{O}(2^J)$$

coefficients. So the order of approximation is now:

$$||f - f_n|| = \mathcal{O}(n^{-1/2}),$$

while in the one-dimensional case we had $n = J$ and

$$||f - f_n|| = \mathcal{O}(2^{-n}).$$

This is not just squaring the number of coefficients to obtain a comparable error in two dimensions. This dramatic change comes from the difference between a point singularity in one dimensional signals and a line singularity in two dimensions. Of course, point singularities also exist in images, but they are far less important, and, after all, line singularities certainly do not exist in one dimensional signals. A point has no dimension, at each scale it only interferes with a fixed number of basis functions. A line has however a certain length. Consequently, the number of basis functions meeting this line increases for finer scales.

For a piecewise smooth function of the form $h = g + f$, with $g \in C^{\alpha}$, we have $\|g - g_J\| = \mathcal{O}(2^{-J\alpha})$, provided that the wavelet basis has $p \geq \alpha$ vanishing moments. This linear approximation uses $n = \mathcal{O}(2^{2J})$ coefficients, so the order of approximation is $\mathcal{O}(n^{-\alpha/2})$. We need coefficients at $\lceil 2J\alpha \rceil$ resolution levels to represent f with the same the same order of accuracy as g. This means $\mathcal{O}(2^{2J\alpha})$ additional non-zero coefficients. The total number of coefficients to achieve $\|h - h_n\| = \mathcal{O}(2^{-J\alpha/2})$ is then $n = \mathcal{O}(2^{2J\alpha} + 2^J) = \mathcal{O}(2^{2J\alpha})$. A wavelet approximation for a piecewise smooth function in two dimensions thus has an accuracy of $\mathcal{O}(n^{-1/2})$. Unlike in the one-dimensional case, the line singularity does have an important impact on the quality of the wavelet approximation: all the benefits from using more than one vanishing moment seem to be lost.

6.1.3 Smoothness spaces

As discussed in Section 3.5.4, Besov spaces are well characterized by wavelet coefficients: wavelet bases are unconditional bases for these spaces.

On the other hand, members of Besov spaces also show good wavelet approximation properties: if $\|f\|_{B^{\alpha}_{p,q}} < \infty$, then f can be approximated with an accuracy of $\mathcal{O}(n^{-\alpha/2})$ by n coefficients [53].

Since for a simple image as in the previous section, this order of approximation is $\mathcal{O}(n^{-1/2})$, this seems to suggest that typical images are in Besov spaces with relatively low α, even if the regions between the edges are very smooth. Typical images are reported to live in Besov spaces with values of α between 0.3 and 0.6 [53].

6.1.4 Other basis functions

From the previous analysis, we conclude that wavelets may not provide the ultimate representation for images, and, consequently, Besov spaces may not be the optimal way to describe images. It is of course true that wavelets and Besov spaces *are* successful, but looking for better generalizations of the wavelet idea for more-dimensional applications is an interesting — though difficult — challenge. The previous argument comes from approximation theory, but it has consequences in statistical estimation: a basis that performs well in approximation of piecewise smooth functions is appropriate for noise reduction. This is a motivation for the development of new types of basis functions, like ridgelets [27].

This text takes a different approach: it applies the classical two-dimensional wavelets and concentrates on the coefficients in the basis for a description of edges. This description is based on a random prior model for these coefficients and leads to a Bayesian algorithm, the philosophy of which is described in Section 2.6.

6.2 The Bayesian approach

6.2.1 Motivation and objectives

In one dimension, as in two dimensions, wavelet basis functions are localized in space and scale (frequency). As a consequence, manipulating a coefficient has a local effect, both in space and frequency. This is an important advantage of wavelet based methods.

On the other hand, usual *classification* rules are local too, and do not take into account all the correlations that exist among neighboring coefficients. Although a wavelet transform has decorrelating properties, this decorrelation is not complete (a wavelet transform is sometimes seen as an *approximation* of a Karuhnen-Loève-transform). We distinguish two types of correlations:

1. Important image features correspond to large coefficients at different scales: these coefficients are of course correlated. This type of correlation is inherent to all wavelet decompositions: it reflects the multiscale nature of it. In Chapter 5 we proposed, cited and discussed a couple of *deterministic* algorithms that take this multiresolution character into account. Other algorithms start from different variations of a stochastic 'tree' model for uncorrupted wavelet coefficients in a multiscale structure [33, 44, 105].

2. The second type of correlation is within one scale and is specific for two-dimensional inputs, like images: important coefficients tend to be clustered on the location of edges.

We assume that classical thresholding, possibly extended to deal with interscale correlations, performs sufficiently well for the first type of intercoefficient dependencies. This chapter concentrates on the second type of correlations. For the stochastic description of these structures, we need *geometrical* prior models. This leads to a multiscale version of *Markov Random Field Models* (MRF). Similar approaches are in [15, 20, 108, 107, 106].

The basis for our approach remains the thresholding philosophy. The minimum MSE threshold is based on a global compromise between noise and data: this is not the best thing we can do: instead of applying one threshold for all coefficients at a given level, we would like to decide for each coefficient separately what is best: keeping or killing. If we know the noise deviation σ and if an "oracle" would tell us the noise-free magnitude of each coefficient, we could apply the best possible selection from Section 3.4.1, i.e. the minimum risk selection: keep coefficients with uncorrupted value above σ and replace the others by zero. We remind that this is not thresholding, because the decisions are based on the uncorrupted values, not on the noisy ones. Thresholding is one particular example of this general idea of coefficient selection and the minimum risk selection is another one. This remains an ideal benchmark, but we hope that the incorporation of a prior model helps in mimicking this oracle. The Bayesian approach aims at two objectives at once: by taking into account the geometrical structures in the coefficients, we want to come closer to the ideal coefficient selection. As becomes clear from the subsequent sections, both objectives are reflected by the Bayesian model that we use.

6.2.2 Plugging the threshold procedure into a fully random model

Whereas typical threshold algorithms are based on this heuristical approach that the largest coefficients capture the essential image features, *Bayesian* methods start from a full model for wavelet coefficients of the following type:

$$\boldsymbol{W} = \boldsymbol{V} + \boldsymbol{N}$$

This is an additive model for wavelet coefficients where $\boldsymbol{N}$ is the noise vector, $\boldsymbol{V}$ is the uncorrupted wavelet coefficient vector, and $\boldsymbol{W}$ is the input (empirical) wavelet coefficient vector. Both the noise and the noise-free data are viewed as realizations of a probability distribution. We now describe how threshold procedures fit into this model.

A wavelet threshold algorithm consists of three steps: first, the observational data are transformed into empirical wavelet coefficients. The next step is a manipulation of the coefficients and finally, an inverse transform of the modified coefficients yields the result. When extending this thresholding with a Bayesian approach, we leave the three steps intact, but we build in more uncertainties in the second step. As explained in Section 2.6, the selection criterion used in the second step is based on a measure of *regularity*. This measure of significance $\boldsymbol{M}$ is a function of the observation:

$$\boldsymbol{M} = m(\boldsymbol{W}),$$

Wavelet coefficients with a significance below a threshold λ, are classified as noisy. With each wavelet coefficient W_s, the algorithm associates a ‘label’ or ‘mask’ variable X_s such that:

$$X_s = \begin{cases} 0, & \text{if } W_s \text{ is noisy according} \\ & \text{to the criterion, i.e. if } M_s < \lambda \\ 1, & \text{then } W_s \text{ is sufficiently clean, i.e. if} \\ & M_s \geq \lambda \end{cases} \tag{6.1}$$

In these and following equations, s represents the ‘multidimensional’ index of a wavelet coefficient on a given resolution level j and for a given component (vertical, horizontal, or diagonal): $s = (k, l)$. To avoid overloaded notations we omit the resolution level j and the component m in our equations, and use the simple index s. So, if no confusion is possible, we write W_s instead of $W^m_{j;s}$ or $W^m_{j;k,l}$. This classification is followed by the modification step: If $W_{\lambda s}$ denotes the modified coefficient, with subscript λ referring to the threshold value, we write:

$$W_{\lambda s} = h(W_s, M_s, X_s),$$

for some *action* $h(W_s, M_s, X_s)$. The classic *hard-threshold* procedure corresponds to

$$h(W_s, M_s, X_s) = W_s X_s.$$

It keeps the 'uncorrupted' coefficients and replaces the noisy ones by zero.

6.2.3 Threshold mask images

Figure 6.5 visualizes the binary label image $\boldsymbol{X}$, i.e. it shows in black the position of the selected wavelet coefficients for the horizontal subband at the one but finest resolution level from the non-decimated wavelet transform of the noisy image in Figure 5.10. The one but finest scale in the wavelet transform is two scales below the original image resolution, and, as before, we use the variation on the CDF-(spline)-filters "with less dissimilar lengths" [38, 11]. Primal and dual wavelets have four vanishing moments. The mask on the left-hand side was obtained by soft-thresholding using the minimum MSE threshold. The mask on the right-hand side is obtained by a generalized cross validation threshold. Applying soft-thresholding using this mask (and its analogues for other components and scales) leads to the output in Figure 5.12.

If we apply the same threshold to the noise-free coefficients, we get the left picture in Figure 6.6. We see that many of the isolated pixels have disappeared: they were due to noise. Applying the optimal selection, inspired by the 'oracle' information leads to an even more structured image in Figure 6.6(b). To conclude this discussion, we compare the result from soft-thresholding with level- and subband-dependent GCV-threshold with the result from the oracle selection, also referred to as the optimal (clairvoyant) diagonal projection. Only the three finest scales were processed. Signal-to-noise ratio is respectively 18.02 dB and 21.05 dB. The GCV result is in Figure 5.12, while Figure 6.7 contains the output from the ideal selection.

6.2.4 Binary image enhancement methods

A comparison of the different label images clearly illustrates that thresholding each coefficient separately does not take into account the image structures. An obvious way to recover the optimal mask of Figure 6.6 (b), is trying classic enhancement methods. Figure 6.8 (a) shows the label image after applying a median filter to the approximate minimum MSE labels in Figure 6.5. Another possibility is the application of so called erosion-dilation methods: these methods proceed in two steps:

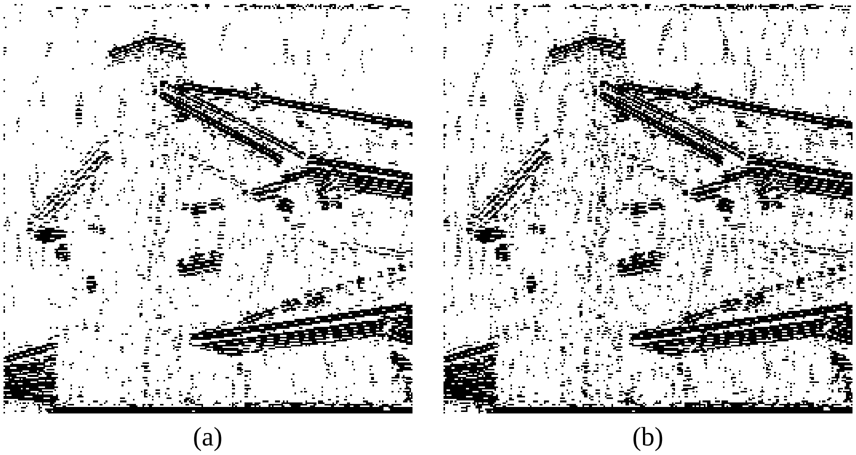

(a) (b)

Figure 6.5: Mask or label images, corresponding to the horizontal component of the one but finest scale. Black pixels represent coefficients with magnitude above the threshold. Left: using the minimum MSE threshold. Right: using a GCV estimate of this threshold.

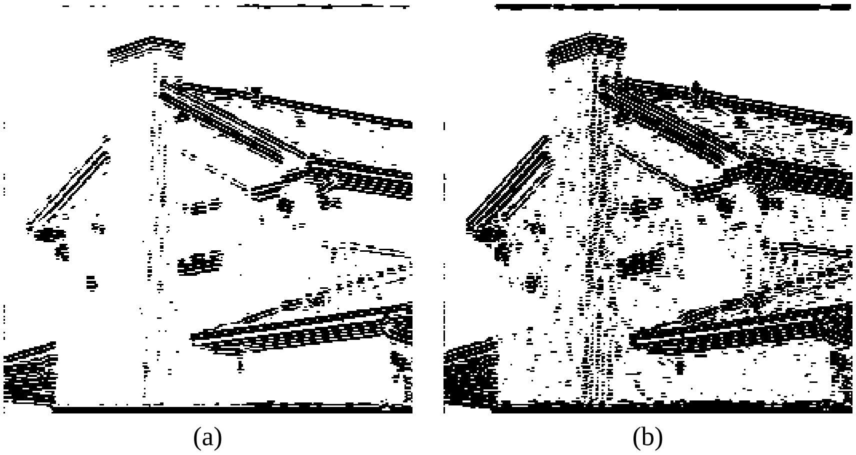

(a) (b)

Figure 6.6: Same mask images as in Figure 6.5, here based on noise-free coefficients. Left: black pixels indicate noise-free coefficients with magnitude above the previous threshold. Right: black pixels indicate noise-free coefficients with magnitude larger than noise deviation. This corresponds to the ideal wavelet selection: if an “oracle” [60] tells us whether or not a coefficient is dominated by noise, this is the best thing we can do.

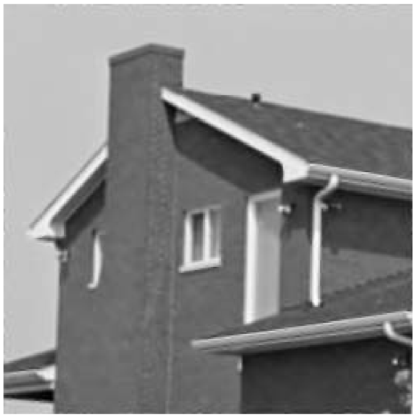

Figure 6.7: Output from the optimal (clairvoyant) diagonal projection, applied to three resolution levels. SNR $= 21.05$ dB.

in the first step, black pixels with less than, for instance, two black neighbors are removed. This erosion can be repeated several times, before going to the dilation. This second step tries to restore the eroded objects by turning white background pixels into black object pixels, if there is already an object in the neighborhood. (This neighborhood is typically a 3×3 box containing the actual pixel in its center.) Figure 6.8 (b) contains the result of this operation. It is hard to preserve the fine edge structures, while removing the noisy pixels. These operations act on the label images only and forget about the background behind them: these pixels come from a wavelet coefficient classification. We would prefer a method that can deal with the geometry *and* the local coefficient values at the *same* time. Bayes' rule tells us how we can do so.

6.2.5 Bayesian classification

The classification (6.1) in a threshold algorithm is a deterministic function of the empirical coefficients: thresholding on magnitudes corresponds to a simple step function, as illustrated in Figure 6.9. Recall that, in this text, the measure of significance is the coefficient magnitude: $\boldsymbol{M} = |\boldsymbol{W}|$. However, it would be interesting to examine measures based on interscale-correlations: e.g. $M_{j;s}^{m} = \prod_i W_{j+i;s}^{m}$, where j is the current resolution level and m the orientation ($m = \text{HOR}, \text{VER}, \text{DIAG}$).

Because we want to take the spatial configurations into account, we give up this tight relation between a coefficient value and its classification. We introduce a *prior model* for coefficient classification configurations $\boldsymbol{X}$. This prior should express the belief that clusters of noise-free coefficients have a higher probability

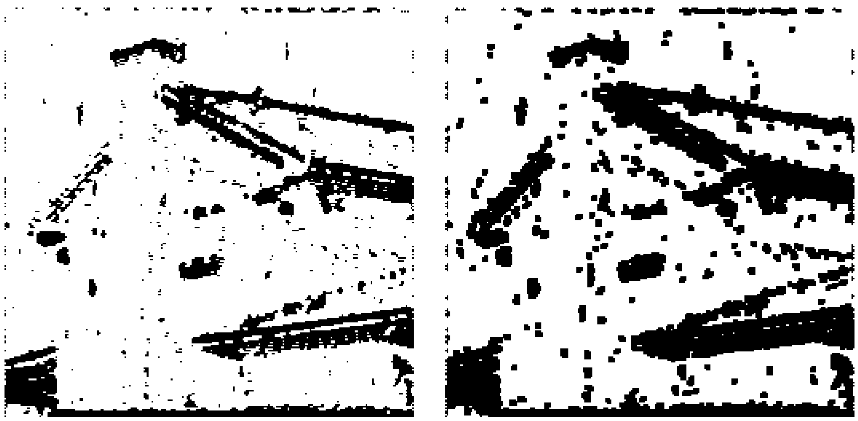

(a) (b)

Figure 6.8: Result of elementary binary image enhancement methods on the approximate minimum MSE label image in Figure 6.5. Left: a median filter; Right: an erosion-dilation procedure.

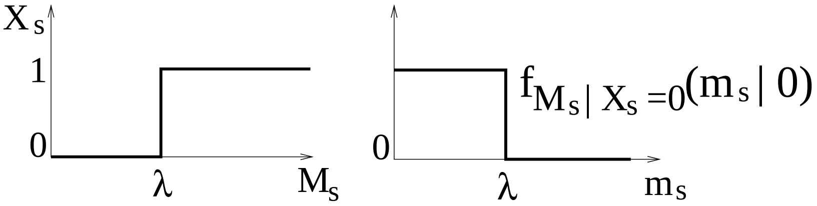

(a) (b)

Figure 6.9: Left: The deterministic classification function for coefficient magnitude thresholding: if a coefficient magnitude M is below the threshold value λ, it is classified as noisy ($X = 0$), otherwise it is called sufficiently clean ($X = 1$). Right: this deterministic approach is a special case of the Bayesian model, where the conditional density is zero for coefficient magnitudes above the threshold if $X = 0$ and beneath the threshold if $X = 1$.

than configurations with many isolated labels. In particular, edge-shaped clusters should be promoted. The prior model rests on the *classification* of the coefficients, not on the uncorrupted coefficients themselves. A similar idea is the use of Hidden Markov Models [33, 44, 105, 15, 20].

Next, the *conditional model* (likelihood function) states that if the classification label for a coefficient equals one, this coefficient is *probably* above the threshold. A zero label means that the corresponding coefficient is probably small. The classical, deterministic approach can be seen as an extreme case of this probability model, where, for example, a label $X = 0$ tells that the coefficient is *certainly* in the range $[-\lambda, \lambda]$. This appears in Figure 6.9(b).

If we have a prior distribution $\mathrm{P}(\boldsymbol{X} = \boldsymbol{x})$ and a conditional model $f_{\mathbf{M}|\mathbf{X}}(\boldsymbol{m}|\boldsymbol{x})$, then Bayes' rule allows to compute the *posterior* probability:

$$\mathrm{P}(\boldsymbol{X} = \boldsymbol{x}|\boldsymbol{M} = \boldsymbol{m}) = \frac{\mathrm{P}(\boldsymbol{X} = \boldsymbol{x}) f_{\mathbf{M}|\mathbf{X}}(\boldsymbol{m}|\boldsymbol{x})}{f_{\mathbf{M}}(\boldsymbol{m})}$$

In a given experiment, where $\boldsymbol{m}$ is fixed, the denominator is a constant. As we explain later, it is sufficient to know the *relative* probabilities of configurations, and therefore we write:

$$\mathrm{P}(\boldsymbol{X} = \boldsymbol{x}|\boldsymbol{M} = \boldsymbol{m}) = C \cdot \mathrm{P}(\boldsymbol{X} = \boldsymbol{x}) f_{\mathbf{M}|\mathbf{X}}(\boldsymbol{m}|\boldsymbol{x})$$

6.3 Prior and conditional model

6.3.1 The prior model

As explained above, we are looking for a multivariate model for a binary image $\boldsymbol{X}$. Expressing a probability function for all 2^{NM} possible values in a N by M label image may be cumbersome. We therefore construct the model starting from local descriptions of clustering. The prior probability function can always be written as:

$$\mathrm{P}(\boldsymbol{X} = \boldsymbol{x}) = \frac{1}{Z} \exp[-H(\boldsymbol{x})], \qquad (6.2)$$

with the *partition function* Z :

$$Z = \sum_{\boldsymbol{x}} \exp[-H(\boldsymbol{x})].$$

$H(\boldsymbol{x})$ is the *energy function* of a configuration $\boldsymbol{x}$: the lower the energy, the higher the prior probability. To express that this energy comes from *local* interactions only, we first define for each pixel index s in the lattice S its set of neighbors, i.e. the set of indices $\partial s \subset S$ that interact with s. We assume that $s \notin \partial s$ and

$s \in \partial t \Leftrightarrow t \in \partial s$. A set of indices that are all neighbors to each other is called a *clique*. The set of all cliques is

$$\mathcal{C} = \{C \in 2^S \mid \forall s, t \in C : t \in \partial s\}$$

If the total energy of a configuration equals the sum of its clique potential functions:

$$H(\boldsymbol{x}) = \tau \sum_{C \in \mathcal{C}} U_C(\boldsymbol{x}_C),$$

the probability function $\mathrm{P}(\boldsymbol{X} = \boldsymbol{x})$ is named a *Gibbs distribution* with respect to the given neighborhood system $\{S, \partial\}$, after the American theoretical physicist and chemist, Josiah Gibbs, who used this model in statistical mechanics [67]. The hyperparameter τ measures the *rigidity* of the configuration. The higher τ, the less likely are status changes due to noise. As the equation indicates, the clique potential U_C only depends on the values of $\boldsymbol{x}$ in the sites that belong to C.

Whereas Gibbs distributions are based on local energies, Markov Random Fields (MRF) are based on local statistical dependencies. A Markov Random Field, relative to a neighborhood system $\{S, \partial\}$ is a probability function P with the two-dimensional Markov property:

$$\mathrm{P}(X_s = x_s | \boldsymbol{X}_{S \setminus \{s\}} = \boldsymbol{x}_{S \setminus \{s\}}) = \mathrm{P}(X_s = x_s | \boldsymbol{X}_{\partial s} = \boldsymbol{x}_{\partial s}).$$

This definition does not use the notion of *clique*.

The Hammersly-Clifford theorem states that MRF's and Gibbs distributions are the same:

Theorem 6.1 (Hammersly-Clifford) *A probability function is a Markov Random Field with respect to a neighborhood system if and only if it is a Gibbs distribution with respect to same neighborhood system.*

Proofs are in [18, 151]. This theorem facilitates the computation of conditional probabilities in the lattice of a Gibbs distribution: this computation only uses local information. The computation of marginal probabilities of a MRF is well served by the Gibbs distribution property. Especially in expressions like

$$\frac{\mathrm{P}_{\mathbf{X}}(\boldsymbol{u})}{\mathrm{P}_{\mathbf{X}}(\boldsymbol{v})}$$

where $\boldsymbol{u}$ and $\boldsymbol{v}$ differ in a couple of lattice points s only, it is easy to use the theorem and limit the calculations to the potentials of cliques that contain one of these points s:

$$\frac{\mathrm{P}_{\mathbf{X}}(\boldsymbol{u})}{\mathrm{P}_{\mathbf{X}}(\boldsymbol{v})} = \exp\left(-\tau \sum_{s} \sum_{C \in \mathcal{C}, s \in C} U_C(\boldsymbol{u}_C) - U_C(\boldsymbol{v}_C)\right).$$

Actually, a Gibbs distribution is mostly the only practically possible specification of a Markov Random Field: it is hard to check whether a collection of local conditional probabilities form a coherent set for a Markov Random Field [66].

The application of this MRF's and Gibbs distributions in image analysis and image processing is still growing and our list [66, 78, 143, 151] is nothing but a snapshot. An often used Gibbs distribution is the Ising model, named after the German physicist Ising, who used it to explain ferromagnetism [80]. The neighbors of a pixel with index s is a 3×3 submatrix, excluding s in its center. The model only considers pairs of neighbors. Other cliques in the system have no energy. The total energy is:

$$H(\boldsymbol{x}) = \sum_{\{s,t\} \in \mathcal{C}} x_s x_t.$$

For our experiments, we use a slightly different model, in a 5×5-neighborhood system. This model is slightly better in describing edge structures than the Ising model and yet does not require too much computational effort. We only consider 3×3 cliques, i.e. the largest possible type in a 5 by 5 neighborhood system. The potentials of all other types of cliques are set to zero. For a 3 by 3 clique C we set:

$$U_C(\boldsymbol{x}_C) = \frac{\sum_{s \in C} x_s \sum_{t \in C \cap \partial s} (1 - 2 x_s x_t)}{\sum_{s \in C} x_s},$$

i.e. for each $x_s = 1$, we subtract the number of neighbors within the clique with value one from the number of neighbors with zero value. The sum of these results is divided by the number of labels with value $x_s = 1$, to obtain a mean value. The idea behind this potential function is to compute a kind of “average degree of isolation” within the clique for the pixels with value one. The background pixels are considered to be neutral. Unlike the classical Ising model, this function is not symmetric for interchanges of ones and zeros.

6.3.2 The conditional model

We also need a conditional density $f_{\mathbf{M}|\mathbf{X}}(\boldsymbol{m}|\boldsymbol{x})$. Whereas the prior describes the clustering of significant wavelet coefficients, this conditional model deals with the *local* significance measure. Therefore we write

$$f_{\mathbf{M}|\mathbf{X}}(\boldsymbol{m}|\boldsymbol{x}) = \prod_{s \in S} f_{M_s|X_s}(m_s|x_s).$$

This density expresses that if the label $X_s = 1$, i.e. if the corresponding wavelet coefficient is sufficiently noise-free, a large value of M_s is probable. Referring to the ideal selection procedure, we now impose the idea that selected coefficients should have an untouched value above the noise deviation σ. This means that if

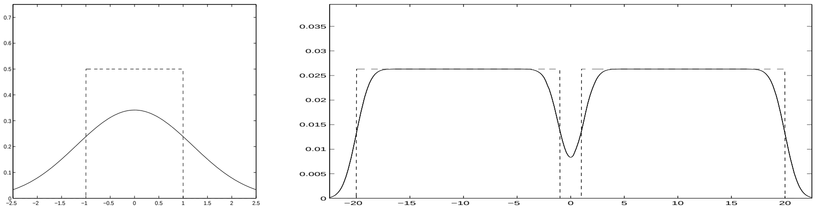

(a): $f_{W_s|X_s}(w|0)$ (b): $f_{W_s|X_s}(w|1)$

Figure 6.10: Conditional probability densities in Bayesian model. The model expresses that if a label $X_s = 0$, the corresponding coefficient *probably* has a small magnitude, but magnitude is no longer a strict selection criterion: a small coefficient might be important and a large coefficient might be replaced by zero.

$X_s = 1$, V_s is for instance uniformly distributed on $[-\mu, -\sigma] \cup [\sigma, \mu]$, μ being the maximum coefficient magnitude, which is a parameter of the model that has to be determined. If the noise $N_s \sim n(0, \sigma)$ has a Gaussian density, it is easy to verify that

$$f_{W_s|X_s}(w|1) = \frac{1}{2(\mu - \sigma)} \left[\Phi(w+\mu) - \Phi(w+\sigma) + \Phi(w-\sigma) - \Phi(w-\mu)\right],$$

where $\Phi(z)$ is the cumulative Gaussian distribution. A similar argument leads to the following conditional model for coefficients dominated by noise:

$$f_{W_s|X_s}(w|0) = \frac{1}{2\sigma} \left[\Phi(w+\sigma) - \Phi(w-\sigma)\right].$$

Figure 6.10 shows these density functions for $\sigma = 1$ and $\mu = 20$. This model expresses that if a label $X_s = 0$, the corresponding coefficient *probably* has a small magnitude, but magnitude is no longer a strict selection criterion: a small coefficient might be important and a large coefficient might be replaced by zero.

Other, perhaps more realistic models follow from the assumption that the important, noise-free coefficients are exponentially distributed:

$$f_{V_s|X_s}(v|1) = \frac{\rho \mathrm{e}^{\rho\sigma}}{2} \mathrm{e}^{-\rho|v|}.$$

This leads to the following expression for the coefficients corrupted by noise:

$$\begin{aligned} f_{W_s|X_s}(w|1) &= \frac{\rho\, \mathrm{e}^{\sigma\rho + \sigma^2\rho^2/2}}{2} \\ &\quad \left[\mathrm{e}^{-\rho w}\Phi(w - \sigma - \sigma^2\rho) + \mathrm{e}^{\rho w}(1 - \Phi(w + \sigma + \sigma^2\rho))\right]. \end{aligned}$$

Even more general models for noise-free wavelet coefficients are Laplacian distributions [129]:

$$f_V(v) = K\,\mathrm{e}^{-|kv|^{\kappa}}.$$

Typical values for κ range between 0.5 and 0.8.

6.4 The Bayesian algorithm

6.4.1 Posterior probabilities

From Bayes' rule, we can compute the posterior probabilities

$$\mathrm{P}(\boldsymbol{X}=\boldsymbol{x}|\boldsymbol{M}=\boldsymbol{m}) = \frac{\mathrm{P}(\boldsymbol{X}=\boldsymbol{x}) f_{\mathbf{M}|\mathbf{X}}(\boldsymbol{m}|\boldsymbol{x})}{f_{\mathbf{M}}(\boldsymbol{m})}$$

With these probabilities, a *Bayesian decision rule* leads to an estimation of the optimal label. The Maximum A Posteriori (MAP) procedure chooses the mask $\boldsymbol{x}$ with the highest posterior probability. The Maximal Marginal Posterior (MMP) rule is a more local approach: it computes in each site s the marginal probabilities:

$$\mathrm{P}(X_s=1|\boldsymbol{M}=\boldsymbol{m}) = \sum_{\boldsymbol{x}} x_s \mathrm{P}(\boldsymbol{X}=\boldsymbol{x}|\boldsymbol{M}=\boldsymbol{m}),$$

and if this probability is more than 0.5, the pixel gets value 1. Both decision rules have a binary outcome: each coefficient is classified as noisy ($X=0$) or relatively uncorrupted ($X=1$). We would like to exploit the entire posterior probability: the posterior mean value

$$E(X_s|\boldsymbol{M}=\boldsymbol{m}) = \mathrm{P}(X_s=1|\boldsymbol{M}=\boldsymbol{m})$$

preserves all information. It is a minimum least squares estimator. This classification leads to a posterior 'expected action':

$$\begin{aligned}\mathrm{E}(W_{\lambda s}|\boldsymbol{M}) = {} & h(W_s, m_s(\boldsymbol{W}), 1)\mathrm{P}(X_s=1|\boldsymbol{M}) \\ & + h(W_s, m_s(\boldsymbol{W}), 0)\mathrm{P}(X_s=0|\boldsymbol{M}).\end{aligned}$$

If $h(W_s, M_s, X_s) = X_s W_s$, this is:

$$\mathrm{E}(W_{\lambda s}|\boldsymbol{M}) = W_s \mathrm{E}(X_s|\boldsymbol{M}=\boldsymbol{m}) = W_s \mathrm{P}(X_s=1|\boldsymbol{M}).$$

Unlike most thresholding methods, this is not a binary procedure: using the posterior probability leads to a more continuous approach.

6.4.2 Stochastic sampling

The computation of $\mathrm{P}(X_s = 1|\boldsymbol{W})$ involves the probability of all possible configurations $\boldsymbol{x}$. Because of the enormous number of configurations, this is an intractable task. The sum we have to compute is of the following form:

$$\mu_s = \sum_{\boldsymbol{x}} f_s(\boldsymbol{x})\mathrm{P}(\boldsymbol{X} = \boldsymbol{x}|\boldsymbol{M} = \boldsymbol{m})$$

where in this case $f_s(\boldsymbol{x}) = x_s$ and $\mu_s = \mathrm{P}(X_s = 1|\boldsymbol{M} = \boldsymbol{m})$.

To estimate this type of sum (or integral for random variables on a continuous line), one typically uses stochastic samplers. These methods generate subsequent samples $\boldsymbol{X}^{(i)}$, not selected uniformly, but in proportion to their probability. This allows to approximate the matrix of required marginal probabilities by the mean value of the generated masks:

$$\hat{\mu}_s = \sum_i X_s^{(i)}.$$

Mostly, the samples are generated, not independently of each other, but in a chain, hence the name Markov Chain Monte Carlo (MCMC) estimation. The next sample is generated, starting from the previous one. One advantage of this procedure is that knowledge of the *relative* probabilities of the candidates is sufficient. The probability ratio of two subsequent samples:

$$r^{(i)} = \frac{\mathrm{P}(\boldsymbol{X}^{(i+1)}|\boldsymbol{M})}{\mathrm{P}(\boldsymbol{X}^{(i)}|\boldsymbol{M})}$$

is the only quantity needed by the algorithm, and if

$$\mathrm{P}(\boldsymbol{X} = \boldsymbol{x}|\boldsymbol{M}) = \frac{1}{Z f_{\mathbf{M}}(\mathbf{m})} \exp[-H(\boldsymbol{x})] f_{\mathbf{M}|\mathbf{X}}(\boldsymbol{m}|\boldsymbol{x}),$$

there is no need for the enormous computation of the partition function $Z f_{\mathbf{M}}(\mathbf{m})$.

We use the classic Metropolis MCMC sampler [114]. The chain of states is started from an initial state $\boldsymbol{X}^{(0)}$. The successive samples $\boldsymbol{X}^{(i)}$ are then produced as follows: a candidate intermediate state is generated by a local random perturbation of the actual state. Then the probability ratio r of the actual state and its perturbation is computed. Since the Gibbs distribution is based on local potential functions, only positions s whose mask labels are switched by the perturbation or which have a switched label in their neighborhood ∂s are involved in the computation. If the candidate has a higher probability than the actual state, i.e. if the probability ratio is larger than one, then the new state is accepted, otherwise it is accepted with probability equal to r. To generate a completely new sample, we repeat this local switching for all locations in the grid.

6.5 Parameter estimation

6.5.1 Parameters of the conditional model

The conditional model $f_{V_s|X_s}(v|1)$ or $f_{W_s|X_s}(w|1)$ is for instance uniform or exponential. This model contains a hyperparameter. It is not so hard to fill in this parameter using the observed, noisy wavelet coefficients. In our approach, we mostly use the uniform model on $[\sigma, \mu]$ for which it is easy to prove that the expected highest magnitude $\mathrm{E}|V|_{\max}$ equals:

$$\mathrm{E}|V|_{\max} = \frac{N\mu + \sigma}{N+1}.$$

A good measure for the noise variance is the average energy removed by the minimum MSE-threshold:

$$\hat{\sigma}^2 = \sum_{i=1}^{N} (W_{\lambda i} - W_i)^2.$$

Since the influence of the noise on the largest coefficients is relatively small, we take:

$$\hat{\mu} = \frac{(N+1)|W|_{\max} - \hat{\sigma}}{N}.$$

6.5.2 Full Bayes or empirical Bayes

The prior energy model contains a parameter τ:

$$H(\boldsymbol{x}) = \tau \sum_{C \in \mathcal{C}} U_C(\boldsymbol{x}_C)$$

It determines the local rigidity of the prior. The higher its value, the larger the energy difference between the two states of a given pixel in the label image. The choice $\tau = 0$, for instance, disregards spatial structures.

To find a good value for this parameter, there exists at least two approaches. The *fully* Bayesian approach considers this parameter as an instance of still another density and assigns a prior distribution f_τ to τ. The posterior density for this parameter is then:

$$f_{\tau|\mathbf{X}}(\tau|\boldsymbol{x}) \propto f_\tau(\tau)\mathrm{P}(\boldsymbol{X} = \boldsymbol{x}|\tau).$$

The posterior probability of the full set of unknowns $\boldsymbol{X}$, and τ, given the observation $\boldsymbol{M} = \boldsymbol{m}$ then satisfies:

$$\mathrm{P}(\boldsymbol{X} = \boldsymbol{x}, \tau|\boldsymbol{M} = \boldsymbol{m}) \propto f_{\mathbf{M}|\mathbf{X}}(\boldsymbol{m}|\boldsymbol{x})\mathrm{P}(\boldsymbol{X} = \boldsymbol{x}|\tau)f_\tau(\tau).$$

From these expressions, we can — for instance — find values for $\boldsymbol{M}$ and τ with maximum posterior probability.

The *empirical* Bayes approach maximizes the likelihood of the actual label image $\boldsymbol{x}$:

$$\mathrm{L}(\tau) = \mathrm{P}(\boldsymbol{X} = \boldsymbol{x}),$$

where the probability function on the right hand side depends on the rigidity τ through the energy function $H(\boldsymbol{x})$. This maximum likelihood estimation (MLE) has two practical problems. First, the computation of the likelihood function is extremely hard, due to the intractable partition function in (6.2). Therefore, and since the rigidity parameter controls the local behavior of the label image, we use a pseudo-likelihood method: we maximize the product of "local" likelihood functions:

$$\mathrm{PL}(\tau) = \prod_{s \in S} P(X_s = x_s | \boldsymbol{X}_{\partial s} = \boldsymbol{x}_{\partial s}, \tau).$$

This maximum pseudo likelihood estimation (MPLE) leaves us with the second problem: we have no real instance of the probability function $\mathrm{P}(\boldsymbol{X} = \boldsymbol{x})$, because we only have *noisy* measurements $\boldsymbol{M}$. The probability function of $\boldsymbol{X}$ supposes that $\boldsymbol{X}$ is the optimal selection of wavelet coefficients. This selection is based on the uncorrupted values $\boldsymbol{V}$ being above or below σ, which we do not know. Nevertheless, we assume that the *local* behavior of the mask obtained by thresholding the *noisy* coefficients approaches the rigidity of the optimal selection. The choice of the threshold is of course crucial in this approximation: we cannot take $\lambda = \sigma$, pretending $\boldsymbol{W} \approx \boldsymbol{V}$, since this would generate highly noisy masks, with little structure from the optimal selection. A mask generated by the minimum MSE or GCV is generally still too noisy, as becomes clear from a comparison of the labels in Figure 6.5 with the ideal one in Figure 6.6(b). This can be helped by applying a median filter to the minimum GCV labels, as in Figure 6.8. As mentioned before, this median filter does not take into account the background of the individual labels, like the conditional density in a Bayesian approach. Therefore it is less appropriate for the actual correction of the label images, but it may do a good job in estimating the rigidity factor τ of the optimal selection mask on a local basis. Another possibility is the universal threshold: this threshold eliminates all noise with high probability, at the risk of loosing parts of the underlying structure.

6.6 The algorithm and its results

6.6.1 Algorithm overview

This is a schematic overview of the subsequent steps of the algorithm:

1. Compute the non-decimated wavelet transform $\boldsymbol{W}$ of the input.
2. At each level and for each component, select the appropriate threshold. This threshold generates an initial label image $\boldsymbol{X}^{(0)}$.
3. Apply a median filter to $\boldsymbol{X}^{(0)}$ and estimate the prior parameter α from the result, using a maximum pseudo-likelihood estimator.
4. Run a stochastic sampler to estimate for each coefficient at the given resolution level the probability $\mathrm{P}(X_s|\boldsymbol{W})$. Use $\boldsymbol{X}^{(0)}$ from the previous step as the starting sample. A Markov Chain Monte Carlo algorithm produces the sequence of samples.
5. $\hat{W}_{\lambda s} \leftarrow W_s \mathrm{P}(X_s = 1|\boldsymbol{W})$.
6. Inverse wavelet transform yields the result.

6.6.2 Results and discussion

We now apply the procedure to the image with artificial noise in Figure 5.10. Figure 6.11(a) shows the mask image after ten MCMC-iterations. To be more correct: this image represents for each coefficient the posterior probability $\mathrm{P}(X_s = 1|\boldsymbol{W})$ of its label being one. More iterations (up to 100) did not improve the output quality. This output appears in Figure 6.11(b). Signal-to-noise ratio is 18.50 dB. Looking at the posterior probabilities, and comparing this with the objective mask in Figure 6.6(b), we see that most spurious labels from the threshold procedure indeed have a low posterior probability. The important structures that are present in the label image corresponding to the MSE-threshold, are preserved: the coefficients belonging to these structures have high probabilities. Nevertheless, it seems to be hard to recover clusters of small coefficients, even if these structures appear in the optimal selection.

We also illustrate the method with the ‘realistic” MRI-image of a knee in Figure 5.18. Figure 6.12(a) has the output of the Bayesian algorithm, applied to the first and second resolution level. Figure 6.12(b) shows the label image for the vertical subband at the second resolution level, to be compared with the selection of a minimum GCV-threshold, depicted in Figure 6.12(c). The latter selection is based on local regularity (magnitude) and shows far less geometrical structure.

6.6.3 Related methods

Our prior model was designed to describe geometrical correlations among coefficients within a given subband (scale and component). This type of correlation typically appears in two-dimensional wavelet transforms, especially in image analysis. Interscale correlations, present in all dimensions, are not captured by our prior model, although this is possible, as in [44].

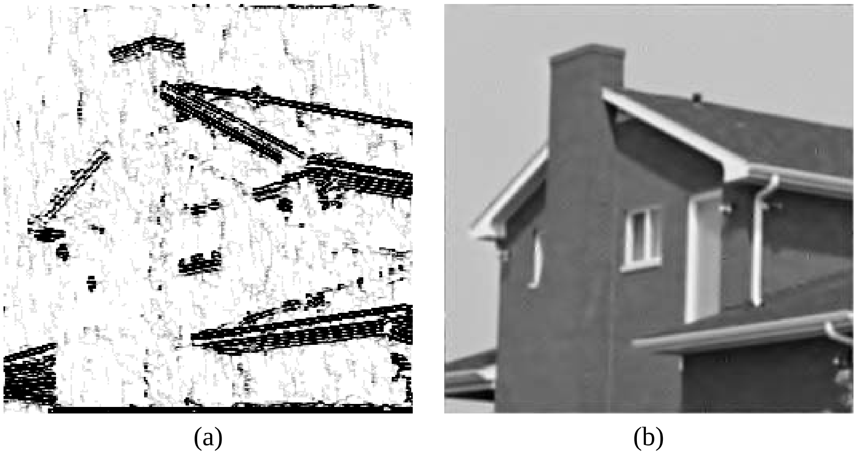

Figure 6.11: Left: label image for the wavelet coefficients of the image in Figure 5.10 after ten MCMC iterations. Consequently, this image has 11 grey values. A pixel value is an estimate of the marginal posterior probability $\mathrm{P}(X_s = 1|\boldsymbol{M})$. Right: the algorithm output. Three resolution levels were processed. Signal-to-noise ratio is 18.50 dB.

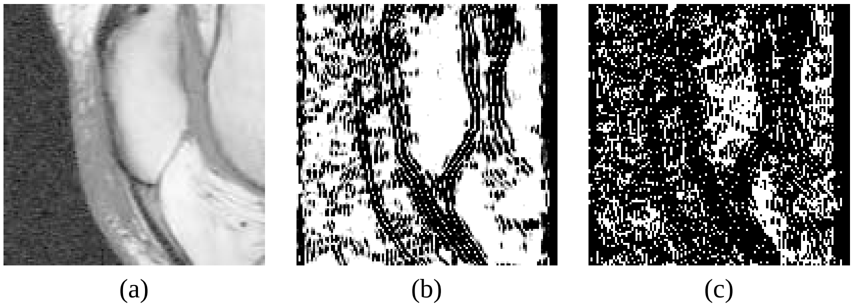

Figure 6.12: (a) Output of the Bayesian algorithm, applied to the first and second resolution level of the image in Figure 5.18. (b) and (c): Selection masks for vertical subband at the one but finest resolution level. The image in (b) has eleven grey levels, it represents for each coefficient an MCMC-estimate of the posterior probabilities of being important. The MCMC procedure used ten iterations, hence eleven grey levels, from zero to one. The last image is binary: black pixels correspond to coefficients that are preserved by a minimum GCV-threshold. This selection is based on local regularity (magnitude) and shows far less geometrical structure.

Another difference is the meaning of the label values X_s, and, consequently the design of the conditional model. Unlike the labels in [35, 44], a label one in our algorithm means that the corresponding noise-free coefficient is certainly larger than σ. The conditional model is explicitly inspired by the idea of finding the optimal diagonal projection of [60]. We do not compute a posterior mean $\mathrm{E}(V_s|\boldsymbol{W})$, but rather a posterior expected action: $\mathrm{E}(W_{\lambda s}|\boldsymbol{W})$.

This algorithm was inspired by previous work by Malfait et al. [108, 107], although their algorithm is based on Hölder regularity, and therefore looks at the evolution of coefficients through scales. Our algorithm uses coefficient magnitudes at one scale only, because this leads to more stable computations. Second, unlike the work by Malfait et al. the algorithm described in this text aims at the optimal coefficient selection, and the conditional model has been designed with this objective in mind. Third, all model parameters in our algorithm are determined automatically, in an empirical or heuristical way: there is no need for learning, the algorithm adapts itself to a given image.

6.7 Summary and conclusions

This chapter has investigated the possibilities of a Bayesian procedure to improve the results of a wavelet thresholding procedure. This procedure was designed for application in image noise reduction and it combines two objectives:

1. We want to capture the correlations in wavelet coefficients due to edge singularities. This type of singularities is specific for more-dimensional data, like images. The *prior* model in our procedure takes these line singularities into account: the model is based on *geometrical* properties: it favors clusters of important coefficients.

2. With the aid of this geometrical prior, we aim at mimicking the optimal coefficient selection. This is reflected in the *conditional* model.

The algorithm succeeds in finding more structure in the coefficient selection, which results in an output with better preserved edges. It would be interesting to quantify this gain in contrast. A more sophisticated conditional model, based on Laplacian distributions for uncorrupted wavelet coefficients, as well as the never ending search for good prior models are other topics for further research.

“Bei Tag, bei Nacht, im Wachen, im Traum,
Ihr gilt das alles gleich,
Wenn sie nur wandern, wandern kann,
Dann ist sie überreich!

Sie wird nicht müd, sie wird nicht matt,
Der Weg ist stets ihr neu;
Sie braucht nicht Lockung, braucht nicht Lohn,
Die Taub’ ist so mir treu! ”

—Johann Gabriel Seidl, *(1804–1875), Die Taubenpost, set to music by* *Franz Schubert* *(1797–1828), Schwanengesang, D. 957.14.*

Chapter 7

Smoothing non-equidistantly spaced data using second generation wavelets and thresholding

“ – Cerchiamo di ricominciare da capo, Adso, e ti assicuro che cerco di spiegarti una cosa sulla quale neppura io credo di possedere la verità.
(...)
– Perché non prendete posizione, perché non mi dite dove sta la verità?
(...)
– Ecco, il massimo che si può fare è guardare meglio.
(...)
– Quindi, se ben capisco, fate, e sapete perché fate, ma non sapete perché sapete che sapete quel che fate? ”
—Umberto Eco, *Il Nome della Rosa, terzo giorno, nona.*

A classical (first generation) wavelet transform assumes the input to be a regularly sampled signal. In most applications of digital signal processing or digital image processing, this assumption corresponds to reality. In many other applications however, data are not available on a regular grid, but rather as non-equidistant samples. Examples in this chapter illustrate what happens if we use classical wavelet transforms, pretending that the data are equispaced: the irregularity of the grid is reflected in the output.

Working with wavelets on irregular grids guarantees a smooth reconstruction [48]. This chapter investigates closeness of fit: it turns out that stability issues make it hard to hit this target from the wavelet domain. A close fit in terms of wavelet coefficients may be not so good after reconstruction. As a consequence of this, the connection between coefficient magnitude and importance is not so clear anymore: omitting a small coefficient may cause an important bias after reconstruction.

Nearly all existing wavelet based regression of non-equispaced data combines a traditional equispaced algorithm for fitting with a “translation” of the input into an equispaced problem, for instance by interpolation in equidistant points [76, 96], or a projection of the result onto the irregular grid by projection [25].

The second generation wavelets approach for de-noising non-equidistant samples is new. A discussion of the unbalanced Haar transform [68] for regression appears in [51], which also contains an excellent overview of first generation approaches. The origin of the stability problems when using second generation wavelets is not yet fully understood. This chapter proposes some possible explanations.

7.1 Thresholding second generation coefficients

7.1.1 The model and procedure

For this text, we suppose that the data live on a fixed, irregular grid:

$$y_i = f(x_i) + \eta_i, \quad i = 1, \ldots, N.$$

Some methods based on classical wavelets use a ‘preconditioning’ of the data (by interpolation in equidistant points, for instance). In that case, it may make a difference starting from a random model for the data points:

$$y_i = f(X_i) + \eta_i, \quad i = 1, \ldots, N,$$

where the X_i come from a random distribution. In our approach, however, there is no need for specifying how the data points were selected.

We just apply a second generation wavelet transform to the input. Since this transform takes into account the lattice of the data, the noise standard deviation is different for each coefficient, even if the noise on the input data had a constant standard deviation. This lack of homoscedasticity makes thresholding difficult: if the amount of noise is different for each coefficient, it is hard to remove it decently by only one threshold.

Nevertheless, if we know the covariance structure Q of the input noise, we can compute the variance fluctuation in the wavelet domain, as in (2.20):

$$S = \tilde{W} Q \tilde{W}^T$$

If Q is a banded matrix, S can be computed in a linear amount of time. In practical cases, the exact values of Q are often unknown, but the structure of Q may be known, i.e. Q may be known up to a constant. The case of stationary white noise, for instance, corresponds to: $Q = \sigma^2 I$, with I the identity matrix.

The normalised coefficients

$$\tilde{w}_i = w_i / \sqrt{S_{ii}}$$

do have a constant variance and thresholding these coefficients makes more sense than thresholding the original ones.

7.1.2 Threshold selection

The matrix Q may not contain the exact variances, but only the structure of the covariance matrix. This is the case if we know the structure of the correlation of the input noise. In many practical situations, for instance, it is reasonable to assume that the noise is white and stationary without specifying the exact noise level.

To find a good threshold without using an estimate for this noise level, we rely on the GCV-procedure of Chapter 4:

$$GCV(\lambda) = \frac{\frac{1}{N}\|\tilde{\boldsymbol{w}} - \tilde{\boldsymbol{w}}_{\boldsymbol{\lambda}}\|^2}{[\frac{N_0}{N}]^2}.$$

In this equation $\tilde{\boldsymbol{w}}_{\boldsymbol{\lambda}}$ is the vector of thresholded normalized coefficients and, as usual, N_0/N stands for the fraction of coefficients replaced by zero by this particular threshold value λ.

7.1.3 Two examples

We illustrate the effect of using second generation wavelets with two examples. In the first example, the grid was obtained by selecting $N = 2048$ points x_k at random between 0 and 1. These points were ordered and used as sampling points for the “heavisine” function [61]:

$$\begin{aligned} f(x) &= 4\sin(4\pi x) - \mathrm{sign}(x - 0.3) - \mathrm{sign}(0.72 - x) \\ y_k &= f(x_k) + \eta_k, k = 1, \ldots, N \end{aligned}$$

The figures 7.1 show a detail of 600 points. The algorithm used a lifting scheme, based on cubic interpolation for prediction and a two-taps update filter. We can neglect the grid structure, i.e. we run the algorithm with an equidistant grid, this means that we are smoothing the data (k, y_k) instead of (x_k, y_k). The result is noisy, because the regular grid transform does not correspond to the real grid. The spikes in the result are inherent for this simple threshold algorithm. More sophisticated algorithms should be able to remove them. The curve in between these spikes however is much smoother if we use second generation wavelets.

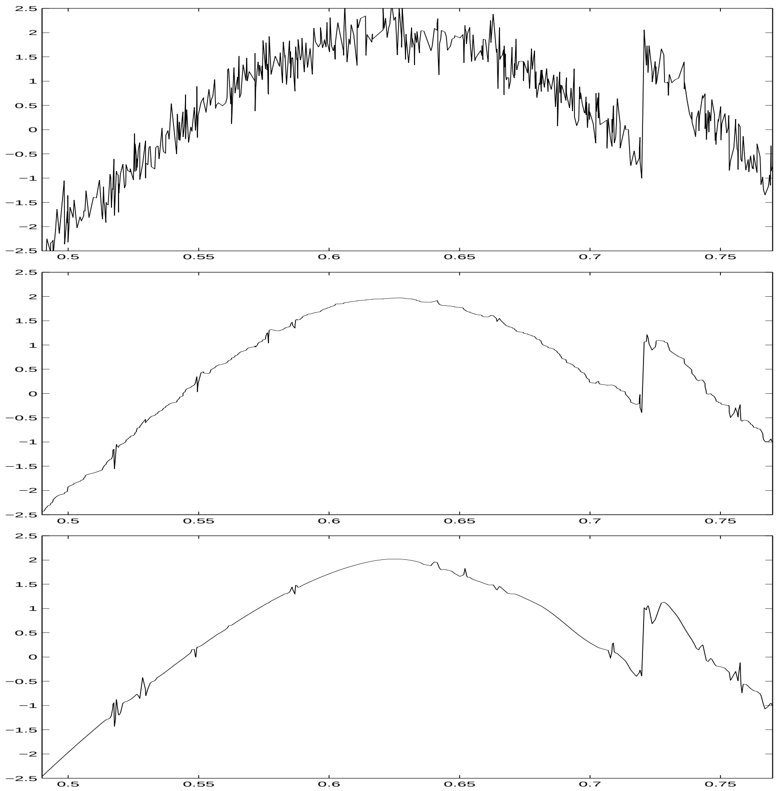

Figure 7.1: Example 1: Top: noisy ‘HeaviSine’ function on a “not too” irregular grid. The grid was obtained as an ordered set of uniformly chosen points on the interval $[0, 1]$. Middle: result of a threshold algorithm on a classical wavelet transform. We run the lifting scheme but tell the algorithm that the grid is regular. The result is noisy, because the regular grid transform does not correspond to the real grid. Bottom: result of the same algorithm based on the actual grid. In both cases, we use GCV to estimate the MSE-threshold.

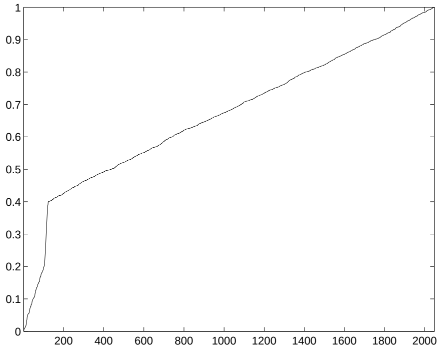

Figure 7.2: The grid of Example 2: this very irregular grid was constructed as follows: we choose approximately 100 samples at random between 0 and 0.2, about 10 samples between 0.2 and 0.4 and about 1940 samples between 0.4 and 1.

A second example is a damped sine ($f(x) = \mathrm{e}^{-x} \sin 4\pi x$) on an extremely irregular grid. This grid was constructed as follows: we choose approximately 100 samples at random between 0 and 0.2, about 10 samples between 0.2 and 0.4 and about 1940 samples between 0.4 and 1. Figure 7.2 plots the grid point versus the point number. If we add white and stationary noise to this function, we get the upper plot of Figure 7.3. The left part of this plot looks less noisy, but this is because data points in the right tail are much closer to each other. As for the previous example, second generation wavelets give a generally smoother result, but in this case, this scheme introduces a tremendous bias, not only in the region with few data points, but also at places where data are given close to each other. One could argue that this example is somehow artificial. Moreover, the phenomena seem to appear mostly at coarse scale, and it is a common practice to leave coefficients at coarse scales untouched. Nevertheless, if we run the same algorithm pretending the grid to be regular, the result is quite fair, apart from the grid irregularities, of course. We now investigate where this bias comes from and what we can do to make the second generation algorithm perform at least as well as the “first” generation wavelets.

7.2 The bias

7.2.1 The problem

The bias comes from the fact that the second generation wavelet transform may be far from orthogonal. This appears in several effects, which sometimes enhance each other.

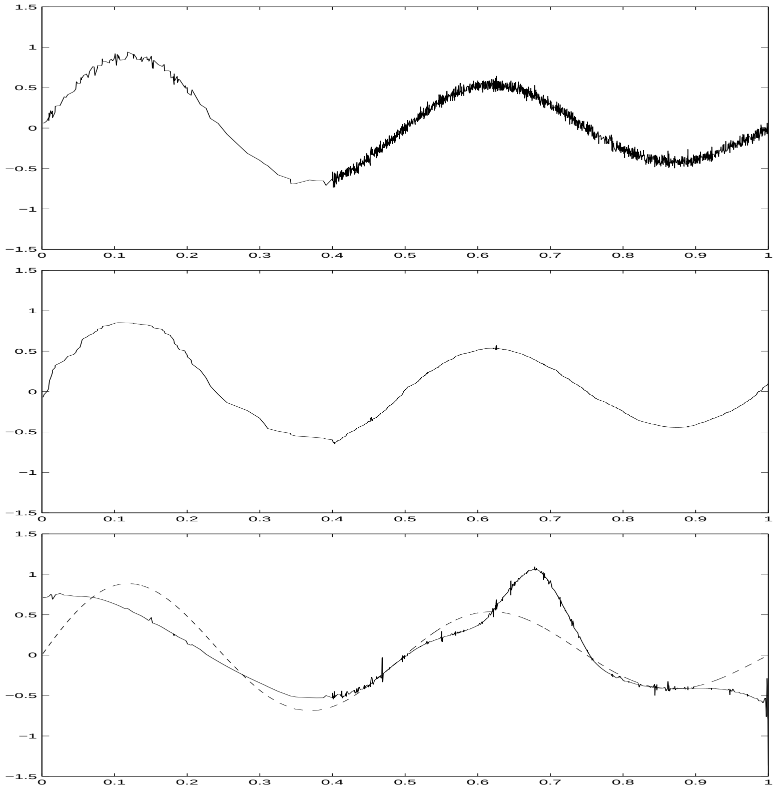

Figure 7.3: Example 2: Top: noisy signal ($f(x) = \mathrm{e}^{-x} \sin 4\pi x$) on the grid of Figure 7.2. Middle: result of a threshold algorithm on a classical wavelet transform. The lack of smoothness in this result reflects the irregularity of the grid. Using second generation wavelets leads to a much smoother result, but for this example, this scheme causes an unacceptable bias.

1. A small coefficient may have a wide *impact*, especially when it is related to a region with only a few samples. Thresholding it causes an important effect in the original domain.

2. Basis functions sometimes have a large overlap, especially in the neighborhood of boundaries. Large individual coefficients may then compensate each other, resulting in a signal with a relatively small energy. Thresholding these coefficients destroys the balance between the large coefficients and causes artifacts: hidden components suddenly become visible.

3. A transform has a bad condition number if it is sensible to errors on the input. As a matter of fact, thresholding can be considered as an artificial error on the input, and typically, the threshold is much larger than machine-precision! If the transform is not stable, there is no guarantee that the output is close to the input, even if it is so in wavelet-domain.

4. The threshold is proportional to the standard deviation of a coefficient. Unlike in the stable case, coefficients with large variance may correspond to basis functions with large energy. Or, equivalently, dividing wavelet coefficients by their standard deviation may cause important coefficients to become relatively small.

The bad condition of such a wavelet transform plays a role in other applications too, of course. From the statistical point of view, we are specifically interested in the interaction between variance normalization and bias, as described in the last item of this enumeration. In short, a bad conditioned transform makes it difficult, if not impossible, to predict the effect of a threshold on a coefficient.

7.2.2 Condition of the wavelet transform

Table 7.1 compares the condition number for different wavelet transforms on different lattices. The first row contains the condition numbers of first generation wavelets, treating the boundaries by periodic extension. For the second row, we still have an equidistant grid, but now the boundaries are processed in the second generation way. The third row was obtained for a transform on the “close-to-regular” grid, as in Figure 7.1, i.e. the input is defined on an ordered set of uniformly chosen points on the interval $[0, 1]$. The next row corresponds to the extremely irregular grid in Figure 7.2. The last row has results for an evenly irregular grid, but this time, the zone with little data is right in the middle of the interval, instead of at the left side. In this example, there should be less interaction of the sparse data zone with the boundary. All transforms use $N = 2048$ data points and $\tilde{n} = 2$ vanishing moments for the primal wavelet function, which corresponds to a two-taps update filter in the lifting scheme. The prediction is a linear interpolation in the first column and a cubic interpolation in the second one.

	linear interpolation	cubic interpolation
(1)	.754E1	.607E1
(2)	.194E3	.755E2
(3)	.104E4	.247E5
(4)	.400E4	.253E6
(5)	.272E3	.172E6

Table 7.1: Condition numbers for wavelet transforms on different lattices: (1) equidistant grid, periodic extension, (2) equidistant grid, 2nd generation, (3) uniformly random samples, (4) lattice of Figure 7.2, (5) an evenly irregular lattice as (4) but this time, the sparse zone is in the middle of the interval. The notation $q\mathrm{E}a$ stands for $q \times 10^a$.

To eliminate all normalization effects, and to concentrate on the obliqueness of the basis, we consider transforms that map coefficients in a normalized scaling basis onto coefficients in a normalized wavelet basis. The according normalization at the beginning and at the end is included in the condition numbers.

7.2.3 Where does the bad condition come from?

As Table 7.1 indicates, bad condition follows from several factors and from the interaction between those:

1. The primal lifting (update) step plays an important role in this phenomenon: it turns out that an update filter with two taps $A_{j,k}$ and $B_{j,k+1}$ defines a wavelet function at scale j and place k as a combination of scaling function at two scales [138]:

   $$\psi_{j,k} = \varphi_{j+1,2k+1} + A_{j,k}\varphi_{j,k} + B_{j,k+1}\varphi_{j,k+1}.$$

   If the update filter coefficients are large, ψ_{jk} is close to the subspace spanned by the scaling functions $\varphi_{j,k}$ at the same scale.

2. These problems appear to have most consequences close to the boundaries of the interval, and less in the middle. Scaling functions at the boundaries tend to have heavy tails and these tails cause an important overlap of $\psi_{j,k}$ with $\varphi_{j,k}$ or $\varphi_{j,k+1}$.

3. Pretending the grid to be regular eliminates a great deal of the bias. This indicates that not only boundary problems have an impact: the irregularity itself also creates or enhances instability.

4. It is clear that the lifting theory as such neglects the notion of scale: if a sequence of dense samples is followed by a large gap, the transform operates

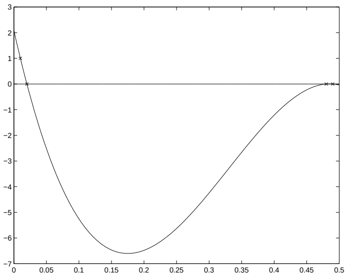

Figure 7.4: Effect on the interpolating polynomial of an error in the first interpolating point. This function is the difference between the correct interpolating polynomial (not shown here) and the polynomial that comes out if the error in the first interpolating point (0.01) equals one. This illustrates the problem that this error function may become large if the interpolating points are far from equidistant.

on phenomena at different scales in one single step. In one way or another, the transform should be re-organized so that it deals with phenomena at one scale in each step. This reordering of downsampling the coefficients however does not seem so easy.

We remark that at least the Haar transform remains orthogonal on an irregular grid. For the CDF 2,2-transform, which corresponds to linear interpolation prediction and a simple update, the problems remain marginal. In both cases, there is almost no mixture of scales possible: one (for Haar) and even two (CDF 2,2) prediction points never show a structure with two different scales. In a cubic interpolation scheme, however, the four interpolation points may reflect phenomena at two different scales, for instance, if three points are close to each other and the fourth is at a long distance from this cluster.

5. Heavy tails are partly a consequence of the prediction (dual lifting) step, which determines the primal scaling functions. So, the interaction of both prediction and update seems to be responsible for at least part of the problem. Figure 7.4 illustrates that a small error in one of the interpolation points may cause a serious error in the points where this interpolating polynomial is used as a prediction. The figure shows the errors caused by a unit error in one of the interpolation points: this function is the *difference* between the correct interpolating polynomial (not shown here) and the polynomial that comes out if the error in the first interpolating point (0.01 in the example) equals one. This difference or error function itself is a Lagrange interpolating polynomial.

7.3 How to deal with the bias?

Essentially, there are two possible ways to overcome the problem of the bad condition. The first is trying to modify the transform so that it becomes more stable. Since at this moment we do not completely understand the origin of the instability, and because we believe that reorganizing the algorithm would be a rather hard job, we prefer an alternative solution. We examine which coefficients are dangerous to threshold, and how to find an appropriate value for these coefficients.

7.3.1 Computing the impact of a threshold

In the first instance we try to save the coefficients that correspond to large energy basis functions from thresholding. We examine for each coefficient the influence of a threshold proportional to its noise level $\lambda = k\sigma_i$. We have that

$$\sigma_i = \sqrt{(\tilde{W} Q \tilde{W}^T)_{ii}}.$$

We assume that the input noise is uncorrelated (white) and second order stationary: $Q = \sigma^2 I$. Each coefficient w_i corresponds to a basis function. The 2-norm of this function can be computed as:

$$E_i = \int_{-\infty}^{\infty} \psi_i^2(x)\, dx = \sqrt{(W^T T_J W)_{ii}} = \sqrt{\left[(\tilde{W} T_J^{-1} \tilde{W}^T)^{-1}\right]_{ii}},$$

where $W = \tilde{W}^{-1}$ is the inverse wavelet transform matrix and T_J is a diagonal matrix containing the squared norms of the scaling function at the initial, fine resolution:

$$T_{J,kk} = \int_{-\infty}^{\infty} \varphi_{J,k}^2(x)\, dx \approx \int_{(x_{k-1}+x_k)/2}^{(x_k+x_{k+1})/2} 1^2\, dx.$$

This norm E_i is a measure for the effect of a “unit-threshold”. The total effect $\Delta \boldsymbol{y}$ of thresholding is given by the following expression of impact:

$$\Delta \boldsymbol{y} = k \sqrt{(\tilde{W} Q \tilde{W}^T)_{ii} \left[(\tilde{W} T_J^{-1} \tilde{W}^T)^{-1}\right]_{ii}}.$$

For orthonormal transforms on a regular grid and with uncorrelated, stationary noise, this effect would be independent of W: it only depends on the threshold value $\Delta \boldsymbol{y} = k\sigma = \lambda$. Figure 7.5 shows the result if we preserve coefficients with a large impact from thresholding. The most serious bias has gone, but the result has lost smoothness and it is difficult to define a threshold between coefficients with large and small impact.

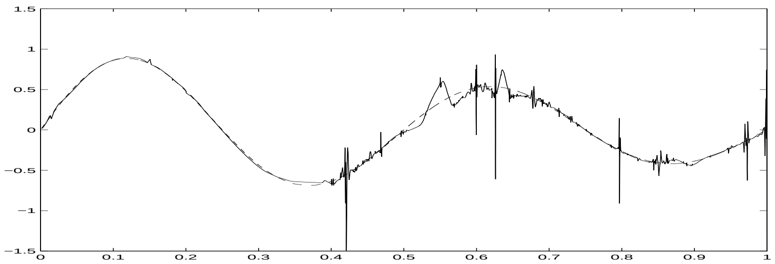

Figure 7.5: Result if we preserve coefficients with a large impact from thresholding. The most serious bias has gone, but the result has lost smoothness and it is difficult to define a threshold between coefficients with large and small impact.

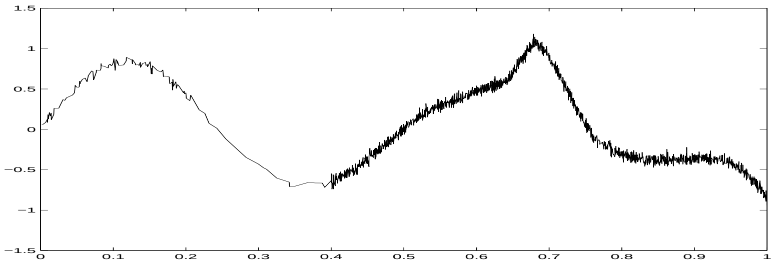

Figure 7.6: Reconstruction after removing one coefficient from the noisy transform. The effect is enormous, but the coefficient was rather big.

7.3.2 Hidden components and correlation between coefficients

The computation in the previous section only takes into account the 2-norm of separate basis functions. The inner product of two functions, which is responsible for inter-coefficient correlations, does not appear in the algorithm. The peaks in the result are the consequence of this approach, as illustrates the following example. Figure 7.6 shows an experiment where one particular second-generation wavelet coefficient of the noisy signal was replaced by zero. Inverse transform reveals a tremendous effect. The coefficient had a rather large magnitude, and apparently also a wide impact, but comparison of the results in Figure 7.6 and Figure 7.3 indicates that the same coefficient was classified as not important by the threshold algorithm. This is because not only its magnitude was large, but so was its variance. If we remove the same threshold from the noise-free wavelet coefficients, we get the reconstruction in Figure 7.7. The difference with the original function is hardly visible. The threshold algorithm was right to remove it. A simple example in $\mathbb{R}^3$ makes clear what happens. Suppose we have the basis vectors $\{(-1/2, \sqrt{3}/2, 0), (-1/2, -\sqrt{3}/2, 0), (1, 0, \varepsilon)\}$. If ε is small, this basis has an

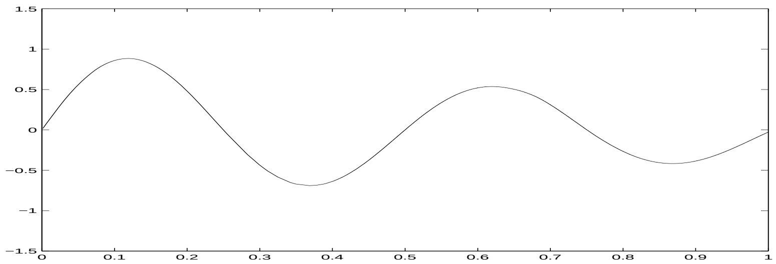

Figure 7.7: Reconstruction after removing the same coefficient as in Figure 7.6 from the noise-free transform. The effect is quasi nihil.

extremely bad condition. Suppose the noise is $(0, 0, \varepsilon)$ in the canonical basis, then its coordinates in this oblique basis are $(1, 1, 1)$. If one or two of these coordinates are thresholded, “hidden components” become clear. This bad condition can only be detected with a global analysis: none of the basis vectors is close to another one. In the example of Figure 7.6, the noise made small coefficients big, because it did not fit well into the oblique basis. Removing some of these coefficients uncovers these hidden components. The result of Figure 7.5 does not contain the same bias as in Figure 7.6. This means that the computation of the impact of the coefficients saved the coefficient of Figure 7.6 from being thresholded. This is not what we want: not only it does not correspond to what the noise-free coefficient says (this is what Donoho and Johnstone call the “oracle”), but also, if we keep this large, purely noisy coefficient, we have to keep all the others that compensate for its effect. These are hard to find, and if we find them, we end up with a result without any noise-*reduction* at this place. We would like to remove all of these large noise coefficients and therefore we want a reliable estimation of the noise-free signal: this estimation does not have to be smooth, but it should learn us which of the big coefficients are really important and which are due to noise. Unlike the classical (bi-)orthogonal transform, the second-generation transform no longer guarantees that coefficients with a large magnitude are important.

Another unpleasant consequence is the fact that scaling coefficients which are not further transformed may carry a lot of noise too. Most algorithms do not threshold scaling coefficients, and this may uncover, once more, hidden noise components. A reliable estimation of the noise-free signal could give us an idea of the effect of the noise on the low-resolution scaling coefficients.

7.3.3 Starting from a first-generation solution

We know that if the transform neglects the grid structure, the result reflects the irregularity of the grid. The result is non-smooth, which means that it has no sparse representation in a second-generation basis. Apart from that, the result is fairly reliable, in the sense that bias is restricted by the Riesz-constants of the transform: if we are thresholding in the wavelet domain, we know what we are doing in the original signal domain. Let $\boldsymbol{w}^{(1)}$ be the second generation wavelet coefficients of this first generation solution $\boldsymbol{y}^{(1)}$. Our objective is to find a sparsely represented signal close to $\boldsymbol{y}^{(1)}$. To this end, we use the thresholded coefficients $\boldsymbol{w}_{\boldsymbol{\lambda}}$ of the second-generation transform of the noise.

If a coefficient w_i corresponds to a wavelet that lies on an interval where the second-generation solution $\boldsymbol{y}_{\boldsymbol{\lambda}}$ shows no bias, we can choose as output:

$$\hat{w}_i = w_{\lambda i}$$

To do so, we have to define in which data points $\boldsymbol{y}_{\boldsymbol{\lambda}}$ is biased and we have to mark the coefficients that correspond to these points. We say that $y_{\lambda i}$ is biased if

$$|y_{\lambda i} - y_i^{(1)}| > \hat{\sigma},$$

where:

$$\hat{\sigma} = \sqrt{\frac{1}{N}\sum_{i=1}^{N}(y_i - y_i^{(1)})^2}$$

is an estimate of the noise variance (we suppose that the noise is stationary). This definition is subject to the remaining noise and the irregular grid effects in $y_i^{(1)}$. Because we expect that bias has typically a range of more than one data point, we first filter out isolated points that were classified as biased, before the actual marking of the corresponding wavelet coefficients.

For all these marked coefficients w_i we compute the value of

$$(w_{\lambda i} - w_i^{(1)})^2 \int_{-\infty}^{\infty} \psi_i^2(x)\,dx = (w_{\lambda i} - w_i^{(1)})^2 (W^T T_J W)_{ii},$$

which quantifies the effect on the output if we replace $w_i^{(1)}$ by $w_{\lambda i}$. If we compute the sum of these effects over all marked coefficients, we see that a few of them are responsible for the major part of the bias. These coefficients, together with the untouched scaling coefficients, keep their value $w_i^{(1)}$. All others undergo the same procedure as the unmarked coefficients.

This procedure eliminates large noise coefficients that do not interfere with biased reconstruction points. This is how the algorithm gets rid of most hidden noise components.

Instead of marking wavelet coefficients that correspond to intervals with bias, we can also compute for *all* coefficients the value of:

$$B_i = (w_{\lambda i} - w_i^{(1)})^2 \int_{-\infty}^{\infty} \psi_i^2(x)\chi_{\text{bias}}(x)\,dx.$$

$\chi_{\text{bias}}(x)$ is an indicator function which is one on all intervals with bias. The above value measures the participation of w_i in the bias. If M is a diagonal matrix with $M_{kk} = 1$ if the corresponding data point x_k has been marked as biased and $M_{kk} = 0$ otherwise, B_i can be computed as:

$$B_i = (w_{\lambda i} - w_i^{(1)})^2 (W^T (T_J M) W)_{ii}.$$

Marking the coefficients with the highest values gives results very close to the first selecting procedure.

7.3.4 The proposed algorithm

The objective of the algorithm is to combine the smooth reconstruction of a second-generation procedure with the reliable estimation of the classical transform. We call $\tilde{W}$ and W the forward and inverse second generation transform, as before, and $\tilde{U}$ and U are the transform matrices if we do not take into account the grid structure. The algorithm goes as follows:

1. Compute $\boldsymbol{w} = \tilde{W}\boldsymbol{y}$ and $\boldsymbol{u} = \tilde{U}\boldsymbol{y}$.

2. Compute the structure of the covariance matrix of the wavelet coefficients:

   $$S = \tilde{W} Q \tilde{W}^T,$$

   and similarly for $\tilde{U}$. Q contains the covariance matrix of the input (up to constant; we do not use an estimate of the noise variance). We assume that the noise is stationary and uncorrelated: $Q = I$. In that case, the computation of S has linear complexity.

3. Normalize the coefficients with these variances and select for both sets of wavelet coefficients a threshold λ and μ, e.g. by minimizing $\text{GCV}_{\boldsymbol{w}}(\lambda)$ and $\text{GCV}_{\boldsymbol{u}}(\mu)$. And apply a soft-threshold to get the thresholded vectors $\boldsymbol{w}_{\boldsymbol{\lambda}}$ and $\boldsymbol{u}_{\boldsymbol{\mu}}$.

4. Compute $\boldsymbol{y}^{(\mathbf{1})} = U\boldsymbol{u}_{\boldsymbol{\mu}}$ and $\boldsymbol{w}^{(\mathbf{1})} = \tilde{W}\boldsymbol{y}^{(\mathbf{1})}$. Use the not further transformed scaling coefficients in $\boldsymbol{w}^{(\mathbf{1})}$ as an estimate for the corresponding noise-free scaling coefficients. Replace the noisy scaling coefficients in $\boldsymbol{w}_{\boldsymbol{\lambda}}$ by these values and compute $\boldsymbol{y}_{\boldsymbol{\lambda}} = W\boldsymbol{w}_{\boldsymbol{\lambda}}$.

5. Estimate the noise standard deviation by:

   $$\hat{\sigma} = \sqrt{\frac{1}{N}\sum_{i=1}^{N}(y_i - y_i^{(1)})^2}.$$

   Among all data points $i = 1, \ldots, N$ we mark those for which $|y_{\lambda i} - y_i^{(1)}| > \hat{\sigma}$, $y_{\lambda i}$ as biased. We filter out isolated labels, since we consider bias as a more-than-one-point phenomenon. We mark all coefficients corresponding to basis functions on intervals with bias.

6. Compute the 2-norm of each basis function, these can be found in the diagonal of the matrix $W^T T_J W$. The computation of this diagonal is of linear complexity.

7. Among all marked coefficients $w_{\lambda i}$, unmark those for which

$$(w_{\lambda i} - w_i^{(1)})^2 (W^T T_J W)_{ii}$$

is too small. Make sure that all scaling coefficients are marked.

8. For all coefficients $i = 1, \ldots, N$ select the appropriate value:

   (a) If a coefficient is marked, let: $\hat{w}_i = w_i^{(1)}$,

   (b) for the others, select: $\hat{w}_i = w_{\lambda i}$.

9. The output is:

$$\hat{\boldsymbol{y}} = W \hat{\boldsymbol{w}}.$$

This algorithm requires 3 forward and 3 inverse transforms, but the order of complexity is still linear. The computation of $W^T T_J W$ and $\tilde{W} Q \tilde{W}^T$ are the most time consuming steps.

7.3.5 Results and discussion

Figure 7.8 contains a plot of the result of the proposed algorithm. It is smooth and close to the noise-free signal. Figure 7.9 focuses on a detail and illustrates the importance of the grid: if neglect the grid structure, the result is non-smooth. The wavelet transform used a cubic interpolation as prediction filter, followed by a two taps update-filter, designed to create the dual wavelets with two vanishing moments. The input signal had $N = 2048$ data points, and we leave 8 scaling coefficients untransformed, and so untouched by the threshold. For the reconstruction, only 18 from the 2048 wavelet coefficients, including the 8 scaling coefficients, were taken from $\boldsymbol{w}^{(1)}$, all the others were based on the thresholded second generation coefficients.

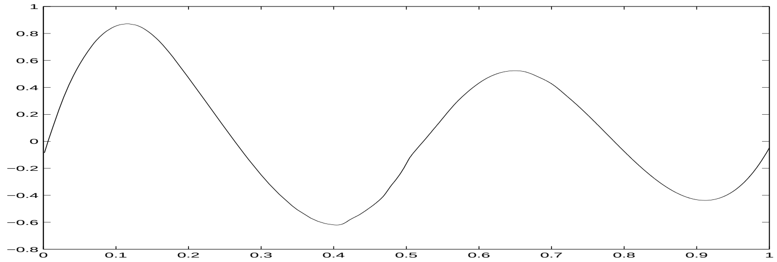

Figure 7.8: Result of the proposed algorithm. It is smooth and close to the noise-free signal.

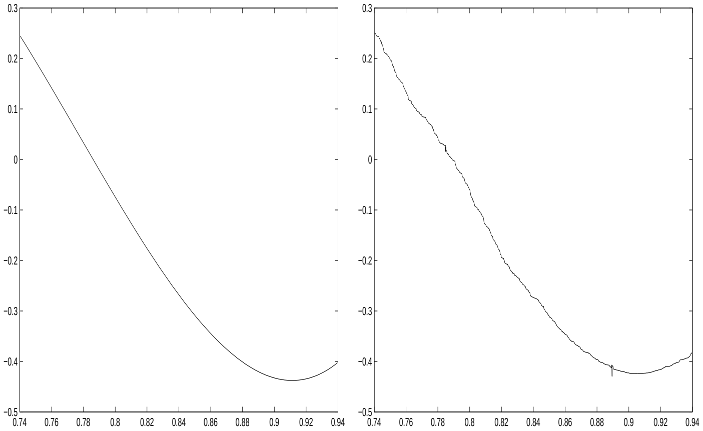

Figure 7.9: Left: detail of Figure 7.8. Right: the reconstruction of classical procedure (no grid structure) on the same interval. This reconstruction carries the irregularity of the grid.

Chapter 8

Overview of contribution and concluding remarks

"O wandern, wandern, meine Lust, o wandern
O wandern, wandern, meine Lust, o wandern
Herr Meister und Frau Meisterin,
lasst mich in Frieden weiterziehen,
und wandern, und wandern,
und wandern, und wandern!"
—Wilhelm Müller, *(1794–1827), Die Schöne Müllerin, set to music by* Franz Schubert *(1797–1828), D. 795.1.*

8.1 Contribution

This dissertation has investigated several aspects of wavelet thresholding. After two chapters of introduction, the description of our own research starts in Chapter 3. We studied [83] the behavior of the minimum risk threshold and proved that for piecewise polynomials, this threshold grows asymptotically as:

$$\lambda^* \sim \sqrt{2 \log N} \sigma,$$

if the number of samples N tends to infinity. This is exactly the same expression as for the *universal threshold*. For piecewise Lipschitz α functions, this needs a slight correction:

$$\lambda^* \sim \sqrt{\frac{2\alpha}{2\alpha+1}} \sqrt{2 \log N} \sigma.$$

Although the risk function and minimum risk threshold have been studied extensively, these results are new as far as we know.

We use this asymptotic result in Chapter 4, where we introduce the method of generalized cross validation to estimate the minimum risk threshold. This method is well known in the framework of linear regression, like spline smoothing [148]. Weyrich and Warhola [149] formulated the definition of GCV for wavelet-thresholding:

$$GCV(\lambda) = \frac{\frac{1}{N} \cdot \|\boldsymbol{y} - \boldsymbol{y_\lambda}\|^2}{\left(\frac{N_0(\lambda)}{N}\right)^2}.$$

$GCV(\lambda)$ is a function of the threshold value through the output $\boldsymbol{y}_{\boldsymbol{\lambda}}$ and the number of killed coefficients $N_0(\lambda)$. This function has asymptotically the same minimizer as the mean square error function. More precisely, Chapter 4 shows that if $\lambda^* = \mathit{arg}\min R(\lambda)$ and $\hat{\lambda} = \mathit{arg}\min GCV(\lambda)$, then for $N \to \infty$, both minimizers yield a result of the same quality:

$$\frac{\mathrm{E}R(\hat{\lambda})}{\mathrm{E}R(\lambda^*)} \downarrow 1.$$

Our proof was inspired by the spline proof by Wahba [148], but the non-linear character of the threshold operation caused several additional problems. The reason why we need the results of Chapter 3 is the following: $GCV(\lambda)$ is badly behaving for small threshold values, because of discontinuities in the denominator. This is why we want the minimum risk threshold to move away from the origin.

The proof of the asymptotic optimality of GCV not only motivates its use in the standard setting of white, stationary noise and orthogonal transforms. Inspecting the assumptions also shows the way to extend the method to correlated (colored) noise, biorthogonal transforms. Chapter 5 also studies GCV for non-decimated wavelet transforms and tries to incorporate GCV and soft-thresholding into a tree structured approach. These techniques and ideas are rather common and obvious, but the introduction and motivation of GCV in these approaches is new [87, 90, 82]. We argued that the advantages of GCV may play an important role, for instance in level-dependent thresholding, to avoid an explicit noise variance estimation at each level.

Chapter 6 concentrates on two-dimensional problems. We illustrate how additional difficulties show up when proceeding from one dimension to two dimensions. We propose a Bayesian approach based on a geometrical prior for configurations of important wavelet coefficients. The idea is based on previous work by Malfait [106], but the elaboration is different [85, 86, 84], as we pointed out in Section 6.6.3. This elaboration was inspired by two clear objectives: we want to mimic an “oracle” which tells the optimal coefficient selection and at the same time we want to deal with line singularities. This type of singularities is specific for two-dimensional data and is relatively badly captured by classical two-dimensional wavelets.

The last chapter is dedicated to a new application: regression of non-equispaced data. Unlike all existing methods, we tried the second generation wavelets way [88]. We encountered several stability problems, and although the precise influence of the different phenomena and their interaction is not yet completely understood, we present an algorithm which performs satisfactorily in practical examples.

8.2 Open problems and suggestions for further research

8.2.1 Non-Gaussian noise

Automatic threshold assessment in various situations has been one of the central issues in this thesis. As for the noise, we limited discussion to stationary, Gaussian densities. Other types, like shot-noise (also known as salt-and-pepper noise), were not treated. An important class of heteroscedastic noise is *multiplicative* or *Poisson* noise:

$$\mathrm{P}(y_i|f_i) = \frac{e^{-f_i} f_i^{y_i}}{y_i!}.$$

The noisy data can only take integer values. This is a good model in situations where intensity (image grey values) are proportional to the result of counting incoming light particles. CT (computer tomography) scanning is an example of this situation. This model also appears in some algorithms for statistical density estimation. Suppose we want to estimate the density $f_X(x)$ of some random variable X, and we have n observations. If we denote by y_i the number of evaluations that fall between x_{i-1} and x_i, $i = 1, \ldots, N$, then

$$f_i := \mathrm{E}y_i = n \int_{x_{i-1}}^{x_i} f_X(x)dx,$$

and y_i has a Poisson distribution. Most density estimation algorithms proceed slightly different: they start from unbiased estimates for scaling coefficients f_k at the finest scale. The density function is expanded as:

$$f_X(x) = \sum_k f_k \varphi_{J,k}(x),$$

with:

$$f_k = \int_{-\infty}^{\infty} \tilde{\varphi}_{J,k}(x) f_X(x)dx,$$

and the initial, noisy estimates are:

$$y_k = \sum_{l=1}^{n} \tilde{\varphi}_{J,k}(X_l).$$

In a Haar basis, this corresponds to simply counting the number of observations in subsequent intervals, but even in the general case, the assumption of normality does not hold.

Shot noise does not cause the typical small, noisy coefficients and the heteroscedastic character of Poisson noise makes it difficult to remove it by one threshold, even if this threshold is scale-adaptive. Anscombe's [8] transformation

$$z_i = 2\sqrt{y_i + 3/8}$$

yields data with a distribution closer to the Gaussian. Using this transformation as a preprocessing step allows for a more successful application of thresholding. Alternatively, one could seek for adapted threshold schemes [95]. In spite of the numerous Poisson phenomena, this application has not yet been studied extensively. Automatically selected thresholds for other types of heteroscedastic and locally stationary noise [147] merit further investigation.

8.2.2 Bayesian correction

We introduced a geometrical prior model for configurations of important two-dimensional wavelet coefficients. This model was combined with a threshold algorithm for noise reduction. Instead of just using coefficient magnitudes, one could involve interscale correlations. One possibility are multiscale Markov Random Fields [44], where the interlevel correlation appears in the prior model. Alternatively one could build interlevel correlations into the measure of regularity to be used in the conditional model. To our knowledge, this possibility has not been investigated so far. This approach relies on a correlation driven deterministic algorithm, like [152] and it should be faster than a multiscale prior model in a Bayesian procedure.

Further experiments with other priors and different models for noise-free coefficients, like Laplacian distributions, are other possible extensions.

While looking for more sophisticated models, one should pay attention to the algorithm complexity: this is a crucial factor in this Bayesian approach. Especially the parameter estimation by the MPLE method could be examined for simplification. This estimation is already much faster than a full MLE, but yet requires a lot of computation. It is also interesting to reconsider the problem that we observe noisy masks: hence, we cannot be sure of the rigidity of the ideal selection mask. Is there any method to estimate this rigidity, taking this perturbation into account?

The introduction of the prior yields a better structured selection, but the effect on the output is fair, at least in terms of signal-to-noise ratio. It may be true that most of the quality gain lies in the enhancement of contrast near the edges and SNR is not an ideal contrast quantifyer. Therefore, a validation of the method with more attention to contrast could give a better idea of the real quality of the Bayesian approach and indicate possible improvements in the prior and conditional model.

8.2.3 Stable transformations for non-equispaced data

In Section 7.2.3, we pointed out several possible explanations for the bad condition of second generation wavelet transforms on irregular grids. Further experiments should reveal how these factors mutually enhance each other. This could lead to a more quantitative study of the stability issue.

Next, this could motivate modifications to the second generation wavelet transform, which reduces the instability, and yet keeps the smoothness of the second generation setting and the locality of a wavelet transform.

A third step is the application to noise reduction.

“ Über allen Gipfeln
Ist Ruh,
In allen Wipfeln
Spürest du
Kaum einen Hauch;
Die Vögelein schweigen im Walde,
Warte nur, balde
Ruhest du auch! ”

—Johann Wolfgang von Goethe, *(1749–1832), set to music (among others) by*
Franz Schubert *(1797–1828), Wandrers Nachtlied, D. 768.*

Bibliography

[1] F. Abramovich, T. C. Bailey, and Th. Sapatinas. Wavelet analysis and its statistical applications. *The Statistician - Journal of the Royal Statistical Society, Ser. D*, To appear, 2000.

[2] F. Abramovich and Y. Benjamini. Adaptive thresholding of wavelet coefficients. *Computational Statistics and Data Analysis*, 22:351–361, 1996.

[3] F. Abramovich, F. Sapatinas, and B. W. Silverman. Wavelet thresholding via a Bayesian approach. *Journal of the Royal Statistical Society, Series B*, 60:725–749, 1998.

[4] F. Abramovich and B.W. Silverman. Wavelet decomposition approaches to statistical inverse problems. *Biometrika*, 85:115–129, 1998.

[5] A. N. Akansu and R. A. Haddad. *Multiresolution Signal Decomposition: Transforms, Subbands, and Wavelets*. Academic Press, 1250 Sixth Ave., San Diego, CA 92101-4311, 1992.

[6] U. Amato and D. T. Vuza. Besov regularization, thresholding and wavelets for smoothing data. *Numer. Funct. Anal. Optimization*, 18:461–493, 1997.

[7] U. Amato and D. T. Vuza. Wavelet approximation of a function from samples affected by noise. *Revue Roum. Math. Pures Appl.*, 42(7–8):481–493, 1997.

[8] F. Anscombe. The transformation of Poisson, binomial and negative binomial data. *Biometrika*, 35:246–254, 1948.

[9] J.-P. Antoine. The continuous wavelet transform in image processing. *CWI Q.*, 11(4):323–345, 1998.

[10] J.-P. Antoine, P. Carrette, R. Murenzi, and B. Piette. Image analysis with two-dimensional continuous wavelet transform. *Signal Processing*, 31(3):241–272, 1993.

[11] M. Antonini, M. Barlaud, P. Mathieu, and I. Daubechies. Image coding using the wavelet transform. *IEEE Transactions on Image Processing*, 1(2):205–220, 1992.

[12] A. Arneodo, E. Bacry, S. Jaffard, and J.F. Muzy. Singularity spectrum of multifractal functions involving oscillating singularities. *J. Fourier Anal. Appl.*, 4(2):159–174, 1998.

[13] R. Baraniuk. Optimal tree approximation with wavelets. In M. A. Unser, A. Aldroubi, and Laine A. F., editors, *Wavelet Applications in Signal and Image Processing VII*, volume 3813 of *SPIE Proceedings*, pages 206–214, July 1999.

[14] O. E. Barndorff-Nielsen and D. R. Cox. *Asymptotic Techniques for Use in Statistics*. Chapman and Hall, 11 New Fetter Lane, London EC4P 4EE, U.K., 1989.

[15] M. G. Bello. A combined Markov Random Field and wave-packet transform-based approach for image segmentation. *IEEE Transactions on Image Processing*, 3(6):834–846, 1994.

[16] Y. Benjamini and Y. Hochberg. Controlling the false discovery rate: A practical and powerful approach to multiple testing. *Journal of the Royal Statistical Society, Series B*, 57:289–300, 1995.

[17] K. Berkner and R. O. Wells, Jr. Correlation-dependent model for denoising via nonorthogonal wavelet transforms. Technical report, C. M. L., Dept. Mathematics, Rice University, June 1998.

[18] J. E. Besag. Spatial interaction and the spatial analysis of lattice systems. *Journal of the Royal Statistical Society, Series B*, 36:192–236, 1974.

[19] Ch. Blatter. *Wavelets. A primer*. Natick, MA: A K Peters, 1998.

[20] C. A. Bouman and M. Shapiro. A multiscale random field model for Bayesian image segmentation. *IEEE Transactions on Image Processing*, 3(2):162–177, 1994.

[21] L. Breiman, J. H. Friedman, R. A. Olshen, and C. J. Stone. *Classification and regression trees (CART)*. Wadsworth, Monterey, CA, USA, 1984.

[22] S. C. Brenner and L. R. Scott. *The Mathematical Theory of Finite Element Methods*. Springer-Verlag, 175 Fifth Avenue, New York 10010, USA, 1994.

[23] A.G. Bruce and H.-Y. Gao. Waveshrink with firm shrinkage. *Statistica Sinica*, 4:855–874, 1997.

[24] C. S. Burrus, R. A. Gopinath, and H. Guo. *Introduction to Wavelets and Wavelet Transforms*. Prentice Hall, Upper Saddle River, New Jersey 07458, 1998.

[25] T. Cai and L.D. Brown. Wavelet shrinkage for nonequispaced samples. *Annals of Statistics*, 26(5):1783–1799, 1998.

[26] R. Calderbank, I. Daubechies, W. Sweldens, and B.-L. Yeo. Wavelet transforms that map integers to integers. *Appl. Comput. Harmon. Anal.*, 5(3):332–369, 1998.

[27] E. Candes. *Ridgelets: theory and applications*. PhD thesis, Department of Statistics, Stanford University, August 1998.

[28] R. A. Carmona. Extrema reconstructions and spline smoothing: Variations on an algorithm of Mallat & Zhong. In A. Antoniadis and G. Oppenheim, editors, *Wavelets and Statistics*, volume 103 of *Lecture Notes in Statistics*, pages 83–94, 1995.

[29] A. Chambolle, R. A. DeVore, N.-Y. Lee, and B. J. Lucier. Nonlinear wavelet image processing: Variational problems, compression, and noise removal through wavelet shrinkage. *IEEE Transactions on Image Processing*, 7(3):319–355, March 1998.

[30] G. Chang, B. Yu, and M. Vetterli. Adaptive wavelet thresholding for image denoising and compression. *submitted*, 1999.

[31] G. Chang, B. Yu, and M. Vetterli. Spatially adaptive wavelet thresholding based on context modeling for image denoising. *submitted*, 1999.

[32] G. Chang, B. Yu, and M. Vetterli. Wavelet thresholding for multiple noisy image copies. *IEEE Transactions on Image Processing*, To appear, 1999.

[33] P. Charbonnier, L. Blanc-Féraud, and M. Barlaud. Noisy image restoration using multiresolution Markov Random Fields. *Journal of Visual Communication and Image Representation*, 3(4):338–346, 1992.

[34] S. Chen and D. L. Donoho. Atomic decomposition by basis pursuit. Technical Report 479, Department of Statistics, Stanford University, May 1995.

[35] H. Chipman, E. Kolaczyk, and R. McCulloch. Adaptive Bayesian wavelet shrinkage. *J. Amer. Statist. Assoc.*, 92:1413–1421, 1997.

[36] H. Choi and Baraniuk R. G. Wavelet statistical models and besov spaces. In M. A. Unser, A. Aldroubi, and A. F. Laine, editors, *Wavelet Applications in Signal and Image Processing VII*, volume 3813 of *SPIE Proceedings*, page To Appear, July 1999.

[37] M. Clyde, G. Parmigiani, and B. Vidakovic. Multiple shrinkage and subset selection in wavelets. *Biometrica*, 85:391–401, 1998.

[38] A. Cohen, I. Daubechies, and J. Feauveau. Bi-orthogonal bases of compactly supported wavelets. *Comm. Pure Appl. Math.*, 45:485–560, 1992.

[39] I. Cohen, I. Raz, and D. Malah. Orthonormal shift-invariant adaptive local trigonometric decomposition. *Signal Processing*, 57(1):43–64, 1997.

[40] I. Cohen, I. Raz, and D. Malah. Orthonormal shift-invariant wavelet packet decomposition and representation. *Signal Processing*, 57(3):251–270, 1997.

[41] R. R. Coifman, Y. Meyer, and V. Wickerhauser. Size properties of wavelet packets. In M. B. Ruskai, G. Beylkin, R. Coifman, I. Daubechies, S. Mallat, Y. Meyer, and L. Raphael, editors, *Wavelets and their Applications*, pages 453–470. Jones and Bartlett, Boston, 1992.

[42] R. R. Coifman and M. L. Wickerhauser. Entropy based algorithms for best basis selection. *IEEE Transactions on Information Theory*, 38(2):713–718, 1992.

[43] P. Craven and G. Wahba. Smoothing noisy data with spline functions. *Numerische Mathematik*, 31:377–403, 1979.

[44] M. S. Crouse, R.D. Nowak, and R. G. Baraniuk. Wavelet-based signal processing using hidden markov models. *IEEE Transactions on Signal Processing*, 46, Special Issue on Wavelets and Filterbanks:886–902, 1998.

[45] W. Dahmen, A. J. Kurdila, and P. Oswald. *Multiscale wavelet methods for partial differential equations*. Academic press New York, 1997.

[46] I. Daubechies. *Ten Lectures on Wavelets*. CBMS-NSF Regional Conf. Series in Appl. Math., Vol. 61. Society for Industrial and Applied Mathematics, Philadelphia, PA, 1992.

[47] I. Daubechies, I. Guskov, P. Schröder, and W. Sweldens. Wavelets on irregular point sets. *Phil. Trans. R. Soc. Lond. A*, To be published.

[48] I. Daubechies, I. Guskov, and W. Sweldens. Regularity of irregular subdivision. *Constructive Approximation*, 15:381–426, 1999.

[49] I. Daubechies and W. Sweldens. Factoring wavelet transforms into lifting steps. *J. Fourier Anal. Appl.*, 4(3):245–267, 1998.

[50] P. De Gersem, B. De Moor, and M Moonen. Applications of the continuous wavelet transform in the processing of musical signals. In *Proc. of the 13th International Conference on Digital Signal Processing (DSP97)*, pages 563–566, 1997.

[51] V. Delouille. Nonparametric regression estimation using design-adapted wavelets. Master's thesis, Institut de Statistique, UCL, Belgium, 1999.

[52] R. A. DeVore, B. B. Jawerth, and V. Popov. Compression of wavelet decompositions. *Amer. J. Math.*, 114:737–785, 1992.

[53] R. A. DeVore, B. Jawerth, and B. J. Lucier. Image compression through wavelet transform coding. *IEEE Transactions on Information Theory*, 38(2):719–746, 1992.

[54] R. A. DeVore and V Popov. Interpolation of Besov spaces. *Trans. Amer. Math. Soc.*, 305:397–414, 1988.

[55] D. L. Donoho. Wavelet shrinkage and W.V.D. – a ten-minute tour. In Y. Meyer and S. Roques, editors, *Progress in Wavelet Analysis and Applications*, pages 109–128. Editions Frontières: Gif-sur-Yvette, 1993.

[56] D. L. Donoho. De-noising by soft-thresholding. *IEEE Transactions on Information Theory*, 41(3):613–627, May 1995.

[57] D. L. Donoho. Nonlinear solution of linear inverse problems by wavelet-vaguelette decomposition. *Appl. Comput. Harmon. Anal.*, 2(2):101–126, 1995.

[58] D. L. Donoho. CART and best-ortho-basis: a connection. *Ann. Statist.*, 25(5):1870–1911, 1997.

[59] D. L. Donoho and I. M. Johnstone. Minimax estimation via wavelet shrinkage. Technical Report 402, Stanford University, 1992.

[60] D. L. Donoho and I. M. Johnstone. Ideal spatial adaptation via wavelet shrinkage. *Biometrika*, 81:425–455, 1994.

[61] D. L. Donoho and I. M. Johnstone. Adapting to unknown smoothness via wavelet shrinkage. *J. Amer. Statist. Assoc.*, 90:1200–1224, 1995.

[62] D. L. Donoho, I. M. Johnstone, G. Kerkyacharian, and D. Picard. Wavelet shrinkage: Asymptopia? *Journal of the Royal Statistical Society, Series B*, 57(2):301–369, 1995.

[63] R. Fletcher. *Practical methods of optimization*. Wiley-interscience publications. Wiley, Chichester, 1981.

[64] M. W. Frazier. *An Introduction to Wavelets through Linear Algebra*. Springer-Verlag, New York, 1999.

[65] H.-Y. Gao. Wavelet shrinkage denoising using the non-negative garrote. *Journal of Computational and Graphical Statistics*, 7(4):469–488, December 1998.

[66] S. Geman and D. Geman. Stochastic relaxation, Gibbs distributions, and the Bayesian restoration of images. *IEEE Transactions on Pattern Analysis and Machine Intelligence*, 6(6):721–741, 1984.

[67] J. W. Gibbs. *Elementary principles in statistical mechanics*. Yale University Press, New Haven, 1902. Reprinted by Ox Bow Press, Woodbridge, 1981.

[68] M. Girardi and W. Sweldens. A new class of unbalanced Haar wavelets that form an unconditional basis for L_p on general measure spaces. *J. Fourier Anal. Appl.*, 3(4):457–474, 1997.

[69] S. Goedecker. *Wavelets and their application for the solution of partial differential equations in physics*. Cahiers de Physique. 4. Presses Politechniques et Universitaires Romandes, Lausanne, 1998.

[70] S. Goedecker and O. Ivanov. Solution of multiscale partial differential equations using wavelets. *Computers in Physics*, 12(6):548–555, 1998.

[71] A. Haar. Zur Theorie der orthogonalen Funktionen-Systeme. *Math. Ann.*, 69:331–371, 1910.

[72] P. Hall and I. Koch. On the feasibility of cross-validation in image analysis. *SIAM J. Appl. Math.*, 52(1):292–313, 1992.

[73] P. Hall and P. Patil. Formulae for mean integrated squared error of nonlinear wavelet-based density estimators. *Annals of Statistics*, 23(3):905–928, 1995.

[74] P. Hall and P. Patil. Effect of threshold rules on performance of wavelet-based curve estimators. *Stat. Sin.*, 6(2):331–345, 1996.

[75] P. Hall and P. Patil. On the choice of smoothing parameter, threshold and truncation in nonparametric regression by non-linear wavelet methods. *Journal of the Royal Statistical Society, Series B*, 58(2):361–377, 1996.

[76] P. Hall and B. A. Turlach. Interpolation methods for nonlinear wavelet regression with irregularly spaced design. *Annals of Statistics*, 25(5):1912 – 1925, 1997.

[77] M. Hansen and B. Yu. Wavelet thresholding via MDL: simultaneous denoising and compression. *submitted*, 1999.

[78] J. Heikkinen and H. Högmander. Fully Bayesian approach to image restoration with an application in biogeography. *Applied Statistics*, 43(4):569–582, 1994.

[79] H. M. Hudson. A natural identity for exponential families with applications in multiparameter estimation. *Annals of Statistics*, 6(3):473–484, 1978.

[80] E. Ising. Beitrag zur Theorie des Ferromagnetismus. *Zeitschrift für Physik*, 31:253–258, 1925.

[81] S. Jaffard. Pointwise smoothness, two-microlocalisation and wavelet coefficients. *Publicacions Matemàtiques*, 35:155–168, 1991.

[82] M. Jansen and A. Bultheel. Experiments with wavelet based image denoising using generalized cross validation. In K. M. Hanson, editor, *Medical Imaging 1997: Image Processing*, volume 3034 of *SPIE Proceedings*, pages 206–214, February 1997.

[83] M. Jansen and A. Bultheel. Asymptotic behavior of the minimum mean squared error threshold for noisy wavelet coefficients of piecewise smooth signals. TW Report 294, Department of Computer Science, Katholieke Universiteit Leuven, Belgium, October 1999.

[84] M. Jansen and A. Bultheel. Empirical bayes approach to improve wavelet thresholding for image noise reduction. TW Report 296, Department of Computer Science, Katholieke Universiteit Leuven, Belgium, October 1999.

[85] M. Jansen and A. Bultheel. Geometrical priors for noisefree wavelet coefficient configurations in image de-noising. In P. Müller and B. Vidakovic, editors, *Bayesian inference in wavelet based models*, pages 223–242. Springer-Verlag, 1999.

[86] M. Jansen and A. Bultheel. Geometrical priors in a Bayesian approach to improve wavelet threshold procedures. In M. A. Unser, A. Aldroubi, and Laine A. F., editors, *Wavelet Applications in Signal and Image Processing VII*, volume 3813 of *SPIE Proceedings*, pages 580–590, July 1999.

[87] M. Jansen and A. Bultheel. Multiple wavelet threshold estimation by generalized cross validation for images with correlated noise. *IEEE Transactions on Image Processing*, 8(7):947–953, July 1999.

[88] M. Jansen and A. Bultheel. Smoothing irregularly sampled signals using wavelets and cross validation. TW Report 289, Department of Computer Science, Katholieke Universiteit Leuven, Belgium, April 1999.

[89] M. Jansen, M. Malfait, and A. Bultheel. Generalized cross validation for wavelet thresholding. *Signal Processing*, 56(1):33–44, January 1997.

[90] M. Jansen, G. Uytterhoeven, and A. Bultheel. Image de-noising by integer wavelet transforms and generalized cross validation. *Medical Physics*, 26(4):622–630, April 1999.

[91] B. Jawerth and W. Sweldens. An overview of wavelet based multiresolution analyses. *SIAM Review*, 36(3):377–412, 1994.

[92] I. M. Johnstone and B. W. Silverman. Wavelet threshold estimators for data with correlated noise. *Journal of the Royal Statistical Society, Series B*, 59:319–351, 1997.

[93] G. Kaiser. *A Friendly Guide to Wavelets*. Birkhäuser, 675 Massachusetts Ave., Cambridge, MA 02139, U.S.A., 1994.

[94] E. D. Kolaczyk. A wavelet shrinkage approach to tomographic image reconstruction. *J. Amer. Statist. Assoc.*, 91:1079–1090, 1996.

[95] E. D. Kolaczyk. Wavelet shrinkage estimation of certain Poisson intensity signals using corrected thresholds. *Stat. Sin.*, 9(1):119–135, 1999.

[96] A. Kovac and B. Silverman. Extending the scope of wavelet regression methods by coefficient-dependent thresholding. *J. Amer. Statist. Assoc.*, 95:To appear, 2000.

[97] J. Kovačević and W. Sweldens. Wavelet families of increasing order in arbitrary dimensions. *IEEE Transactions on Image Processing*, 1999.

[98] J. Kovačević and M. Vetterli. Nonseparable multidimensional perfect reconstruction filter banks and wavelet bases for $\mathbf{R}^n$. *IEEE Transactions on Information Theory*, 38(2):533–555, March 1992.

[99] F. Labaere, P. Vuylsteke, P. Wambacq, E. Schoeters, and C. Fivez. Primitive-based contrast enhancement method. In M. Loew and K. Hanson, editors, *Medical Imaging 1996: Image Processing*, volume 2710 of *SPIE Proceedings*, pages 811–820, April 1996.

[100] G. Lang, H. Guo, J. E. Odegard, C. S. Burrus, and R. O. Wells. Noise reduction using an undecimated discrete wavelet transform. *IEEE Signal Processing Letters*, 3(1):10–12, 1996.

[101] M. Lang, H. Guo, J. E. Odegard, C. S. Burrus, and R. O. Wells. Nonlinear processing of a shift-invariant discrete wavelet transform (dwt) for noise reduction. In H. H. Szu, editor, *Wavelet Applications II*, pages 640–651, April 1995.

[102] M. R. Leadbetter, G. Lindgren, and H. Rootzén. *Extremes and Related Properties of Random Sequences and Processes*. Springer Series in Statistics. Springer, 175 Fifth Avenue, New York 10010, USA, 1983.

[103] A. K. Louis, P. Maaß, and A. Rieder. *Wavelets: Theory and Applicaltions*. John Wiley & Sons, 605 Third Avenue, New York, NY 10158-0012, USA, 1997.

[104] J. Lu, D. M. Healy Jr., and J. B. Weaver. Contrast enhancement of medical images using multiscale edge representation. *Optical Engineering*, special issue on Adaptive Wavelet Tansforms:pages 1251–1261, July 1994.

[105] M. R. Luettgen, W. C. Karl, A. S. Willsky, and R. R. Tenney. Multiscale representations of Markov Random Fields. *IEEE Transactions on Signal Processing*, 41(12):3377–3395, December 1993.

[106] M. Malfait. *Stochastic Sampling and Wavelets for Bayesian Image Analysis*. PhD thesis, Department of Computer Science, K.U.Leuven, Belgium, 1995.

[107] M. Malfait. Using wavelets to suppress noise in biomedical images. In A. Aldroubi and M. Unser, editors, *Wavelets in Medicine and Biology*, Chapter 8, pages 191–208. CRC Press, 1995.

[108] M. Malfait and D. Roose. Wavelet based image denoising using a markov random field a priori model. *IEEE Transactions on Image Processing*, 6(4):549–565, 1997.

[109] S. Mallat and W. L. Hwang. Singularity detection and processing with wavelets. *IEEE Transactions on Information Theory*, 38(2):617–643, 1992.

[110] S. Mallat and Z. Zhang. Matching pursuits with time-freuency dictionaries. *IEEE Transactions on Signal Processing*, 41(12):3397–3415, 1993.

[111] S. Mallat and S. Zhong. Characterization of signals from multiscale edges. *IEEE Transactions on Pattern Analysis and Machine Intelligence*, 14:710–732, 1992.

[112] S. G. Mallat. A theory for multiresolution signal decomposition: The wavelet representation. *IEEE Transactions on Pattern Analysis and Machine Intelligence*, 11(7):674–693, 1989.

[113] S. G. Mallat. *A Wavelet Tour of Signal Processing*. Academic Press, 525 B Street, Suite 1900, San Diego, CA, 92101-4495, USA, 1998.

[114] N. Metropolis, M. Rosenbluth, et al. Equation of state calculations by fast computing machines. *Journal of Chemical Physics*, 21:1087–1092, 1953.

[115] G. P. Nason. Wavelet regression by cross validation. Preprint, Department of Mathematics, University of Bristol, UK, 1994.

[116] G. P. Nason. Wavelet shrinkage using cross validation. *Journal of the Royal Statistical Society, Series B*, 58:463–479, 1996.

[117] G. P. Nason and B. W. Silverman. The stationary wavelet transform and some statistical applications. In A. Antoniadis and G. Oppenheim, editors, *Wavelets and Statistics*, Lecture Notes in Statistics, pages 281–299, 1995.

[118] G. P. Nason and R. von Sachs. Wavelets in time series analysis. *Philosophical Transactions of the Royal Society London, Series A: Mathematical, Physical and Engineering Sciences*, 357:2511–2526, 1999.

[119] G. P. Nason, R. von Sachs, and G. Kroisandt. Wavelet processes and adaptive estimation of the evolutionary wavelet spectrum. *Journal of the Royal Statistical Society, Series B*, To appear, 2000.

[120] M. H. Neumann and R. von Sachs. Wavelet thresholding in anisotropic function classes and application to adaptive estimation of evolutionary spectra. *Annals of Statistics*, 25:38–76, 1997.

[121] Y. Nievergelt. *Wavelets made easy*. Birkhaeuser, Boston, MA, 1999.

[122] R.D. Nowak and R. G. Baraniuk. Optimal weighted highpass filters using multiscale analysis. *IEEE Transactions on Image Processing*, 1996. submitted.

[123] R.D. Nowak and R. G. Baraniuk. Wavelet-domain filtering for photon imaging systems. *IEEE Transactions on Image Processing*, 1998. submitted.

[124] T. Ogden and E. Parzen. Change-point approach to data analytic wavelet thresholding. *Statistics and Computing*, 6:93–99, 1996.

[125] T. Ogden and E. Parzen. Data dependent wavelet thresholding in nonparametric regression with change-point applications. *Computational Statistics and Data Analysis*, 22(1):53–70, 1996.

[126] J.-C. Pesquet, H. Krim, and H. Carfantan. Time invariant orthonormal wavelet representations. *IEEE Transactions on Signal Processing*, 44(8):1964–1970, 1996.

[127] L. Prasad and S. S. Iyengar. *Wavelet Analysis with Applications to Image Processing*. CRC Press, 2000 Corporate Blvd., N.W., Boca Raton, Florida 33431, 1997.

[128] F. Ruggeri and B. Vidakovic. A Bayesian decision theoretic approach to the choice of thresholding parameter. *Statistica Sinica*, 9:183–197, 1999.

[129] E. Simoncelli. Modeling the joint statistics of images in the wavelet domain. In M. A. Unser, A. Aldroubi, and Laine A. F., editors, *Wavelet Applications in Signal and Image Processing VII*, volume 3813 of *SPIE Proceedings*, pages 206–214, July 1999.

[130] E. P. Simoncelli and E.H. Adelson. Noise removal via Bayesian wavelet coring. In *proceedings 3rd International Conference on Image Processing*, September 1996.

[131] E.P. Simoncelli and E.H. Adelson. Non-separable extensions of quadrature mirror filters to multiple dimensions. *Proceedings of the IEEE*, 78:652–664, April 1990.

[132] C. Stein. Estimation of the mean of a multivariate normal distribution. *Annals of Statistics*, 9(6):1135–1151, 1981.

[133] G. Strang and T. Nguyen. *Wavelets and filter banks*. Wellesley-Cambridge Press, Box 812060, Wellesley MA 02181, fax 617-253-4358, 1996.

[134] W. Sweldens. *The Construction and Application of Wavelets in Numerical Analysis*. PhD thesis, Department of Computer Science, K.U.Leuven, Belgium, 1994.

[135] W. Sweldens. The lifting scheme: A new philosophy in biorthogonal wavelet constructions. In A. F. Laine and M. Unser, editors, *Wavelet Applications in Signal and Image Processing III*, pages 68–79. Proc. SPIE 2569, 1995.

[136] W. Sweldens. The lifting scheme: A custom-design construction of biorthogonal wavelets. *Appl. Comput. Harmon. Anal.*, 3(2):186–200, 1996.

[137] W. Sweldens. The lifting scheme: A construction of second generation wavelets. *SIAM J. Math. Anal.*, 29(2):511–546, 1997.

[138] W. Sweldens and P. Schröder. Building your own wavelets at home. In *Wavelets in Computer Graphics*, ACM SIGGRAPH Course Notes, pages 15–87. ACM, 1996.

[139] A. Teolis. *Computational signal processing with wavelets*. Applied and Numerical Harmonic Analysis. Birkhaeuser, Boston, MA, 1998.

[140] G. Uytterhoeven. *Wavelets: software and applications*. PhD thesis, Department of Computer Science, K.U.Leuven, Belgium, April 1999.

[141] G. Uytterhoeven and A. Bultheel. The Red-Black wavelet transform. TW Report 271, Department of Computer Science, Katholieke Universiteit Leuven, Belgium, December 1997.

[142] G. Uytterhoeven, F. Van Wulpen, M. Jansen, D. Roose, and A. Bultheel. WAILI: Wavelets with Integer Lifting. TW Report 262, Department of Computer Science, Katholieke Universiteit Leuven, Belgium, July 1997.

[143] D. Vandermeulen. *Methods for registration, interpolation and interpretation of three-dimensional medical image data for use in 3-D display, 3-D modelling and therapy planning*. PhD thesis, K.U.Leuven, 1991.

[144] T. Verhaeghe. Het algoritme van Carmona voor wavelet-gebaseerde signaalreconstructie. Master's thesis, Department of Computer Science, K.U.Leuven, Belgium, 1997.

[145] M. Vetterli and C. Herley. Wavelets and filter banks: theory and design. *IEEE Transactions on Signal Processing*, 40(9):2207–2232, 1992.

[146] B. Vidakovic. Nonlinear wavelet shrinkage with Bayes rules and Bayes factors. *J. Amer. Statist. Assoc.*, 93:173–179, 1998.

[147] R. von Sachs and B. MacGibbon. Non-parametric curve estimation by wavelet thresholding with locally stationary errors. *Scandinavian Journal of Statistics*, To appear, 2000.

[148] G. Wahba. *Spline Models for Observational Data*, chapter 4, pages 45–65. CBMS-NSF Regional Conf. Series in Appl. Math. Society for Industrial and Applied Mathematics, Philadelphia, PA, 1990.

[149] N. Weyrich and G. T. Warhola. De-noising using wavelets and cross validation. In S.P. Singh, editor, *Approximation Theory, Wavelets and Applications*, volume 454 of *NATO ASI Series C*, pages 523–532, 1995.

[150] N. Weyrich and G.T. Warhola. Wavelet shrinkage and generalized cross validation for image denoising. *IEEE Transactions on Image Processing*, 7(1):82–90, January 1998.

[151] G. Winkler. *Image analysis, random fields and dynamic Monte Carlo methods*. Applications of Mathematics. Springer, 1995.

[152] Y. Xu, J. B. Weaver, D. M. Healy, and J. Lu. Wavelet transform domain filters: a spatially selective noise filtration technique. *IEEE Transactions on Image Processing*, 3(6):747–758, 1994.

Index

The research leading to this thesis was made possible with the financial support of the following institutions:

Katholieke Universiteit Leuven

Fonds voor Wetenschappelijk Onderzoek Vlaanderen (FWO)

Vlaams Instituut voor de bevordering van het Wetenschappelijk Technologisch onderzoek in de industrie (IWT)

Vlaamse Leergangen Leuven

Stanford University

Duke University

Nederlandse vertaling van sommige citaten

English translations of some quotations

Page xi.
A certain amount of dreaming is good, like a narcotic in discreet doses. It lulls to sleep the fevers of the mind at labor, which are sometimes severe, and produces in the spirit a soft and fresh vapor which corrects the over-harsh contours of pure thought, fills in gaps here and there, binds together and rounds off the angles of the ideas. But too much dreaming sinks and drowns. Woe to the brain-worker who allows himself to fall entirely from thought into revery! He thinks that he can re-ascend with equal ease, and he tells himself that, after all, it is the same thing. Error!
Thought is the toil of the intelligence, revery its voluptuousness. To replace thought with revery is to confound a poison with a food.
(English translation: Isabel F. Hapgood)

Pagina 7.
'Bengt', zei William tegen mij,' is ten prooi gevallen aan een grote wellust, die niet die van Berenger noch die van de cellarius is. Zoals velen die zich met studie bezig houden, wordt hij beheerst door de lust tot weten. Tot weten om het weten. Toen hij van een deel van dit weten was uitgesloten, wilde hij zich ervan meester maken. Nu heeft hij zich ervan meester gemaakt. Malachias kende zijn man en heeft het beste middel aangewend om het boek terug te krijgen en de lippen van Bengt te verzegelen. Jij zult me nu vragen waartoe het dient zulk een schat aan wetenschap in beheer te hebben als men de voorwaarde aanvaardt deze niet aan anderen ter beschikking te stellen. Maar daarom juist sprak ik van wellust. De dorst naar kennis van Roger Bacon, die de wetenschap wilde aanwenden om het volk Gods gelukkiger te maken en dus niet het weten om het weten zocht, was geen wellust. Die van Bengt is alleen maar onverzadigbare nieuwsgierigheid, hoogmoed van het verstand, een van de manieren, voor een monnik, om de lusten van zijn lenden een andere vorm te geven en tot rust te brengen, of het innerlijk vuur dat een ander tot strijder voor het geloof, of voor de ketterij maakt. We kennen niet alleen de wellust van het vlees.
(Nederlandse vertaling: Jenny Tuin, Pietha de Voogd en Henny Vlot)

Page 45
But you wander up and down,
from the eastern cradle to the western grave,
on your pilgrimage from land to land;
and wherever you are, you are at home.
(...)
o happy is he who, wherever he goes,
still stands on native ground!
(English translation: Emily Ezust)

Page 79
Midway in the journey of our life
I found myself in a dark wood,
for the straight way was lost.
Ah, how hard it is to tell what that
wood was, wild, rugged, harsh;
the very thought of it renews the fear!
(English translation: Charles S. Singleton)

Pagina 101
En vaak is de stap van extatisch visioen naar de razernij van zonde maar al te klein.
(...)
'Wat ik wilde zeggen, is dat er weinig verschil bestaat tussen het vuur van de Serafijnen en het vuur van Lucifer: allebei volgen ze uit een extreme ontvlamming van de wil.'
'O, maar dat verschil is er wel, en ik ken het het!', zei Ubertino begeesterd,'Jij wil zeggen dat tussen het goede willen en het kwade willen er maar een kleine stap bestaat, omdat het er altijd op neerkomt dezelfde wil te richten. Dat is waar. Maar het verschil zit in het voorwerp, en het voorwerp is onmiskenbaar: aan de ene kant God, aan de andere kant de duivel.
(eigen vertaling)

Pagina 125
Het leven der eenvoudigen, heer abt, wordt niet verlicht door de wijsheid en door waakzame zin voor onderscheid die ons verstandig maakt. Hun leven wordt beheerst door ziekte en armoede, onwetendheid maakt hen tot stotteraars. Dikwijls is voor velen van hen een ketterij alleen een manier als een andere om hun wanhoop uit te schreeuwen. Men kan het huis van een kardinaal in brand steken, ofwel omdat men het leven van de clerus wil uitzuiveren, ofwel omdat men gelooft dat de hel die hij voorhoudt, niet bestaat. Men doet het altijd omdat de aardse hel bestaat.

(eigen vertaling)

Page 152
By day, by night, in waking, in dreaming,
They are all the same to her,
So long as she can wander,
She is more than satisfied!

She never becomes tired, she never grows exhausted,
The route always feels new;
She needs no enticement, needs no reward,
This pigeon is so true to me.
(English translation: Philip Sternberg)

Pagina 153
– Laten we van voorafaan proberen, Adso, en ik verzeker je, ik probeer je iets uit te leggen waarvan zelfs ik niet geloof de waarheid in pacht te hebben.
– Waarom neemt u geen stelling in, waarom zegt u me niet waar de waarheid ligt?
– Kijk, het beste wat men kan doen, is beter kijken.
– Dus als ik goed begrijp, doet u iets, en weet u waarom u dat doet, maar weet u niet waarom u weet dat u weet wat u dat doet?
(eigen vertaling)

Page 169
Oh, wandering, wandering, my joy,
Oh, wandering, wandering, my joy,
Oh, wandering!
Oh, Master and Mistress,
Let me continue in peace,
And wander, and wander,
and wander, and wander!
(English translation: Emily Ezust)

Page 174
Over all the peaks
It is peaceful,
In all the treetops
You feel
Hardly a breath of wind;
The little birds are silent in the forest,
Only wait; soon
You will rest as well!
(English translation: Emily Ezust)